The University of Manchester

A Computational Model of Human Iron Metabolism

A thesis
submitted to The University of Manchester
for the degree of
doctor of philosophy (PhD)
in the faculty of Engineering and Physical Sciences

Simon Mitchell

School of Computer Science
2013

CONTENTS

Final word count: 33095

LIST OF FIGURES

LIST OF TABLES

LIST OF ABBREVIATIONS

Table 1: **List of Abbreviations**

Abbreviation	Description
Cp	Ceruloplasmin
Dcytb	Duodenal cytochrome B
DMT1	Divalent metal transporter 1
EPO	Erythropoietin
Fe	Iron
Ft	Ferritin
HCP1	Haem carrier protein 1
HFE	Human haemochromatosis protein
HIF	Hypoxia inducible factor
HRE	Hypoxia responsive element
IRE	Iron responsive element
IRP	Iron response protein
KO	Knockout
LIP	Labile iron pool
ODE	Ordinary differential equations
PrP	Cellular prion protein
RBC	Red blood cell
SBML	Systems biology markup language
SPR	Surface plasmon resonance
TBI	Transferrin-bound iron
Tf	Transferrin
Tf-Fe	Transferrin-bound iron
TfR1/2	Transferrin receptor 1/2
WBC	White blood cell

ABSTRACT

A THESIS SUBMITTED TO THE UNIVERSITY OF MANCHESTER
FOR THE DEGREE OF DOCTOR OF PHILOSOPHY (PHD)
SIMON MITCHELL
2013

Iron is essential for virtually all organisms, yet it can be highly toxic if not properly regulated. Only the Lyme disease pathogen *Borrelia burgdorferi* has evolved to not require iron (Aguirre et al., 2013). Recent findings have characterised elements of the iron metabolism network, but understanding of systemic iron regulation remains poor. To improve understanding and provide a tool for *in silico* experimentation, a computational model of human iron metabolism has been constructed.

COPASI was utilised to construct a model that included detailed modelling of iron metabolism in liver and intestinal cells. Inter-cellular interactions and dietary iron absorption were included to create a systemic computational model. Parameterisation was performed using a wide variety of literature data.

Validation of the model was performed using published experimental and clinical findings, and the model was found to recreate quantitatively and accurately many results. Analysis of sensitivities in the model showed that, despite enterocytes being the only route of iron uptake, almost all control over the system is provided by reactions in the liver. Metabolic control analysis identified key regulatory factors and potential therapeutic targets.

A virtual haemochromatosis patient was created and compared to a simulation of a healthy human. The redistribution of control in haemochromatosis was analysed in order to improve our understanding of the condition and identify promising therapeutic targets.

Cellular prion protein (PrP) is an enigmatic protein, implicated in disease when misfolded, but its physiological role remains a mystery. PrP was recently found to have ferric-reductase capacity. Potential sites of ferric reduction were simulated and the findings compared to PrP knockout mice experiments. I propose that the physiological role of PrP is in the chemical reduction of endocytosed ferric iron to its ferrous form following transferrin receptor-mediated uptake.

DECLARATION

The University of Manchester

Candidate Name: Simon Mitchell

Faculty: Engineering and Physical Sciences

Thesis Title: A Computational Model of Human Iron Metabolism

I declare that no portion of this work referred to in this thesis has been submitted in support of an application for another degree or qualification of this or any other university or other institute of learning.

COPYRIGHT

ACKNOWLEDGEMENTS

First, I would like to thank my supervisor Professor Pedro Mendes for his support and guidance throughout my studies. Pedro proposed the project, developed the software I used for modelling, and contributed valuably when I had difficulties. I'd like to thank everyone at Virginia Tech, Wake Forest University and the Luxembourg Centre for Systems Biomedicine who made my visits possible; namely, Suzy Torti, Frank Torti, Rudi Balling and Reinhard Laubenbacher. I am grateful to Neena Singh for many discussions and data shared, Anthony West for sharing binding data, and Douglas Kell for the productive discussions. I thank all the members of the Mendes group and all my colleagues in the Manchester Institute of Biotechnology for selflessly assisting me whenever they could and motivating me throughout. This work was funded by the BBSRC and I am thankful for the opportunity to do this research and attend many interesting conferences.

I would like to thank my parents for always being incredibly supportive, patient and inspiring. Finally, I am grateful for my friends who distracted me when required, but also showed genuine interest in my progress which motivated me to do my best work.

CHAPTER

ONE

INTRODUCTION

Iron is an essential element required by virtually all studied organisms from Archaea to man (Aisen et al., 2001). Iron homeostasis is a carefully controlled process which is essential since both iron overload and deficiency cause cell death (Hentze et al., 2004). The challenge of avoiding iron deficiency and overload requires cellular and whole system-scale control mechanisms.

Iron is a transition metal that readily participates in oxidation-reduction reactions between ferric (Fe^{3+}) and ferrous (Fe^{2+}) states (Kell, 2009). This one-electron oxidation-reduction ability not only explains the value of iron but also its toxicity.

Iron is incorporated into a number of essential proteins where it provides electron transfer utility. The mitochondrial electron transport chain requires iron-sulphur clusters. ACO2, an aconitase in the tricarboxylic acid (TCA) cycle, is an iron-sulphur containing protein.

Iron's ability to donate and accept electrons can facilitate dangerous chemistry leading to the harmful over production of free radicals. Therefore free iron must be carefully regulated in order to be adequate for incorporation in essential complexes and yet prevent dangerous radical production. Here I describe some of the key cellular components that regulate iron metabolism to ensure free iron is carefully controlled.

1.1 Cellular Iron Metabolism

Iron metabolism has been widely studied for many years and in recent years a more comprehensive picture of the iron metabolism network is emerging. Some components of iron metabolism are well understood while others remain elusive. Here I present some of the more actively studied elements within the iron metabolic network.

1.1.1 Iron Uptake

Extracellular iron circulates and is transported by plasma protein transferrin (Tf). Transferrin binds two ferric iron molecules. The high affinity of transferrin for iron

(4.7×10^{20} M^{-1} at pH 7.4) leaves iron nonreactive but difficult to extract (Aisen et al., 1978). Transferrin then delivers iron to cells by binding to Tf receptors (TfR1/TfR2) on the cell surface (Richardson and Ponka, 1997). TfR1 is the most comprehensively studied of the transferrin-dependent uptake mechanisms (Cheng et al., 2004).

Transferrin receptor 2 (TfR2) was identified more recently (Kawabata et al., 1999) and was found to be homologous to TfR1. TfR2 binds Tf with much lower affinity than TfR1 and is restricted to a few cell types (Hentze et al., 2004). It has been suggested that the primary role of TfR2 is as an iron sensor rather than an importer as its expression is increased by transferrin (Robb and Wessling-Resnick, 2004). It is also thought that holo-transferrin may facilitate TfR2 recycling; however, this remains poorly understood (Johnson et al., 2007).

Transferrin-dependent iron uptake is well-described (Huebers and Finch, 1987; Ponka et al., 1998). Transferrin-bound iron binds to the Tf receptor and induces receptor-mediated endocytosis. The low pH in the endosome facilitates iron's release from the transferrin receptor. The receptor and holo-transferrin are recycled to the surface while the released iron must be reduced to the ferrous form before it can be exported by divalent metal transporter 1 (DMT1) into the labile iron pool (LIP) within the cell.

There is some evidence for a Tf-independent transport system. While TfR1 knockout is lethal in mice, TfR1 knockout mice show some tissue development, this tissue development suggests some iron uptake mechanism exists (Levy et al., 1999). Humans with low transferrin show iron overload in some tissues despite anaemia (Kaplan, 2002).

Human haemochromatosis protein (HFE) is a protein with which holo-transferrin competes for binding to the transferrin receptors. HFE binds to TfRs (TfR1/TfR2) blocking iron binding and therefore reducing iron uptake (Salter-Cid et al., 1999). It is thought that both TfR2 and HFE alter expression of the iron regulatory hormone hepcidin through bone morphogenetic protein (BMP) and SMAD signalling (Wallace et al., 2009). It has been shown that a complex forms between HFE and TfR2 (D'Alessio et al., 2012) that promotes hepcidin expression. The role of HFE in general iron metabolism is still the subject of much debate (Chorney et al., 2003); however, a consensus on its role is beginning to emerge. Modelling may be able to provide testable predictions of how HFE and TfR2 can function as iron sensors to promote hepcidin expression.

It has been observed that neutrophil gelatinase-associated lipocalin (NGAL) binds to a bacterial chromophore and that this contains an iron atom. Bacterial infections require free iron and the body lowers labile iron in response to infections. Worsening conditions have been observed in patients with bacterial infection given iron supplements (Weinberg, 1984). Bacteria in a limited iron environment secrete iron chelators (siderophores) (Braun, 1999), which bind iron much more tightly than transferrin. NGAL binds iron with an affinity that can compete with *E. coli* (Goetz et al., 2002) and therefore can function as a bacteriostatic agent. Yang et al. (2002) showed that iron obtained through NGAL was internalised and was able to regulate iron-dependent genes. NGAL is also recycled

similarly to Tf, however NGAL and Tf-dependent iron uptake differ in many ways (Yang et al., 2002).

Direct (transferrin/NGAL-independent) iron absorption has been identified in intestinal epithelial cells through the action of divalent metal transporter 1 (DMT1) (Gunshin et al., 1997). DMT1 is important for transport of iron across membranes as it transports ferrous iron into the labile iron pool from both the plasma membrane and the endosome (Ma et al., 2006b). DMT1 is a ubiquitous protein (Gunshin et al., 1997).

The identification of iron transporter DMT1 in the duodenum led to the discovery of a haem transporter, haem carrier protein 1 (HCP1) on the apical membrane of the duodenum (Shayeghi et al., 2005). However the primary role of HCP1 was questioned when it was discovered that HCP1 transports folate with a greater affinity than it demonstrates for haem (Andrews, 2007). HCP1 is present in many human organs and therefore it may contribute to iron homeostasis in some of these tissues types (Latunde-Dada et al., 2006).

1.1.2 Ferritin

The capacity of iron to be toxic led to it becoming an active area of research and early studies focused on two molecules that were both abundant and easy to isolate: ferritin and transferrin (Andrews, 2008). Ferritin and transferrin protect the body from the damaging effects of ferrous iron by precluding the Fenton chemistry that promotes formation of oxygen radicals. Ferritin was the second of all proteins to be crystalised (Laufberger, 1937).

Ferritin is a predominately cytosolic protein, which stores iron after it enters the cell if it is not needed for immediate use. Ferritin is ubiquitous and is present in almost all organisms. Ferritin storage counters the toxic effects of free iron by storing up to 4500 iron atoms within the protein shell as a chemically less reactive ferrihydrite (Harrison, 1977). Usually twenty-four subunits make up each ferritin protein. Two distinct types of ferritin subunit (heavy - H and light - L) are present in different ratios depending on the tissue-type (Boyd et al., 1985). The predominant subunit in liver and spleen is L, while in heart and kidney the H subunit is more highly expressed (Arosio et al., 1976). The two subunit types are the product of distinct genes and have distinct functions. The H subunits perform a ferroxidase role while L subunits contains a site for nucleation of the mineral core (Levi et al., 1992). Despite the distinct roles of the two subunits both appear involved in the formation of ferroxidase centers. A 1:1 ratio of H and L chains leads to maximal redox activity of recombinant human ferritin (Johnson et al., 1999). It is thought that the ratio of the two subunits adjusts the function of ferritin for the requirements of each organ. Ferritin H subunits convert Fe^{2+} to Fe^{3+} as the iron is internalised. The kinetics of this reaction change between low and high iron-loadings of ferritin (Bou-Abdallah et al., 2005b). The ratio of the two ferritin subunits in each tissue type is not fixed and responds to a wide variety of stimuli including inflammation and infection (Torti and Torti, 2002).

Ferritin is found in serum and this is regularly used as a diagnostic marker however

the source and role of serum ferritin remains unclear. It is thought that serum ferritin is a product of the same gene as L subunit ferritin (Beaumont et al., 1995).

Iron release from ferritin is less well understood than the internalisation process. It has been suggested that degradation of ferritin in the lysosome is the only method of iron release (Kidane et al., 2006). However contradictory research has suggested that iron chelators are able to access iron within ferritin through the eight pores in its shell (Jin et al., 2001). Ferritin pores, while mainly closed (Liu et al., 2003), are thought to allow iron to pass out of the shell in iron deficiency and haemoglobin production (Liu et al., 2007).

Mitochondrial ferritin is distinct from cytosolic ferritin. While it contains a similar subunit structure, 12 of the 24 ferroxidase sites are inoperative (Bou-Abdallah et al., 2005a). The kinetics of mitochondrial ferritin differ as a result of the inoperative sites with an overall lower rate of mineral core formation and a lower change between low iron saturation and high iron saturation kinetics.

1.1.3 Haemosiderin

Iron overload disorders such as haemochromatosis result in iron being deposited in heterogeneous conglomerates known as haemosiderin (Granick, 1946). Formation of haemosiderin is generally associated with high cellular iron levels. Haemosiderin is thought to form as a degradation product of ferritin (Wixom et al., 1980) and contains a mix of partly degraded ferritin and iron as ferrihydrite. The composition of haemosiderin varies between normal individuals, those with haemochromatosis and those with a secondary iron overload as a result of a disorder such as thalassemia (Andrews et al., 1988; St Pierre et al., 1998). The ease at which iron can be mobilised from haemosiderin also varies between primary and secondary iron overload. Iron is generally more easily mobilised from haemosiderin of primary iron overload than from ferritin, but more easily mobilised from ferritin than haemosiderin of secondary iron overload (Andrews et al., 1988; O'Connell et al., 1989).

1.1.4 Haem Biosynthesis

Haem is a compound containing ferrous iron in a porphyrin ring. Haem is best known for its incorporation in the oxygen-transport protein haemoglobin.

Haem biosynthesis is a well studied process as reviewed by Ferreira (1995). Once haem production is complete, haem is transported into the cytoplasm where it can be degraded by haem oxygenase 1 and 2. Haem regulates its own production through delta aminolevulinate synthase (ALAS), which is the catalyst for the first step of haem synthesis (Ferreira and Gong, 1995). ALAS2 is present exclusively in erythroid cells and ALAS1 is present in non-erythroid cells (Bishop, 1990). Haem inhibits the transport of ALAS1 into the cytoplasm and also inhibits ALAS1 at the level of translation (Yamamoto et al.,

1983; Dailey et al., 2005).

Frataxin is a mitochondrial protein the function of which is not fully understood. However, frataxin is known to facilitate iron-sulphur crystal formation through binding to ferrous iron and delivering it to the scaffold protein (ISU) where iron-sulfur crystals are formed (Rötig et al., 1997; Yoon and Cowan, 2003). Mature frataxin is located solely in the mitochondria (Martelli et al., 2007); however, it has been suggested that iron-sulfur clusters can form in the cytoplasm (Tong and Rouault, 2006). Frataxin is also thought to facilitate haem synthesis through the delivery of iron to ferrochelatase (a catalyst in haem production) (Yoon and Cowan, 2004).

Haem biosynthesis regulation differs greatly in erythroid cells when compared to other cell types (Ponka, 1997). Liver and kidney cell haem biosynthesis are similar however overall synthesis rate is slower in the kidney. This may be due to the the larger free haem ratio to overall haem activity in liver (Woods, 1988).

1.1.5 Ferroportin

Ferroportin is the only identified iron exporter (Abboud and Haile, 2000). Ferroportin is expressed in many cell types. Located at the basolateral-membrane of enterocytes, ferroportin controls iron export into the blood. In some cell types, caeruloplasmin (Cp) is required to convert Fe^{2+} into Fe^{3+} for export by ferroportin and transport by transferrin (Harris et al., 1999). In other cell types, hephaestin is the catalyst for the oxidation (Ma et al., 2006b).

Ferroportin is the target of hepcidin, the regulatory hormone for system-wide control of iron metabolism. The effect of changes in hepcidin levels varies depending on the cell type: blocking iron export from the intestine effectively blocks iron import into the body thereby reducing systemic iron levels, whereas blocking iron export from other tissues, such as the liver, may increase their iron stores. Modelling may be able to explain better the effect of system-wide modulations of ferroportin.

1.1.6 Haem Exporters

Ferroportin is the only currently identified iron exporter; however, two haem exporters have been found on the cell surface. Feline leukemia virus C receptor (FLVCR) was shown to export haem after it was first cloned as a feline leukemia virus receptor (Quigley et al., 2004). It has recently been shown *in vivo* that FLVCR is essential for iron homeostasis and performs a haem export role (Keel et al., 2008).

ATP-binding cassette (ABC) transporters are able to transport substrates against a concentration gradient through coupling to ATP hydrolysis. ABCG2 is an ABC transporter that uses this to prevent an excess of haem building up within a cell (Krishnamurthy and Schuetz, 2006). Although ABCG2 is expressed in multiple cell types it is not ubiquitous (Doyle and Ross, 2003).

1.1.7 Human Haemochromatosis Protein

Hereditary haemochromatosis is an iron overload disease which leads to accumulation of iron within organs (Aisen et al., 2001). Human haemochromatosis protein (HFE) was found to be the protein defective in patients with hereditary haemochromatosis, but the role of HFE in iron metabolism remained unknown for some time. The first important finding linking HFE with iron metabolism was the discovery that HFE forms a tight complex and co-precipitates with TfR in tissue culture cells (Feder et al., 1998). HFE association with TfR negatively regulates iron uptake by lowering the affinity of transferrin for TfRs approximately 10-fold. HFE expression gives a low ferritin phenotype, which is the result of an increase in iron-responsive element-binding protein (IRP) mRNA binding activity (Corsi et al., 1999). TfR2-HFE binding is still the subject of much debate however HFE binding to TfR2 has been suggested as a mechanism for mammalian iron sensing (Goswami and Andrews, 2006). There are also some recent findings showing that HFE and TfR2 form a complex (D'Alessio et al., 2012). While HFE knockout animals show deficient hepcidin leading to a haemochromatosis phenotype, it appears the liver is still able to sense serum iron levels without HFE (Constante et al., 2006). HFE deficient animals have been shown to have normal hepcidin induction in response to iron changes, but the basal level of hepcidin requires HFE (Constante et al., 2006). Reduced hepcidin levels as a result of loss of HFE leads to the over abundance of ferroportin and the iron overload phenotype of haemochromatosis. The proposed method for HFE-independent hepcidin induction is through TfR2, which has been shown to localise to lipid raft domains and induce MAP kinase (MAPK) signalling (Calzolari et al., 2006). MAPK signalling cross-talks with the bone morphogenetic protein signalling pathway usually associated with hepcidin induction. Specifically, transferrin binding to TfR2 has been shown to induce MAPK signalling, which could allow TfR2 to sense serum iron levels without a requirement for HFE.

1.1.8 Caeruloplasmin

Ferrous iron oxidation in vertebrates is catalyzed by caeruloplasmin (Cp) and hephaestin (Heph) (Osaki et al., 1966; Chen et al., 2004). Caeruloplasmin's significance is demonstrated by the accumulation of iron in various tissues in patients with an inherited Cp deficiency (acaeruloplasminemia). The ferroxidase activity of Cp is supported by radiolabelled iron experiments (Harris et al., 2004). However, this role appears to be limited to release from tissue stores as Cp transcript is not present in intestinal cells and iron absorption is normal in $Cp^{-/-}$ mice (Harris et al., 1999).

Heph is a Cp paralog that is mutated in mice with sex-linked anaemia (SLA)(Vulpe et al., 1999). Heph is proposed to be responsible for basolateral iron transport from enterocytes with ferroportin (Chen et al., 2003). Although Cp and Heph appear to have different roles as they are located in different cell types, the mild phenotype when either

is deleted suggests at least a partial compensatory role of each for the other (Hahn et al., 2004).

1.1.9 Ferrireductase

Dietary iron is predominantly in ferric form (Fe^{3+}) and must first be reduced before it can be transported across the brush border membrane. Several yeast ferrireductase genes were identified before a mammalian candidate was found (Dancis et al., 1990, 1992). A candidate mammalian ferric reductase was identified (McKie et al., 2001) and duodenal cytochrome B (Dcytb) has been widely accepted as the mammalian ferric reductase. However, this was challenged when Dcytb knockout mice were generated and it was shown that Dcytb was not necessary for iron absorption (Gunshin et al., 2005). Following this, Steap3 was identified as the major erythroid ferrireductase (Ohgami et al., 2005). Further research questioned the finding that Dcytb was not required for iron metabolism (McKie, 2008), and investigations with knockout mice using radiolabelled iron demonstrated that Dcytb does affect iron absorption.

It is likely that Dcytb is the predominant mammalian ferrireductase. However, due to observations that knockout mice do not exhibit severe iron deficiency it is likely that other mechanisms for ferric iron reduction can substitute this role. Steap3 is a good candidate for this substitution.

Iron must also be reduced following endocytosis of the transferrin receptor complex, so that it can be exported out of the endosome by DMT1 (Section 1.1.1). Iron is released from transferrin due to the low endosomal pH. DMT1 exports iron out of the endosome, but it can only translate ferrous iron. Which reductase is responsible for endosomal reduction still remains to be confirmed; however, Steap3 appears a good candidate.

1.1.10 Hypoxia Sensing

The iron metabolism network and hypoxia-sensing pathways are closely linked. Hypoxia induces an increased rate of erythropoiesis, which is a major iron sink. Increased erythropoiesis in hypoxia is driven by the hypoxia-inducible factors (HIF1 and HIF2) (Semenza, 2009). HIFs consist of α and β subunits both of which are widely expressed. Degradation of the α subunit is highly sensitive to hypoxia (Huang et al., 1996; Powell, 2003). In normoxia, HIF is degraded rapidly; however, in hypoxia, HIF rapidly accumulates and induces a wide array of gene expression. Prolyl hydroxylase domains (PHDs), the most abundant of which is PHD2, control the degradation of HIFα in an oxygen-dependent manner. PHDs form a complex including iron and oxygen that hydroxylates HIFα leading to its binding to a von Hippel Lindau (VHL) ubiquitin ligase complex and subsequent proteosomal degradation (Ivan et al., 2001). As iron is a necessary co-factor in the post-translational modification of HIFα, the hypoxia-sensing pathway will also respond to perturbations in iron (Peyssonnaux et al., 2008). Both low iron and low tissue

oxygen cause an HIF increase leading to activation of a number of genes and increased erythropoiesis. The HIF heterodimer, made of both the α and β subunits, induces transcription of its target genes by binding directly to hypoxia response elements (HREs). This is analogous to the IRE/IRP binding system for iron metabolism (Section 1.1.11).

Iron is not only able to regulate and be regulated by hypoxia-sensing through erythropoiesis, but also more directly. A number of iron-related genes contain HREs. TfR contains an HRE and is up-regulated in hypoxia to accommodate the extra iron requirement for erythropoiesis (Lok and Ponka, 1999). Caeruloplasmin, which is required for oxidising iron prior to binding to transferrin, is induced by HIF1 thereby ensuring iron is available to various tissues (Mukhopadhyay et al., 2000). Haem iron availability is also increased in hypoxia by induction of haem oxygenase (Lee et al., 1997). The distinct roles of HIF1 and 2 are still poorly understood, however HIF2 is known to target uniquely a number of iron-related genes. HIF2 increases iron absorption from the diet by regulating transcription of DMT1. Up-regulation of DMT1 in hypoxia is essential to provide the increased iron required for erythropoiesis. The complex cross-talk between the iron metabolism and hypoxia-sensing networks is further complicated by the discovery of an iron-responsive element in the 5' untranslated region of HIF2α (Sanchez et al., 2007).

Overall, this presents a comprehensive response to hypoxia in the iron metabolism network, which aims to increase available iron and iron uptake into tissues that require it for erythropoiesis. The increased iron requirement in erythropoiesis has been used to treat anaemia more effectively by reducing required erythropoietin (EPO) doses through iron supplementation (Macdougall et al., 1996). Computational modelling may be able to provide insight into the interaction of the iron metabolism and hypoxia networks.

1.1.11 Cellular Regulation

Coordinated regulation of the uptake, storage and export proteins is required to maintain the careful balance between the damaging effects of iron overload and iron deficiency. This is achieved essentially through post-transcriptional regulation. Untranslated mRNAs that encode proteins involved in iron metabolism contain iron responsive elements (IREs) (Hentze and Kühn, 1996). IREs are a conserved stem-loop structure that can regulate iron metabolism through the binding of iron-responsive element-binding proteins (IRPs).

IRPs perform a different regulatory role depending on the location of the IRE to which they bind. IRE/IRP binding in the 5' untranslated region (UTR) of mRNAs inhibit translation (Muckenthaler et al., 1998). The 5' UTR contains an IRE in the mRNA encoding ferritin (Hentze et al., 2004) and ferroportin (Hentze and Kühn, 1996). If the location of the IRE is in the 3' UTR of the mRNA then IRE/IRP binding stabilises the mRNA. The 3' UTR contains an IRE in the mRNA encoding DMT1 (Hubert and Hentze, 2002). Multiple IRE sites can exist within a single region to provide finer controlled regulation (Hentze and Kühn, 1996).

Transcriptional regulation has also been reported for iron-related proteins including

TNF-α and interleukin-6, which stimulate ferritin expression and reduce TfR1 expression (Torti and Torti, 2002). Cytokines induce a change in iron metabolism; DMT1 is induced while ferroportin is inhibited by interferon-γ (IFN-γ) (Ludwiczek et al., 2003).

Pantopoulos et al. (1995) inhibited protein synthesis in murine fibroblasts and found the half-life of IRP-1 to be about 12 hours. It was also found that iron perturbations do not affect this half-life, which is in contrast to previous studies (Tang et al., 1992). IRPs do not respond to iron-perturbations through altered degradation. The total number of IRP-1 molecules (active and non-active) in a mouse fibroblast and human rhabdomyosarcoma cell line is normally within the range 50000-100000 (Müllner et al., 1989; Haile et al., 1989a; Hentze and Kühn, 1996).

1.2 Systemic Iron Metabolism

Iron homeostasis requires delicate control of many iron-related proteins. Cells that are responsible for iron uptake must "communicate" with cells that require iron to ensure systemic iron conditions are optimal. Iron is taken up through a tightly controlled pathway in intestinal cells; however, unlike copper which can be excreted through the biliary route, the iron metabolism network has no excretory pathway (Hentze et al., 2004). This means iron overload cannot be compensated for by the body excreting iron. Instead, iron uptake must be carefully controlled to ensure adequate but not excessive uptake for the body's requirements.

The method of systemic iron regulation has been the topic of much debate. The accepted model until recently was that immature crypt cells were programmed to balance iron absorption correctly (as reviewed by Frazer and Anderson (2003)). This view is based on the lag time before iron absorption responds to stimuli (several days) corresponding with the time for immature crypt cells to mature and migrate to the villus (Wessling-Resnick, 2006).

The discovery of hepcidin as an iron regulatory hormone challenged the crypt cell maturation model (Krause et al., 2000). Synthesis of hepcidin mainly takes place in the liver (Park et al., 2001). Time is required to alter hepcidin expression levels and this delay corresponds to the lag period observed before a response to stimuli is seen (Frazer et al., 2004). Changes in absorption occur rapidly after circulating hepcidin levels are increased, the lag period is a consequence of the time required to alter hepcidin expression levels.

The hepcidin receptor remained elusive for some time following the discovery of hepcidin. However it has recently been shown that hepcidin binds to ferroportin and induces its internalisation and subsequent degradation within the lysosomes (Nemeth et al., 2004b).

Constitutive expression of hepcidin in mice leads to iron deficiency (Nicolas et al., 2002a). Hepcidin responds to stimuli with increased expression in the event of iron overload and decreased response in the event of iron deficiency (Nicolas et al., 2002b; Pi-

geon et al., 2001). Hepcidin expression is regulated by the bone morphogenetic protein BMP/SMAD signal transduction pathway (Babitt et al., 2006). Inactivation of SMAD4 leads to a similar iron overload phenotype to hepcidin knockout (Wang et al., 2005). Expression of hepcidin is increased by treatment with BMPs (Babitt et al., 2006). There is cross-talk with inflammatory cytokines including interleukin-6 (IL-6), which induce hepcidin transcription in hepatocytes (Nemeth et al., 2004a). This is a result of binding of the signal transducer and activator of transcription 3 (STAT3) regulatory element to the hepcidin promoter (Wrighting and Andrews, 2006). There is also evidence that when transferrin binds to TfR2 the ERK1/2 and p38 MAP kinase pathways are activated leading to hepcidin expression (Calzolari et al., 2006).

1.3 Iron-sulphur Clusters

Iron-sulphur (Fe-S) clusters are present in active sites of many enzymes. Fe-S clusters are evolutionarily conserved across all domains of life and thus seem to be essential. Fe-S proteins have utility for electron transfer, enzymatic reaction catalysis and regulatory roles. Mitochondrial complex I and II both contain iron-sulphur clusters essential for their role in oxidative phosphorylation. Iron metabolism and Fe-S biogenesis are closely linked. The iron response proteins (IRPs) are Fe-S cluster-containing proteins and Fe-S clusters are sensitive to oxidative stress (Bouton and Drapier, 2003). Defects in Fe-S cluster synthesis lead to dangerous mitochondrial iron overload. Mitochondrial iron overload as a result of abnormal Fe-S protein biogenesis is found in patients with Friedreich's ataxia (Puccio and Kœnig, 2000). A number of related diseases including ISCU myopathy and sideroblastic anaemia are caused by reduced Fe-S cluster biogenesis leading to mitochondrial iron overload.

1.4 Iron Disease

1.4.1 Haemochromatosis

As previously mentioned (Section 1.2), iron metabolism has no direct excretory mechanism and as a result excess iron is not lost except by losing iron-containing cells, for example through bleeding or intestinal shedding. Hereditary haemochromatosis is an iron overload disorder, resulting from excess iron uptake, which cannot be compensated for due to the bodies inability to discard excess iron. It is the most common genetic disorder in Caucasian populations, affecting around 1 in 200 Europeans (Olsson et al., 1983). Haemochromatosis is characterised as a progressive parenchymal iron overload which has a potential for multi-organ damage and disease. Haemochromatosis initially leads to an increase in transferrin saturation as a result of massive influx of iron from enterocytes. Macrophages also release more than normal levels of iron (Camaschella et al., 2000).

Pathogenic mutation in the HFE gene was discovered to be present in the majority of hereditary haemochromatosis patients (Feder et al., 1996). However this was complicated when mutations in other iron-related genes were found to lead to the same phenotype as haemochromatosis. Hepcidin (Roetto et al., 2003), TfR2 (Camaschella et al., 2000), ferroportin (Montosi et al., 2001) and haemojuvelin (Papanikolaou et al., 2003) perturbations have all been attributed to various haemochromatosis types. HFE mutations lead to type 1 hereditary haemochromatosis (HH) which causes liver fibrosis and diabetes; Type 1 HH is the most common form of HH. Mutations in the gene for haemojuvelin (HJV) lead to type 2 (juvenile) haemochromatosis and this is often fatal. TfR2 mutations lead to type 3 HH and mutations in ferroportin cause type 4.

Recent findings suggest that the multiple haemochromatosis types with similar phenotype may be a result of HFE, TFR2 and HJV all being regulators of hepcidin in the liver, as haemochromatosis in all mutations is characterised by inadequate hepcidin synthesis (Gehrke et al., 2003). Mutations in the ferroportin gene cause the transporter to be insensitive to hepcidin regulation, which can lead to haemochromatosis.

1.4.2 Iron-deficiency Anaemia

Iron deficiency is more common than the iron overload associated with haemochromatosis. Iron-deficiency anaemia may be the most common nutritional defect worldwide (Clark, 2008) with over 30% of the world's population suffering from some form of anaemia (Benoist et al., 2008). Anemia is commonly caused by caused by inadequate iron uptake, bleeding and Inflammation (Clark, 2008). It has been shown that iron-deficiency anaemia can be caused without significant bleeding by infection with *H pylori* (Marignani et al., 1997).

Genetic defects in iron-related genes can also cause iron-deficiency anaemia. A mutation in the gene encoding DMT1 has been shown to cause genetic microcytic anaemia (Mims et al., 2005).

Hypotransferrinemia is an extremely rare disorder resulting from mutations in the gene encoding transferrin. Hypotransferrinemia is characterised as very low transferrin levels in the plasma. Iron delivery is interrupted and a futile increase in intestinal iron absorption leads to tissue iron deposition (Trenor et al., 2000). Incorrect levels of caeruloplasmin can also cause mild iron-deficiency anaemia (Harris et al., 1995). *Mask* mice have demonstrated iron deficiency anaemia which is attributed to elevated hepcidin expression (Andrews, 2008).

Anaemia is common in intensive care units (ICUs) due to a combination of repeated blood sampling, underlying injuries and infections. Ninety-seven per cent of patients in ICU are anaemic after their first week (Hayden et al., 2012). The risk presented by this anaemia is somewhat unknown as much of it can be attributed to the potential protective affects of the "anaemia of inflammation". The aim of this anaemia may be to reduce iron availability for invading micro-organisms. However there is a strong correlation between

severity of anaemia and poor patient outcome (Mehdi and Toto, 2009; Salisbury et al., 2010; Go et al., 2006).

1.4.3 Malaria and Anaemia

Malaria, while not a disorder of iron metabolism, has been shown to be highly dependent on iron regulatory processes. In areas where malaria is most prevalent there is also a high prevalence of anaemia. Trials that preventatively treat anaemia in these areas have proved contentious as malaria infection rates increase with iron supplementation (Oppenheimer et al., 1986). Malaria preferentially infects iron replete red blood cells and increased hepcidin expression following an initial malaria infection confers protection against a second infection. If we could better understand iron metabolism to ensure free iron is minimised without inducing anaemia we may be able to treat both malaria and anaemia more effectively.

1.4.4 Neurodegenerative Disorders

Neurodegenerative disorders are among the most highly studied diseases associated with iron metabolism. Unusually high levels of iron accumulation in various regions of the brain has emerged as a common finding in neurodegenerative disorders including: Parkinson's disease (Youdim et al., 1993), Alzheimer's disease (Gooman, 1953), Huntington's disease (Bartzokis et al., 2007a), and normal age-related neuronal degeneration (Bartzokis et al., 1994). With improvements in magnetic resonance imaging it has become increasingly possible to characterise the altered localisation of iron in neurodegeneration (Collingwood and Dobson, 2006). While many neurodegenerative disorders have been found to share misregulated iron metabolism, they have distinct phenotypes. The variety of neurodegenerative phenotypes may be attributed to the specific causative alterations leading to iron accumulation in distinct cell-types or sub-cellular locations in each disorder. If the destination of poorly liganded iron can be identified in each neurodegenerative disorder, then iron chelation and anti-oxident therapeutics may be effective treatements for a wide variety of highly prevelant neurodegenerative disorders (Kell, 2010).

1.5 Tissue Specificity

Iron metabolism is not an identical process in all cell types. Differences have been shown in gene expressions between different tissues and cell types (Polonifi et al., 2010). pH has been shown to greatly affect the kinetics of iron-related reactions and endosomal pH varies with cell type, ranging from 6 to 5.5 and occasionally as low as 4.3 (Mellman et al., 1986; Lee et al., 1996). Based on data from the literature, Hower et al. (2009) created multiple iron metabolism networks that showed the specific iron metabolism factors present in different tissue types.

1.5.1 Hepatocytes

Hepatocytes are key regulators of iron metabolism. The liver is a site of major iron storage which leads to liver damage in iron overload disorders and hepcidin is predominantly expressed in the liver (Park et al., 2001). For the correct regulation of hepcidin, which is released into the serum to regulate whole body iron metabolism, hepatocytes must be accurate sensors of serum iron levels. TfR2 is highly expressed in hepatic tissue and is thought to facilitate the iron-sensing role of hepatocytes. HFE is also more highly expressed in hepatocytes and is thought to assist with TfR2 in an iron-sensing/signalling role.

1.5.2 Enterocytes

Intestinal absorptive cells (enterocytes) differ from many other cell types as they are responsible for uptake of iron directly from the diet. Iron in the diet is not bound to transferrin and therefore cannot be taken up through the action of transferrin receptors. Transferrin receptor 1 is still expressed in enterocytes where it appears to play a role outside iron uptake in maintaining the structural integrity of the enterocyte. Enterocytes do not express hepcidin but are one of the major sites of hepcidin-targeted regulation. As hepcidin induces the degradation of enterocyte ferroportin, it has the potential to block the only route of iron uptake from the diet into the body. Controlling enterocyte iron uptake either locally or through the action of hepcidin is key to understanding and treating iron-related disorders. Enterocytes take up non-haem iron (iron not derived from haemoglobin or myoglobin in animal protein sources) through the action of divalent metal transporter 1 (Gunshin et al., 1997); the mechanism and kinetics of this process differ from transferrin receptor-mediated endocytosis found in cell types that import transferrin-bound iron from serum. Enterocytes are polarised meaning they take up iron from the brush border and export iron through the basolateral membrane into the serum. This polarised structure provides a one-way route for iron taken up from the diet with no possibility of iron returning to the gut lumen once it has been exported by ferroportin into the serum. This one-way route for iron, and the lack of an iron export pathway in general, leads to conditions of iron overload when iron is misregulated.

1.5.3 Reticulocyte

Reticulocytes are immature red blood cells, which still have both mitochondria and ribosomes. In their mature form, red blood cells contain haemoglobin. Haemoglobin A (HbA), the primary haemoglobin type in adults, is composed of 2 peptide globin chains. Regulation of HbA is by haem-regulated eIF2a kinase (HRI). Once activated, HRI phosphorylates eIF2a, which inhibits globin synthesis. Haem binds to HRI and deactivates it when haem levels are high. Haem detaches from HRI in haem deficiency leading to activation (Han et al., 2001). An alternative haemoglobin regulator, α haemoglobin-stabilizing

protein (AHSP), stabilises aHb and promotes haemoglobin synthesis (Yu et al., 2007).

Reticulocytes take up iron through the standard Tf-TfR pathway, but ferritin receptors also exist on the cell-surface, which provide an alternative iron uptake mechanism (Meyron-Holtz et al., 1994). Following internalisation through ferritin receptors, ferritin is degraded in the lysosome, which releases iron into the labile iron pool (Vaisman et al., 1997; Leimberg et al., 2008).

Regulatory differences in the erythroid-specific form of ALAS (i.e. ALAS2) mean it is unaffected by haem (Ponka, 1999). An IRE in the 5'UTR is present only in ALAS2 (Bhasker et al., 1993).

The action of DMT1 differs in reticulocytes. Although DMT1 is not known to play an iron import role in reticulocytes, and a non-IRE form is most prevalent, there is mRNA evidence of the presence of the IRE-containing form (Kato et al., 2007).

1.5.4 Macrophage

The main role of the macrophage in iron metabolism is iron recycling from haemoglobin back into circulation. Most of the iron in circulation is a result of recycling existing iron as opposed to new iron uptake. The majority of this iron is recovered from senescent erythrocytes (Alberts et al., 2007). Phagocytosis of senescent erythroid cells begins in the binding of cell-surface receptors to the senescent red blood cells. The red blood cell is then absorbed by the activated receptor in the phagosome which in turn fuses with the lysosome. The red blood cell and haemoglobin are then degraded by hydrolytic enzymes which leave them haem free. Recycled iron is then transported out of the phagosome by Nramp1 (Soe-Lin et al., 2008).

Recycling of haemoglobin can also begin with cluster of differentiation 163 (CD163) mediated endocytosis of haptoglobin:haemoglobin (Hp-Hb) complexes (Fabriek et al., 2005). CD163 exists on the cell surface of macrophages and is a member of a family of scavenger receptor cystine-rich (SRCR) receptors. Once Hp-Hb is internalised into the lysosome, haem is released and degraded by haem oxygenases (Madsen et al., 2001). CD163 is also known to detach from the plasma membrane; however, the function of free soluble CD163 remains unknown (Droste et al., 1999).

1.6 Existing Models

1.6.1 General Systems Biology Modelling

Molecular biology approaches have been used to study the steps of iron metabolism in detail, revealing facts such as protein properties and genome sequences. However, the fundamental principle of systems biology is that knowledge of the parts of a network does not lead to complete understanding without knowledge of the interaction dynamics. Cells, tissues, organs, organisms and ecological systems are constructed of components

with interactions that have been defined by evolution (Kitano, 2002). Understanding these interactions is key to understanding the emergent behaviour and developing treatments for iron metabolism related disorders. Developing tools to integrate the large amounts of highly varied data (gene expression, proteomic, metabolomic) is a central goal of systems biology.

A consistent target of systems biology is to develop an *in silico* model of a full organism. Constructing a comprehensive model of iron metabolism contributes not only to understanding of iron metabolism, but also towards the completeness of a full virtual human.

The biological complexity of a network's interactions can rise exponentially with the scale of the system. Each extra component in the system can add multiple interactions, which can change the systems behaviour. If a system is large, there is a risk that too few interactions are understood and quantified. Therefore, it is important that a system of an appropriate scale is chosen for study. Iron metabolism is a system of multiple components interacting in a complex network as shown in the map constructed by Hower et al. (2009), and therefore is a suitable candidate for systems biology modelling provided the scale of the system is appropriate. The general map of iron metabolism (Hower et al., 2009) contains 107 reactions and transport steps. However, some of these are small steps that may have trivial kinetics, or there may be multiple-stage processes that can be approximated to a simple process. Many of the subcellular localisation steps may not be required for an initial model of iron metabolism. The kinetic data from the literature provides information relevant to modelling the main, central interactions at the core of the network. Therefore, a cellular-scale mechanistic model of human iron metabolism is achievable and that this could potentially be extended to include multiple cell types responsible for regulation and iron absorption.

1.6.2 Hypoxia Modelling

Qutub and Popel (2006) constructed a computational model of oxygen sensing and hypoxia response. The mechanistic ordinary differential equation model included kinetics derived from the literature and some parameter estimation. The model included iron, ascorbate, oxygen, 2-oxoglutarate, PHD and HIF1. The modelling was performed in MATLAB (MATLAB, 2010). However, the kinetics used were not clearly described by the authors. The methods describe the catalytic rate (k_{cat}) being set to zero for fast reactions, whereas a zero k_{cat} would actually model a stopped reaction with zero flux. To attempt to gain a better understanding of the modelling methods, a MATLAB file was obtained through correspondence with the authors. This file confirmed the modelling decisions to set k_{cat} values to zero. In the following sample from the code obtained the final component of dy(7) and dy(9) both evaluate to zero and therefore have no effect on any kinetics.

```
%Compound y(7) = PD2-Fe2-DG-O2
```

```
%Compound y(8) = AS, ascorbate
%Compound y(9) = PD2-Fe2-DG-O2-AS
kcatAS=0;
kcatO2=0;
dy(7) = k1O2*y(5)*y(6)-k_1O2*y(7)-kcatO2*y(7);
dy(8) = k_1AS*y(9)-k1AS*y(7)*y(8)-kASFe*y(13)*y(6)*(y(15))^2*y(8);
dy(9) = k1AS*y(7)*y(8)-k_1AS*y(9)-kcatAS*y(9);
```

Furthermore, species 9, which is a complex of 7 and 8, appears to consume only species 8 in its production. Species 7 contains no term dependent on the production rate of species 9 and therefore does not obey mass conservation.

The authors found that the response to hypoxia could vary greatly in magnitude and dynamics depending on the molecular environment. Iron and ascorbate were found to be the metabolites that limited the response in various conditions. Ascorbate had the highest effect on hypoxia response when iron was low. The result of HIF1 regulation, including the feedback into the iron metabolism network, was not considered.

If this modelling work is to be incorporated into a larger model of iron metabolism, then care should be taken to describe accurately the biochemical processes when expressing them in computational code. The paper's (Qutub and Popel, 2006) parameters and proposed complex formation reactions could guide the construction of a new model.

1.6.3 Existing Iron Metabolism Models

As the importance of iron and its distribution in the body became apparent a number of attempts to create mathematical models of iron metabolism have been made. A number of different modelling techniques have been applied to iron metabolism and the scope of models has varied from whole body to single cell.

Some existing studies of iron metabolism have focused on a compartmental approach, which have led to comprehensive physiological models of iron distribution over time. These are not mechanistic models, they are instead physiological and concerned with recreating the phenotype of iron metabolism, but are important in construction and verification of a multiscale model. Compartmental models are the initial stages of a top-down systems model and molecular models are the initial stage of a bottom-up systems modelling approach.

Early modelling by Berzuini et al. (1978) constructed a compartmental model of iron metabolism (Figure 1.1a). Parameters were estimated using radiation based techniques and an optimisation algorithm. The erythropoietic and storage circuit were considered separately and then the interaction between the two was modelled, which demonstrates, in a minimal way, the multiscale modelling approach required to investigate iron metabolism. Computing limitations inhibited the accuracy of variable estimations and many experimental parameters that are currently available were not available when the model was constructed. This model was extended by Franzone et al. (1982) (Figure 1.1b).

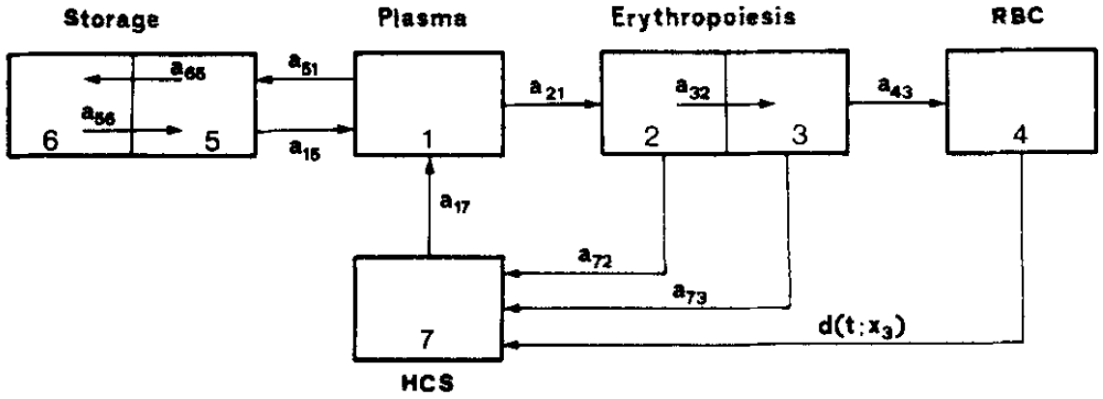

(a) Minimal Compartmental Iron Metabolism Model (Berzuini et al., 1978) (Reproduced with permission). RBC: Red Blood Cells, HCS: Haemoglobin Catabolic System.

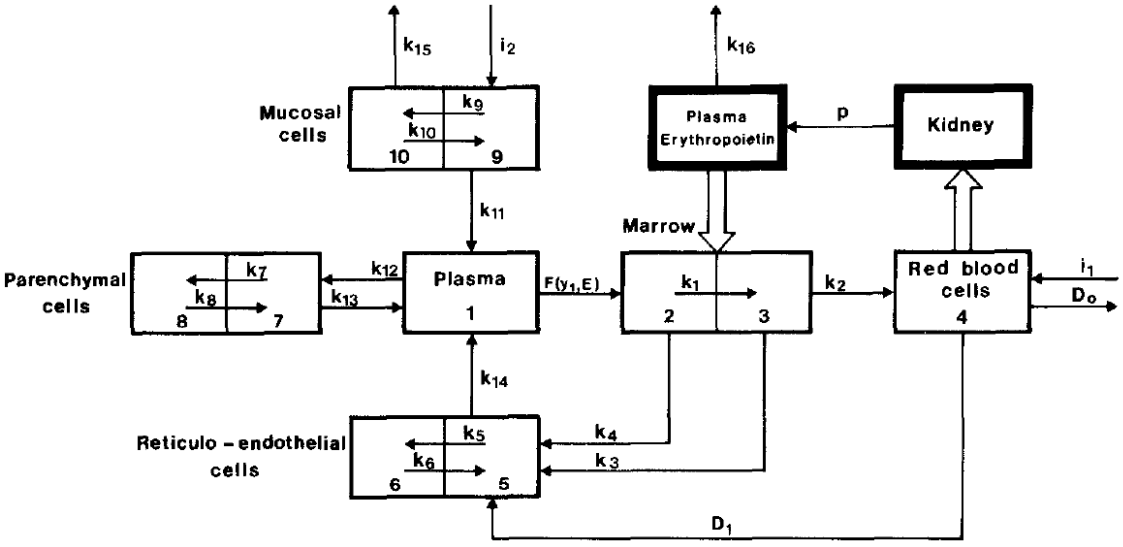

(b) Compartmental Iron Metabolism Model (Franzone et al., 1982) (Reproduced with permission). Thin contour blocks represent iron pools while heavy contour blocks the control mechanism. Thin arrows represent material flows (iron or erythropoietin) while large arrows the input-output signals of the control mechanism.

Figure 1.1: **Compartmental models of iron metabolism and intercellular levels of iron using radiation based ferrokinetic data.**

The model of Franzone et al. (1982) was verified by experimental data and provided reasonably accurate predictions of iron content in various iron pools. This work focused on modelling the effects of therapeutic treatment; events such as blood donation and therapeutic treatments of erythroid disorders were simulated and verified. The numerical accuracy and length of simulation was limited by computational power available at the time.

Recent work (Lopes et al., 2010) used similar radiation tracing to calculate steady-state fluxes and iron distribution between different organs. Three different dietary iron levels were studied. This work focused on modelling the effects of dietary changes. The model produced was a more accurate and complete model in part due to the increased computational power available. Although the ferrokinetic data were collected from mouse experiments the findings should be scalable to human models.

Early, small scale intra-cellular, molecular models were minimal. A model con-

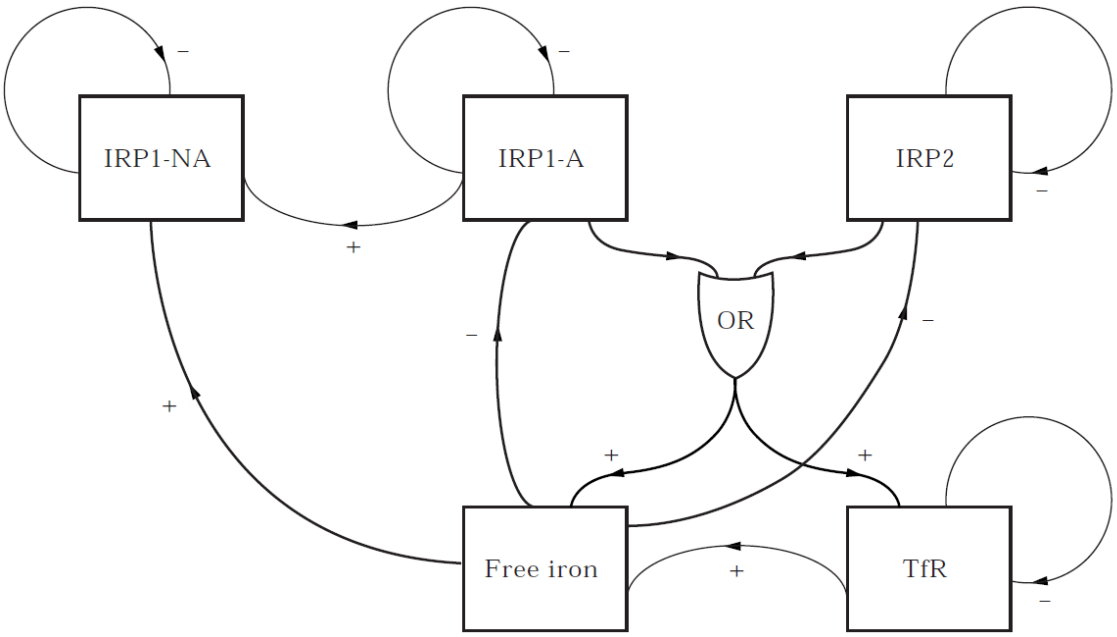

Figure 1.2: **Minimal Intra-cellular Iron Metabolism Model (Omholt, 1998) (Reproduced with permission).** The feedback-loop structure of the iron regulatory system used for constructing the model. IRP1-NA and IRP1-A are the non-IRE binding and the IRE-binding version of iron regulatory protein 1 respectively. Ferritin and eALAS (erythroid 5-aminolaevulinate synthase) are not included as state variables of the model, but their interactions are incorporated by indirect means. Thick lines refer to sigmoidal regulation, while thin lines refer to proportional regulation (ordinary decay).

structed by Omholt (1998) (Figure 1.2) contains only negative feedback. It has 5 metabolites with an 'OR' switching mechanism. Many of the kinetic constants were estimated from half-life values and therefore may not be as accurate as affinity kinetics.

A recent model (Salgado et al., 2010) of ferritin iron storage dynamics provided a detailed mechanistic model that matched experimental data well. The conventional storage role for ferritin was questioned in favour of a role as a 3-stage iron buffer that protects the cell from fluctuations in available iron. The model was constructed using Michaelis Menten-like kinetics with kinetic constants approximated from the literature. This produced a model that matched the observed data well; however, some potentially inaccurate assumptions were made, which would require further validation before incorporation into a larger model of iron metabolism. Diffusional phenomena were ignored and a perfectly mixed system was assumed. An analysis identified a rate-limiting step, but this view has been shown to be incorrect and should be replaced with the idea of distributed control in future analysis (Westerhoff et al., 2009).

Recently, a core model of cellular iron metabolism was published by Chifman et al. (2012). The model consisted of 5 ordinary differential equations representing the LIP, ferritin, IRP, ferroportin and TfR1 (Figure 1.3a). It is a strictly qualitative model and makes no attempts to use experimental or fitted parameters. The model is of breast epithelial tissue and therefore considered hepcidin to be a fixed external signal to the cellular system with which they were concerned. The model was validated by its ability to recreate the

single result that ferroportin and ferritin show an inverse correlation in both the simulation and breast epithelial cell lines. However, this result is intrinsically constructed into the model, as up-regulation of either ferroportin or ferritin leads to a decrease in LIP and subsequent increase in IRP, which regulates the other factor in an inverse manner. Therefore, further validation should be performed with data other than those used to construct the model.

Chifman et al. (2012) argued that, due to having 15 undetermined numerical parameters, parameter estimation was not feasible for the iron metabolism network. Instead, through a combination of analytical techniques and sampling, they demonstrated that the model properties are inherent in the topology and interactions included, as opposed to the parameters chosen. A more extensive model that includes variable hepcidin will be required to see emergent behaviour and provide utility as a hypothesis-generation tool.

Mobilia et al. (2012) constructed a core model of iron metabolism with similar scope to Chifman et al. (2012), but with the aim of modelling an erythroid cell. The iron metabolism network was chosen as a system to demonstrate a novel approach to parameter-space reduction. Initial parameter upper and lower bounds were assigned from the literature where estimates were found. Where estimates were not found in the literature a broad range of chemically feasible concentrations was permitted. Known behaviour of the iron metabolism network was then used to construct temporal logic formulae (Moszkowski, 1985). Temporal logic formulae encapsulate time-dependent phenomena, such as a metabolite increase leading to a decrease in a second metabolite after some time. These temporal logic formulae were used to restrict further the parameter space through a process of repeatedly sampling parameters and testing the truth of the logical formulae. Regions of parameter space that did not fully meet the logical requirements were excluded. This led to a much reduced parameter space (often by multiple orders of magnitude) in which any set of parameters match known behaviour of the iron metabolism network.

Overall iron metabolism modelling efforts have focused at a cellular scale on the roles of ferritin, IRPs and TfR1. While existing models have confirmed the experimentally observed role for these proteins, due to the limited scope of the mechanistic modelling efforts (i.e. including only a few key proteins), and the limited experimental data incorporated into these models, the predictive power of systems biology approaches remains to be demonstrated. By increasing the modelling scope to include iron-sensing in hepatocytes, hepcidin expression and dietary iron uptake, we should better understand iron disorders. To construct a model with predictive utility, a comprehensive, translational approach to data acquisition (from various experimental techniques and the clinic) should be taken. Care should be taken to consider the potential errors that arise as a result of integrating multiple data sources. However, due to improving experimental techniques it should be possible to construct a more ambitious fully parameterised model of human iron metabolism.

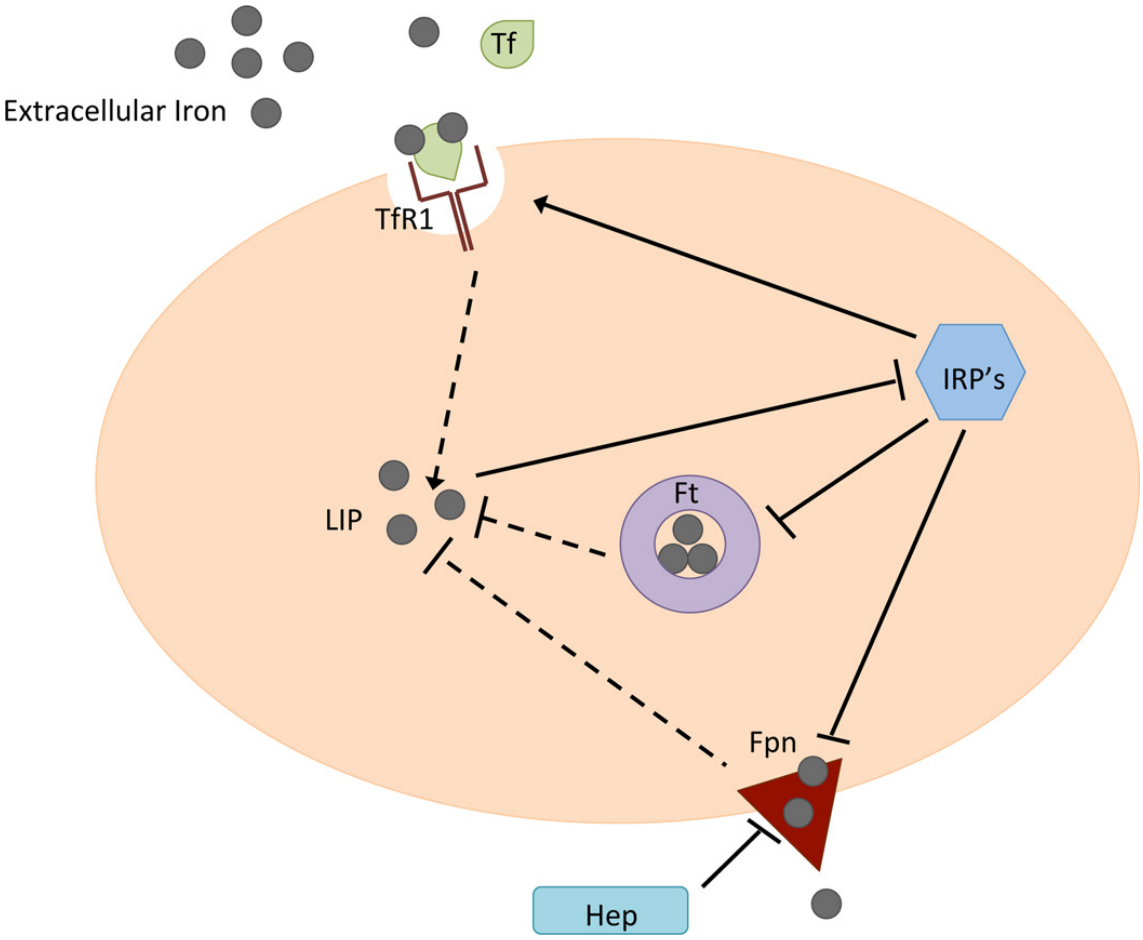

(a) The Chifman et al. (2012) model contains the basic components of cellular iron metabolism (reproduced with permission).

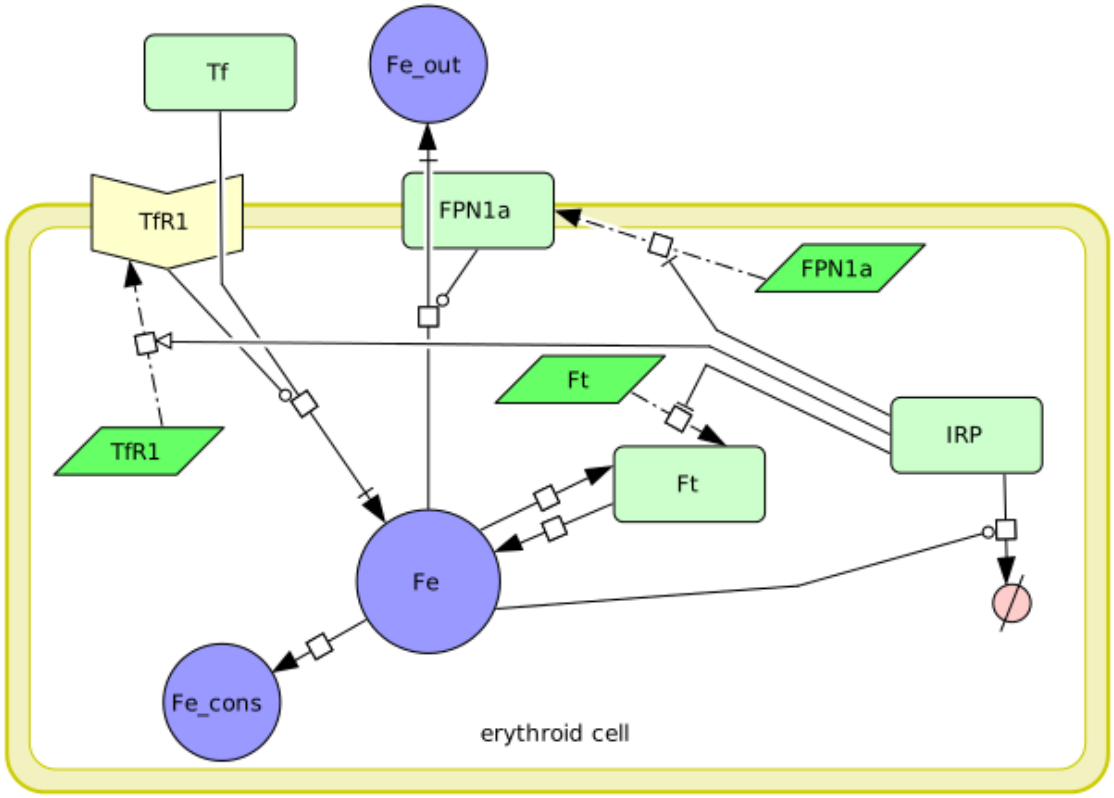

(b) The Mobilia et al. (2012) model covers similar core components.

Figure 1.3: **Core models of iron metabolism contain similar components.**

1.7 Network Inference

One of the fundamental challenges in constructing systems biology models is the network inference from systems level data (Stolovitzky et al., 2007). A number of approaches have been developed to tackle this problem. Statistical modelling approaches such as Bayesian inference and ARACNe provide a measure of correlation between network nodes (Laubenbacher et al., 2009). The ARACNe algorithm (Basso et al., 2005) is based on relevance networks that use information criterion in a pair-wise manner across gene expression profiles to identify possible edges. ARACNe adds further processing to avoid indirect interactions. Bayesian network methods (Friedman et al., 2000) can require more data than are typically available from gene expression experiments (Pe'er et al., 2001). A review of reverse engineering, network inference, methodologies was performed by Camacho et al. (2007). The authors found that methods based on individual gene perturbations, such as the methods of de la Fuente et al. (2002), outperformed methods that used comparatively more data for inference, such as time-series analysis (Yu et al., 2004), or statistical techniques (De La Fuente et al., 2004).

1.7.1 Map of Iron Metabolism

Network inference is at an advanced stage for iron modelling and this is best shown by an iron metabolism map that has been constructed by Hower et al. (2009) with 151 chemical species and 107 reactions and transport steps. Tissue-specific subnetworks were also created for liver, intestinal, macrophage and reticulocyte cells. The chemical species in each tissue-specific subnetwork was determined by assessing the literature for evidence; however, this should be verified before incorporation into a model. The inclusion of some species were based on mRNA evidence, which may be less reliable than some proteomic data now available, for example from the Human Protein Atlas (Berglund et al., 2008). The Human Protein Atlas (Section 2.1.1) can provide an initial verification of the network, specifically in the case where negative expression has been shown for a species previously included in the network based on mRNA evidence.

The addition of kinetic data to the validated network or subnetworks should provide an excellent systems biology model and is the basis for the work presented here.

1.8 Modelling Techniques

1.8.1 Discrete Networks

Discrete networks, the simplest of which are Boolean networks, are a simulation method that are often applied to reverse-engineering gene regulatory networks from expression data. Boolean networks simplify continuous models to become deterministic, where the state of a species at a time-point represents whether it is expressed (1) or has

negative expression (0). Time is also descretised so that a species will only change state when the time-point progresses to the next "tick". Discrete networks are used widely when systems biology networks do not have sufficient high quality data to build detailed quantitative models using ordinary differential equations (ODEs) (Veliz-Cuba et al., 2010). Discrete modelling can also be more accessible to life scientists due to the logical correlation between "activation" and a 1 in the state space. Discrete modelling techniques have many disadvantages including the loss of all concentration information. Discrete models can not perform a time-course showing how concentrations change over a defined time period. An artifact of discrete modelling can be false stable osciliatory behaviour, as the reduced resolution provided can ignore the effect of dampening on damped oscillations tending towards a stable concentration. All findings from ODE models can be recreated using thresholding techniques and therefore ODE models can make the most use of existing data and models for parameterisation and validation.

1.8.2 Petri Nets

Petri nets are an alternative form of discrete modelling that have been successfully applied in a systems biology context (Chaouiya et al., 2008; Grunwald et al., 2008). Petri nets offer the ability to analyse systems from either quantitative or qualitative perspectives. A petri net is a graph theoretic technique in which nodes are transitions and places interconnected by arrows (arcs) showing the direction of flow. Petri nets are discrete as each token in the network can represent a single molecule but can equally represent 1 mol. Tokens move from one place to another when a connecting transition is activated (or fired) as seen in Figure 1.4. Petri net models can be easily constructed since the stoichiometry matrix of a metabolic network corresponds directly with the incidence matrix of a petri net. A general approach to re-write multi-level logical models into petri nets has been defined by Chaouiya et al. (2008). Petri net modelling reduces some of the issues with low resolution discrete modelling. However, petri net modelling still fails to capture the full information available from an ordinary differential equation based model.

1.8.3 Ordinary Differential Equation Based Modelling

Ordinary differential equation (ODE) based models are made up of a differential equation for each metabolite, representing its rate of change. The terms of the differential equations simulate the effect each reaction has on the metabolite which the equation represents. ODE models have been successfully applied to a wide variety of biological systems from human coagulation (Wajima et al., 2009) to phosphorylation in signal transduction cascades (Ortega et al., 2006). ODE models are best used for well characterised systems where kinetic data for the processes are available. Where parameters are not available they can be estimated, but caution must be taken with this process. While skepticism over parameter accuracy is often raised with ODE models, these parameters are what provides

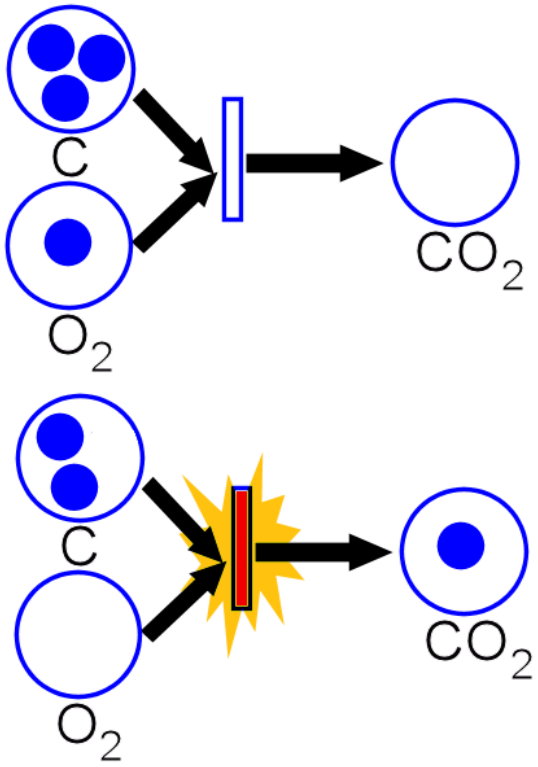

Figure 1.4: **Petri nets - tokens move between places when transitions fire**

the model's quantitative and predictive power. Parameter-free models or less quantitative modelling techniques cannot take full advantage of all available data.

The study presented in this thesis ambitiously aimed to construct an ordinary differential equation based model. This was reevaluated throughout the modelling process to ensure the that this was the correct modelling approach, for the entire system and individual components, given the amount and quality of available data.

1.9 Graph Theory

The scale of the iron metabolism network offers opportunity for mathematical analysis with graph theory techniques. Each species in the network is represented by a node and each interaction is an edge between one node and another. The degree of a node is a measure of the number of edges that begin or end at that node. Node degree can measure the significance of a biochemical species in a network (Han et al., 2004; Fraser et al., 2002). Hower et al. (2009) analysed the map of the iron metabolic network from a graph theory approach and showed that consistently, for all tissue-specific subnetworks, LIP, cytosolic haem and cytosolic reactive oxygen species had the highest degree. Some cellular networks are thought to have scale-free degree distributions (Jeong et al., 2000). This is significant as it differs from random graphs where the node-degrees are closely clustered around the mean degree. In scale-free structures, "hubs" exist that have an unusually high degree and this has biological impact on the robustness of a network to random node failure or attack (Albert et al., 2000). Affecting those hubs with large degrees can alter the

behaviour of a biological network more efficiently than targeting non-hub nodes that can have little effect on the overall behaviour of a system.

Average path length and diameter of biochemical networks are small when compared to the size of the network. A biological network of size n has average path length in the same order of magnitude as $log(n)$ (Jeong et al., 2000; Wagner and Fell, 2001). This property can be thought of as the number of steps a signal must pass through before a species can react and, therefore, the speed at which information can be transmitted through the network.

Clustering analysis of metabolic networks has revealed that, when compared to random networks, the clustering coefficient of the metabolic network is at least an order of magnitude higher (Reed and Palsson, 2003). The clustering coefficient measures how likely the neighbours of a given node are to be themselves linked by an edge. Furthermore, as the degree of a node increases, the clustering coefficient decreases. This may be due to the network structure of metabolic networks being made of different modules linked by high-degree hub nodes.

Centrality measures have been shown to be linked to essentiality of a gene/protein. This could be applied to identify effective drug targets (Jeong et al., 2003). Degree centrality is the same as degree for undirected graphs. However, degree centrality can be either in-degree or out-degree for directed graphs. Closeness centrality is a measure that assumes important nodes will be connected to other nodes with a short path to aid quick communication. It was shown by Wuchty (2003) that the highest centrality scores in *S. cerevisiae* were involved in signal transduction reactions. Betweenness centrality assumes that important nodes lie on a high proportion of paths between other nodes. Joy et al. (2005) measured betweenness centrality for the yeast protein interaction network and found that essential proteins had an 80% higher average betweenness centrality value than non-essential proteins.

By performing further graph theoretic analysis on the map of iron metabolism it will be possible to identify which metabolites are most central. Central nodes identified by graph theory, combined with literature review for metabolites regarded as highly important and well characterised, should point to the starting point for modelling.

1.10 Tools

1.10.1 Systems Biology Mark up Language

A standard approach to modelling complex biological networks is a deterministic strategy through integration of ordinary differential equations (ODEs). To facilitate sharing and collaboration of modelling work, a number of tools and standards have been developed. The Systems Biology Mark up Language (SBML) (Hucka et al., 2003) is an open source file format based on eXtensible Markup Language (XML) and is used for representing biochemical reaction networks. SBML offers a number of different specification

levels with varying features: Level 1 provides the most simple and widely supported implementation; Level 2 adds a number of features (Le Novère et al., 2008); and Level 3 (the latest implementation) provides the most comprehensive set of features (Hucka et al., 2010). Through these multiple levels, SBML is able to represent many biological systems which can then be simulated in a number of different ways (ODEs, stochastic, petri nets etc) using various software tools (Sections 1.10.4-1.10.7). CellML (Lloyd et al., 2004) offers similar functionality to SBML, and is an alternative, although SBML has wider support and compatibility than CellML and has been more widely accepted. COPASI (Section 1.10.4) can import and export SBML.

Both experimental data and systems models have adopted data standards. However, until recently there were no standards to associate models with modelling data. Systems Biology Results Markup Language (SBRML) was created for this purpose (Dada et al., 2010). Like SBML, SBRML is an XML-based language, but SBRML links datasets with their associated parameters in a computational model.

1.10.2 Systems Biology Graphical Notation

The analogy between electrical circuits and biological circuits is often used when explaining the methodology of systems biology. In neither field can a knowledge of the network's components in isolation lead to an understanding of the network without knowledge of the interactions. Systems Biology Graphical Notation (SBGN) (Novere et al., 2009) is to systems biology what circuit diagrams are to electrical engineering. SBGN is a visual language that was developed to represent biochemical networks in a standard unambiguous way. SBGN consists of three diagram types. The SBGN process diagrams are used to represent processes that change the location, state or convert a physical entity into another, and therefore are most relevant here. These diagrams can be created in CellDesigner (Section 1.10.7).

1.10.3 Stochastic and Deterministic Simulations

A deterministic systems biology model is usually made up of a system of ordinary differential equations. These equations are solved using numerical or analytical methods. Stochastic simulations differ from deterministic approaches due to the evolution of the stochastic system being unpredictable from the initial conditions and parameters. A large, repeated stochastic simulation where the results are averaged may reveal what appears to be deterministic results; however, simulations with a small sample size will demonstrate stochastic effects. An identical stochastic system run twice can reveal very different results.

Biological systems are inherently noisy and stochastic models include simulation of this effect. From gene expression (Raj and van Oudenaarden, 2008) to biochemical reactions, the importance of noise is apparent at all scales of a biological system (Samoilov

et al., 2006). The behaviour of a system modelled stochastically can vary from deterministic predictions (Srivastava et al., 2002). Stability analysis of the steady states of deterministic systems can reveal unstable nodes, which stochastic simulations can reach and remain at (Srivastava et al., 2002).

Hybrid stochastic-deterministic methods have been developed to attempt to overcome the limitations of both individual methods. Hybrid algorithms first partition a network into subnetworks with different properties with the aim of applying an appropriate simulation method to each of the subnetworks. This retains the computationally expensive stochastic techniques for the subnetworks where they are needed. For example COPASI (Section 1.10.4) uses a basic particle number partitioning technique for this purpose. A model can be constructed once (i.e. without re-modelling) and then simulated using both stochastic and deterministic approaches using COPASI.

1.10.4 COPASI

COPASI is a systems biology tool that provides a framework for deterministic and stochastic modelling (Hoops et al., 2006). COPASI can transparently switch between deterministic chemical kinetic rate laws and appropriate discrete stochastic equivalents. This allows both approaches to be explored without remodelling.

COPASI also offers the ability to calculate and analyse the stability of steady states. Steady states are calculated using a damped Newton method and forward or backward integration.

When analysing the dynamics of a system, repeated simulation can be a powerful tool. Repeating a stochastic simulation with consistent parameters can refine the distribution of solutions; repeating a deterministic simulation with a random perturbation to parameters can establish the sensitivity of a model to the accuracy of the kinetic parameters. COPASI offers the ability to repeat simulations with consistent parameters or to perform an automated parameter scan.

COPASI provides tools to perform easily metabolic control analysis, which is a powerful technique for identifying reactions that have the most control over a network. Time courses can also be performed in COPASI. These COPASI time courses are useful for model validation from experimental time courses and are also useful for providing detailed time courses that would be difficult to perform in the laboratory. Events can also be scheduled for specific time points to simulate experimental conditions such as injections or meals.

1.10.5 DBSolve Optimum

DBSolve Optimum is a recently developed simulation workbench that improves on DBSolve 5 (Gizzatkulov et al., 2010). DBSolve is highly user-friendly offering advanced visualisation for the construction, verification and analysis of kinetic models. Simulation

results can be dynamically animated which is a useful tool for presentation. Although DBSolve is an alternative to COPASI it lacks the wide adoption of COPASI, possibly due to not being a multi-platform tool. COPASI offers advanced stochastic modelling features, which may be important to modelling a large complex network such as iron metabolism.

1.10.6 MATLAB

Mathworks MATLAB is a high level programming language and interactive development environment that can be used for systems biology modelling. Although it is possible to input ODEs representing a biochemical system directly into MATLAB an additional piece of software (toolbox) is often used to facilitate this process as MATLAB is not designed for ease of use with bioscience applications. With the aid of these toolboxes, MATLAB can provide much of the functionality available in COPASI. For example, the Systems Biology Toolbox (Schmidt and Jirstrand, 2006) provides tools for ODE based modelling, sensitivity analysis, estimation and algorithm. MATLAB provides increased flexibility for modelling systems outside biochemistry, for example, population level models, which are not easily supported in COPASI. However MATLAB-based models are less reproducible because a MATLAB and toolbox licence is required to reproduce results. The advanced complexity and increased availability of various modelling techniques offered by MATLAB is not necessary for the work presented here modelling iron metabolism. The network being investigated is a cellular scale mechanistic model extending to multiple compartments which is fully supported within COPASI.

1.10.7 CellDesigner

CellDesigner (Funahashi et al., 2008) was used by Hower et al. (2009) to construct the general and tissue-specific maps of iron metabolism. It is a freely available Java application and therefore is cross-platform (i.e. Windows, Mac and Linux). CellDesigner was initially created as a diagram editor for biochemical networks and has since grown into a complete modelling/simulation tool. It is able to create, export and import systems biology models in systems biology markup language (SBML) file format. This allows diagrams created in CellDesigner to be imported into tools such as COPASI for stochastic or deterministic simulation. CellDesigner uses systems biology graphical notation to represent models, and includes many features similar to those offered by other tools such as COPASI, including parameter search and time-course simulation. Simulations can be run directly from CellDesigner without exporting into another tool using the integrated SBML ODE solver; however, stochastic simulations cannot be performed directly. CellDesigner also interfaces directly with established modelling databases to allow users to browse, edit and refer to existing models within CellDesigner. A model created in a tool such as COPASI can be imported into CellDesigner for the creation of figures. This was the most

appropriate application of CellDesigner to the present project due to the superior model building and analysis framework offered by COPASI.

On balance, given the nature of the iron metabolism network, the scope of modelling, and the type of analysis that was required, COPASI was the most appropriate modelling tool for model construction and analysis. The choice of COPASI (Section 1.10.4) was re-assessed throughout the project.

1.10.8 Workflows

A workflow can be designed that combines all the previously discussed approaches of model inference and experimental data integration. Li et al. (2010b) proposed such a workflow which is suitable for modelling of any organism. The workflow was constructed in Taverna, an open-source workflow management software application (Hull et al., 2006). This work automates construction of metabolic networks. Qualitative networks are initially constructed using a "minimal information required in the annotation of models" (MIRIAM)-compliant genome-scale model. This is parameterised using experimental data from applicable data repositories. The model is then calibrated using a web interface to COPASI to produce a quantitative model. Although this workflow can not be directly applied to the human iron metabolism system due to the unavailability of a genome scale human MIRIAM-compliant model and a lack of comprehensive data sources, the overall methodology may be applied effectively in supervised manner without the use of Taverna. Instead, the present project aimed to improve the quality of the model through the detailed manual approach taken to network inference by Hower et al. (2009), and through the thorough model construction process presented here.

1.10.9 BioModels Database

Due to the increased use of modelling in various bioscience areas, the number of published models is growing rapidly. Existing centralised literature databases do not offer the features needed to facilitate model dissemination and reuse. BioModels Database was developed to address these needs (Li et al., 2010a). BioModels Database offers high quality, peer-reviewed, quantitative models in a freely-accessible online resource. Simulation quality is verified before addition to the database, annotations are added, and links to relevant data resources are established. Export into various file formats is offered. BioModels Database has become recognised as a reference resource for systems biology modelling. Several journals also recommend deposition of models into the database. Although no similar model of iron metabolism is currently found in the database, existing models were checked for data relevant to modelling iron metabolism and the work presented here has been uploaded to the BioModels Database (MODEL1302260000 and MODEL1309200000).

1.11 Parameter Estimation

Since many iron-related processing steps have only recently been investigated or still remain unknown, kinetic data are not available for the entire network. This is a common problem with creating systems biology models of complex networks. Parameter estimation techniques aim to optimise kinetic parameters to fit experimental data as closely as possible. Parameter optimisation is a special case of a mathematical optimisation problem where the objective function to be minimised is some measure of distance between the experimental data and the modelling results. COPASI uses a weighted sum of squares differences as the objective function (Hoops et al., 2006).

Optimisation algorithms fall into two categories: global and local optimisation. Local optimisation is a relatively computationally easy problem that identifies a minimum point; however, the minimum point may not be a global minimum, but only a local minimum point within a small range based on the initial point. Due to the nonlinear differential constraints of many biochemical networks, local optimisation algorithms often reach unsatisfactory solutions (Moles et al., 2003). Deterministic and stochastic global optimisation methods attempt to overcome this limitation. Although stochastic algorithms such as evolution strategies do not tend to the global optimum solution with certainty, they do offer a robust and efficient method of minimising a cost function for parameter estimation.

With the large amount of literature data available for the individual reactions for human iron metabolism (Chapter 2), there was no use of parameter optimisation techniques in this study. Optimisation algorithms were only used for identifying maximum and minimum control coefficients in global sensitivity analysis (Section 1.13.2).

1.12 Similar Systems Biology Studies

Laubenbacher et al. (2009) provide a detailed study of how various systems biology techniques have been applied to cancer. Cancer is a systems disease that shares many properties with iron metabolism.

The multiscale nature of cancer (molecular scale, cellular scale and tissue scale) is reflected in the multiscale modelling approach needed. The complexity of cancer leaves it unfeasible to model initially with a bottom-up, kinetic approach. Alternative approaches, which model these low level interactions, such as Bayesian statistical network models and Boolean networks, are assessed by Laubenbacher et al. (2009).

The fields of cancer systems and iron metabolism differ in that the interaction networks for cancers remain mainly unknown whereas, with maps such as Hower et al. (2009), the volume of research has lead to a reasonably comprehensive picture of the process of iron metabolism, therefore a bottom-up kinetic approach was feasible here.

1.13 Systems Biology Analytical Methods

As the network structure of iron metabolism is reasonably well elucidated, investigation of the dynamics is possible. Although analysis of dynamics usually follows network structure discovery, the two process are often overlapping as unknown interactions can be predicted from dynamic analysis. Depending on the quality and availability of biological knowledge for modelling, different analytical techniques can be used.

1.13.1 Flux Balance Analysis

Flux balance analysis (FBA) is a constraint-based modelling approach. Constraint-based analysis assumes that an organism will reach a steady state satisfying the biochemical constraints and environmental conditions. Multiple steady states are possible due to constraints that are not completely understood (Segrè et al., 2002). Flux balance analysis uses the stoichiometry of the network to constrain the steady-state solution. Although stoichiometry alone cannot determine an exact solution, a bounded space of feasible fluxes can be identified (Schilling et al., 2000). Constraints can be refined by adding experimental data and general biochemical limitations.

The general procedure for modelling with flux balance analysis begins with network construction. Mass balance analysis is then carried out to create a stoichiometric and flux matrix. As there are more fluxes than metabolites, the steady-state solution is unavailable without additional constraints. Further constraints such as allowable ranges of fluxes are incorporated. Finally, optimisation techniques can be used to estimate parameters with the assumption that the system is optimised with respect to some objective function (Segrè et al., 2002). Flux balance analysis techniques successfully predicted switching behaviour in the *Escherichia coli* metabolic network, which was later experimentally confirmed (Edwards et al., 2001).

As many of the reactions involved in iron metabolism are well characterised, it was not necessary to perform FBA and a full kinetic model was constructed in this study. This enables the capture of time-course information, which is vital to understanding perturbations involved in the regulation of human iron metabolism.

1.13.2 Sensitivity Analysis

If some knowledge of the steady-state rate constants is already available, sensitivity analysis can provide insight into the systems dynamics. Sensitivity analysis is used to identify significant parameters, for which accuracy is required, and less significant parameters, for which estimated values will be suitable. Sensitivity analysis techniques can either be global or local. Local methods vary single parameters and measure the effect on the output of the model; however, this can fail to capture large parameter changes of multiple parameters. Global sensitivity analysis (GSA) involves a full search of the

parameter space. This fully explores the possible dynamics of the model. Multiple parameters can be varied at the same time as, often, combinations of parameters have a much greater sensitivity than expected from the sensitivity of the individual components. GSA methods are able to analyse parameter interaction effects, even those that involve nonlinearities (Saltelli et al., 2000). Disease states may differ from health simulation in a number of ways. Therefore, a scan of a large parameter space provided by GSA is important to ensure simulations are accurate in health and disease. GSA methods can be highly computationally expensive and therefore this can limit the extent to which the parameter space can be explored.

Metabolic control analysis (MCA) is a type of local sensitivity analysis used to quantify the distribution of control across a biochemical network (Kacser and Burns, 1973; Heinrich and Rapoport, 1974). The values obtained through MCA are control coefficients. These can be considered the percentage change of a variable given a 1% change in the reaction rate. Where the variable being considered is the steady state concentration of a metabolite the output is a concentration control coefficient. Where a steady state flux is of interest the result is a flux control coefficient.

1.13.3 Overcoming Computational Restraints

Using a distributed processing system, to make use of idle time on unused workstation computers, such as Condor (Litzkow et al., 1988), can drastically reduce the time it takes to run computationally intensive tasks such as global optimisation (Litzkow and Livny, 1988). Condor pools are applicable to global optimisation, regardless of the software used to assist with the task, as the software is sent to each workstation along with the data for analysis.

To fascilitate the distribution of biochemical analysis tasks to Condor pools, Kent et al. (2012b) developed Condor-COPASI. This server-based software tool enables tasks from COPASI (Section 1.10.4) that can be run in parallel, to be intelligently split into parts and automatically submitted to a Condor pool. The results are collected from the distributed jobs and presented in a number of useful formats when tasks are complete.

Distributed systems are optimised for high throughput computing tasks that can be split into a number of smaller tasks. For highly computationally expensive tasks, which cannot be isolated, a high performance solution is more suitable. One option (which still requires task-splitting but which can facilitate communication between the sub-tasks) is to utilise the programmable parallel processor of modern graphics processing units (GPUs). Originally developed for rendering of computer graphics, GPUs have recently been applied to general computational tasks. Nvidia developed the Compute Unified Device Architecture (CUDA) (Lindholm et al., 2008), which extends the C programming language and allows an application to use both central processing unit (CPU) and GPU computation. Although GPU-based processing has not been widely used for systems biology modelling, the matrix algebra of computational modelling is similar to the matrix-

based computation required for computer graphics rendering.

1.14 Purpose and Scope

Due to recent experimental advances, significant progress has been made towards understanding the network and the individual interactions of the human iron metabolism system. Despite increasing understanding of individual interactions, an holistic view of iron metabolism and the mechanisms of systemic control of iron metabolism remain to be elucidated.

Many diseases are shown to demonstrate a misregulation of iron metabolism, yet, due to a lack of understanding of systemic control, iron-related therapeutic targets have been difficult to identify. Misregulation of iron metabolism contributes to iron deficiency, which is a global problem not easily addressable by dietary changes. It may be possible, with a greater understanding of the iron metabolism system, to improve iron absorption and retention to combat iron deficiency. Iron overload disorders such as haemochromatosis are highly prevalent and an increasing body of evidence suggests that iron overload may be more harmful than anaemia. The regulatory control demonstrated by the iron metabolism network has impact on other systems. Crosstalk between networks such as signalling networks and other metal metabolism networks are poorly understood.

Here a systems biology approach is used to improve understanding of human iron metabolism. To gain holistic understanding of the whole organism, mathematical modelling techniques are used. An ordinary differential equation model of iron metabolism, which includes cellular and systemic regulation, is developed. A mechanistic modelling approach is used and includes known cellular processes such as: complex association and dissociation, enzyme catalyzed reactions, transport, and induced expression and degradation. Both the cellular-scale regulation, provided by IRPs, and the systemic-scale regulation, provided by hepcidin, is modelled. Multiple tissue types have been modelled, as has the interaction between different tissue types. To parameterise accurately such a comprehensive model, a translational approach to incorporating data from a large number of literature sources is used. The model was constructed in COPASI by bringing together information from the literature in a comprehensive manner. The model was validated using experimental results. A sensitivity analysis and metabolic control analysis of the model determined which reactions had the strongest impact on systemic iron levels.

The model was analysed in health and disease. Dynamics and redistribution of control in disease were investigated to identify potential therapeutic targets.

Additionally, the model was applied to test potential hypotheses for a role for cellular prion protein (for which no physiological role is currently known) within iron metabolism, and a potential site of action was identified.

CHAPTER

TWO

DATA COLLECTION

2.1 Existing Data

To construct the most detailed and accurate model possible, a thorough review of the data available in the literature was performed. A highly integrative approach was taken to data collection. While some of the data collected may not be directly applicable to model construction, due to experimental conditions or the qualitative nature of the result, all data were considered to be of value for assisting with validation. Where no human data were available, animal model, cell-line and *in vitro* data were used as an estimate, but care was taken with conversions and validation to ensure these data were as applicable as possible.

2.1.1 Human Protein Atlas

The Human Protein Atlas (HPA) (Berglund et al., 2008) is a database that contains tissue-specific expression data for over 25% of the predicted protein-coding genes of the human genome. Both internally generated and commercially available protein-specific antibody probes are used. All genes predicted by the joint scientific project between the European Bioinformatics Institute and the Wellcome Trust Sanger Institute, Ensembl (Flicek et al., 2008) are included in the HPA. However, due to difficulty obtaining verified antibodies for many proteins, not all these contain expression data. Validation of internally-generated antibodies was performed by protein microarrays and specificity was determined by a fluorescence-based analysis. Further western blot and immunohistochemistry verification were performed.

The HPA contains valuable information to validate tissue-specific models although it is incomplete. High confidence results showing negative expression could be used to exclude species from a model and reduce its size. Expression data in the HPA are collected specifically for inclusion in the HPA, which ensures the quality of the results; however, the level of completeness could be improved by incorporating expression data from other sources.

2.1.2 Surface Plasmon Resonance

When collecting data from the literature it is important to identify the experimental techniques that provide data of the type and quality required for computational modelling.

Surface plasmon resonance (SPR) is a technique that can provide kinetic data useful as rate constants for modelling (Jönsson et al., 1991; Lang et al., 2005). Biosensors have been developed to provide label-free investigations of biomolecular interactions with the use of SPR (Walker et al., 2004). SPR determines association and disassociation constants (Hahnefeld et al., 2004). To perform SPR, one reactant must be immobilised on a thin gold layer and the second component then introduced using a microfluidics system. As the mass of the immobilised component changes, when binding occurs, the binding can be detected through optical techniques. The refractive index in the vicinity of the surface changes with the mass of the reactants and this can be measured with sensitive instrumentation using total internal reflection. Once the association (k_{on}) and disassociation (k_{off}) rate constants have been obtained, the equilibrium dissociation constant (K_d) can be determined. Many papers only report the K_d, but this is less useful for modelling than the individual rate constant. In such cases the authors were contacted to obtain the specific k_{on} and k_{off} rate constants.

SPR is highly sensitive with a lower limit on detection of bio-material at about 0.1 pg$\cdot$ mM^{-2}. Large macromolecular systems with fast binding kinetics can be limited by diffusion phenomena (De Crescenzo et al., 2008). This limitation of SPR, known as the mass transport limitation (MTL), has been studied in depth (Goldstein et al., 1999) and approaches have been developed that provide a good approximation in this situation (Myszka et al., 1998).

2.1.3 Kinetic Data

Accurate modelling requires experimental kinetic data for estimation of parameters and validation. Some interactions within the iron metabolic network have well characterised kinetics while others remain relatively unstudied. Some of the most interesting kinetics for model construction and validation published for iron-related interactions are given here (Table 2.1).

Early kinetic studies showed that iron uptake by reticulocytes followed the saturation kinetics characteristic of carrier-mediated transport. Kinetics were measured by Egyed (1988) for the carrier-mediated iron transport system in the reticulocyte membrane. Rabbit reticulocytes were studied as a model using radioactive iron (^{59}Fe) to determine iron uptake rates (Table 2.1).

Transferrin was then studied in great detail as reviewed (Thorstensen and Romslo, 1990). When these authors reviewed the literature only one transferrin receptor had been identified; this receptor binds transferrin prior to internalisation. Transferrin receptor kinetics results differ throughout the literature and binding was found to be strongly affected

Table 2.1: **Data collected from the literature for the purpose of model parameterisation and validation.**

Reaction/Metabolites	Result	Reference
Reticulocyte iron uptake	$K_m = 8.8 \pm 3.8 \mu M$	Egyed (1988)
Reticulocyte iron uptake	$V_{max} = 1.1 \pm 0.2 ng/10^8$reticulocytes/min	Egyed (1988)
Tf Fe^{3+} binding	$\log K_{on} = 20.2$ pH 7.4	Thorstensen and Romslo (1990)
Tf Fe^{3+} binding	$\log K_{on} = 12.6$ pH 5.5	Thorstensen and Romslo (1990)
Tf Fe^{3+} binding	K_d of 10^{-24} pH 7	Kaplan (2002)
Tf Fe^{3+} binding	$K_d = 10^{-23}$M	Richardson and Ponka (1997)
TfR1 diferric Tf binding	K_d of 10^{-24} pH 7.4	Kaplan (2002)
TfR1 diferric Tf binding	$(0.34 - 1.6) \times 10^7 M^{-1}$ pH 7.4 Rat Hepatocyte	Thorstensen and Romslo (1990)
TfR1 diferric Tf binding	$1.1 \times 10^8 M^{-1}$ pH 7.4 Rabbit reticulocytes	Thorstensen and Romslo (1990)
TfR1 diferric Tf binding	$1.4 \times 10^8 M^{-1}$ pH 7.4 Human HepG2	Thorstensen and Romslo (1990)
TfR1 diferric Tf binding	$7.7 \times 10^7 M^{-1}$ pH 5.5 Human HepG2	Lebron (1998)
TfR1 monoferric Tf binding	$2.6 \times 10^7 M^{-1}$ pH 7.4 Rabbit reticulocytes	Lebron (1998)
TfR1 apo-Tf binding	$4.6 \times 10^6 M^{-1}$ pH 7.4 Rabbit reticulocytes	Lebron (1998)
TfR1 apo-Tf binding	$7.7 \times 10^7 M^{-1}$ pH 5.5 Rabbit reticulocytes	Lebron (1998)
TfR1 Tf binding	$K_d = 5 \times 10^{-9} M$ Ph 7.4 K562 cells	Richardson and Ponka (1997)
Mobilferrin Fe binding	$K_d = 9 \times 10^{-5} M$	Richardson and Ponka (1997)
Tf TfR2 binding	$K_{d1} = 27nM$	West et al. (2000)
Tf-TfR2 Tf binding	$K_{d2} = 350nM$	West et al. (2000)
Tf TfR1 binding	$K_{d1} = 1.1nM$	West et al. (2000)
Tf-TfR1 Tf binding	$K_{d2} = 29nM$	West et al. (2000)
HFE TfR binding	$K_d \sim 300nM$	Bennett et al. (2000)

Michaelis constant (K_m), maximal velocity (V_{max}), turnover number (K_{cat}), equilibrium binding constant (K_d and K_{d1}, K_{d2} if two staged binding), association rate (K_{on}).

by pH and iron bound to transferrin, as can be seen in Table 2.1.

Richardson and Ponka (1997) reviewed the essential steps of iron metabolism and estimated the affinity with which transferrin binds two Fe^{3+} atoms (Table 2.1). They also reviewed the binding strengths of calreticulin (mobilferrin) and the strength of IRP/IRE binding (Table 2.1).

The discovery of TfR2 and refinement of surface plasmon resonance-based techniques have led to more accurate results from later research. Previously, fluorescence-based techniques had been used, which provided less accurate estimates (Breuer et al., 1995b). More recently, binding affinity of TfR1 and TfR2 was also measured by West et al. (2000). Using surface plasmon resonance techniques, TfR2 was attached to a sensor chip, and this was followed by a series of Tf and HFE injections. The binding of Tf to TfR2 was found to have a 25-fold lower affinity than Tf to TfR1. Although only the K_d values were given in the published literature, the k_{on} and k_{off} rates were obtained through personal correspondence.

HFE:TfR1 was found to have a 2:2 stoichiometry by Aisen (2004) although 1:2 has also been observed (Bennett et al., 2000).

TfR2-HFE binding assays using TfR1 as positive control found a $K_d \gg 10\mu M$ (West et al., 2000) Therefore, binding between membrane HFE and TfR2 was thought to be unlikely. This was also verified by observations that TfR1 but not TfR2 coimmunoprecipitates with HFE. The difference in binding is unsurprising as half the TfR1 residues that form contacts with HFE are replaced by different amino acids in TfR2. However, recent studies found TfR2 does in fact bind to HFE (Goswami and Andrews, 2006) in an important regulatory role.

The number of TfRs on cell surfaces is reported to be highly variable. Non-dividing cells have very low levels of TfR1 expression. However, up to 100,000 TfRs are present per cell in highly proliferating cells (Gomme et al., 2005). This allows iron accumulation from transferrin at a rate of around 1,100 ions/cell/s (Iacopetta and Morgan, 1983). The intake rate of iron per TfR1 has been estimated to be 36 iron atoms hr^{-1} at normal transferrin saturation levels.

Binding of apo neutrophil gelatinase-associated lipocalin (NGAL) to the low-density lipoprotein-receptor family transmembrane protein megalin occurs with high affinity as investigated by Hvidberg et al. (2005) and similar results are seen with siderophore-bound NGAL.

The affinity of Fe-TF for immobilised TfR1 was determined in the absence of HFE to have a K_d of $\sim$1 nM (Lebrón et al., 1999). This is consistent with published data for membrane bound TfR1 ($K_d = 5nM$) and soluble TfR1 ($K_d \sim 3nM$). The affinity of soluble HFE for immobilized TfR1 was determined by Bennett et al. (2000) (Table 2.2).

DMT1 acts as a proton-coupled symporter with stoichiometry $1Fe^{2+} : 1H^+$ with K_m values of 6 and $1 - 2\mu M$, respectively (Gunshin et al., 1997).

Ferroportin - hepcidin binding was studied by Rice et al. (2009) using surface plas-

Table 2.2: **Biosensor Analyses of TfR1 Binding to Tf and HFE (Lebron, 1998)** a,b,c,d,e,f and g represent different experimental conditions and derivations; * = experiment could not be performed, N.B. = no significant binding at concentrations up to 1 μM; details in experimental methods of Lebron (1998).

	$K_{d,eq^a}(nM)$	$K_{d,calc^b}(nM)$	$K_{on}(sec^{-1}M^{-1})$	$K_{off}(sec^{-1})$
TfR1 immobilised				
Fe-Tf (pH 7.5)$_c$	*	5.7	3.1×10^5	1.8×10^3
Fe-Tf (pH 7.5)$_d$	1.9	0.81 ± 0.1	$(1.6 \pm 0.04) \times 10^6$	$(1.3 \pm 0.2) \times 10^3$
apo-Tf (pH 6.0)$_e$	< 15	1.3 ± 0.2	$(7.3 \pm 0.7) \times 10^5$	$(9.4 \pm 2) \times 10^4$
apo-Tf + PP$_i$ (pH 7.5)$_e$	>8,000	N.B.	N.B.	N.B.
HFE (pH 7.5)$_f$	350	130 ± 10	$(8.1 \pm 0.9) \times 10^5$	$(1.1 \pm 0.1) \times 10^1$
HFE (pH 6.0)$_f$	$> 10,000$	N.B.	N.B.	N.B.
HFE immobilised				
TfR1 (pH 7.5)$_g$	0.91	0.33 ± 0.02	$(3.8 \pm 0.2) \times 10^6$	$(1.2 \pm 0.1) \times 10^3$
TfR1 (pH 6.0)$_g$	*	N.B.	N.B.	N.B.
Fe-Tf (pH 7.5)$_g$	N.B.	N.B.	N.B.	N.B.
apo-Tf (pH 6.0)$_g$	N.B.	N.B.	N.B.	N.B.

Equilibrium binding constant (K_d), association rate (K_{on}), dissociation rate (K_{off}), iron chelator pyrophosphate (PPi).

mon resonance. The data did not fit a 1:1 binding model and therefore an accurate K_d could not be calculated. This was probably due to complex binding events relating to the aggregation of injected hepcidin. However, they were able to establish a low micromolar K_d.

TfR2 human liver protein concentrations were estimated by Chloupková et al. (2010) to be 1.95 nmol $\cdot$ g protein^{-1}. This was scaled using a typical weight of human liver (around 1.5 kg; Heinemann et al. (1999)) to give an estimate of 3 μM for TfR2. Chloupková et al. (2010) also measured TfR1 protein concentration in human liver and found it to be around 4.5 times lower than TfR2 levels. The level of HFE protein was found to be lower than 0.53 nmol/g and this was scaled in the same way as with TfR2. The half-life (λ) of TfR2 was measured by Johnson and Enns (2004) to be 4 hours in the absence of Tf and up to 14 hours in the presence of Tf. The half-life of TfR1 is much longer at ~ 23 hours. The half-life of HFE was shown to be 2-4 hours by Wang et al. (2003b). These half-life values were converted into degradation rates using Equation 2.1.1:

$$\lambda = \frac{\ln 2}{\text{degradation rate}}. \tag{2.1.1}$$

With the degradation rates and expected steady-state concentrations obtained, it was possible to derive expression rates that are rarely measured experimentally. At steady state, the change of protein concentration should be zero. The concentration of the protein is known, as is the degradation rate and therefore we could use the following Equation 2.1.2:

$$\frac{d[P]}{dt} = k - d[P] = 0. \tag{2.1.2}$$

This was solved for k where $[P]$ is the steady-state concentration of the protein and d is the degradation rate obtained from the half-life using Equation 2.1.1.

The stability of the IRP protein was found to be relatively long (>12 hours) by Pantopoulos et al. (1995). Steady-state IRP concentrations were estimated by combining a number of sources. Cairo et al. (1998) gives an estimate of 700000 IRP proteins per cell, which is around 1.16×10^{-18} mol$\cdot$cell^{-1} and with hepatocyte volume around 1×10^{-12} L this gives a concentration of around 1.16 μM. Chen et al. (1998) measured mRNA binding of IRPs and found a total of 0.164 pmol $\cdot$ mg^{-1} which is 0.164 μmol $\cdot$ Kg^{-1}; this is one order of magnitude lower than the previous estimate. However Chen et al. (1998) also measured total IRP by 2-ME induction, which is a measure of total IRP protein (as opposed to mRNA binding) and found 8.06 pmol $\cdot$ mg^{-1} which is 8 μmol $\cdot$ Kg^{-1}; slightly higher than the previous estimate. These were used to estimate an expression rate using Equation 2.1.2.

Hepcidin half-life was estimated to be around two hours using Rivera et al. (2005). The concentration of hepcidin in healthy adults was calculated to be around 72.9 ng $\cdot$ mL^{-1}, which was converted to an appropriate concentration using the molecular weight of hepcidin (2789 Da) and approximate volume of human liver (Heinemann et al., 1999). As both the degradation rate and steady-state concentration were calculated, the expression rate could be derived as described previously.

Haem oxygenation rate was taken from Kinobe et al. (2006) who calculated the K_m and V_{max} of around $2 \pm 0.4\mu$M and 38 ± 1pM $\cdot$ (min $\cdot$ mg)$^{-1}$, respectively, using rat haem oxygenase. The V_{max} was converted to s $\cdot$ Kg^{-1}.

The rate at which iron is released from transferrin following receptor-mediated endocytosis was measured by Byrne et al. (2010). The release of iron from each lobe of transferrin was described in detail at endosomal pH, but the rates (~ 0.83 L $\cdot$ s^{-1}) are fast and therefore it may be unnecessary to consider this level of detail when modelling.

All ferritin-related kinetic constants were obtained from Salgado et al. (2010) who estimated and verified rates for iron binding to ferritin, its subsequent internalisation, iron release, as well as ferritin degradation kinetics. Salgado et al. (2010) discretised ferritin kinetics into discrete iron packets of 50 iron atoms per package; some adjustments were made to convert this to a continuous model of ferritin loading. To model the dependence on current iron loading of the iron export rate out of ferritin, Salgado et al. (2010) defined an equation for each loading of ferritin. This rate of iron export had the form:

$$v = \mathrm{K_{loss}}(1 + (\mathrm{k} \cdot \mathrm{i})/(1 + \mathrm{i})) \tag{2.1.3}$$

where K $= 2.4$ and i $=$ the number of "iron packages" stored in ferritin. This equation was modified for the present model to remove the need for discrete "iron packages". 'i' was replaced with $\frac{\text{iron in ferritin}}{\text{amount of ferritin}}$ which is the amount of of iron stored per ferritin. K was divided by 50 to adjust for the 50 iron atoms per "iron package" used by Salgado et al. (2010).

Haem oxygenase's half-life was estimated by Pimstone et al. (1971) to be around 6 hours which was converted to a degradation rate using Equation 2.1.1. The steady-state concentrations of haem oxygenase were taken from Bao et al. (2010) and used to derive the expression rates as described previously.

Haem uptake and export are thought to be mediated by haem carrier protein 1 (HCP1) and ATP-binding cassette (ABC) transporter ABCG2, respectively. The kinetics for haem iron uptake by HCP1 were characterised by Shayeghi et al. (2005), who found a V_{max} of 3.1 pM $\cdot (\text{min} \cdot \mu\text{g})^{-1}$ and K_m of 125 μM. ABCG2 kinetics were calculated by Tamura et al. (2006), who found a V_{max} of 0.654 nmol $\cdot (\text{min} \cdot \text{mg})^{-1}$ and $K_m = 17.8$ μM. The V_{max} in both cases were converted to $\text{M} \cdot (\text{s} \cdot \text{liver})^{-1}$ using estimates described previously.

2.1.4 Intracellular Concentrations

Recent advances in fluorescent dyes and digital fluorescence microscopy have meant that fluorescence-based techniques have become important for the detection of intracellular ions (Petrat et al., 1999). The intracellular concentrations of iron have been measured in various cell types for a number of years and a reasonably comprehensive picture of systemic iron concentrations is emerging. The findings are summarised in Table 2.3.

Table 2.3: **Intracellular Iron Concentrations**

Probe	Cell type	[Fe] (μM)	Reference
Phen Green SK	Hepatocytes	9.8	Petrat et al. (1999)
Phen Green SK	Hepatocytes	2.5	Petrat (2000)
Phen Green SK	Hepatocytes	3.1	Rauen et al. (2000)
Phen Green SK	Hepatocyte Cytosol	5.8	Petrat et al. (2001)
Phen Green SK	Hepatocyte Mitochondria	4.8	Petrat et al. (2001)
Phen Green SK	Hepatocyte Nucleus	6.6	Petrat et al. (2001)
Phen Green SK	Liver Endothelial Cell Cytosol	7.3	Petrat et al. (2001)
Phen Green SK	Liver Endothelial Cell Mitochondria	9.2	Petrat et al. (2001)
Phen Green SK	Liver Endothelial Cell Nucleus	11.8	Petrat et al. (2001)
Phen Green SK	Human Erythroleukemia K562 Cells	4.0	Petrat et al. (1999)
Phen Green SK	Guinea Pig Inner Hair Cells	1.3	Dehne (2001)
Phen Green SK	Guinea Pig Hensen Cells	3.7	Dehne (2001)
Calcein	K562 Cells	0.8	Konijn et al. (1999)
Calcein	K562 Cells	0.2-0.5	Breuer et al. (1995a)
Calcein	Erythroid and Myeloid Cells	0.2-1.5	Epsztejn et al. (1997)
Calcein	Hepatocytes	0.2	Zanninelli et al. (2002)
CP655	Hepatocytes	5.4	Ma et al. (2006a)
CP655	Human Lymphocytes	0.57	Ma et al. (2007)
Rhodamine B	Hepatocyte Mitochondria	12.2	Petrat et al. (2002)

CHAPTER

THREE

HEPATOCYTE MODEL

Parts of this chapter have been published in Mitchell and Mendes (2013b) A Model of Liver Iron Metabolism. PLOS Computational Biology. This publication is also available at arXiv.org (Mitchell and Mendes, 2013a).

3.1 Introduction

The liver has been proposed to play a central role in the regulation of iron homeostasis (Frazer and Anderson, 2003), through the action of the recently discovered hormone hepcidin (Park et al., 2001). Hepcidin is expressed predominantly in the liver (Pigeon et al., 2001) and distributed in the serum to control systemic iron metabolism. Hepcidin acts on ferroportin to induce its degradation. Ferroportin is the sole iron-exporting protein in mammalian cells (Van Zandt et al., 2008), therefore hepcidin expression inhibits iron export into the serum from enterocytes, and prevents iron export from the liver. Intracellular iron metabolism is controlled by the action of iron response proteins (IRPs) (Hentze and Kühn, 1996). IRPs post-transcriptionally regulate mRNAs encoding proteins involved in iron metabolism, and IRPs combined with ferritin and the transferrin receptors (TfR) make up the centre of cellular iron regulation. Ferritin is the iron-storage protein forming a hollow shell, which counters the toxic effects of free iron by storing iron atoms in a chemically less reactive form, ferrihydrite (Harrison, 1977). Extracellular iron circulates bound to transferrin (Tf), and is imported into the cell through the action of membrane bound proteins, transferrin receptors 1 and 2 (TfR1 and TfR2). Human haemochromatosis protein (HFE) competes with transferrin bound iron for binding to TfR1 and TfR2 (West et al., 2001).

Systems biology provides an excellent methodology for elucidating our understanding of the complex iron metabolic network through computational modelling. A quantitative model of iron metabolism allows for a careful and principled examination of the effect of the various components of the network. Modelling allows one to do "what-if" experiments leading to new hypotheses that can later be put to test experimentally. However, no comprehensive model of liver iron metabolism exists to date. Models have been pub-

lished that cover specific molecular events only, such as the binding of iron to ferritin (Salgado et al., 2010). A qualitative map of iron metabolism provides a detailed overview of the molecular interactions involved in iron metabolism, including in specific cell types (Hower et al., 2009). A qualitative core model of the iron network has been recently described (Chifman et al., 2012), which suggests that the dynamics of this network is stable, yet this model includes only a few components. One of the problems of modelling iron metabolism quantitatively and in detail arises from the lack of parameter values for many interactions. Recently, several of those parameters have been described in the literature (Table 3.3), particularly using technologies like surface plasmon resonance. This has enabled us to construct a detailed mechanistic kinetic model of human hepatocyte iron metabolism. The model has been validated by being able to reproduce data from several disease conditions — importantly, these physiological data were not used in constructing the model. This validation provides a sense of confidence that the model is indeed appropriate for understanding liver iron regulation and for predicting the response to various environmental perturbations.

3.2 Materials and Methods

3.2.1 Graph Theory

To focus initial modelling efforts on key components in the iron metabolism network, graph theory techniques were used to identify central metabolites. To perform graph theory analysis on the iron metabolism maps (Hower et al., 2009) the diagrams had to be converted into a suitable format.

CellDesigner (Funahashi et al., 2008) was used to create the maps of iron metabolism networks by Hower et al. (2009). CellDesigner uses Systems Biology Graphical Notation (SBGN) (Novere et al., 2009) to represent biochemical networks; however, this format is not suitable for direct analysis by graph theory algorithms.

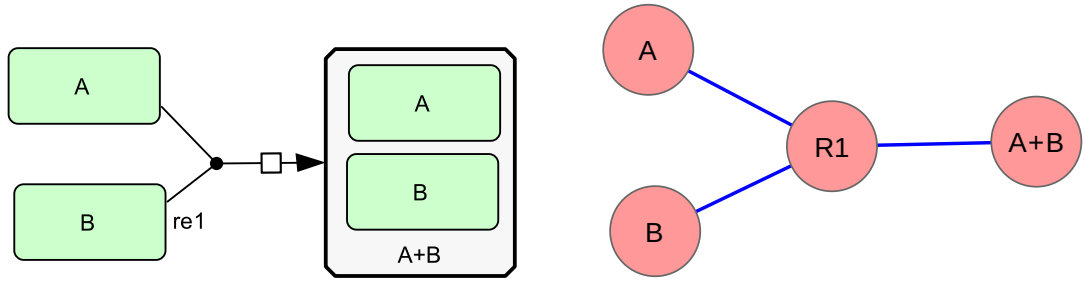

(a) Example SBGN Binding from CellDesigner (b) SBGN Nodes

Figure 3.1: **The node and edge structure of SBGN.** A, B and A+B are metabolites participating in reaction R1.

An example SBGN reaction generated by CellDesigner is given in Figure 3.1a. This

figure appears to have metabolites as graph nodes connected by edges representing reactions; however, this is not the case as each reaction is also a node. Edges only exist between reaction nodes and metabolite nodes. As can be seen from Figure 3.1b reactants and products of a reaction are not linked by a single edge in SBGN, but rather by a 2-edge path through a reaction.

Directly analysing SBGN as a graph is counter intuitive as reactants and products should be neighbours in a graph where edges represent a biological significance. This means measures such as clustering coefficients, which measure connectedness between immediate neighbours of a node, are inaccurate if applied directly to SBGN maps. The clustering coefficient of any node in any graph taken directly from SBGN is zero as a nonzero clustering coefficient would require reaction-reaction or species-species connections.

To provide accurate graph theory analysis, the SBGN networks from Hower et al. (2009) were converted into graphs where two species were linked with an edge if a perturbation in one species would directly affect the other through a single reaction. A function f was applied to the SGBN graph G such that

$$f : G(V, E) \rightarrow G'(M, E') \tag{3.2.1}$$

where

$$E, E' \text{: sets of edges,}$$

$$M \text{: set of metabolite nodes,}$$

$$R \text{: set of reaction nodes,}$$

$$V : M \cup R.$$

An edge $((a, b)|a, b \in M) \in E'$ iff $\exists$ a directed path in G from a to b of the form:

$$P(a, b) = \{(a, r), (r, b)|a, b \in S, r \in R\}. \tag{3.2.2}$$

This ensured all nodes were metabolites and all edges were between metabolites that participated in the same reaction.

In the case where no reaction modifiers exist, the undirected graph as seen in Figure 3.2 is adequate. The edges are bidirectional as increasing levels of product directly affect substrate by mass action. However for the iron metabolism network, the directionality of edges was important as reaction modifiers such as enzymes affected reactants, but were not affected themselves by other reactants. This led to a directed graph as seen in Figure 3.3. The converted graph of the whole iron metabolism network was imported into the Cytoscape software (Smoot et al., 2011) for calculating graph properties.

Cytoscape's network analysis plugin was used to calculate node degree distribution and betweenness centrality values for each node. These data were used, along with as-

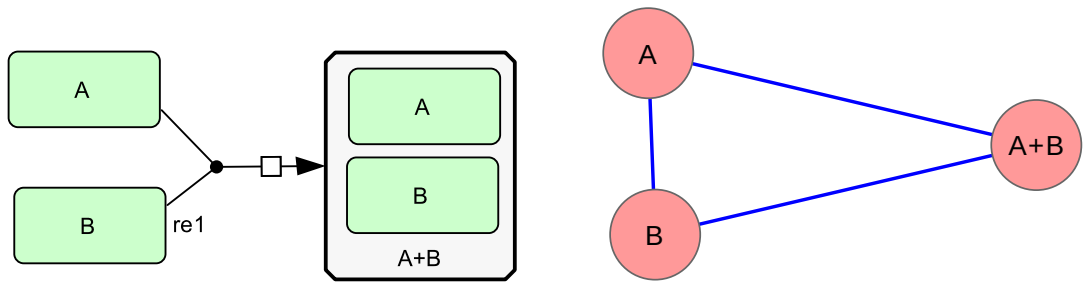

(a) Example SBGN Binding (b) Conversion to Graph

Figure 3.2: **Example conversion from SBGN**

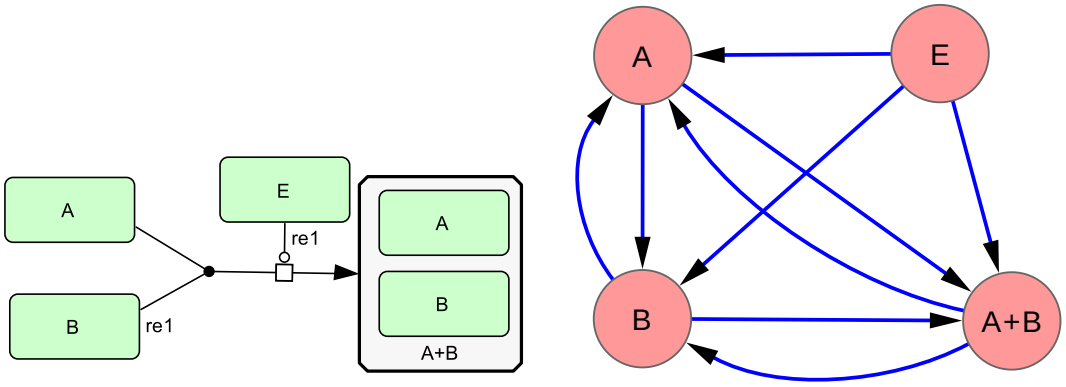

(a) Example SBGN Binding with enzyme (b) Conversion to Graph with enzyme

Figure 3.3: **Example conversion of enzyme-mediated reaction from SBGN.** A, B and A+B are metabolites participating in reaction re1, which is mediated by enzyme E. It is important to consider that enzymes affect a reactions rate but are not themselves affected by the other participants of the reaction.

sessment of the availability of appropriate data, to decide which metabolites from the map of iron metabolism to include in the model presented here.

3.2.2 Modelling

The model is constructed using ordinary differential equations (ODEs) to represent the rate of change of each chemical species. COPASI (Hoops et al., 2006) was used as the software framework for model construction, simulation and analysis. CellDesigner (Funahashi et al., 2008) was used for construction of an SBGN process diagram (Figure 3.5).

The model consists of two compartments representing the serum and the liver. Concentrations of haem and transferrin-bound iron in the serum were fixed to represent constant extracellular conditions. Fixed metabolites simulate a constant influx of iron through the diet as any iron absorbed by the liver is effectively replenished. A labile iron pool (LIP) degradation reaction is added to represent various uses of iron and create a flow

through the system. Initial concentrations for metabolites were set to appropriate concentrations based on a consensus from across literature (Table 3.1). All metabolites formed through complex binding were set to zero initial concentrations (Table 3.1).

Table 3.1: **Initial Concentrations of all Metabolites**

Parameter	Initial Concentration (M)	Source
LIP	1.3×10^{-6}	Epsztejn et al. (1997)
FPN1	1×10^{-9}	
IRP	1.16×10^{-6}	Haile et al. (1989b)
HAMP	5×10^{-9}	Zaritsky et al. (2010)
haem	1×10^{-9}	
2(Tf-Fe)-TfR1_Internal	0	
2(Tf-Fe)-TfR2_Internal	0	
Tf-Fe-TfR2_Internal	0	
Tf-Fe-TfR1_Internal	0	
Tf-TfR1_Internal	0	
Tf-TfR2_Internal	0	
Fe-FT	0	
FT	1.66×10^{-10}	Cozzi (2003)
HO-1	3.56×10^{-11}	Mateo et al. (2010)
FT1	0	
Tf-Fe_intercell	5×10^{-6}	fixed, Johnson and Enns (2004)
TfR	4×10^{-7}	Chloupková et al. (2010)
Tf-Fe-TfR1	0	
HFE	2×10^{-7}	Chloupková et al. (2010)
HFE-TfR	0	
HFE-TfR2	0	
Tf-Fe-TfR2	0	
2(Tf-Fe)-TfR1	0	
2HFE-TfR	0	
2HFE-TfR2	0	
2(Tf-Fe)-TfR2	0	
TfR2	3×10^{-6}	Chloupková et al. (2010)
haem_intercell	1×10^{-7}	Sassa (2004)

The concentration of a chemical species at a time point in the simulation is determined by integrating the system of ODEs. For some proteins a half-life was available in the literature, but sources could not be found for synthesis rate (translation). In this occurrence, estimated steady-state concentrations were used from the literature and a synthesis rate was chosen such that at steady state the concentration of the protein would be approximately accurate, following Equation 3.2.3:

$$\frac{d[\mathrm{P}]}{dt} = k - d[\mathrm{P}] = 0. \tag{3.2.3}$$

This is solved for k where $[\mathrm{P}]$ is the steady-state concentration of the protein and d is the degradation rate obtained from the half-life (λ) using:

$$d = \frac{\ln 2}{\lambda}. \tag{3.2.4}$$

Complex formation reactions, such as binding of TfR1 to Tf-Fe for iron uptake, are modelled using the on and off rate constants for the appropriate reversible mass action reaction. For example:

$$\text{TfR1} + \text{Tf-Fe} \rightleftharpoons \text{Tf-Fe-TfR1} \tag{3.2.5}$$

is modelled using two reactions:

$$\text{TfR1} + \text{Tf-Fe} \xrightarrow{k_a} \text{Tf-Fe-TfR1} \tag{3.2.6}$$

$$\text{Tf-Fe-TfR1} \xrightarrow{k_d} \text{TfR1} + \text{Tf-Fe} \tag{3.2.7}$$

Where K_a is the association rate and K_d is the dissociation rate. There is one ODE per each chemical species. The two reactions 3.2.6 and 3.2.7 add the following terms to the set of ODEs:

$$\begin{aligned}
\frac{d[\text{TfR1}]}{dt} &= -\,k_a[\text{TfR1}][\text{TF-Fe}] + k_d[\text{Tf-Fe-TfR1}]\ldots \\
\frac{d[\text{Tf-Fe}]}{dt} &= -\,k_a[\text{TfR1}][\text{TF-Fe}] + k_d[\text{Tf-Fe-TfR1}]\ldots \\
\frac{d[\text{Tf-Fe-TfR1}]}{dt} &= +\,k_a[\text{TfR1}][\text{TF-Fe}] - k_d[\text{Tf-Fe-TfR1}]\ldots
\end{aligned} \tag{3.2.8}$$

Intracellular haem levels are controlled by a balance between uptake, export and oxygenation. Haem import through the action of haem carrier protein 1 (HCP1), haem export by ATP-binding cassette sub-family G member 2 (ABCG2), and oxygenation by haem oxygenase-1 (HO-1) follow Michaelis-Menten kinetics. HO-1 expression is promoted by haem through a Hill function (Equation (3.2.9)).

$$v = [\text{S}] \cdot a \cdot \left(\frac{[\text{M}]^{n_H}}{K^{n_H} + [\text{M}]^{n_H}} \right), \tag{3.2.9}$$

$$v = [\text{S}] \cdot a \cdot \left(1 - \frac{[\text{M}]^{n_H}}{K^{n_H} + [\text{M}]^{n_H}} \right). \tag{3.2.10}$$

Where v is the reaction rate, S is the substrate, M is the modifier, a is the turnover number, K is the ligand concentration which produces half occupancy of the binding sites of the enzyme, and n_H is the Hill coefficient. Values of n_H larger than 1 produce positive cooperativity (i.e. a sigmoidal response); when $n_H = 1$ the response is the same as Michaelis-Menten kinetics. A Hill coefficient of $n_H = 1$ was assumed unless there is literature evidence for a different value. Where K is not known it has been estimated to

be of the order of magnitude of experimentally observed concentrations for the ligand.

IRP/Iron-responsive elements (IRE) regulation is represented by Hill kinetics using Equation (3.2.9) to simulate the 3' binding of IRP promoting the translation rate, and Equation (3.2.10) to represent the 5' binding of IRP reducing the translation rate. Ferroportin degradation is modelled using two reactions: one representing the standard half-life and the other representing the hepcidin-induced degradation. A Hill equation (Equation 3.2.9) is used to simulate the hepcidin-induced degradation of ferroportin.

Hepcidin expression is the only reaction modelled using a Hill coefficient greater than 1. Due to the small dynamic range of HFE-TfR2 concentrations, a Hill coefficient of 5 was chosen to provide the sensitivity required to produce the expected range of hepcidin concentrations. The mechanism by which HFE-TfR2 interactions induce hepcidin expression is not well understood, but is thought to involve the mitogen-activated protein kinase (MAPK) signalling pathway (Wallace et al., 2009). The stimulus/response curve of the MAPK has been found to be as steep as that of a cooperative enzyme with a Hill coefficient of 4 to 5 (Huang and Ferrell, 1996), making the steep Hill function appropriate to model hepcidin expression.

Ferritin modelling is similar to Salgado et al. (2010). Iron from the LIP binds to, and is internalised in, ferritin with mass action kinetics. Internalised iron release from ferritin occurs through two reactions. The average amount of iron internalised per ferritin affects the iron release rate and this is modelled using Equation 3.2.11 (adapted from Salgado et al. (2010)):

$$v = [\mathrm{S}] \cdot k_{\mathrm{loss}} \cdot \left(1 + \frac{0.048 \cdot \frac{[\mathrm{FT1}]}{[\mathrm{FT}]}}{1 + \frac{[\mathrm{FT1}]}{[\mathrm{FT}]}} \right). \tag{3.2.11}$$

Where S is internalised iron, k_{loss} is the rate constant and $\mathrm{FT1}/\mathrm{FT}$ is the ratio of iron internalised in ferritin to total ferritin available. Iron is also released from ferritin when the entire ferritin cage is degraded. The kinetics of ferritin degradation are mass action. However, the amount of iron released when a ferritin cage is degraded is an average based on ferritin levels and total iron internalised in ferritin. Incorporating mass action and ferritin saturation ratio gives the following rate law for $\mathrm{FT1} \rightarrow \mathrm{LIP}; \mathrm{FT1}$ FT.

$$v = [\mathrm{S}] \cdot k \cdot \frac{[\mathrm{FT1}]}{[\mathrm{FT}]}. \tag{3.2.12}$$

Iron export rate was modelled using a Hill equation (Equation 3.2.9), with ferroportin as the modifier and a Hill coefficient of 1. K^{n_H} was assumed to be around the steady state concentration of ferroportin. A rate (V) of $40\mathrm{pM} \cdot (10^6 \text{ cells} \cdot 5\mathrm{min})^{-1}$ was used from Sarkar et al. (2003). These values were substituted into the equation and solved for a.

Ferroportin expression rates and degradation rates are poorly understood. Ferroportin abundance data (Wang et al., 2012) led to an estimate of ferroportin concentration around $0.16\mu M$. The hepcidin induced degradation of ferroportin is represented in the model by a rate law in the form of Equation 3.2.9 with a Hill coefficient $n_H = 5$ (see above) and

a K^{n_H} equal to the measured concentration of hepcidin (Zaritsky et al., 2010) (see Table 3.1). A maximal rate of degradation of 1 nMs^{-1} was then assumed, and using the steady state concentration of ferroportin, the rate constant can be estimated as 0.0002315 s^{-1}. The ferroportin synthesis rate was then calculated to produce the required steady-state concentration of ferroportin at the nominal hepcidin concentration.

The HFE-TfR2 binding and dissociation constants were also not available and so it was assumed that they were the same as those of TfR1-HFE. Finally, the HFE-TfR and HFE-TfR2 degradation rates are also not known; a value was used that is an order of magnitude lower than the half life for unbound TfR (i.e. it was assumed that the complex is more stable than the free form of TfR).

Although DMT1 may contribute towards transferrin bound iron uptake in hepatocytes, this contribution has been found to be minor. DMT1 knockout has little affect on iron metabolism (Wang and Knutson, 2013) and therefore DMT1 was not included in the model.

The two iron response proteins (IRP1 and IRP2), which are responsible for cellular iron regulation, were modelled as a single metabolite in this study as the mechanistic differences in their regulatory roles is poorly understood. Equivalent regulation by both IRPs has been found in multiple studies (Kim et al., 1995; Ke et al., 1998; Erlitzki et al., 2002).

Global sensitivity analysis was performed as described in Sahle et al. (2008). The sensitivities obtained were normalized and represent flux and concentration control coefficients in metabolic control analysis (Kacser and Burns, 1973; Heinrich and Rapoport, 1974). The control coefficients were optimised to find a maximum and minimum value, which they could reach when all parameters were constrained within 10% of their chosen values. A particle swarm optimisation algorithm (Eberhart and Kennedy, 1995) was chosen as an efficient but reliable method of finding the maximum and minimum coefficients. Optimisation problems with many variables are computationally difficult and therefore an HTCondor (Litzkow et al., 1988) distributed computing system was used to perform the control coefficient optimisation calculations. The interface between the HTCondor system and the COPASI software was managed using Condor-COPASI (Kent et al., 2012a).

To perform analysis of receptor response in a similar manner to the EPO system studied by Becker et al. (2010), initial conditions were adjusted to recreate the experimental conditions used for EPO. Haem was fixed at zero to isolate transferrin-bound iron uptake. The LIP depletion reaction was decreased due to the lower iron uptake, which gave iron a similar half-life to EPO. Initial concentrations for all metabolites were set to steady-state concentrations, with the exception of the LIP and iron bound to all receptors which were set to zero. Extracellular transferrin bound iron was allowed to vary and set at increasing concentrations to scan receptor response. Time courses were calculated for Tf-Fe-TfR1, 2(Tf-Fe)-TfR1, Tf-Fe-TfR2 and 2(Tf-Fe)-TfR2 as iron is a two-staged binding process with two receptors. The area under the curve of the receptor response time courses was

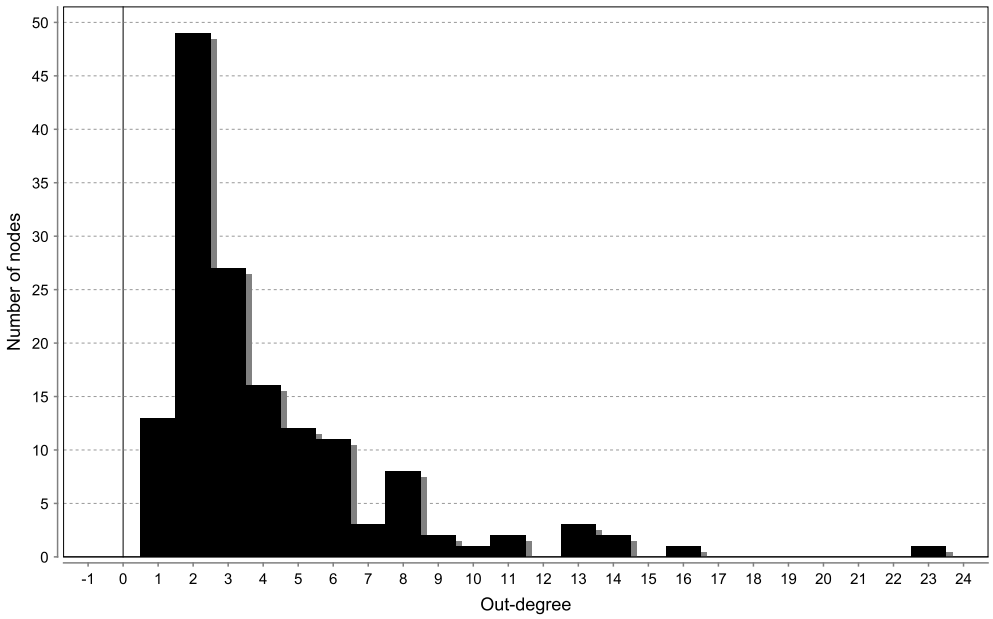

Figure 3.4: **The node degree distribution of the general map of iron metabolism.** A power law distribution was found, which is indicative of the presence of hub nodes.

calculated using COPASI global quantities. The area under both curves, for the two-staged binding process, were calculated for each receptor. Total integral receptor binding for each receptor is a sum of the two areas under the curves. The integral for total TFR1 binding is a sum of the integrals of time courses for Tf-Fe-TfR1 and 2(Tf-Fe)-TfR1.

3.3 Results

3.3.1 Graph Theory Analysis on Map of Iron Metabolism

Initial graph theoretic analysis was used to identify central nodes in the general map of iron metabolism.

The graph of the general map of iron metabolism has 151 nodes with a characteristic path length of 4.722. This low average path length means a signal can travel quickly from one area of a network to another to react quickly to stimuli; this is essential to maintain levels of iron at safe levels despite fluctuating input.

The general map of iron metabolism and all tissue-specific subnetworks show a power-law degree distribution with more hub nodes than a typical random graph. This can be seen in Figure 3.4. The general map's node degree distribution fits $y = 55.381x^{-1.274}$ with $R^2 = 0.705$. The architecture of all the networks suggests each tissue type is resilient to failure of random nodes as there are only a few hub nodes. However the hub nodes identified would be highly sensitive to failure.

Betweenness centrality analysis of the general and tissue-specific maps of iron metabolism are shown in Table 3.2. External Fe^{2+} was found to have high betweenness centrality in all cell types except reticulocytes where Fe^{2+} is a leaf node and therefore

has a betweenness centrality of 0. This was due to no evidence being found for Dcytb-mediated reduction of Fe^{3+} in reticulocytes. Haem has widely varying betweenness centrality across cell types between 0.19 in liver and 0.27 in macrophage. The higher value in the macrophage may be due to haem being a key link between the phagosome and the rest of the cell which is unique to that cell type. Coproporphyrinogen III (COPRO III) is a haem precursor in the haem bio-synthesis pathway that was found to have high betweenness centrality. Metabolites that are transported between subcellular compartments, such as COPRO III, show high betweenness centrality as they link the highly connected subcellular networks. Initial modelling efforts abstracted a cell to a single compartment for simplicity, and therefore metabolites with high centrality due to subcellular relocation were assessed for inclusion based on literature evidence and available data.

Table 3.2: **Betweenness centrality values for general and tissue specific maps of iron metabolism converted from SBGN using the Technique in section 3.2.1**

SBML name	General	Liver	Intestinal	Macrophage	Reticulocyte
Fe^{2+}	0.54	0.52	0.52	0.49	0.49
Fe^{3+}	0.14	0.15	0.14	0.12	0.084
O_2	0.13	0.068	0.066	0.056	0.071
COPRO III	0.11	0.12	0.12	0.096	0.13
haem	0.11	0.19	0.18	0.27	0.23
URO III	0.069	0.076	0.077	0.07	0.084
TfR1	0.064	0.075	0.064	0.057	0.041
HMB	0.056	0.064	0.065	0.059	0.069
Fpn	0.054	0.049	0.019	0.047	0.037
proteins	0.051	0.052	0.063	0.055	0.054
PBG	0.048	0.058	0.058	0.053	0.058
ALAS1	0.044	0.052	0.053	0.048	0
ALA	0.042	0.052	0.052	0.048	0.051
ROS	0.041	0.037	0.03	0.039	0.04
Tf-Fe	0.039	0.045	0.019	0.016	0.037
Fxn	0.039	0.085	0.084	0.065	0
IRP2	0.031	0.036	0.034	0.029	0.039
IRP1-P	0.03	0.035	0.033	0.05	0
IRP1	0.03	0.035	0.033	0.029	0.04
sa109 degraded	0.03	0.022	0.015	0.068	0.003
Fe-S	0.029	0.034	0.035	0.029	0.032
Hepc	0.026	0.027	0	0.014	0
Lf-Fe	0.026	0.03	0.03	0.024	0
Fe-NGAL+R	0.025	0	0.031	0.028	0.076
Tf	0.024	0.027	0.018	0.015	0.023
Hepc	0.024	0.027	0.014	0.012	0.037
NGAL+R+sid	0.023	0.027	0.027	0.025	0.03

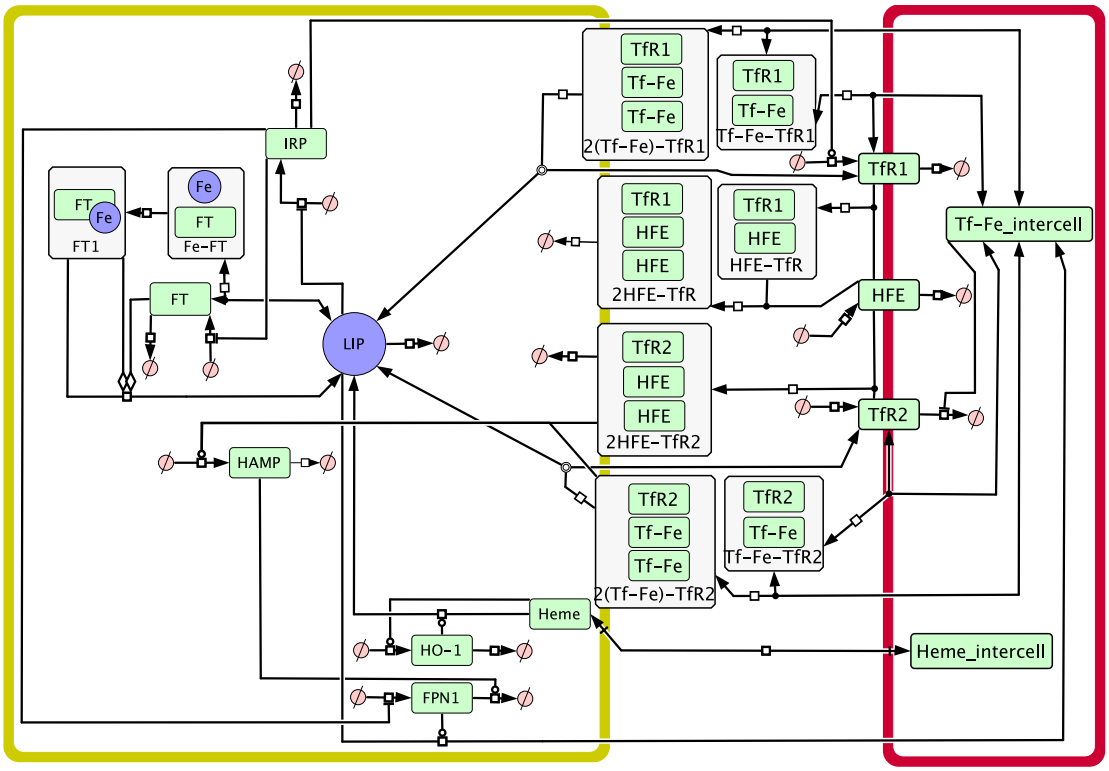

Figure 3.5: **SBGN process diagram of human liver iron metabolism model.** The compartment with yellow boundary represents the hepatocyte, while the compartment with red boundary represents plasma. Species overlayed on the compartment boundaries represent membrane-associated species. Abbreviations: Fe: iron, FPN1: ferroportin, FT: ferritin, HAMP: hepcidin, haem: intracellular haem, haem_intercell: plasma haem, HFE: human haemochromatosis protein, HO-1: haem oxygenase 1, IRP: iron response protein, LIP: labile iron pool, Tf-Fe_intercell: plasma transferrin-bound iron, TfR1: transferrin receptor 1, TfR2: transferrin receptor 2. Complexes are represented in boxes with the component species. In the special case of the ferritin-iron complex symbol, the amounts of each species are not in stoichiometric amounts (since there are thousands of iron ions per ferritin).

3.3.2 Model of Liver Iron Metabolism

The model was constructed based on many published data on individual molecular interactions (Section 3.2.2), and is available from BioModels (http://identifiers.org/biomodels.db/MODEL1302260000) (Le Novère et al., 2006). Figure 3.5 depicts a process diagram of the model, using the SBGN standard (Novere et al., 2009), where all the considered interactions are shown. It is important to highlight that while results described below are largely in agreement with observations, the model was not forced to replicate them. The extent of agreement between model and physiological data provides confidence that the model is accurate enough to carry out "what-if" type of experiments that can provide quantitative explanation of iron regulation in the liver.

3.3.3 Steady State Validation

Initial verification of the hepatocyte model was performed by assessing the ability to recreate biologically accurate, experimentally observed, steady-state concentrations of metabolites and rates of reactions. Simulations were run to steady state using the parameters and initial conditions from Table 3.1 and 3.3. Table 3.4 compares steady state concentrations of metabolites and reactions with experimental observations.

Chua et al. (2010) injected radio-labeled transferrin-bound iron into the serum of mice and measured the total uptake of the liver after 120 minutes. The uptake rate when expressed as mol/s was close to that found at steady state by the computational model (Table 3.4).

A technical aspect of note in this steady-state solution, is that it is very stiff. This originates because one section of the model (the cycle composed of iron binding to ferritin, internalization and release) is orders of magnitude faster than the rest. Arguably this could be resolved by simplifying the model, but the model was left intact because this cycling is an important aspect of iron metabolism and allows the representation of ferritin saturation. Even though the stiffness is high, COPASI is able to cope by using an appropriate numerical method (Newton's method).

Table 3.3: **Reaction Parameters**

Name	**Reaction**	**Function**	**Parameters**	**Source**
Fpn export	LIP → Tf-Fe_intercell; FPN1	Hill function →	$a = 15\ mol \cdot\ s^{-1}$, $n_H = 1$, $K = 1 \times 10^{-6}$ mol	Sarkar et al. (2003)
TfR1 expression	→ TfR; IRP	Hill function →	$a = 6 \times 10^{-12}\ s^{-1}$, $n_H = 1$, $K = 1 \times 10^{-6}$ mol	Chloupková et al. (2010)
TfR1 degradation	TfR →	Mass action	$k = 8.37 \times 10^{-6}\ s^{-1}$	Johnson and Enns (2004)
Ferroportin expression	→ FPN1; IRP	Hill function -|	$a = 4 \times 10^{-9}\ s^{-1}$, $n_H = 1$, $K = 1 \times 10^{-6}$ mol	
Fpn degradation hepc	FPN1 → ; HAMP	Hill function →	$a = 2.315 \times 10^{-5}\ s^{-1}$, $n_H = 1$, $K = 1 \times 10^{-9}$ mol	
IRP expression	→ IRP; LIP	Hill function -|	$a = 4 \times 10^{-11}\ s^{-1}$, $n_H = 1$, $K = 1 \times 10^{-6}$ mol	Pantopoulos et al. (1995)
IRP degradation	IRP →	Mass action	$k = 1.59 \times 10^{-5}\ s^{-1}$	Pantopoulos et al. (1995)

Continued on Next Page...

Table 3.3 – Continued

Name	**Reaction**	**Function**	**Parameters**	**Source**
HFE degradation	HFE $\rightarrow$	Mass action	k = 6.418×10^{-5} s^{-2}	Wang et al. (2003a)
HFE expression	$\rightarrow$ HFE	Constant flux	v = 2.3469×10^{-11} $mol(1 \cdot s)^{-1}$	Wang et al. (2003a)
TfR2 expression	$\rightarrow$ TfR2	Constant flux	v = 2×10^{-11} $mol(1 \cdot s)^{-1}$	Chloupková et al. (2010)
TfR2 degradation	TfR2 $\rightarrow$; Tf-Fe_intercell	Hill function -|	a = 3.2×10^{-05} s^{-1}, $n_H = 1$, $K = 2.5 \times 10^{9}$ mol	Chloupková et al. (2010)
Hepcidin expression	$\rightarrow$ HAMP; 2HFE-TfR2 2(Tf-Fe)-TfR2	Hill function $\rightarrow$	a = 5×10^{-12} s^{-1}, $n_H = 5$, K = 1.35×10^{-7} mol, a = 5×10^{-12} $mol \cdot s^{-1}$, $K = 6 \times 10^{-7}$ mol	Zaritsky et al. (2010)
Hepcidin degradation	HAMP $\rightarrow$	Mass action	k = 9.63×10^{-5} s^{-1}	Rivera et al. (2005)

Continued on Next Page...

Table 3.3 – Continued

Name	Reaction	Function	Parameters	Source
Haem oxygenation	Haem → LIP; HO-1	Henri-Michaelis-Menten	kcat = $17777.7\ s^{-1}$, Km = $2 \times 10^{-6}\ mol \cdot l^{-1}$	Kinobe et al. (2006)
HFE TfR1 binding	HFE + TfR → HFE-TfR	Mass action	k = $1.102 \times 10^{6}\ l(mol \cdot s)^{-1}$	West et al. (2000)
HFE TfR1 release	HFE-TfR → HFE + TfR	Mass action	k = $0.08\ s^{-1}$	West et al. (2000)
TfR1 binding	Tf-Fe_intercell + TfR → Tf-Fe-TfR1	Mass action	k = $837400\ l(mol \cdot s)^{-1}$	West et al. (2000)
TfR1 release	Tf-Fe-TfR1 → Tf-Fe_intercell + TfR	Mass action	k = $9.142 \times 10^{-4}\ s^{-1}$	West et al. (2000)
HFE TfR2 binding	2∗HFE + TfR2 → 2HFE-TfR2	Mass action	k = $3.9438 \times 10^{11}\ l^{2}(mol^{2} \cdot s)^{-1}$	
HFE TfR2 release	2HFE-TfR2 → 2 * HFE + TfR2	Mass action	k = $0.0018\ s^{-1}$	
TfR2 binding	Tf-Fe_intercell + TfR2 → Tf-Fe-TfR2	Mass action	k = $222390\ l(mol \cdot s)^{-1}$	West et al. (2000)
TfR2 release	Tf-Fe-TfR2 → Tf-Fe_intercell + TfR2	Mass action	k = $0.0061\ s^{-1}$	West et al. (2000)
TfR1 binding 2	Tf-Fe-TfR1 + Tf-Fe_intercell → 2(Tf-Fe)-TfR1	Mass action	k = $121400\ l(mol \cdot s)^{-1}$	West et al. (2000)

Continued on Next Page...

Table 3.3 – Continued

Name	Reaction	Function	Parameters	Source
TfR1 release 2	2(Tf-Fe)-TfR1 → Tf-Fe-TfR1 + Tf-Fe_intercell	Mass action	$k = 0.003535\ s^{-1}$	West et al. (2000)
HFE TfR1 binding 2	HFE-TfR + HFE → 2HFE-TfR	Mass action	$k = 1.102 \times 10^6\ l(mol \cdot s)^{-1}$	West et al. (2000)
HFE TfR1 release 2	2HFE-TfR → HFE-TfR + HFE	Mass action	$k = 0.08\ s^{-1}$	West et al. (2000)
TfR1 release 2	2(Tf-Fe)-TfR1 → Tf-Fe-TfR1 + Tf-Fe_intercell	Mass action	$k = 0.003535\ s^{-1}$	West et al. (2000)
TfR1 iron internalisation	2(Tf-Fe)-TfR1 → 4(LIP) + TfR	Mass action	$k = 0.8333\, l \cdot s^{-1}$	Byrne et al. (2010)
TfR2 iron internalisation	2(Tf-Fe)-TfR2 → 4(LIP)-TfR2	Mass action	$k = 0.8333\, l \cdot s^{-1}$	Byrne et al. (2010)
outFlow	LIP →	Mass action (irreversible)	$k = 4 \times 10^{-4}\ s^{-1}$	
Ferritin iron binding	LIP + FT → Fe-FT	Mass action	$k = 4.71 \times 10^{10}\ l(mol \cdot s)^{-1}$	Salgado et al. (2010)
Ferritin iron release	Fe-FT → LIP + FT	Mass action	$k = 22922\ s^{-1}$	Salgado et al. (2010)
Ferritin iron internalisation	Fe-FT → FT1 + FT	Mass action	$k = 108000\ s^{-1}$	Salgado et al. (2010)
Ferritin internalised iron release	FT1 → LIP; FT1 FT	Kloss Hill	$kloss = 13.112\ s^{-1}$	Salgado et al. (2010)

Continued on Next Page...

Table 3.3 – Continued

Name	Reaction	Function	Parameters	Source
ferritin expression	$\rightarrow$ FT; IRP	Hill function -|	a = 2.312×10^{-13} s^{-1}, $n_H = 1$, K = 1×10^{-6} mol	Cozzi (2003)
HO1 degradation	HO-1 $\rightarrow$	Mass action	k = 3.209×10^{-5} s^{-1}	Pimstone et al. (1971)
HO1 expression	$\rightarrow$ HO-1; Haem	Hill function $\rightarrow$	a = 2.1432×10^{-15} s^{-1}, K = 1×10^{-9} mol	Bao et al. (2010)
Ferritin degradation full	FT $\rightarrow$	Mass action	k = 1.203×10^{-5} s^{-1}	Salgado et al. (2010)
Haem uptake	Haem_intercell $\rightarrow$ Haem	Henri-Michaelis-Menten	Km = 1.25×10^{-4} mol, v = 1.034×10^{-5} mol $\cdot$ s^{-1}	Shayeghi et al. (2005)
Haem export	Haem $\rightarrow$ Haem_intercell	Henri-Michaelis-Menten	Km = 1.78×10^{-5} mol, v = 2.18×10^{-5} mol $\cdot$ s^{-1}	Tamura et al. (2006)
Ferritin degradation full iron release	FT1 $\rightarrow$ LIP; FT1 FT	Mass action ferritin	k = 1.203×10^{-5} s^{-1}	Salgado et al. (2010)

Continued on Next Page...

Table 3.3 – Continued

Name	**Reaction**	**Function**	**Parameters**	**Source**
HFE-TfR degradation	2HFE-TfR $\rightarrow$	Mass action	k = 8.37×10^{-7} s^{-1}	
HFE-TfR2 degradation	2HFE-TfR2 $\rightarrow$	Mass action	k = 8.37×10^{-7} s^{-1}	
int iron import DMT1	gutFe2 $\rightarrow$ intLIP; intDMT1 gutFe2	Henri-Michaelis-Menten	C = 3.833, kcat = 4.8×10^{-6}	Iyengar et al. (2009) & Wang et al. (2003b)

Table 3.4: **Steady State Verification**

Metabolite	Model	Experimental	Reference
Labile iron pool	$0.804\ \mu$M	$0.2 - 1.5\ \mu$M	Epsztejn et al. (1997)
Iron response protein	836000 cell^{-1}	$\sim$ 700000 cell^{-1}	Cairo et al. (1998)
Ferritin	4845 cell^{-1}	$3000 - 6000$ cell^{-1} (mRNA), $2.5 - 54600$ cell^{-1} (protein)	Cairo et al. (1998), Summers et al. (1974)
TfR	1.74×10^5 cell^{-1}	$1.6 - 2 \times 10^5$ cell^{-1}	Salter-Cid et al. (1999)
TfR2	$4.63 \times$ [TfR1]	$4.5 - 6.1 \times$ [TfR1]	Chloupková et al. (2010)
Iron per ferritin	2272 average	$\sim$ 2400	Sibille et al. (1988)
Hepcidin	5.32 nM	$3.5 - 8.3$ nM	Swinkels et al. (2008)

Reaction	Model	Experimental	Reference
TBI iron import rate	$2.67\ \mu\text{M} \cdot \text{s}^{-1}$	$2.08\ \mu\text{M} \cdot \text{s}^{-1}$	Chua et al. (2010)

3.3.4 Response to Iron Challenge

An oral dose of iron creates a fluctuation in serum transferrin saturation of approximately 10% (Girelli et al., 2011). The fixed serum iron concentration in the simulation was replaced by a transient increase in concentration, equivalent to a 10% increase in transferrin saturation, as a simulation of oral iron dosage on hepatocytes. The simulated hepcidin response (Figure 3.6) is consistent with the hepcidin response measured by Girelli et al. (2011). The time scale and dynamics of the hepcidin response to iron challenge has been accurately replicated in the simulation presented here. Hereditary haemochromatosis simulations show reduced hepcidin levels and peak response compared to WT (Wild Type) (Figure 3.6). The simulation appears to present an approximation of the two experimental techniques from Girelli et al. (2011) (mass spectrometry and ELISA), reaching a peak between 4 and 8 hours and returning to around basal levels within 24 hours.

3.3.5 Cellular Iron Regulation

The computational model supports the proposed role of HFE and TfR2 as sensors of systemic iron. Figure 3.7A shows that as the concentration of HFE bound to TfR2 (HFE-TfR2) increases with serum transferrin-bound iron (Tf-Fe_intercell), at the same time the abundance of HFE bound to TfR1 (HFE-TfR1) decreases. The increase in HFE-TfR2 complex, even though of small magnitude, promotes increased expression of hepcidin (Figure 3.7B). Increasing HFE-TfR2 complex as a result of HFE-TfR1 reduction induces increased hepcidin. It is through this mechanism that liver cells sense serum iron levels and control whole body iron metabolism through the action of hepcidin. Although the LIP increases with serum transferrin-bound iron in this simulation, this is only because

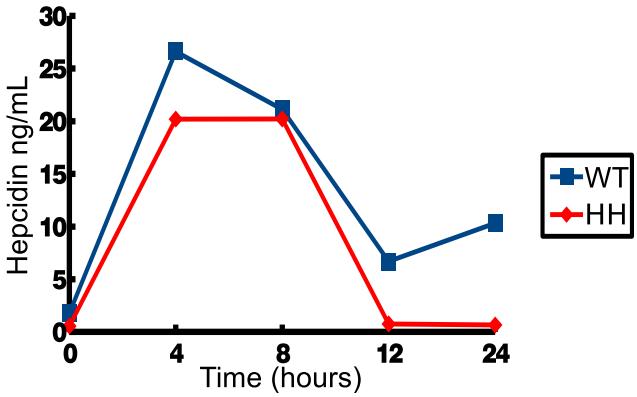

Figure 3.6: **Simulated time course concentrations of hepcidin, in wild type (WT) and hereditary haemochromatosis (HH), in response to changing serum transferrin-bound iron levels.**

the model does not include the action of hepcidin in reducing duodenal export of iron. Expression and secretion of hepcidin will have the effect of degrading intestinal ferroportin which leads to decreased iron export and therefore decreased serum iron.

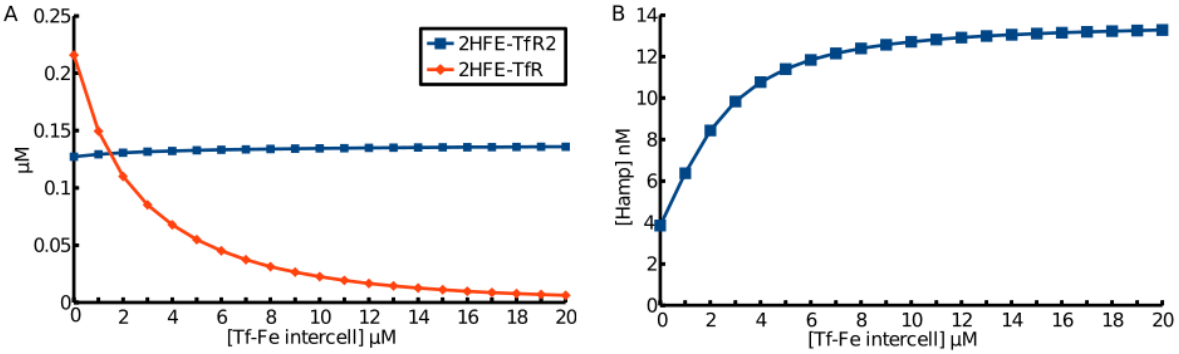

Figure 3.7: **Simulated steady state concentrations of HFE-TfR1/2 complexes (A) and hepcidin (B) in response to increasing serum Tf-Fe.**

3.3.6 Hereditary Haemochromatosis Simulation

Hereditary haemochromatosis is the most common hereditary disorder with a prevalence higher than 1 in 500 (Asberg, 2001). Type 1 haemochromatosis is the most common and is caused by a mutation in the HFE gene leading to a misregulation of hepcidin and consequent systemic iron overload.

To create a simulation of type 1 hereditary haemochromatosis, a virtual HFE knockdown was performed by reducing 100-fold the rate constant for HFE synthesis in the model. 100-fold decrease was chosen as complete inhibition of HFE in experimental organisms could not be confirmed and this approximates the lower limit of detection possible (Riedel et al., 1999). The simulation was run to steady state and results were compared

with experimental findings.

Qualitative validation showed the *in silico* HFE knockdown could reproduce multiple experimental findings as shown in Table 3.5. The simulation of type-1 hereditary haemochromatosis closely matches experimental findings at steady state. Quantitatively the model was unable to reproduce accurately the finding that *HFE -/-* mice have 3 times higher hepatic iron levels (Fleming et al., 2001). This was due to the fixed intercellular transferrin bound iron concentration in the model, unlike in *HFE -/-* mice where there is an increase in transferrin saturation as a result of increased intestinal iron absorption (Fleming et al., 2001).

Table 3.5: **HFE Knockdown Validation**

+ up-regulated, - down-regulated, = no change, $\approx$ no significant change.

Metabolite	Model	Experiment	Reference
IRP	-	-	Riedel et al. (1999)
LIP	+	+	Riedel et al. (1999)
HAMP	-	-	van Dijk et al. (2008)
TfR2	+	+	Robb and Wessling-Resnick (2004)

Reaction	Model	Experimental	Reference
TfR1/2 iron import	+	+	Riedel et al. (1999)
FT expression	+	+	Riedel et al. (1999)
TfR expression	-	-	Riedel et al. (1999)
FPN expression	$\approx$	=	Ludwiczek et al. (2005)

Despite fixed extracellular conditions the model predicted an intracellular hepatocyte iron overload, which would be further compounded by the systemic effects of the misregulation of hepcidin. The simulation recreated increased ferroportin levels despite the expression of ferroportin remaining the same as wild type, which was consistent with mRNA measurements from Ludwiczek et al. (2005). mRNA-based experiments can be used to validate expression rates and protein assays are able to validate steady-state protein concentrations. This is because both expression rates and steady-state protein concentrations are available as results from the computational model. As expression rate was consistent between health and disease changes in ferroportin concentration must be due to changes in degradation rate.

The models of health and haemochromatosis disease were both also able to replicate the dynamics of experimental responses to changing dietary iron conditions. An approximate 2-fold increase in hepatic ferroportin expression is caused by increased dietary iron in both haemochromatosis and healthy mice (Ludwiczek et al., 2005). The model presented here recreated this increase with increasing intercellular iron as can be seen in Figure 3.8. Ferroportin expression rate in the model doubles in response to changing serum iron concentrations as verified experimentally.

HFE knockout has been shown to impair the induction of hepcidin by iron in mouse (Ludwiczek et al., 2005) and human (Piperno et al., 2007) hepatocytes. This was seen in

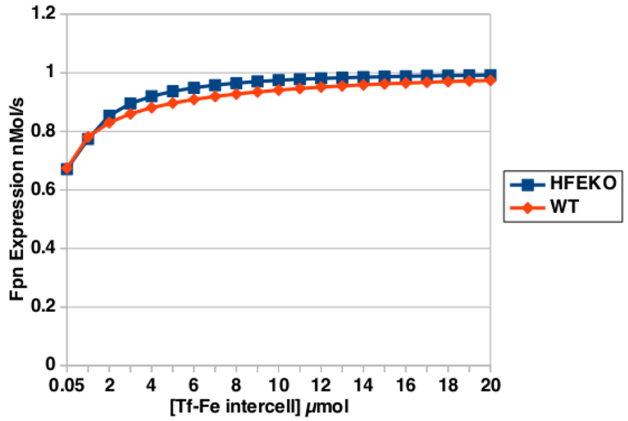

Figure 3.8: **HFE knockdown (HFEKO) HH simulation and wild type (WT) simulation of Tf-Fe against ferroportin (Fpn) expression.**

the computational model as increasing transferrin-bound iron did not induce hepcidin as strongly in HFE knockdown.

Although an increase in transferrin receptor 2 was observed in the model ($1.77\mu M$ health; $2.80\mu M$ type 1 haemochromatosis), the up-regulation was slightly smaller than the change observed *in vivo* (Robb and Wessling-Resnick, 2004). This is due to the model having fixed extracellular transferrin-bound iron concentration, in contrast to haemochromatosis where this concentration increases due to higher absorption in the intestine.

Type 3 haemochromatosis results in similar phenotype as type 1 haemochromatosis, however the mutation is found in the TfR2 gene as opposed to HFE. A virtual TfR2 knockdown mutation was performed by decreasing 100-fold the rate constant of synthesis of TfR2 in the model. Model results were then compared with the findings of Chua et al. (2010). The simulation showed a steady-state decrease of liver TfR1 from $0.29\mu M$ to $0.19\mu M$ with TfR2 knockdown. This is supported by an approximate halving of TfR1 levels in TfR2 mutant mice (Chua et al., 2010). An increase in hepcidin, and consequent decrease in ferroportin, as seen in mice was matched by the simulation.

An iron overload phenotype with increased intracellular iron is not recreated by the model of the TfR2 mutant. This is, again, due to the fixed serum transferrin-bound iron concentration, while in the whole body there would be increased iron absorption from the diet through the effect of hepcidin.

3.3.7 Metabolic Control Analysis

Metabolic control analysis (MCA) is a standard technique to identify the reactions that have the largest influence on metabolite concentrations or reaction fluxes at a steady state (Kacser and Burns, 1973; Heinrich and Rapoport, 1974). MCA is a special type of sensitivity analysis and thus is used to quantify the distributed control of the biochemical network. A control coefficient measures the relative change of the variable of interest caused by a small change in the reaction rate (e.g. a control coefficient can be interpreted

as the percentage change of the variable given a 1% change in the reaction rate).

The control over the concentration of the labile iron pool by each of the model reactions can be seen in Table 3.6. The synthesis and degradation of TfR2, TfR1, HFE and the formation of their complexes were found to have the highest control over the labile iron pool. Synthesis and degradation of IRP were also found to have some degree of control, but synthesis and degradation of hepcidin have, surprisingly, a very small effect on the labile iron pool.

Table 3.6: **Metabolic Control Analysis: Concentration-control coefficients for the labile iron pool.**

Reaction	Local	Minimum	Maximum
TfR2 expression	0.89	0.52	1.4
Fpn export	-0.83	-0.92	-0.7
TfR2 binding	0.57	0.3	0.9
TfR2 degradation	-0.56	-0.9	-0.29
Fpn degradation	0.35	0.19	0.5
Ferroportin expression	-0.35	-0.5	-0.18
HFE expression	-0.31	-0.62	0.35
TfR1 expression	0.26	0.065	0.5
TfR1 binding	0.26	0.066	0.5
TfR1 degradation	-0.26	-0.5	-0.066
IRP expression	0.21	0.075	0.3
IRP degradation	-0.21	-0.35	-0.075
HFETfR2 degradation	-0.034	-0.68	0.00023
Hepcidin expression	0.028	0.00044	0.66
Hepcidin degradation	-0.028	-0.79	-0.00058
HFE degradation	0.016	-0.026	0.039
TfR2 binding 2	0.01	0.3	0.9
TfR2 release	-0.01	-0.019	-0.0043
HFE TfR2 binding	-0.0067	-0.019	0.022
HFE TfR2 release	0.0064	-0.021	0.018
TfR2 iron internalisation	-0.0034	-0.16	0.00056
HFE TfR1 binding	-0.0014	-0.012	0.000074
HFE TfR1 release	0.0014	0.000076	0.012
HFE TfR1 binding 2	-0.0014	-0.012	-0.000074
HFE TfR1 release 2	0.0014	0.000074	0.012
HFETfR degradation	-0.0014	-0.012	-0.000074
Sum	0.00042		

Control over the hepcidin concentration was also measured (Table 3.7), as the ability to control hepatic hepcidin levels could provide therapeutic opportunities to control whole system iron metabolism, due to its action on other tissues. Interestingly, in addition to the expression and degradation of hepcidin itself, the expression of HFE and degradation of HFETfR2 complex have almost as much control over hepcidin. The expression of TfR2 has a considerably lower effect, though still significant.

Flux-control coefficients, which indicate the control that reactions have on a chosen reaction flux, were also determined. The flux-control coefficients for the ferroportin-

Table 3.7: **Metabolic Control Analysis: Concentration-control coefficients for hepcidin.**

Reaction	Local	Minimum	Maximum
Hepcidin expression	1	0.51	1.5
Hepcidin degradation	-1	-1	-1
HFETfR2 degradation	-0.96	-1.4	-0.38
HFE expression	0.91	0.27	1.3
TfR2 expression	0.24	0.098	0.49
TfR2 degradation	-0.15	-0.29	-0.064
TfR2 binding	0.13	0.056	0.27
TfR2 iron internalisation	-0.13	-0.27	-0.056
HFE degradation	-0.047	-0.1	-0.012
HFE TfR2 binding	0.025	0.0063	0.057
HFE TfR2 release	-0.023	-0.056	-0.006
TfR2 binding 2	0.0023	0.00081	0.0059
TfR2 release	-0.0023	-0.0059	-0.00081
HFE TfR1 binding	-0.00093	-0.0073	-0.000052
HFE TfR1 release	0.00093	0.000048	0.007
HFE TfR1 binding 2	-0.00093	-0.0073	-0.000053
HFE TfR1 release 2	0.00093	0.000053	0.0073
HFETfR degradation	-0.00093	-0.0073	-0.000057
TfR1 expression	-0.0008	-0.0061	-0.000044
TfR1 degradation	0.00079	0.000045	0.0062
IRP expresion	-0.00054	-0.0028	-0.000047
IRP degradation	0.00054	0.000042	0.0035
Fpn export	-0.00045	-0.0028	-0.000043
Fpn degradation	0.00019	0.000015	0.0015
Ferroportin expression	-0.00019	-0.0015	-0.000014
TfR1 binding	0.00014	0.0000038	0.0014
TfR2 release 2	-0.000064	-0.00018	-0.000022
Sum	0.00000042		

mediated iron export reaction are given in Table 3.8. This reaction is of particular interest as it is the only method of iron export. Therefore, controlling this reaction rate could be important in treating various iron disorders, including haemochromatosis and anaemia. The reactions of synthesis and degradation of TfR1, TfR2 and HFE were found to have high control, despite not having direct interactions with ferroportin. TfR1 and TfR2 may show consistently high control due to having dual roles as iron importers and iron sensors, which control hepcidin expression.

A drawback of MCA, and any other local sensitivity analysis, is that it is only predictive for small changes of reaction rates. However, the changes that result in disease states are usually large, and experimental parameter estimation can result in large uncertainty. Thus, a global sensitivity analysis was also performed following the method described in Sahle et al. (2008). This generated the maximal and minimal values of the sensitivity coefficients, within a large space of parameter values. This technique is useful; for example, if there is uncertainty about the values of the model parameters, as it reveals the possible

Table 3.8: **Metabolic Control Analysis: Flux-control coefficients for the iron export out of the liver compartment.**

Reaction	Local	Minimum	Maximum
TfR2 expression	0.91	0.45	1.4
TfR2 binding	0.58	0.29	0.87
TfR2 degradation	-0.57	-0.86	-0.28
HFE expression	-0.35	-0.67	-0.19
TfR1 expression	0.27	0.068	0.51
TfR1 binding	0.27	0.068	0.52
TfR1 degradation	-0.27	-0.52	-0.067
IRP expresion	0.18	0.064	0.31
IRP degradation	-0.18	-0.31	-0.066
Fpn Export	0.15	0.063	0.27
Ferroportin Expression	0.065	0.019	0.15
Fpn degradation	-0.065	-0.15	-0.019
HFE degradation	0.018	0.0081	0.04
TfR2 release	-0.01	-0.019	-0.0041
TfR2 binding 2	0.01	0.0041	0.019
HFE TfR2 binding	-0.0077	-0.019	0.0029
HFE TfR2 release	0.0074	-0.0028	0.019
Hepcidin expression	-0.0052	-0.18	-0.000039
Hepcidin degradation	0.0052	0.000058	0.22
HFETfR2 degradation	-0.0023	-0.018	0.2
HFE TfR1 binding	-0.0014	-0.012	-0.000075
HFE TfR1 release	0.0014	0.000075	0.012
HFE TfR1 binding 2	-0.0014	-0.011	-0.000075
HFE TfR1 release 2	0.0014	0.000075	0.012
Ferroportin expression	-0.00019	-0.0015	-0.000014
TfR1 binding	0.00014	0.0000038	0.0014
TfR2 release 2	-0.000064	-0.00018	-0.000022
sum	1		

range of control of each one given the uncertainty. All parameters were allowed to vary within $\pm$ 10% and the maximal and minimal control coefficients were measured (Tables 3.6, 3.7 and 3.8).

In terms of the control of the labile iron pool (Table 3.6), the reactions with highest control in the reference steady state are still the ones with highest control in the global case (i.e. when all parameters have an uncertainty of $\pm 10\%$). However, TfR1 expression, TfR1 binding, TfR1 degradation, IRP expression and IRP degradation, which all have significant (but not the highest) control in the reference state, could have very low control in the global sense. On the other hand, HFETfR2 degradation, hepcidin expression, hepcidin degradation and TfR2 binding 2, have low control in the reference steady state, but could have significant control in the global sense. All other reactions have low control in any situation.

In the case of the control of hepcidin concentration (Table 3.7) the differences between the reference state and the global are much smaller overall, and only a few reactions could

be identified that have moderate control in the reference, but could have a bit less in the global sense (TfR2 expression, TfR2 binding, and TfR2 iron internalisation).

In the case of the control of the flux of iron export (Table 3.8), some reactions were found with high control in the reference that could have low control in the global sense: TfR1 expression, TfR1 biding, TfR1 degradation, IRP expression and IRP degradation. Hepcidin expression, hepcidin degradation, and HFETfR2 degradation have almost no control in the reference, but in the global sense they could exert considerable control. This is very similar to the situation of the control of the labile iron pool.

Chifman et al. (2012) analysed the parameter space of their core model of iron metabolism in breast epithelial cells, and concluded the system behaviour is far more dependent on the network structure than the exact parameters used. The analysis presented here lends some support to that finding, since only a few reactions could have different effect on the system if the parameters are wrong. A further scan of initial conditions for metabolites found that varying initial concentrations over 2 orders of magnitude had no affect on the steady state achieved (Table 3.4), indicating that the steady state found in these simulations is unique.

3.3.8 Receptor Properties

It is known that iron sensing by the transferrin receptors is responsive over a wide range of intercellular iron concentrations (Lin et al., 2007). The present model reproduces this well (Figure 3.10, $1\times$ turnover line). Becker et al. (2010) argued that a linear response of a receptor to its signal over a wide range could be achieved through a combination of the following: high receptor abundance, increased expression when required, recycling to the surface of internalised receptors, and high receptor turnover. This was illustrated with the behaviour of the erythropoietin (EPO) receptor (Becker et al., 2010). Since the present model contains essentially the same type of reactions that can lead to such a behaviour, simulations were carried out to investigate to what extent this linearity of response is present here. In this case, it is the response of the total amount of all forms of TfR1 and TfR2 bound to Tf-Fe against the amount of Tf-Fe_intercell that is important. A variable was created in the model to reflect the total receptor response (Section 3.2.2), and this variable was followed in a time-course response to an iron pulse (Figure 3.9). The simulated response to the iron pulse is remarkably similar, with a distinctive curve, to the response of the EPO receptor to EPO from Becker et al. (2010), their Figure 2B.

Becker et al. (2010) reported that the linearity of EPO-R response, measured by the integral of the response curve, is increased by increasing turnover rate of the receptor and this property was also observed in the simulation of TfR1 response (Figure 3.10). The range of linear response for the transferrin receptor depends on its half-life. This effect was first demonstrated in the EPO receptor by Becker et al. (2010) who found similar behaviour. The range in which the iron response is linear is smaller than that found for EPO (Figure 3.10). As TfR1's half-life in the model matches the experimentally determined

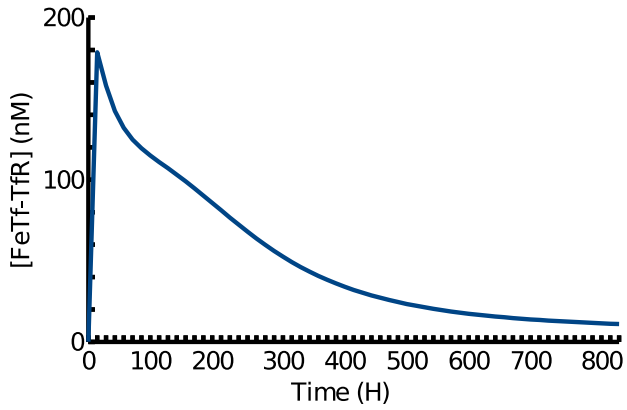

Figure 3.9: **Simulated time course of transferrin receptor complex formation following a pulse of iron.**

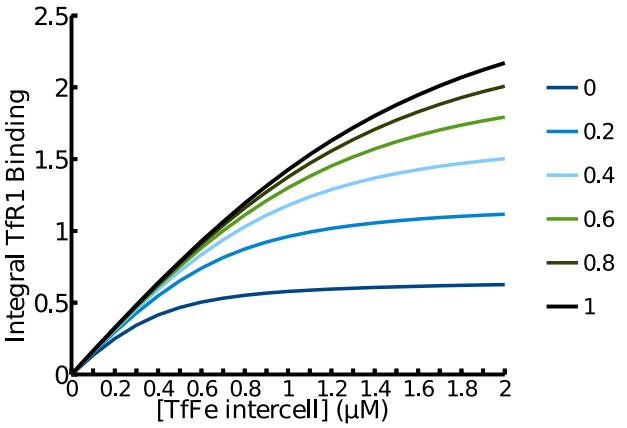

Figure 3.10: **Simulated integral transferrin receptor binding with increasing intercellular iron at various turnover rates.** Integral TfR1 binding is a measure of receptor response. Expression and degradation rate of TfR were simultaneously multiplied by a scaling factor between 0 and 1 to modulate receptor turnover rate.

value (Chloupková et al., 2010) the non-linear receptor response seen in the simulation is expected to be accurate. This suggests that TfR1 is a poor sensor for high levels of intercellular iron. On the other hand, TfR2 is more abundant than TfR1 (Chloupková et al., 2010) and accordingly shows an increased linearity for a greater range of intercellular iron concentrations (Figure 3.11). The response of TfR2 is approximately linear over a wide range of intercellular iron concentrations. This suggests the two transferrin receptors play different roles in sensing intercellular iron levels, with TfR2 providing a wide range of sensing and TfR1 sensing smaller perturbations. The activation of TfR2 directly influences the expression of hepcidin and therefore it is desirable for it to sense large systemic imbalances. TfR1 does not modulate hepcidin expression itself; instead, it plays a primary role as an iron transporter.

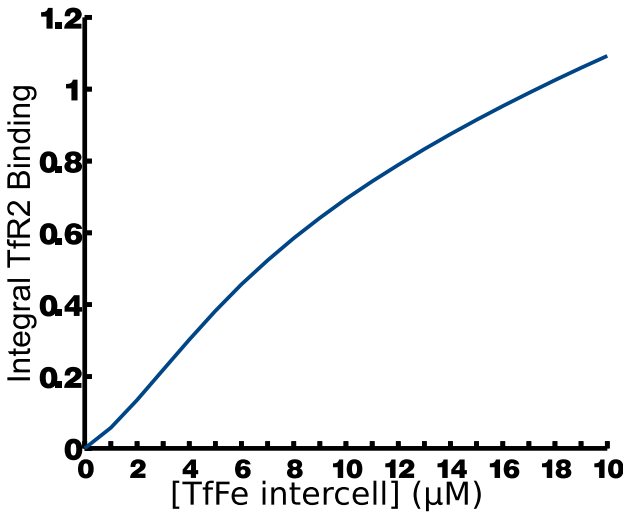

Figure 3.11: **TfR2 response** *versus* **intercellular transferrin-bound iron.**

3.4 Discussion

Iron is an essential element of life. In humans, it is involved in oxygen transport, respiration, biosynthesis, detoxification, and other processes. Iron regulation is essential because iron deficiency results in debilitating anaemia, while iron excess leads to free radical generation and is involved in many diseases (Kell, 2009). It is clear that healthy life depends on tight regulation of iron in the body. The mechanisms involved in iron absorption, transport, storage and regulation form a complex biochemical network (Hower et al., 2009). The liver has a central role in the regulation of systemic iron metabolism through secretion of the peptide hormone hepcidin.

Here I analysed the hepatic biochemical network involved in iron sensing and regulation through a mathematical model and computer simulation. The model was constructed based mostly on *in vitro* biochemical data, such as protein complex dissociation constants. The model was then validated by comparison with experimental data from multiple physiological studies at both steady state and during dynamic responses. Where quantitative data were available the model matched these well and also qualitatively recreated many findings from clinical and experimental investigations. The simulation accurately modelled the highly prevalent iron disorder haemochromatosis. The disease state was simulated through altering a single parameter of the model and showed quantitatively how an iron overload phenotype occurs in patients with an HFE mutation.

Due to the limited availability of quantitative clinical data on human iron metabolism, various other data sources, particularly from *in vitro* experiments and animal models, were integrated for the parameterisation of this model. This computational modelling effort constitutes a clinical translational approach, enabling data from multiple sources to improve our understanding of human iron metabolism. Several arguments could be raised to cast doubt on this approach, such as the the failure of *in vitro* conditions to mimic those *in vivo*, or the difference between animal models and humans. This means

that this type of data integration must be carefully monitored in terms of establishing the validity of the resulting model. Examining the behaviour of the model, by simulating it at different values of initial conditions or other parameters (parameter scans), is important to establish the limits of utility of the model. Global sensitivity analysis is another approach that determines the boundaries of parameter variation that the model tolerates before it becomes too distant from the actual system behaviour. A validation step is also essential to ensure similarity to the biological system; the simulation of haemochromatosis disease presented here matched clinical data (Table 3.5).

The precise regulatory mechanism behind transferrin receptors and HFE controlling hepcidin expression remains to be validated experimentally. However the model presented here supports current understanding that the interaction of TfR2 and HFE form the signal transduction pathway that leads to the induction of hepcidin expression (Gao et al., 2009).

The global metabolic control analysis results support the identification of the transferrin receptors, particularly TfR2, and HFE as potential therapeutic targets; a result that is robust even to inaccuracies in parameter values. Although hepcidin would be an intuitive point of high control of this system (and therefore a good therapeutic target), in the present model this is not the case. It seems that targeting the promoters of hepcidin expression may be more desirable. However this conclusion has to be expressed with some reservation that stems from the fact that the global sensitivity analysis identified the hepcidin synthesis and degradation reactions in the group of those with the largest uncertainty. By changing parameter values by no more than 10% it would be possible to have the hepcidin expression and degradation show higher control. So it seems important that the expression of hepcidin be studied in more detail. I also predict that the control of hepcidin over the system would be higher if the model had included the regulation of intestinal ferroportin by hepatic ferroportin.

The global sensitivity analysis, however, strengthens the conclusions about the reactions for which the reference steady state is not much different from the maximal and minimal values. It turns out that these are the reactions that have the largest and the smallest control over the system variables. For example, the reactions with greatest control on the labile iron pool and iron export are those of the HFE-TfR2 system. But the reactions of the HFE-TfR1 system have always low control. These conclusions are valid under a wide range of parameter values.

Construction of this model required several assumptions to be made due to lack of measured parameter values, as described in Section 3.2. These assumptions may or may not have a large impact on the model behaviour, and it is important to identify those that have a large impact, as their measurement will improve our knowledge the most. Of all the assumptions made, the rates of expression and degradation of ferroportin are those that have a significant impact on the labile iron pool in the model (see Table 3.6). This means that if the values assumed for these rate parameters were to be significantly different, the model prediction for labile iron pool behaviour would also be different. The

model is therefore also useful by suggesting experiments that will optimally improve our knowledge about this system.

Limitations on the predictive power of the model occur due to the scope of the system chosen. Fixed serum iron conditions, which were used as boundary conditions in the model, do not successfully recreate the amplifying feedbacks that occur as a result of hepcidin expression controlling enterocyte iron export. To relieve this limitation, a more advanced model should include dietary iron uptake and the action of hepcidin on that process.

The model predicts a quasi-linear response to increasing pulses of serum iron, similar to what has been predicted for the erythropoietin system (Becker et al., 2010). Our simulations display response of the transferrin receptors to pulses of extracellular transferrin-bound iron that is similar to the EPO receptor response to EPO (Figure 3.10). The integral of this response *versus* the iron sensed deviates very little from linearity in the range of physiological iron (Figure 3.9).

Computational models are research tools whose function is to allow for reasoning in a complex nonlinear system. The present model can be useful in terms of predicting properties of the liver iron system. These predictions form hypotheses that lead to new experiments. Their outcome will undoubtedly improve our knowledge and will also either confirm the accuracy of the model or refute it (in which case it then needs to be corrected). The present model and its results identified a number of predictions about liver iron regulation that should be investigated further:

- changes in activity of the hepcidin gene in the liver have little effect on the size of the labile iron pool,
- the rate of expression of HFE has a high control over the steady state-level of hepcidin,
- the strong effect of HFE is due to its interaction with TfR2 rather than TfR1,
- the rate of liver iron export by ferroportin has a strong dependence on the expression of TfR1, TfR2 and HFE,
- the rate of expression of hepcidin is approximately linear with the concentration of plasma iron within the physiological range.

The present model is the most detailed quantitative mechanistic model of cellular iron metabolism to date, allowing for a comprehensive description of its regulation. It can be used to elucidate the link from genotype to phenotype, as demonstrated here with hereditary haemochromatosis. The model provides the ability to investigate scenarios for which there are currently no experimental data available — thus allowing predictions to be made and aiding in experimental design.

CHAPTER

FOUR

MODEL OF HUMAN IRON ABSORPTION AND METABOLISM

4.1 Introduction

While the liver has been proposed to play a central role in the regulation of iron homeostasis (Frazer and Anderson, 2003), the target of the liver's iron regulatory role had not been studied in detail. Through the action of the hormone hepcidin (Park et al., 2001), which is expressed predominantly in the liver (Pigeon et al., 2001) and distributed in the serum, the liver is thought to control systemic iron metabolism. Hepcidin acts on ferroportin in multiple cell-types to induce its degradation. Ferroportin is the sole iron-exporting protein in mammalian cells (Van Zandt et al., 2008). Therefore, hepcidin expression reduces iron export into the serum from enterocytes, and as a result reduces dietary iron uptake.

I previously described a computational simulation that recreated accurately hepatocyte iron metabolism (Chapter 3). Health and haemochromatosis disease states were simulated. The model did not include the effect of hepcidin expression on intestinal ferroportin and dietary iron uptake. The feedback loop created by the liver sensing serum iron levels, expressing hepcidin, and modulating dietary iron absorption, has not yet been investigated by computation techniques.

Iron in the serum circulates bound to transferrin (Tf), and is imported into the liver cells through the action of membrane bound proteins transferrin receptors 1 and 2 (TfR1 and TfR2). Human haemochromatosis protein (HFE) competes with transferrin bound iron for binding to TfR1 and TfR2 (West et al., 2001). The previous model (Chapter 3) explained how these factors promoted the expression of hepcidin. IRPs along with with ferritin and transferrin receptors (TfR) make up the centre of cellular iron regulation. IRPs in the enterocyte regulate ferroportin expression (Hentze and Kühn, 1996), which will affect total iron imported from the diet.

While many metabolites are conserved, intestinal iron metabolism differs greatly from hepatocyte iron metabolism (Hower et al., 2009). Dietary iron is not bound to transferrin and uptake of dietary iron is through a transferrin-independent mechanism. Divalent

metal transporter has been identified as an importer of iron into intestinal epithelial cells (Gunshin et al., 1997). Cellular iron metabolism within the intestinal absorptive cells may influence system scale iron status, but the interaction between cellular iron metabolism and systemic iron status is not well understood.

Hypoxia has a complex relationship with iron metabolism and it is difficult to predict the prevailing effect of various degrees of hypoxia. Many cell types respond to hypoxia through the action of hypoxia-inducible factors (HIFs) (Wang et al., 1995). HIFs accumulate in hypoxia and up-regulate a number of iron-related proteins through binding to hypoxia-responsive elements (HREs). Hypoxia also induces increased erythropoiesis which results in an increased draw on the iron pool (Cavill, 2002). While simulations of hypoxia have improved understanding of the hypoxia-sensing apparatus (Qutub and Popel, 2006), the interaction with the iron metabolism network and iron regulatory components remains poorly understood.

Through computational modelling, systems biology offers a specialised and valued methodology to aid our understanding of the complexities of the iron metabolism network. By modelling the interaction between cellular iron metabolism and system scale regulation the effect of various components of the network can be better understood.

4.2 Materials and Methods

The methodology for modelling of the combined liver-intestine model of iron metabolism was performed following the protocols described earlier (Section 3.2), unless stated below.

The model is constructed using ordinary differential equations to represent the rate of change of each metabolite. COPASI (Hoops et al., 2006) was used as the software framework for model construction, running simulations and performing analysis. Two compartments were added to the model of hepatocyte iron metabolism; these compartments represented the intestinal absorptive cells and the lumen of the gut where dietary iron is located.

Serum transferrin-bound iron was changed, from a fixed species concentration in the hepatocyte model, to a variable species concentration dependent on a number of reactions. Therefore, transferrin-bound iron was modelled using ordinary differential equations. This had the effect that serum iron was a parameter in the hepatic model and became a variable in the enlarged model. All existing reactions that transferrin-bound iron participated in were conserved. A new reaction was added representing the iron exported by ferroportin from the intestinal compartment to the circulation. The kinetics for the hepatocyte ferroportin-mediated reaction were used for modelling enterocyte ferroportin under the assumption that the two were functionally similar.

The modelling of liver iron following import was also improved to reflect better the mechanism described by Hower et al. (2009). A metabolite representing ferric iron was

added. Iron is released from transferrin in ferric form to be reduced by a ferric reductase. A number of ferric reductases have been proposed in the literature. It appears no single ferric reductase is essential and a compensatory role can be played in the event of mutation. The ferric reduction reaction was modelled with Michaelis-Menten kinetics and parameterised using data by Wyman et al. (2008). Once reduced, ferrous iron in the labile iron pool (LIP) is modelled using the same equations as those used in the hepatocyte model.

Modelled iron uptake into the enterocyte differed from hepatocyte iron uptake. Dietary iron is not found bound to transferrin and therefore the transferrin receptor uptake mechanism modelled previously was not applicable to this cell type. Instead, divalent metal transport (DMT1) is modelled using Michaelis-Menten kinetics.

A typical daily diet was simulated using the estimations of bioavailable iron from Monsen et al. (1978). The sample diet consisted of main meals and snacks taken at typical times throughout a day. The balance of haem and non-haem iron in each food and the bioavailability of the iron sources is considered to provide an estimate of the iron absorbable from each meal. The available iron was converted from grams to moles to ensure model consistency. To simulate this variable dietary iron, the fixed gut iron concentration was permitted to vary. COPASI events were used to simulate the addition of iron from the diet at specific time points. Four events were created and these were triggered once every 24 hours. Each event increased the concentration of gutFe2 (and gutHaem where haem was consumed) by an amount equivalent to the bioavailable iron in the sample food. With meal events included, the time course of gut haem and non-haem iron showed iron spikes as shown in Figure 4.1. This input had a period of 24 hours.

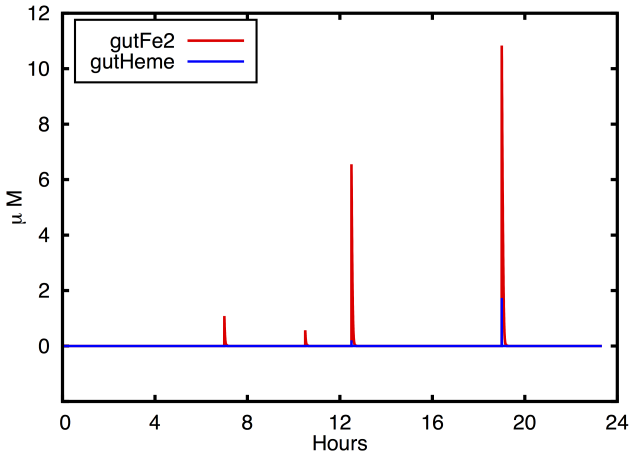

Figure 4.1: **A simulated time course of gut iron in a 24 hour period with meal events.**

Hypoxia sensing through the action of hypoxia inducible factors (HIFs) was modelled using the interactions and parameters from Qutub and Popel (2006). The iron species in Qutub and Popel (2006) were replaced with the labile iron pool from the core model in both enterocyte and hepatocyte cell types.

Both HIF1 and HIF2 expression reactions were included in the two cell compartments as there is evidence that they are expressed and functional in both these tissues (Stroka et al., 2001; Bertges et al., 2002; Mastrogiannaki et al., 2009). The HIF2 degradation pathway was modelled through binding to the same complexes as HIF1. HIF2 degradation is thought to follow the same ubiquitination and proteosomal degradation mechanism as HIF1 (Ratcliffe, 2007). HIF2 mRNA has been shown to differ from HIF1 in that HIF2 contains an IRE in its 5' untranslated region and is therefore responsive to iron status (Sanchez et al., 2007). The IRP-IRE interaction with HIF2 was modelled as a varying expression rate using a Hill Equation with IRP concentration as the modifier.

The targets of HIFs are the HIF-responsive-elements (HREs), which are found in the promoters for many iron and hypoxia related genes including TfR, HO-1 and EPO. These were modelled, similarly to IRPs, using Hill equations to modify the expression rates for the target proteins. It is thought that HIF1 and HIF2 play similar but distinct roles in the response to hypoxia (Ratcliffe, 2007). HIF2 has been shown to modulate DMT1 expression in intestinal epithelial cells while HIF1 has no effect on DMT1 (Mastrogiannaki et al., 2009). HIF2 has also been shown to increase the rate of erythropoiesis (Sanchez et al., 2007). EPO is not explicitly included in the model; however, the variable iron requirement for erythropoiesis is modelled by modulating the outflow of iron with HIF2 levels.

The model developed here is available, in systems biology markup language (SBML), from the BioModels database (http://identifiers.org/biomodels.db/MODEL1309200000).

Metabolic control coefficients were calculated using COPASI, which calculates:

$$\mathrm{C}^{\mathrm{A}}_{\mathrm{v}_i} = \frac{\delta \mathrm{A}}{\delta \mathrm{v}_i} \frac{\mathrm{v}_i}{\mathrm{A}}$$

for each variable A in the system (e.g. concentrations or fluxes) and for each reaction rate v_i.

4.3 Results

The computational model of human iron metabolism can be seen in Figure 4.2 represented using the Systems Biology Graphical Notation [SBGN](Novere et al., 2009).

Two additional compartments, namely enterocyte and lumen of the gut, were added to the previously published model of liver iron metabolism. An enterocyte compartment, representing the total volume of enterocytes, was modelled with a similar approach to the previously created hepatocyte model, however many metabolites and reactions were specific to the enterocyte. To my knowledge this is the first time that the iron uptake pathway through intestinal absorptive cells is modelled in detail.

The two cell types – enterocytes and hepatocytes – were connected together through a compartment that represents the serum. This compartment contains haem and non-haem

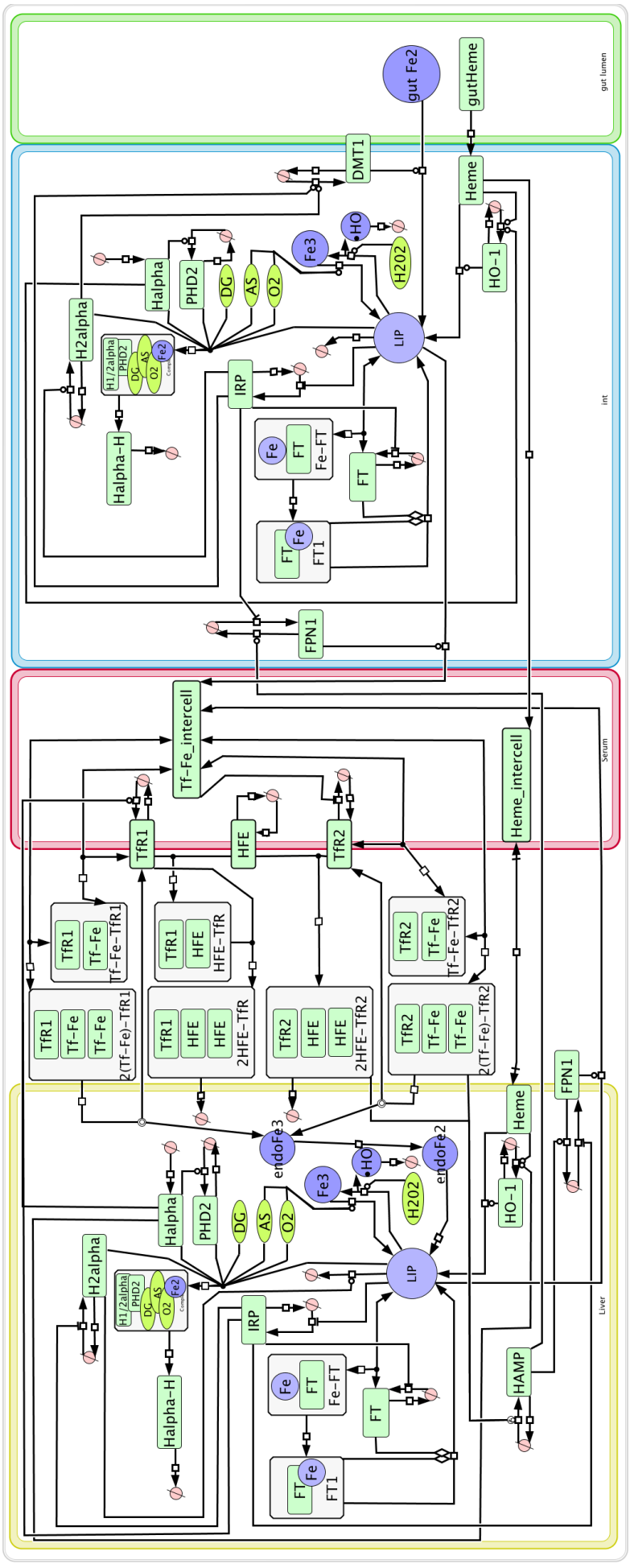

Figure 4.2: **SBGN process diagram of human liver iron metabolism model.** The compartment with yellow boundary represents the total hepatocyte tissue, the compartment with red boundary represents the plasma, the blue border represents the total enterocyte tissue while the green border contains the lumen of the gut. Species located over the compartment boundaries represent membrane-associated species. Abbreviations: Fe: iron, FPN1: ferroportin, FT: ferritin, HAMP: hepcidin, haem: intracellular haem, haem_intercell: plasma haem, HFE: human haemochromatosis protein, HO-1: haem oxygenase 1, IRP: iron response protein, LIP: labile iron pool, Tf-Fe_intercell: plasma transferrin-bound iron, TfR1: transferrin receptor 1, TfR2: transferrin receptor 2, DMT1: divalent metal transporter 1. Complexes are represented in boxes with the component species.

transferrin-bound iron, which has been exported out of enterocytes and hepatocytes. Enterocytes are polarised cells with iron entering through the brush border and being exported through the basolateral membrane into the circulation. The basolateral membrane of the enterocyte model is connected to the intercellular (serum) compartment. A further compartment was added adjacent to the brush border membrane of the enterocyte to represent the lumen of the gut where dietary iron is found (and is a parameter in the model). The hepatocyte compartment is not polarised and imports/exports iron into the serum compartment. Iron taken up through the enterocyte is passed through the plasma (intercellular) compartment for uptake into the hepatocyte. Hepcidin, which is expressed in the hepatocyte compartment, is released into the intercellular compartment and in turn into the erythrocyte where it controls iron export. The erythrocyte is represented here exclusively as a single variable species (Haem_intercell) representing the total iron contained therein.

The model consists of 71 metabolites and 104 reactions represented by 71 ordinary differential equations. A flow through the system was created by fixing the concentrations of dietary haem and non-haem iron in the gut to represent a constant supply in the diet, and adding a reaction representing iron use from the LIP. All compartments were assumed to be 1 litre to simplify the model. This is a fair assumption for the liver (Andersen et al., 2000), an under-estimate for serum (Vander and Sherman, 2001) (however this volume is variable and only a small amount will interact with hepatocytes (Masoud et al., 2008)), and the dimensions of the intestines vary greatly between individuals and to accommodate food (Schiller et al., 2005; Hounnou et al., 2002).

4.3.1 Time Course Simulation

A sample diet was simulated with regular meal events creating iron peaks. Simulated levels of iron in the intestine are lower than those found in the liver compartment (Figure 4.3). This is validated by higher IRP expression in human intestinal tissue than hepatocytes (Uhlen et al., 2010). IRP expression levels have an inverse correlation with iron levels and are more highly expressed in the simulated intestinal cells than the liver (Figure 4.4).

The meal events caused short spikes in intestinal iron that quickly returned to low levels whereas liver LIP levels remained higher for longer following ingested iron (Figure 4.3). The liver LIP under normal conditions remains within the $0.2 - 1.5\mu M$ range predicted by Epsztejn et al. (1997). Various estimates exist for the liver LIP size, generally around $1\mu M$; the simulation suggests the variation in findings may be partly explained by natural LIP variation as a result of dietary fluctuations.

When the simulation was extended for multiple days, although systemic iron levels fluctuated greatly within each 24-hour period no overall increase or decrease in iron levels was seen. The ability of the system to maintain safe iron levels when faced with irregular input is important to prevent damage from excess or depleted iron. The model was not trained or fitted to this input; however, given a physiologically accurate input the

simulation predicts a physiologically plausible time course.

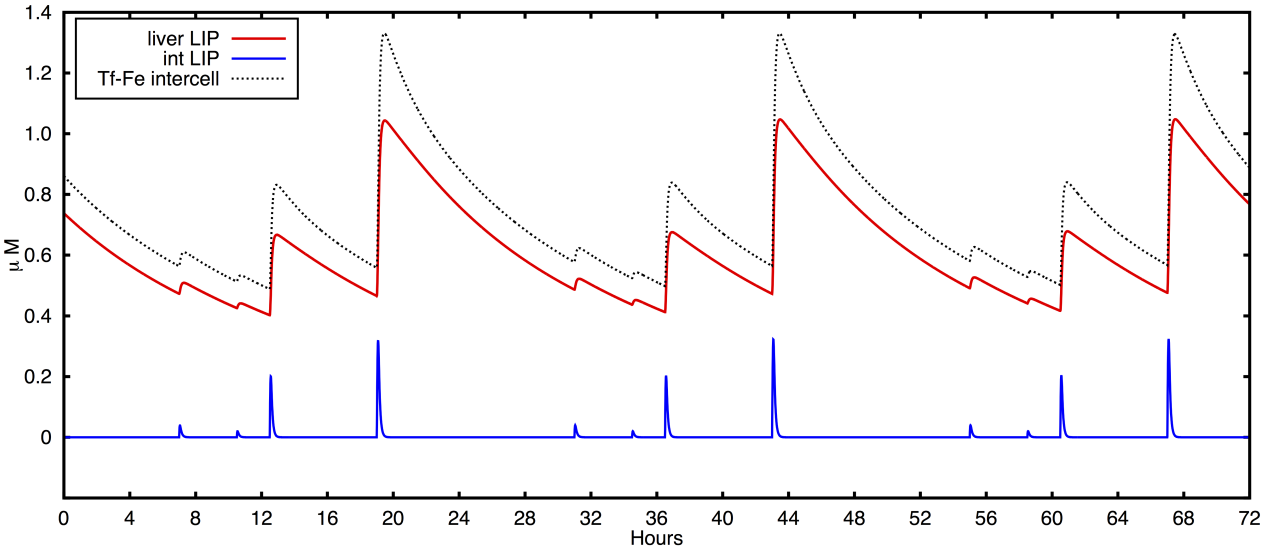

Figure 4.3: **Time course of the simulation with meal events showing iron levels in the liver (liver LIP), intestine (int LIP) and serum (Tf-Fe intercell).**

Simulated IRP in both liver and intestinal cell types had very different dynamics (Figure 4.4). Intestinal IRP decreased sharply after each meal and increased gradually between meals. Liver IRP was found to have a smaller dynamic range and less steep gradients. Only the two largest meal events created maximal inflection points with a smooth decrease and subsequent increase taking place between meal events at 20 to 32 hours. This local minimum in liver IRP between 24-28 hours and repeated on subsequent days appears spontaneous, as no meal events occurred and the liver LIP did not have an inflection point in this period (Figure 4.3). This suggests the expression of IRPs respond to the LIP passing below a threshold value, which is supported by an IRP threshold identified by Mobilia et al. (2012).

Simulated hepcidin (Figure 4.5), expressed in the liver compartment, closely follows intercellular and liver iron levels (Figure 4.3). It is important that hepcidin levels are accurate indicators of systemic iron levels as urinary or serum hepcidin is often used as a diagnostic marker for iron disorder diagnosis and treatment (Kroot et al., 2011). The model supports the use of hepcidin as a biomarker indicative of systemic iron status.

Ferroportin levels in both cell types were found to show a distinctive 'M' shape (Figure 4.6), which is similar to the liver IRP time course. While it may appear that this supports a hypothesis that the local regulation of IRPs controlling ferroportin expression have a stronger effect on ferroportin levels than the intercellular regulation of hepcidin, this is unlikely. The IRPs in the intestinal compartment were found to have different dynamics compared to the IRP in the liver compartment (Figure 4.4), while the ferroportin time courses are very similar in both cell types (Figure 4.6). Hepcidin's influence on both cell types is identical. This supports hepcidin as the main regulator of ferroportin dynamics, through controlling its degradation. The impact of IRPs regulation on ferroportin

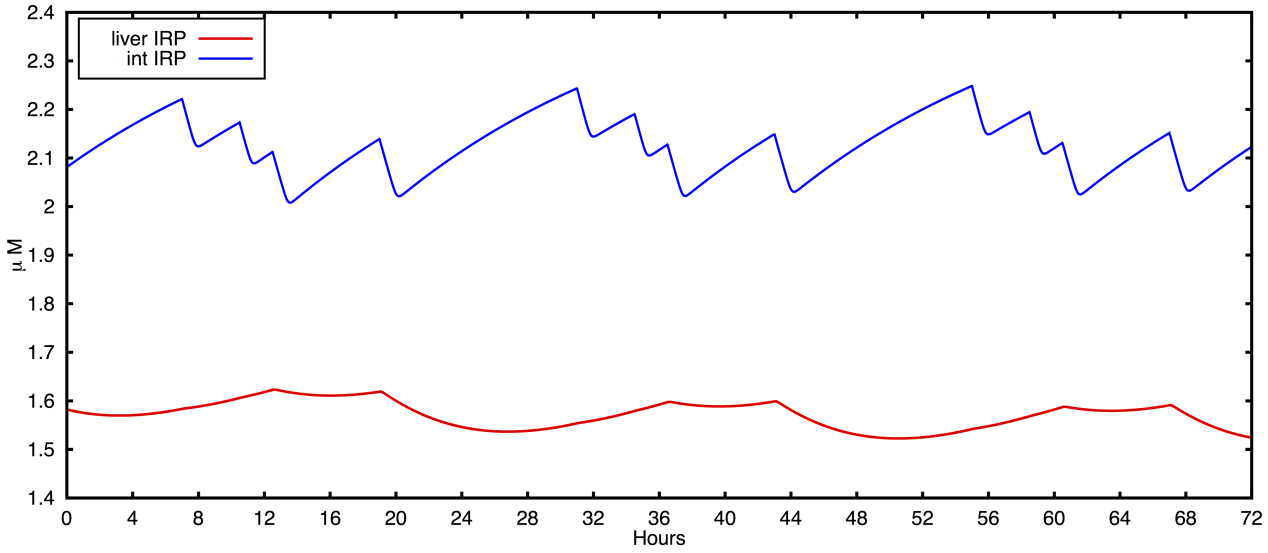

Figure 4.4: **Time course of the simulation with meal events showing iron response proteins levels in the liver (liver IRP) and intestine (int IRP).**

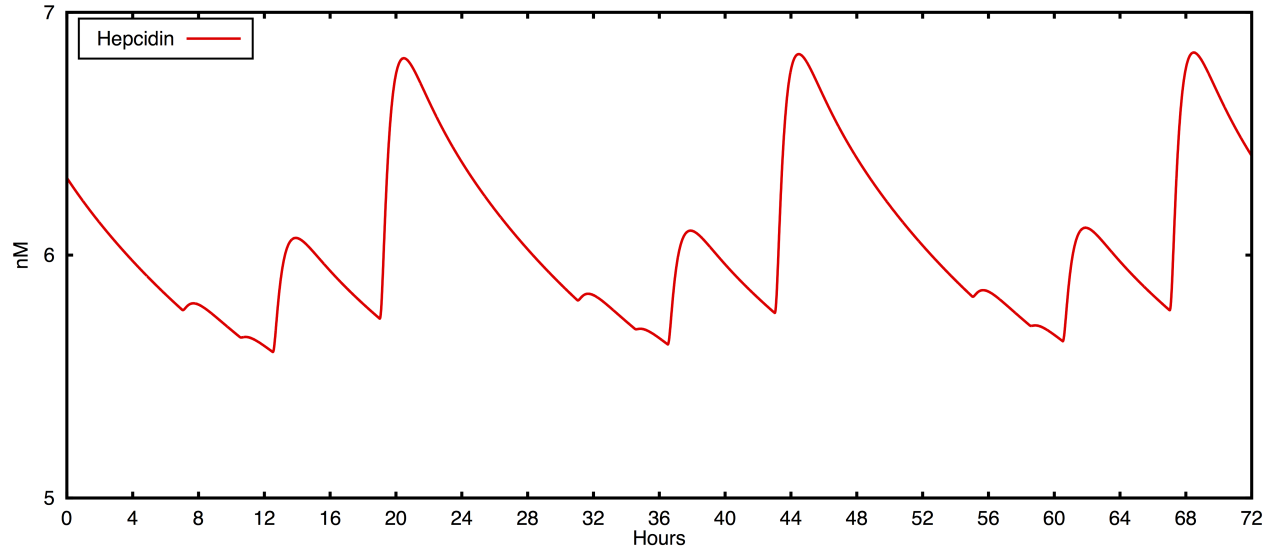

Figure 4.5: **Time course of the simulation with meal events showing hepcidin concentration.** Hepcidin concentrations are the same in both liver and intestine compartments.

expression can be seen in the base-line level of ferroportin and minor difference between the two cell types time courses (Figure 4.6 - around 32 hours). I therefore hypothesize that IRPs control the basal level of ferroportin and hepcidin is responsible for controlling its dynamics.

4.3.2 Steady-State Validation

Initial verification of the computational model was performed by comparing steady-state concentration and reaction fluxes to those in the literature. The model was found to match closely multiple findings including total haem and non-haem iron uptake and ratios

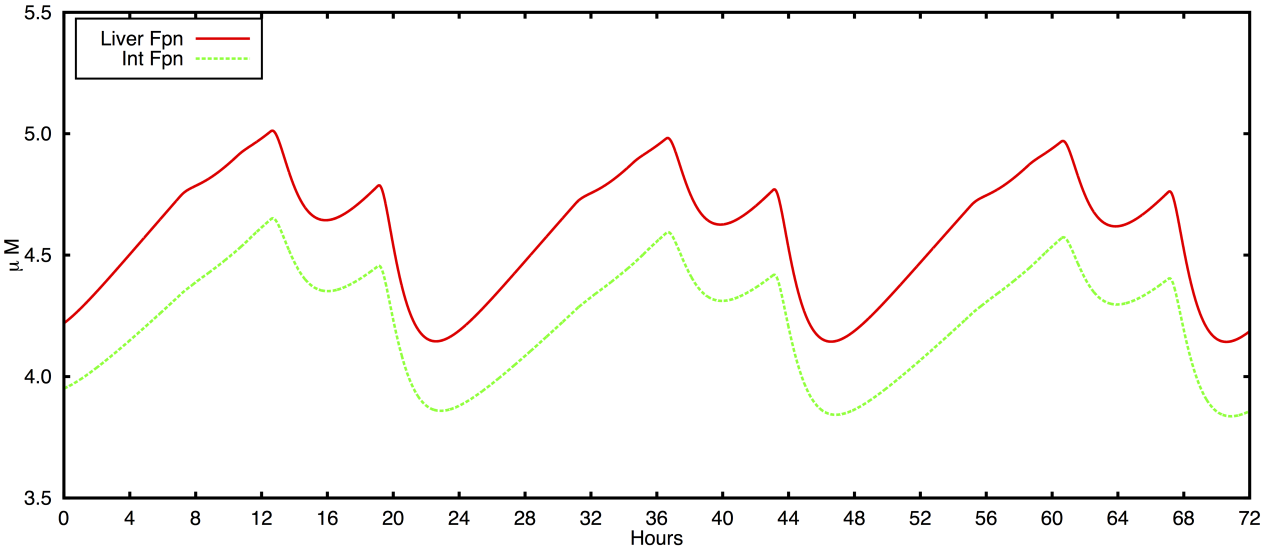

Figure 4.6: **Time course of the simulation with meal events showing ferroportin protein levels in the liver (Liver Fpn) and intestine (Int Fpn).**

Table 4.1: **Steady State Verification of Computational Model**

Metabolite	Model	Experimental	Reference
Labile iron pool	$0.593\ \mu$M	$0.2 - 1.5\ \mu$M	Epsztejn et al. (1997)
Iron response protein	963530 cell^{-1}	$\sim$ 700000 cell^{-1}	Cairo et al. (1998)
Ferritin	4499 cell^{-1}	$3000 - 6000$ cell^{-1} (mRNA), $2.5 - 54600$ cell^{-1} (protein)	Cairo et al. (1998)
TfR	2.599×10^5 cell^{-1}	$1.6 - 2 \times 10^5$ cell^{-1}	Salter-Cid et al. (1999)
Iron per ferritin	1673 average	~ 2400	Sibille et al. (1988)
Hepcidin	6.07 nM	$3.5 - 8.3$ nM	Swinkels et al. (2008)

Reaction	Model	Experimental	Reference
Liver TBI import rate	$1.42\ \mu\text{M} \cdot \text{s}^{-1}$	$2.08\ \mu\text{M} \cdot \text{s}^{-1}$	Chua et al. (2010)
Liver TfR1 uptake %	70%	80%	Calzolari et al. (2006)
Total intestinal iron uptake	0.23 nM $\cdot$ s^{-1}	0.21 nM $\cdot$ s^{-1}	Harju (1989)
Transferrin bound iron uptake	0.096 nM $\cdot$ s^{-1}	1/3 of total	Uzel and Conrad (1998)
Haem uptake	0.14 nM $\cdot$ s^{-1}	2/3 of total	Uzel and Conrad (1998)

TBI: Transferrin Bound Iron.

(Table 4.1). The total iron uptake rate from the dietary compartment of the model was found to be around 1 mg of iron per day, which accurately recreates estimates of human iron uptake requirements. The 1:2 ratio of iron uptake from haem and non-haem iron is accurate given typical concentrations of available dietary iron (Monsen et al., 1978); haem iron is more easily absorbed despite being in lower levels in the diet.

Table 4.2: **Steady State Verification of Computational Model of Haemochromatosis**

Metabolite	Model	Experimental	Reference
Labile iron pool	$0.593 \rightarrow 1.60\ \mu M$	$3\times$ up-regulation	Fleming et al. (2001)
Iron response protein	$+$	$+$	Riedel et al. (1999)
Hepcidin	$6.07 \rightarrow 1.53$ nM	$3.5 - 8.3 \rightarrow 1.88$ nM	van Dijk et al. (2008)
Transferrin receptor 2	$0.769 \rightarrow 1.81\ \mu$M	$\sim 3\times$ up-regulation	Robb and Wessling-Resnick (2004)

Reaction	Model	Experimental	Reference
Liver TBI import rate	$+$	$+$	Riedel et al. (1999)
Ferritin expression	$+$	$+$	Riedel et al. (1999)
TfR expression	$-$	$-$	Riedel et al. (1999)
Total gut iron import	$0.23 \rightarrow 0.64$ nM $\cdot\ s^{-1}$ ($2.7\times$ up-regulation)	$2 - 4\times$ up-regulation	Harju (1989)

$+$ up-regulation, $-$ down-regulation, normal $\rightarrow$ disease (HFE knockdown).

4.3.3 Haemochromatosis Simulation

A virtual type 1 hereditary haemochromatosis disease simulation was performed by reducing the expression rate for HFE and leaving all other parameters consistent with the wild type simulation. This mechanistically recreates the protein mutation found in type 1 haemochromatosis. The haemochromatosis simulation was run to steady state and concentrations of key metabolites and reaction fluxes were compared to literature and clinical findings (Table 4.2).

A three-fold increase in total iron uptake through the gut lumen compartment of the model induced by a single reaction change in the hepatocyte compartment, demonstrates the quantitative, predictive ability of the simulation. It appears that the model of haemochromatosis accurately matches the literature and, where quantitative experimental data are available, the simulation recreates the experimental data within the margin of error between experimental findings.

A virtual type 3 hereditary haemochromatosis disease simulation was also performed. Although the phenotype of type 3 hereditary haemochromatosis is similar to the type 1 (HFE-related) disease, the mutation is found in the gene encoding TfR2 while HFE remains functional. The virtual type 3 haemochromatosis simulation was performed by reducing the expression rate of TfR2 and then comparing steady-state concentrations with experimental observations.

The computational model demonstrated a biologically accurate haemochromatosis phenotype. As predicted by a number of experimental studies, TfR2 knockout leads to greatly decreased levels of hepcidin. An approximate 5-fold increase in simulated DMT1 concentrations was found. This finding is validated in mice by Kawabata et al. (2005) who observed an approximately 4-fold change, which is within the margin of error for the experimental technique used. The DMT1 increase leads to a strong increase being seen in

simulated serum transferrin-bound iron, which is validated by the increase in transferrin saturation seen in haemochromatosis patients by Girelli et al. (2011). The rate of overall liver iron uptake was found to increase in the simulation and was validated by the experimental findings of Chua et al. (2010). The amount of TfR1 was decreased 3-fold in both simulation and mouse models of type 3 haemochromatosis (Chua et al., 2010). The simulation is able to explain the counter-intuitive results from experimental models, which found increased liver iron uptake despite reduced levels of TfR1 and mutational reduction of active TfR2. The greatly increased serum transferrin saturation as a result of misregulation of hepcidin increases the import rate of each transferrin receptor, facilitating an overall increased rate of uptake.

4.3.4 Hypoxia

The hypoxia response of the iron metabolism network was simulated by varying the concentration of O_2 over a wide range of concentrations. Dietary iron was fixed and all other metabolites were simulated as described previously.

The degradation of HIFs requires oxygen and therefore restricting oxygen results in an increased response from HIF. The hypoxia-inducible factors (HIFs) are quickly degraded in normoxia but this process is reduced in hypoxia due to lack of O_2 required for complex formation with prolyhydroxylase (PHD). This results in an increase in HIF in hypoxia, which was seen in Figure 4.7 and validated by Huang et al. (1996). In the simulation of hypoxia both HIF1 and HIF2 alpha subunits were induced similarly.

HIF, which remains undegraded post-transcriptionally, regulates a number of iron related genes that contain hypoxia-responsive elements. Intestinal iron-uptake protein DMT1 is induced by HIF2 to promote increased iron absorption as demonstrated by Mastrogiannaki et al. (2009). Increased intestinal DMT1 expression was seen in the simulation in response to hypoxia (Figure 4.8a), which facilitated increased dietary iron uptake (Figure 4.8b).

HIF2 induces hepatic erythropoiesis in response to hypoxia (Rankin et al., 2007). The increased iron requirement for erythropoiesis in response to hypoxia was recreated in the simulation (Figure 4.9). Simulated HIF2 induces hepatic erythropoiesis to compensate for lack of oxygen availability.

Liver iron is influenced by conflicting perturbations in hypoxia caused by the targets of HIF. Increased iron requirement for erythropoiesis is counteracted by increased iron availability from the diet as a result of DMT induction. Figure 4.10 shows the simulated liver iron time course in hypoxia.

Initially following induction of hypoxia, the requirement for increased hepatic erythropoiesis caused a decrease in LIP. Increasing the severity of hypoxia increased the duration and severity of this iron depletion; however, iron levels are rescued before reaching a severely iron deficient condition. Iron rescue occurred as a result of increased intestinal iron uptake however; increased, iron absorption did not immediately impact systemic

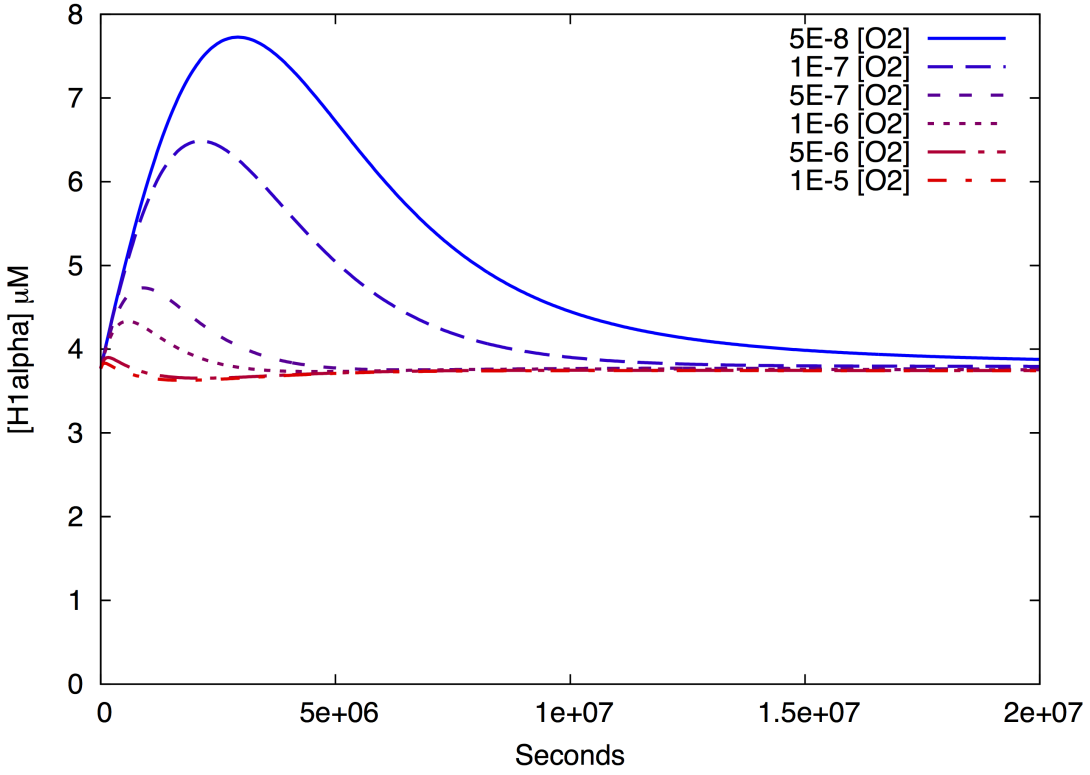

Figure 4.7: **HIF1alpha response to various levels of hypoxia.**

iron levels due to limited intestinal export and buffering through ferritin. After the initial iron recovery, the increased iron absorption became the prevailing perturbation on liver iron levels and increasing hypoxia led to increased liver iron. The increasing dietary iron uptake as a result DMT1 expression induced by HIFs, leads to the LIP returning to normal levels after a transient decrease. This was in agreement with findings that deletion of HIFs (which are abrogated in normoxia) causes decreased liver iron (Mastrogiannaki et al., 2009).

Hepcidin has been shown to be affected by hypoxia; however, it is unknown whether this is a direct effect or whether modulation of the iron metabolism network causes an indirect hepcidin response. To investigate this time course, simulations for hepcidin and its target (ferroportin) were performed in varying degrees of hypoxia (Figure 4.11a and 4.11b).

Hepcidin was found to be transiently down-regulated following hypoxia due to the increased iron requirement for erythropoiesis (Figure 4.11a). This is in agreement with Nicolas et al. (2002b) who found hepcidin to be down-regulated following hypoxia, but returning to basal levels after a number of weeks. The hepcidin down regulation induced an up regulation in intestinal ferroportin (Figure 4.11b), which assisted iron recovery and prevented iron build up in the enterocyte compartment due to DMT1 induction. These results together suggest a full system response to hypoxia, in which the iron metabolism network compensates for increasing iron demands in an elegant fashion to ensure safe levels of iron throughout the system.

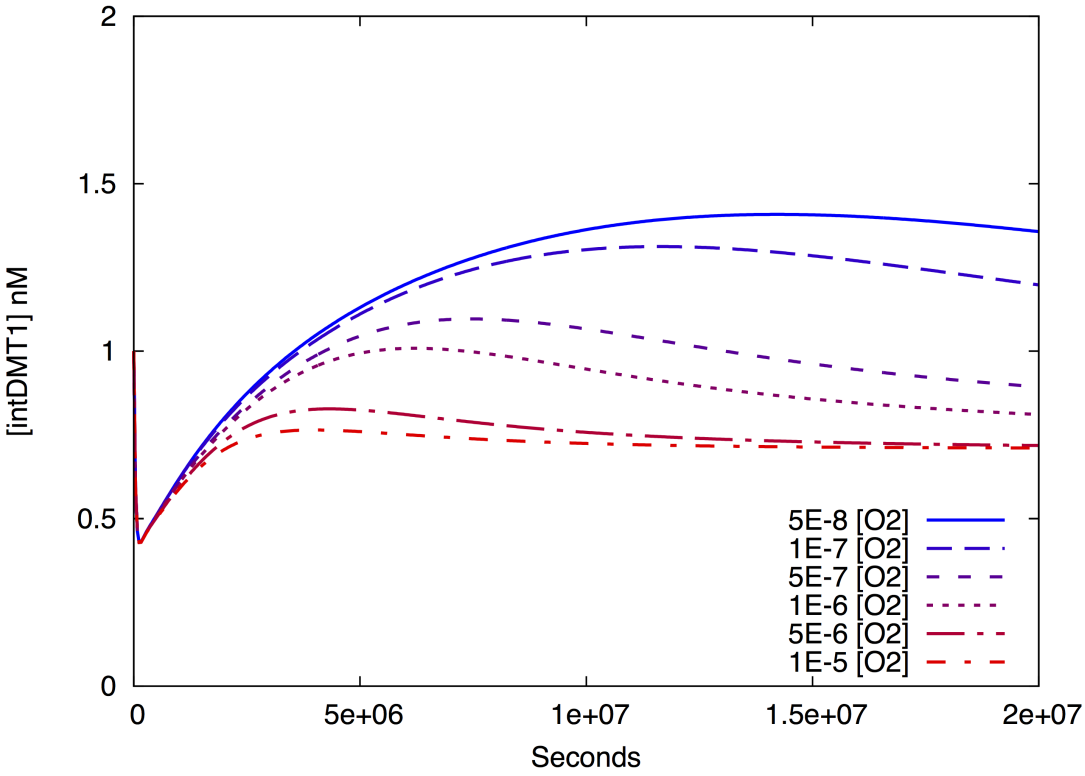

(a) Intestinal DMT1 levels in response to hypoxia.

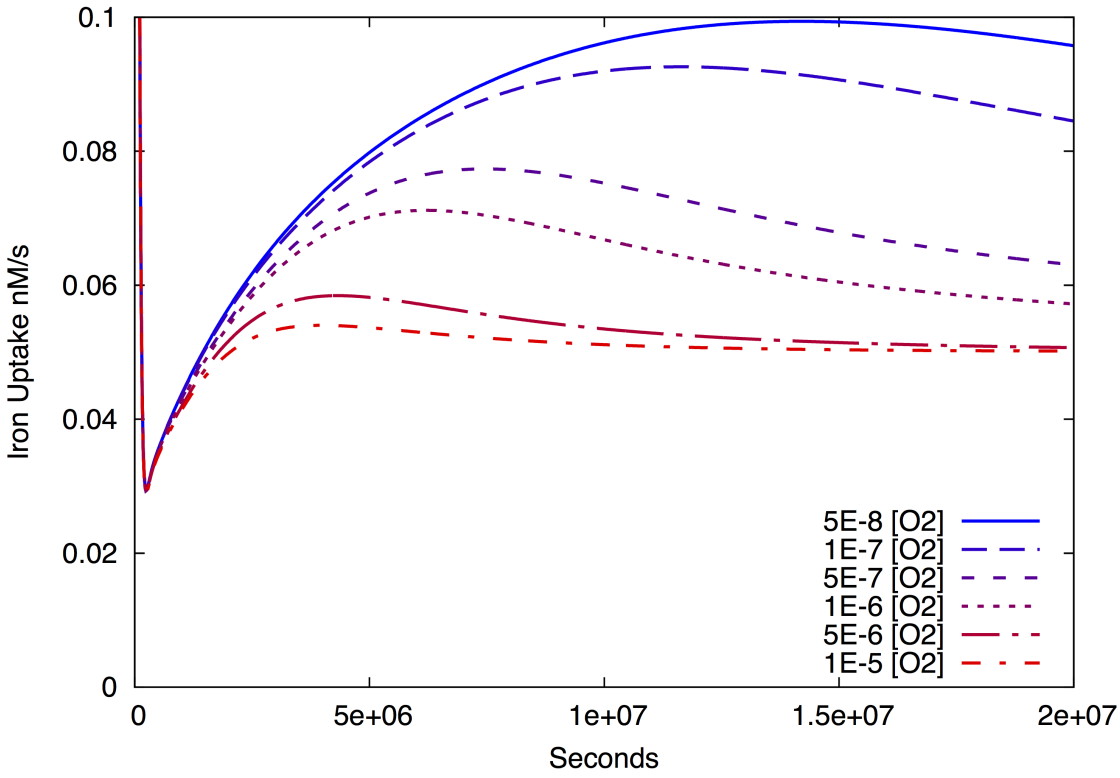

(b) Intestinal iron uptake rate in response to hypoxia.

Figure 4.8: **Simulated intestinal DMT1 and dietary iron uptake in response to various levels of hypoxia.**

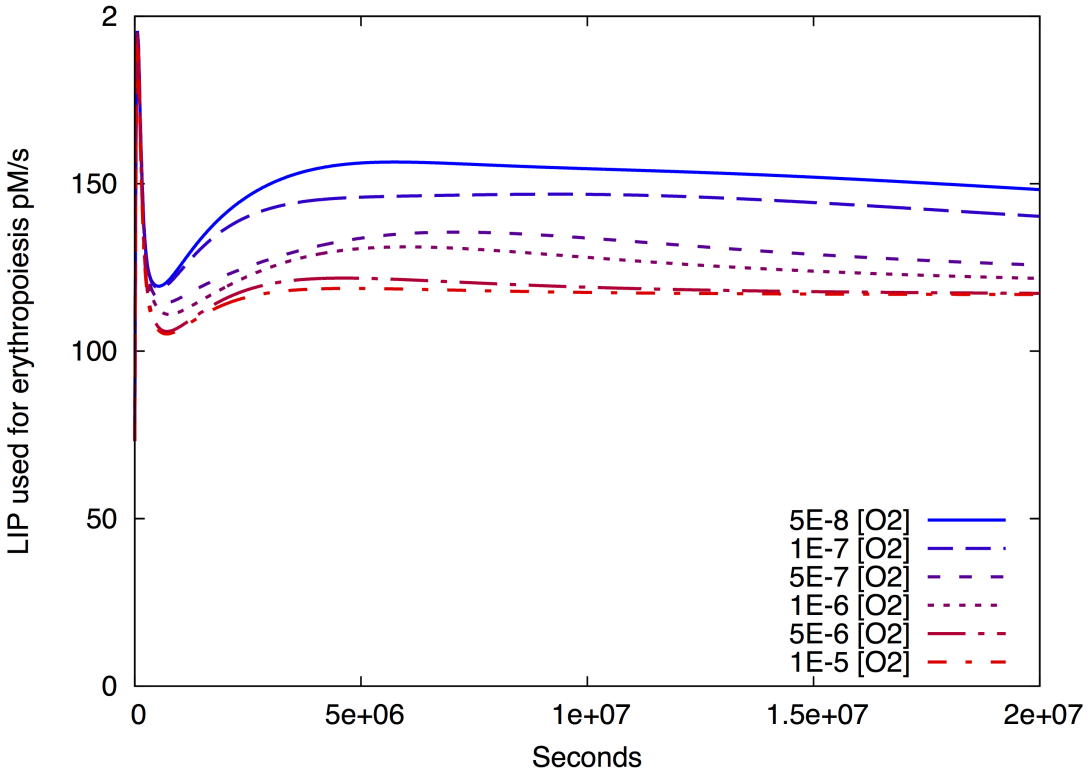

Figure 4.9: **Simulated rate of liver iron use for erythropoiesis in response to hypoxia.**

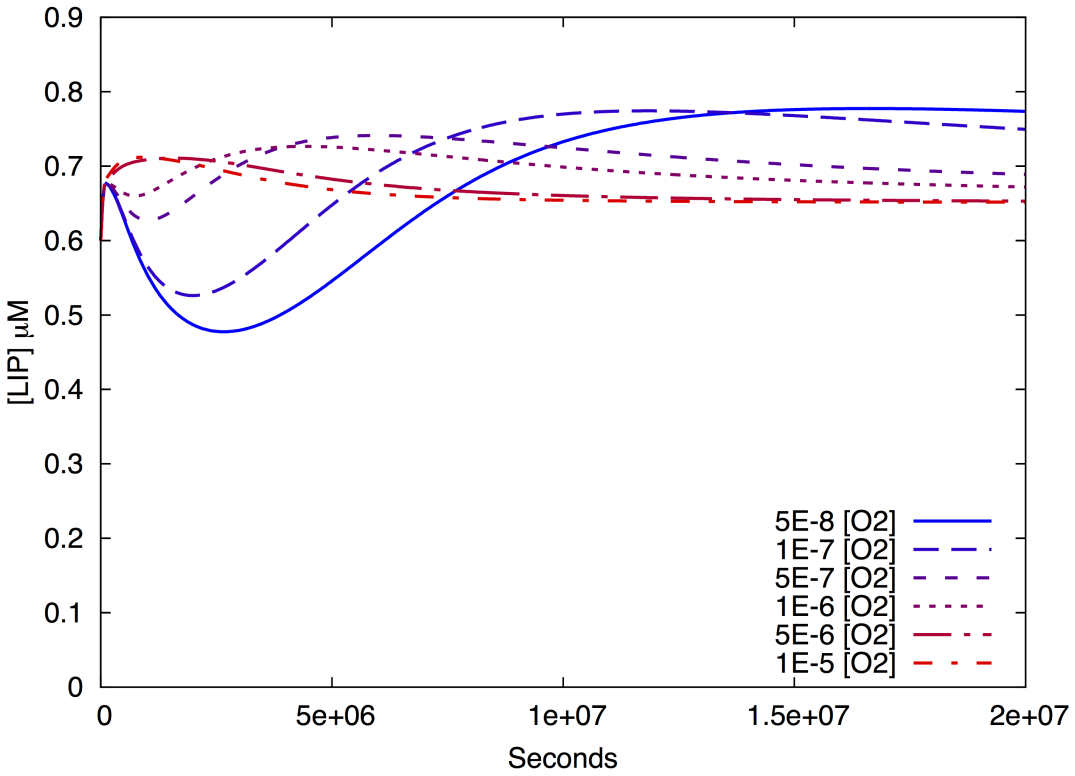

Figure 4.10: **Simulated liver LIP in response to various degrees of hypoxia.**

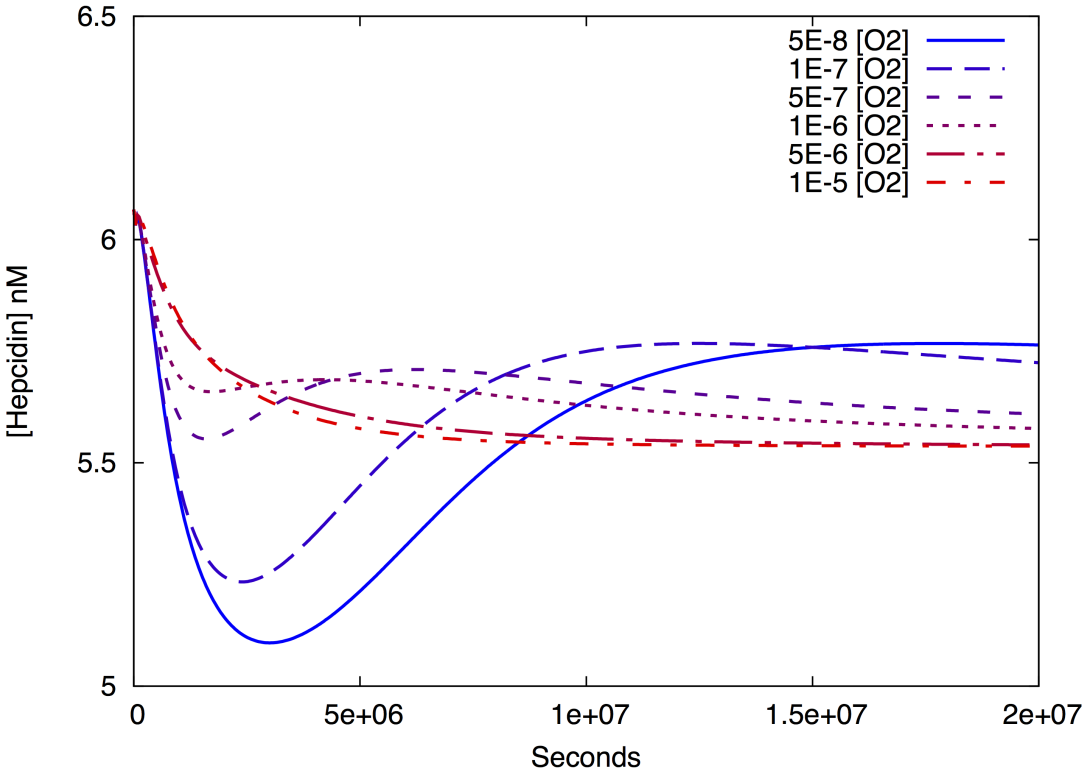

(a) Simulated hepcidin concentrations in response to hypoxia.

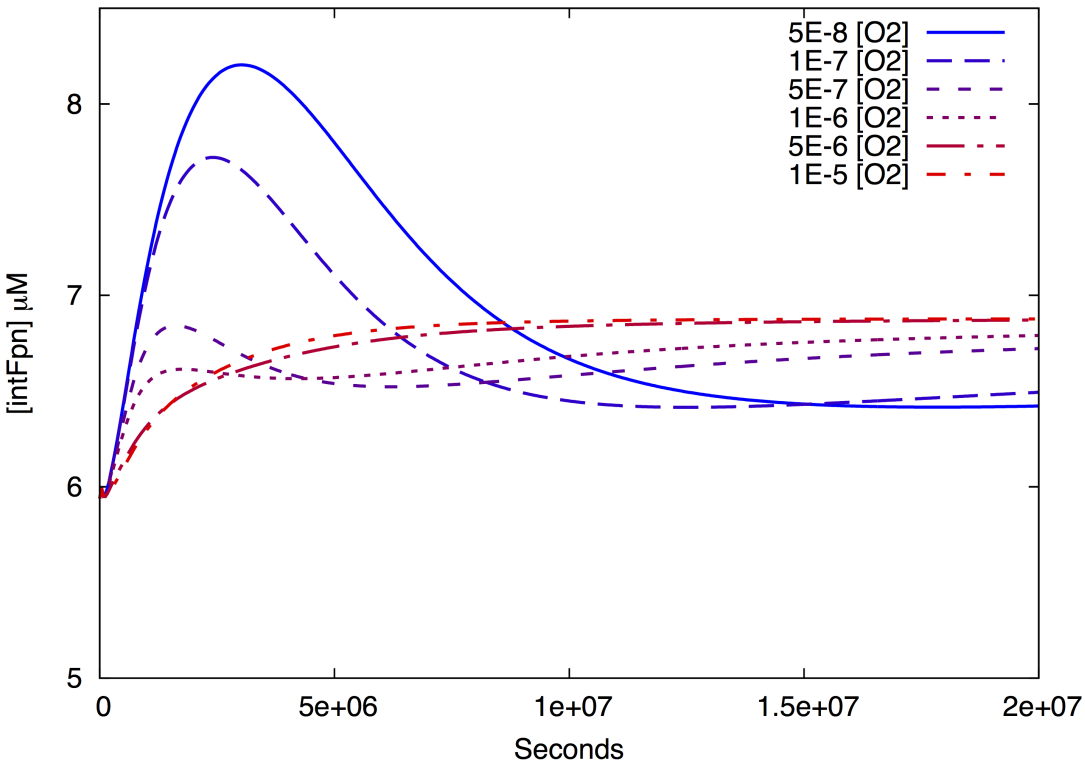

(b) Simulated intestinal ferroportin levels in response to hypoxia.

Figure 4.11: **Simulated response of (a) hepcidin and (b) intestinal ferroportin to Hypoxia.**

4.3.5 Metabolic Control Analysis

Metabolic control analysis was performed to identify the reactions with the highest influence on a reaction/metabolite of interest (Kacser and Burns, 1973; Heinrich and Rapoport, 1974). The results of metabolic control analysis are control coefficients that measure the relative change of the variable of interest as a result of a small change in the reaction rate.

Table 4.3 shows control coefficients for the reactions with highest control over serum iron in the local analysis. It can be seen from this table that the reactions with the highest control are from the liver compartment. These results support the liver's iron-sensing role. The uptake of iron through the intestinal compartment is the only route of iron into the simulated system; despite this, intestinal reactions have significantly lower control than those in the liver compartment. As would be expected if the simulation recreated the latest understanding of human iron regulation, the HFE, TfR2 and TfR iron-sensing apparatus of the liver had the highest control along with the hormone hepcidin that it controls. This served to validate the accurate simulation of the methods by which human iron metabolism is controlled and also identified hepcidin promoters as important therapeutic targets.

Table 4.3: **Local and global concentration-control coefficients with respect to serum iron: normal (wild-type) simulation**

Reaction	Local	Global Min	Global Max
HFETfR2 degradation	1.9	-0.58	3.1
HFE expression	-1.9	-19	8.6
Hepcidin expression	-0.93	-1.2	0.011
Hepcidin degradation	0.93	0	3.9
Fpn Export	0.81	-0.037	110
H2alpha expression	-0.7	-1.5	0
TfR1 binding	-0.65	-1	-0.0014
TfR1 expression	-0.63	-9	0
PHD2 expression	0.63	0	5.4
TfR1 degradation	0.62	0	0.95
TfR2 expression	-0.53	-5.9	-0.004
outFlow erythropoiesis	-0.5	-1.2	0

This local analysis is limited, in its predictive ability, to only a small change of reaction rates. Perturbations to the network such as disease states and stress conditions often result in large changes in multiple parameters simultaneously. To investigate this a global sensitivity analysis was performed following the methods described by Sahle et al. (2008). All parameters were allowed to vary over two orders of magnitude simultaneously, which creates a very large parameter space. This parameter space is searched for the minimum and maximum values of each control coefficients that can be obtained, as shown in Table 4.3. Interestingly, while most reactions only show limited range of control with consistent sign (positive/negative) some reactions were found to have a wide range of possible

control coefficients. HFE expression could have highly negative control as suggested by the local value; however, in the global case this could be significantly positive control over serum iron. Ferroportin export rate had high control in the local case; however the global analysis revealed that the maximum possible control is over 2 orders of magnitude higher than in the reference parameter set. The potential significance of the high variation seen for the control of ferroportin export rate, identifies it as an important parameter to determine accurately experimentally. This is especially so as there have been few experimental measures of this rate to date. The potential variation of HFE between positive and negative control indicates that care must be taken when using hepcidin promoters as therapeutic targets, as since with some parameters they can have the opposite effect on serum iron levels than desired.

Table 4.4: **Concentration-control coefficients with respect to serum iron: iron overload (haemochromatosis) simulation**

Reaction	Control
Fpn Export	0.81
H2alpha expression	-0.73
PHD2 expression	0.62
outFlow erythropoiesis	-0.51
TfR1 expression	-0.5
TfR1 degradation	0.5
TfR1 binding	-0.5
Halpha hydroxylation	-0.45
H2alpha hydroxylation	0.45
int Dmt1 Degradation	-0.38
int DMT1 Expression	0.38
int Iron Import DMT1	0.38

A metabolic control analysis was performed on the haemochromatosis disease simulation to investigate the basis for the misregulation of iron metabolism in haemochromatosis. Concentration-control coefficients for the disease state can be seen in Table 4.4 and can be compared to the health values in Table 4.3. Control was found to shift away from hepcidin and its promoters in the disease simulation, supporting the mechanistic understanding that HFE mutation causes hepcidin deregulation leading to iron overload. Both the hypoxia-sensing and erythropoiesis apparatus retained a large amount of control suggesting that hypoxia could have therapeutic potential for treating haemochromatosis. The control of intestinal iron uptake increased approximately $1.5\times$ in haemochromatosis disease simulation: from 0.243108 in health to 0.384424 in disease. This analysis shows that patients with haemochromatosis are much more sensitive to dietary iron levels as absorption rates cannot be correctly controlled by hepcidin.

As liver iron accumulation is one of the most dangerous effects of haemochromatosis disease, metabolic control analysis was performed with respect to the liver's LIP in health and haemochromatosis disease. The concentration-control coefficients can be seen in Table 4.5 for health and Table 4.6 in disease. In simulation of health (Table 4.5), similar

factors as for serum iron were found to have the highest control over the LIP; however, hepcidin has less effect on the intracellular iron pool. This analysis indicates that the reactions most important to control the liver's iron pool are the HFE-TfR iron-sensing apparatus, hypoxia-sensing pathways, iron response proteins and hepcidin. Concentration-control coefficients with respect to liver LIP in haemochromatosis disease (Table 4.6), when compared to healthy simulation (Table 4.5), indicate that control no longer lies with hepcidin and its promoters. Hypoxia-sensing apparatus and intestinal iron import reactions gain control over the system as it becomes deregulated. In haemochromatosis disease, hypoxia-sensing apparatus and dietary iron uptake have the strongest control on the LIP, as seen for serum iron.

Table 4.5: **Local and global concentration-control coefficients with respect to the liver labile iron pool: normal (wild-type) simulation**

Reaction	Local	Min	Max
HFE expression	-0.7	-2.1	0.1
H2alpha expression	-0.69	-1.7	-0.001
HFETfR2 degradation	0.67	-0.00038	4.3
outFlow erythropoiesis	-0.53	-1	0
PD2 expression	0.5	-0.057	2.2
Halpha hydroxylation	-0.48	-2.1	0
H2alpha hydroxylation	0.48	-8.8	1.3
gutHaem uptake	0.4	0.00066	1.8
IRP expresion	0.34	0.0025	3.1
IRP degradation	-0.34	-1.10	0
Hepcidin degradation	0.33	0	3.4
Hepcidin expression	-0.33	-0.76	0.0017

Table 4.6: **Local and global concentration-control coefficients with respect to the liver labile iron pool: iron overload (haemochromatosis) simulation**

Reaction	Control
H2alpha expression	-0.74
outFlow erythropoiesis	-0.56
PD2 expression	0.53
Halpha hydroxylation	-0.5
H2alpha hydroxylation	0.5
int Dmt1 Degradation	-0.42
int DMT1 Expression	0.42
int Iron Import DMT1	0.42
IRP expression	0.28
IRP degradation	-0.28
int IRP Expression	0.23
int IRP degradation	-0.23

Comparing the metabolic control analysis results, to those obtained for the liver model (Section 3.3.7), shows that the control hepcidin has over the liver's LIP has increased with

the addition of the intestinal compartment. Furthermore, the effect of hepcidin perturbations is inverted in the more extensive model. With respect to the liver's LIP, hepcidin expression was found to have a concentration-control coefficient of 0.028 in the liver model (Table 3.6), and -0.326 in the model including intestinal iron uptake (Table 4.5). This effect is due to increasing hepcidin in an isolated liver compartment resulting in the down-regulation of ferroportin, blocking of iron export and subsequent buildup of iron in the LIP. The prevailing effect on the LIP is the inverse when intestinal iron uptake is added. Increasing hepcidin in the model that includes the gut leads to iron export being blocked from both cell-types. This blocks iron's route into the system from the diet resulting in a decrease in the liver's LIP.

The ferroportin-mediated iron export reaction which showed significant control over the LIP in the liver-only model (Table 3.6) was no longer one of the reactions with the highest control over liver LIP in the multiple cell-type model. This is significant as this reaction is one of the more poorly characterised in the literature.

The HFE-TfR2 degradation reaction showed significantly increased control in the multiple cell type model compared to the liver model. This reaction had a concentration-control coefficient of -0.034 in the liver model (Table 3.6), which increased to 0.672 in the more extensive model (Table 4.5). This strengthens the findings from both models that the HFE-TfR1/2 iron-sensing system is vital to human iron homeostasis.

4.4 Discussion

Iron is essential for many processes throughout the body including oxygen transport and respiration. However, this oxidation and reduction utility also means excess iron is highly dangerous as it leads to the production of dangerous free radicals (Kell, 2009). Therefore, iron must be tightly regulated throughout the body to ensure a minimum amount of free iron is present while still maintaining enough for the essential processes that require it. The complex network of interacting pathways involved in iron absorption, hepcidin regulation, iron storage, and hypoxia-sensing all contribute to human iron homeostasis (Hower et al., 2009).

Here I constructed a mathematical simulation of human iron absorption and regulation that mechanistically recreates the core reactions involving iron in the body. The model was parameterised using a wide variety of data from multiple published experimental studies. The model was then validated by previously published results from clinical studies and model organisms. The disease phenotype of human haemochromatosis was recreated by simulating the causative mutation within the model, demonstrating how a complex phenotype, where all the key biomarkers are perturbed, arises due to a single mutation.

While debate continues over the exact complex formation and signalling steps by which TfR2 and HFE control hepcidin, the model demonstrates that through sensing

serum iron levels and modulating hepcidin expression the liver can control iron export from intestinal absorptive cells to ensure free iron remains safely controlled.

Realistic meal events were created as inputs from the model using estimates of available dietary iron in various foods (Monsen et al., 1978). The simulation was able to regulate tightly free iron pools within safe levels despite irregular iron input. Local iron levels were found to alter the basal levels of ferroportin through the IRPs; however, the dynamic response of ferroportin to meal events was controlled by hepcidin and consistent in each cell type. The IRPs were found to respond to iron decreasing below a threshold level. The model predicts that IRPs control the basal level of ferroportin, but hepcidin is the main factor controlling ferroportin's dynamics. This could be tested with experiments which decrease IRP levels and measure the level of ferroportin compared to a control with normal IRP expression.

Hypoxia results in an increased need for iron for erythropoiesis. Hypoxia-inducible factors accumulate in hypoxia and regulate a number of iron-related proteins. The interaction between the hypoxia network and the iron-regulatory network has been investigated here for the first time here to my knowledge. I found that an increased iron requirement in hypoxia results in a transient reduction in iron pool levels; however, a subsequent increase in iron import factor DMT1 balances this effect. The simulation demonstrates how iron is maintained within safe levels when challenged by a wide variety of different oxygen levels.

As experimentally derived parameters for many of the iron-related reactions are limited, a highly integrative approach to data collection was taken, incorporating data from *in vitro* physical chemistry experiments, cell lines and animal models. Systems modelling allows a wide variety of experimental data to be applicable to human clinical biology. While the applicability of some of these data can raise concerns, extensive validation was performed to ensure that the model was predictive with the parameters available. To further investigate the effects of integrating a wide variety of data, a global sensitivity analysis was performed. This analysis identified many reactions as demonstrating consistent behaviour if perturbed; however, it also identified a couple of important reactions where the effect of modulating the reactions rate would depend on the entire parameter set of the system. While HFE shows high control over the system in the local analysis, the effect of modulating the levels of HFE on serum iron levels was dependent on the rest of the parameters. HFE could show both highly positive, as well as negative control. These findings suggest that the use of hepcidin promoters such as HFE to treat iron disorders would require careful characterisation of the disease state. Potentially a personalised medicinal approach could be adopted where the simulation is parameterised using clinical measurements to create a personal *in silico* patient, which could be used to identify the best point of control for that particular patient. The global sensitivity analysis also identified reactions that had consistently high control such as hepcidin expression/degradation and the hypoxia-sensing factor HIF-prolyl hydroxylase 2 (PHD2) expression; these find-

ings are valid under a wide range of parameter values, and are thus robust results that are unlikely to change even if the parameter values in the model were incorrect.

Comparing sensitivity analysis in health and haemochromatosis disease states shows that control is lost from the hepcidin-promoting apparatus in this disease. The remaining control lies with local iron-regulator proteins and hypoxia-sensing factors. These analyses predict hypoxia should be investigated as a non-invasive treatment for haemochromatosis.

The present model and its results identified a number of predictions about iron regulation that should be investigated further:

- IRPs control the basal level of ferroportin, but hepcidin is the main factor controlling ferroportin's dynamics,
- IRPs respond to iron decreasing below a threshold level,
- hypoxia results in a transient decrease in iron pool levels,
- an increase in iron import factor DMT1 rescues the iron pool levels following hypoxia,
- hepcidin and the hypoxia-sensing factor HIF-prolyl hydroxylase 2 (PHD2) always have high control over the system.

The model presented here is, to my knowledge, the most detailed and comprehensive model of human iron metabolism to date. It mechanistically reproduces the biochemical iron network, which allows the findings to be directly applicable to further experimentation and eventually the clinic. The model provides an *in silico* laboratory for investigating iron absorption and metabolism, and should be the basis for further expansion to investigate the impact of systemic iron levels throughout the body.

CHAPTER

FIVE

IDENTIFYING A ROLE FOR PRION PROTEIN THROUGH SIMULATION

5.1 Introduction

Cellular prion protein PrP^{c} (PrP) is a ubiquitously expressed cell surface protein most widely known as the substrate of PrP-scrapie (PrP^{sc}). PrP^{sc} is implicated in Creutzfeldt-Jakob disease (sCJD) and therefore elucidating the role of PrP in health and disease has become the subject of much research, yet its function has remained elusive. $PrP^{(-/-)}$ mice show no immediately apparent phenotype; however, many perturbations have been reported in neuronal function (Telling, 2000), age related demyelination (Radovanovic et al., 2005), susceptibility to oxidative-stress related neuronal damage (Weise et al., 2006), and recovery from anaemia (Zivny et al., 2008). Iron metabolism appears of particular importance as brains infected with sCJD show iron imbalance, which increases with disease progression and which correlates with PrP^{sc} load (Singh et al., 2009). It is thought that iron forms complexes with PrP^{sc} that remain redox-active and therefore contribute to neurotoxicity (Singh et al., 2009).

The previously described model of iron uptake and regulation in intestinal and liver tissue has been shown to recreate successfully known diseases of iron metabolism (Chapters 3 and 4). However, iron has also been implicated in many diseases that are not traditionally considered diseases of iron metabolism. Perturbations of iron metabolism have been consistently observed in multiple neurodegenerative disorders (Barnham and Bush, 2008; Benarroch, 2009; Boelmans et al., 2012; Gerlach et al., 1994; Ke and Ming Qian, 2003; Kell, 2009; Perez and Franz, 2010; Zecca et al., 2004). The role of iron in neurodegeneration is poorly understood and it is unclear whether it plays a causal role or accumulates as a result of late-stage cellular degeneration. From recent evidence it appears that iron may play a causal role in neurodegeneration (Pichler et al., 2013) and as a result understanding the regulation of iron in neurodegeneration has become a highly promising area of research.

Recently, potential a mechanism for the link between iron metabolism and PrP was found when it was shown that PrP acts as a ferric reductase (Singh et al., 2013). However,

PrP knockout mice show a counter-intuitive phenotype of increased intestinal iron uptake and systemic iron deficiency. To understand better the role of PrP in iron metabolism I investigate whether ferric reductase activity can explain the counter-intuitive phenotype found in $PrP^{(-/-)}$ mice. To test truly the predictive power of the model I modulate only ferric reductase activity in the simulation and compare experimental findings in mice to the simulation results. I test whether a ferric reductive role can fully explain the complex iron-related phenotype observed in modulated PrP expression.

Iron reduction may occur on the membrane of both enterocytes and hepatocytes. Iron from the diet is predominantly in ferric (Fe^{3+}) form and must be reduced before it can be imported into enterocytes by divalent metal transporter. In other cell types (for example, hepatocytes) iron also requires reduction following uptake by the transferrin receptors. Following receptor-mediated endocytosis into hepatocytes, ferric iron is released from the transferrin receptors due to the lower pH. Endosomal iron must then be reduced into the ferrous form before it can be exported, out of the endosome into the labile iron pool. To establish whether PrPs functional role could be at either of these sites (intestinal or transferrin receptor pathways), I simulate modulation of iron reduction at both cell-type membranes and compare the phenotype to PrP knockout mice (Singh et al., 2013).

5.2 Materials and Methods

Much of the modelling of the full system model of iron metabolism was performed using the same methods described previously (Section 3.2), unless stated below. The full computational model of human iron metabolism was used, including intestinal and liver compartments as described in Chapter 4.

Ferric reduction on the intestinal brush border membrane of the simulation was not explicitly modelled as not enough evidence was available for the kinetics and regulation of the intestinal reductase. Therefore, ferrous iron concentrations were used as a surrogate. It is assumed that increasing the rate of reduction of dietary ferric iron, increases the availability of ferrous iron for uptake into the intestinal cells. Therefore to simulate decreased ferric reductase capacity at the intestinal brush border, dietary ferrous iron concentrations were reduced. It is also assumed that an increase in dietary ferric iron reduction at the intestinal brush border, increases the availability of ferrous iron. Therefore to simulate knockout of the reductase, and consequent decrease in dietary ferric iron reduction, ferrous iron availability was decreased.

The only location of explicitly modelled ferric reduction in the simulation was following receptor-mediated uptake of transferrin bound iron from the serum into the liver. While it is thought that Steap3 can perform this ferric reductive role (Section 1.1.9), other proteins may compensate for the role of this in knockout. Therefore, to test the suggested model of PrP as a ferric reductase, the reduction of iron following uptake was modulated. A parameter scan was performed on the V_{max} of iron reduction using COPASI (Hoops

et al., 2006). The V_{max} was varied over 2 orders of magnitude with a time-course task being run with each of 13 logarithmically spaced parameter values. The time course was run for a long period (2×10^7 seconds) to negate the impact of initial conditions, which were kept the same for each time course. If the effect of the modulated parameter took the system a long way from initial conditions, this transient effect is minimised by the advanced time points.

For injection simulation, a COPASI event was added, which triggered once at a defined time-point and increased serum transferrin-bound iron to $10\ \mu$M. The injection event took place after a prolonged period of standard simulation, to ensure that initial conditions had a minimal effect and the system was approximately at steady state. The time displayed in Figure 5.6 is relative to the injection event.

Simultaneous scans of prion protein's potential effect in both enterocyte and hepatocyte cell types were performed by nesting 2 parameter scans within COPASI. The results from the parameter scan were plotted using the open source software gnuplot (http://www.gnuplot.info). The model used here is available, in systems biology markup language (SBML), from the BioModels database (http://identifiers.org/biomodels.db/MODEL1309200000).

5.3 Results

The computational model of human iron metabolism can be seen in Figure 5.1 represented by Systems Biology Graphical Notation (Novere et al., 2009). This figure includes highlights to indicate potential sites of, ferric-reductase activity which could be attributed to cellular prion protein (PrP). The computational model is the same as previously described (Chapter 4), with the exception of the highlighted reactions which were modulated, to simulated PrP activity, as described in Sections 5.3.1-5.3.3.

5.3.1 Intestinal Iron Reduction

To simulate the dietary iron reduction at the brush border, the concentration of ferrous iron was decrease (instead of a detailed mechanistic model of the process). Decreasing reduction rate on the brush border membrane decreases availability of ferrous iron, which was a simulated metabolite. Therefore, to simulate varying rates of ferric iron reduction a parameter scan was performed on the concentration of dietary ferrous iron. The concentration of gut ferrous iron was modulated from 4.50 nM to $1.80\ \mu$M to assess the impact on intestinal iron uptake and the results were compared to the findings of Singh et al. (2013) in PrP knockout mice. Singh et al. (2013) demonstrated that $PrP^{(-/-)}$ mice had significantly decreased liver iron levels compared to controls. The simulated liver LIP was measured with varying rates of ferrous iron availability (Figure 5.2).

The simulated liver iron pool was found to decrease with decreasing ferrous iron availability at the intestinal brush borders, which recreates findings from knockout mice (Singh

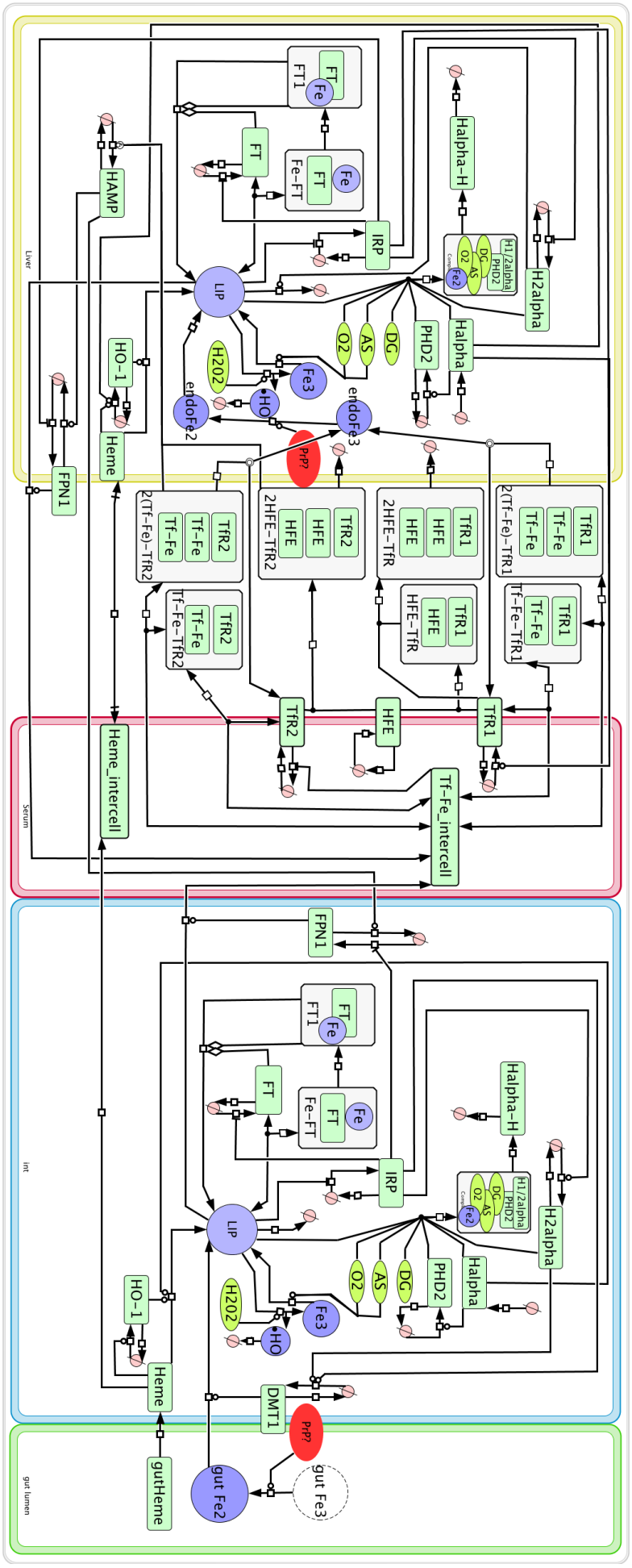

Figure 5.1: **SBGN process diagram of human liver iron metabolism model.** The compartment with yellow boundary represents the hepatocyte, the compartment with pink boundary represents plasma, the blue border represents the enterocyte while the green border contains the lumen of the gut. Species overlayed on the compartment boundaries represent membrane-associated species. Abbreviations: Fe: iron, FPN1: ferroportin, FT: ferritin, HAMP: hepcidin, haem: intracellular haem, haem_intercell: plasma haem, HFE: human haemochromatosis protein, HO-1: haem oxygenase 1, IRP: iron response protein, LIP: labile iron pool, Tf-Fe_intercell: plasma transferrin-bound iron, TfR1: transferrin receptor 1, TfR2: transferrin receptor 2, DMT1: divalent metal transporter 1. Complexes are represented in boxes with the component species. The potential sites of cellular prion protein (PrP) action are marked in red.

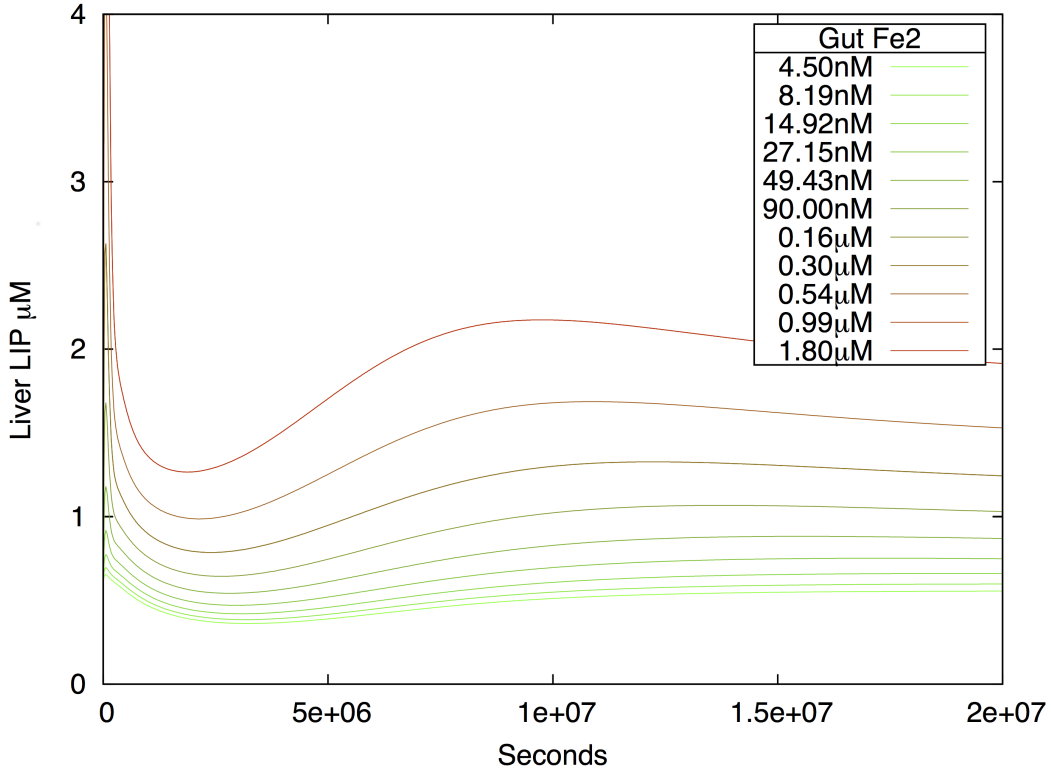

Figure 5.2: **Simulated liver iron pool concentration over time for varying levels of gut ferrous iron availability.**

et al., 2013). Decreasing liver iron pool as a result of decreasing dietary iron availability was not considered sufficient validation that the brush border is the main site of physiological PrP activity, as this finding is intuitive and a natural result of the system; decreased dietary iron availability would naturally result in decreased liver iron pool. In PrP knockout mice it was found that despite the decreased liver iron loading, PrP knockout causes increased iron uptake. These seemingly contradictory properties of increased dietary iron absorption but decreased liver iron pool constitute the distinctive phenotype in PrP knockout mice. The simulation measured the variation in iron uptake depending on intestinal PrP activity represented by ferrous iron availability. Decreased simulated ferrous iron availability decreased the rate of intestinal iron uptake (Figure 5.3). The simulated dietary iron uptake rate decreased as a result of decreased ferrous iron availability at the brush border membrane of the intestinal compartment. The simulation did not recreate the finding of increased intestinal iron uptake in PrP knockout mice compared to wild-type (Singh et al., 2013). This suggested that ferric reduction on the brush border could not fully explain the phenotype observed in PrP knockout animals. It was apparent that ferric reduction at the brush border could not be the only or prevailing physiological role of cellular prion protein.

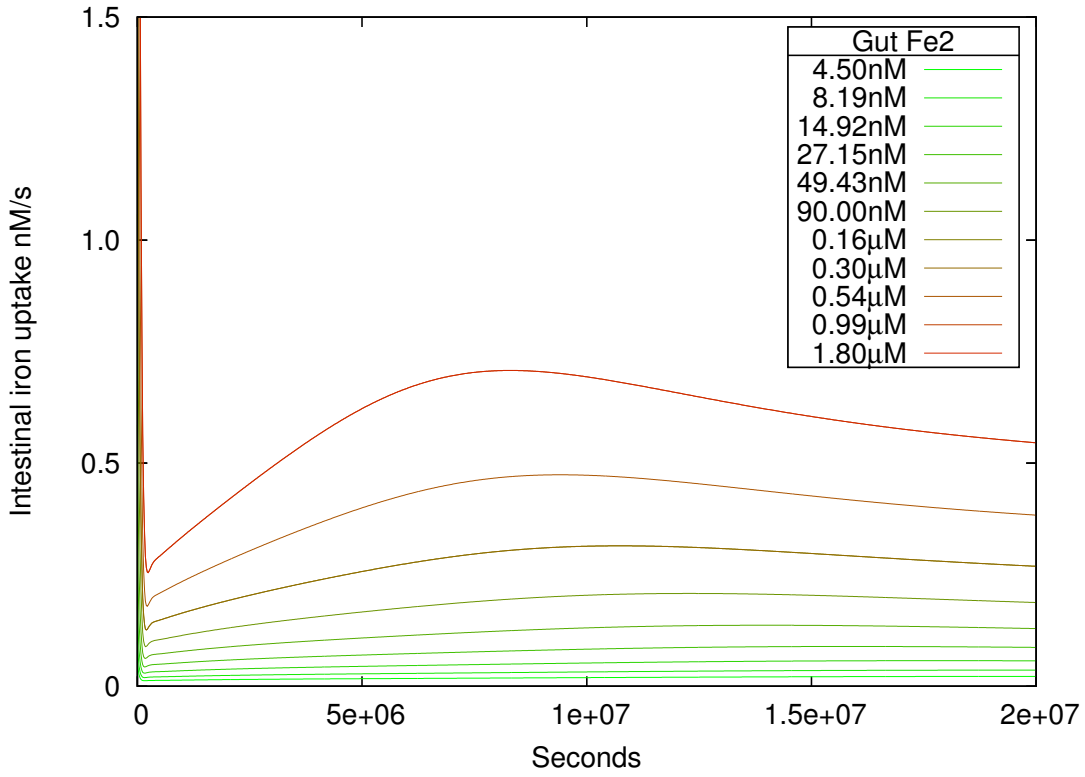

Figure 5.3: **Simulated intestinal iron uptake rate over time for varying levels of gut ferrous iron availability.**

5.3.2 Liver Iron Reduction

An alternative site of ferric reduction was identified in the liver compartment following uptake from transferrin-bound iron. Endocytosed transferrin-bound iron dissociates from the transferrin receptor in the low endosomal pH. However, the iron must be reduced before it can be exported out of the endosome by divalent metal transporter.

A parameter scan on the rate of liver ferric iron reduction was performed with fixed dietary iron conditions. The rate of iron reduction following transferrin-receptor uptake was the only parameter varied and all other parameters and initial conditions were kept constant. A time-course simulation was run for each rate of iron reduction and compared to experimental observations.

Increased dietary uptake is the most significant finding in $PrP^{(-/-)}$ mice and, in the simulation, increasing dietary iron uptake with decreasing ferric reductase activity was also found (Figure 5.4). Increased dietary iron uptake is a surprising finding as the only parameter which was modulated was iron reduction in the liver compartment and a strong effect was seen in the intestinal compartment. While a strong system effect from liver perturbations was previously seen in simulations of haemochromatosis (Section 4.3.3), human haemochromatosis protein (HFE) is involved in hepcidin promotion and therefore a system effect is more expected in haemochromatosis simulation.

To test whether decreasing liver iron reduction could recreate the counter-intuitive

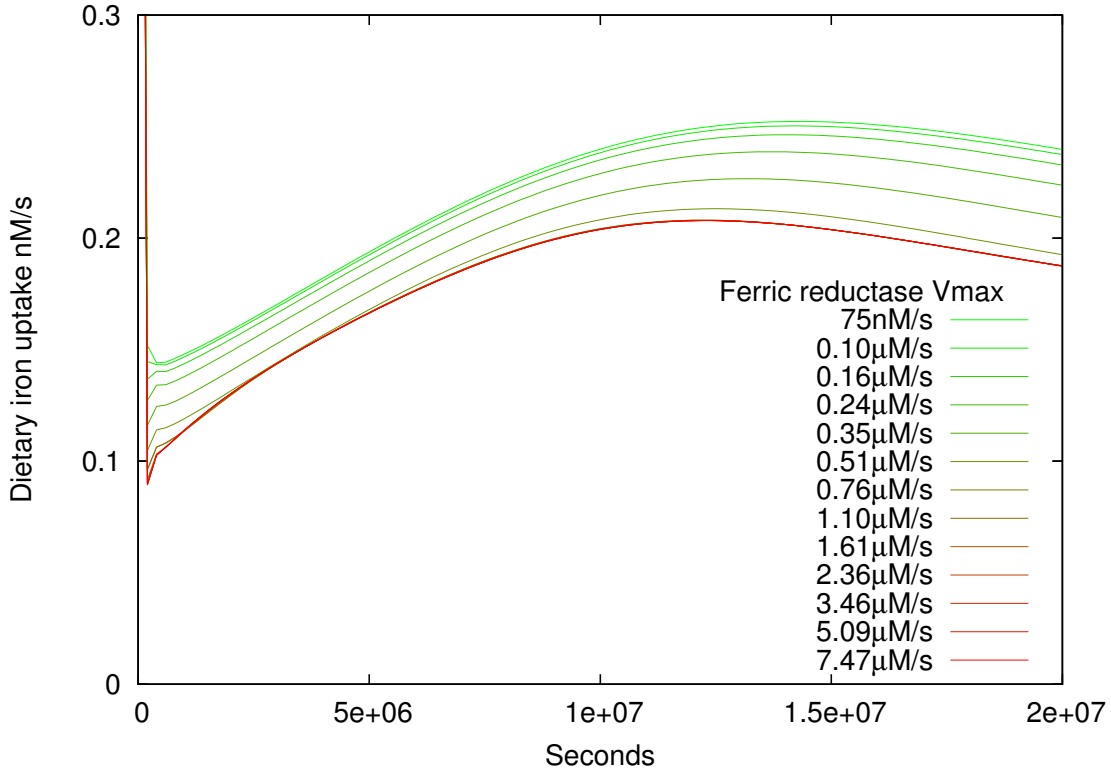

Figure 5.4: **Simulated intestinal iron uptake rate over time for varying iron reduction rates in the hepatocyte compartment.**

phenotype, of increased dietary iron uptake yet decreased liver iron loading, the simulated liver LIP was measured simultaneously during the parameter scan. Decreasing iron reduction rates in the hepatocyte compartment, resulted in a decrease in liver iron pool (Figure 5.5), despite increasing dietary iron uptake (Figure 5.4). This is validated by Singh et al. (2013) in $PrP^{(-/-)}$ mice.

Interestingly, increasing ferric reduction rate had very little effect on both dietary iron uptake and liver iron loading once the V_{max} was above 1 μM/s. This suggests that disorders that are a result of improper iron reduction could be treated if this reduction could be restored, and that there is little concern for over-reduction being harmful. Only greatly inhibited iron-reduction capacity appeared pathological.

To investigate whether the phenotype observed in PrP knockout mice is the result of inadequate iron reduction at the brush-border of intestinal cells or inadequate iron uptake into other organs, Singh et al. (2013) injected iron-dextran into mice. Injection of iron bypasses the intestinal uptake process removing any affect of altered redox state on DMT1-mediated uptake. Singh et al. (2013) found that injected iron was more slowly absorbed by the liver in $PrP^{(-/-)}$ mice. An injection of iron was simulated to mimic the experimental technique by creating a COPASI event to increase serum iron levels. A time course following this injection event was plotted to asses iron uptake into the liver compartment (Figure 5.6).

Simulated iron reductase activity was found to affect the impact of injected iron on

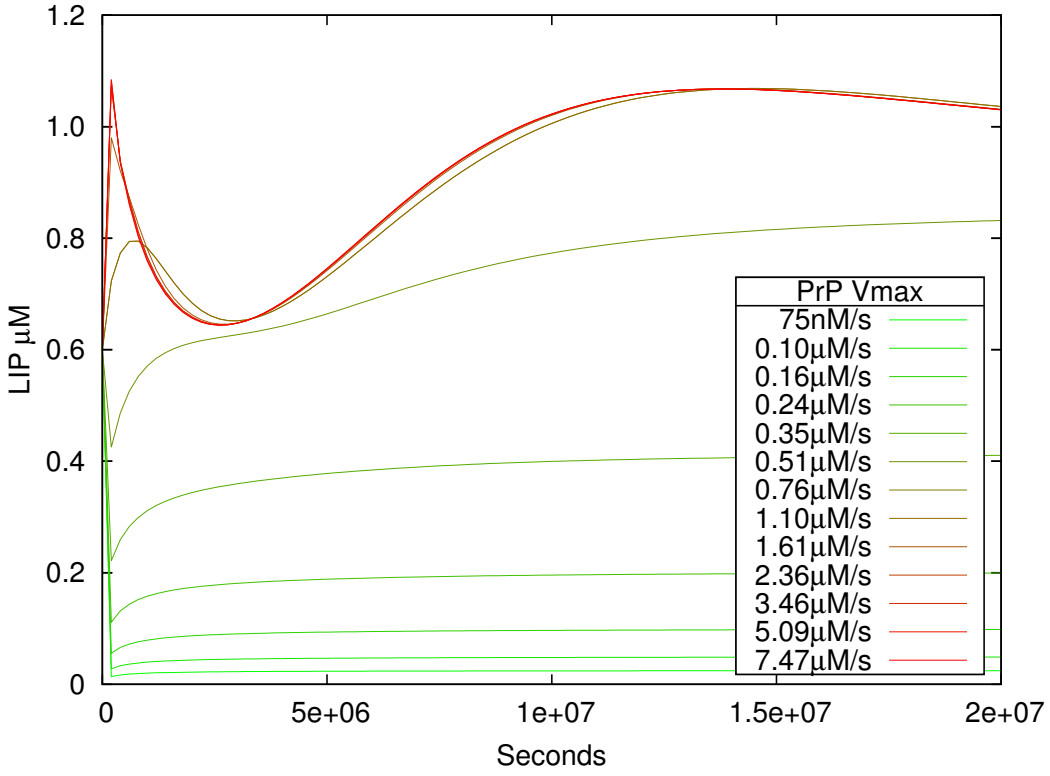

Figure 5.5: **Simulated liver iron pool concentration over time for varying iron reduction rates in the hepatocyte compartment.**

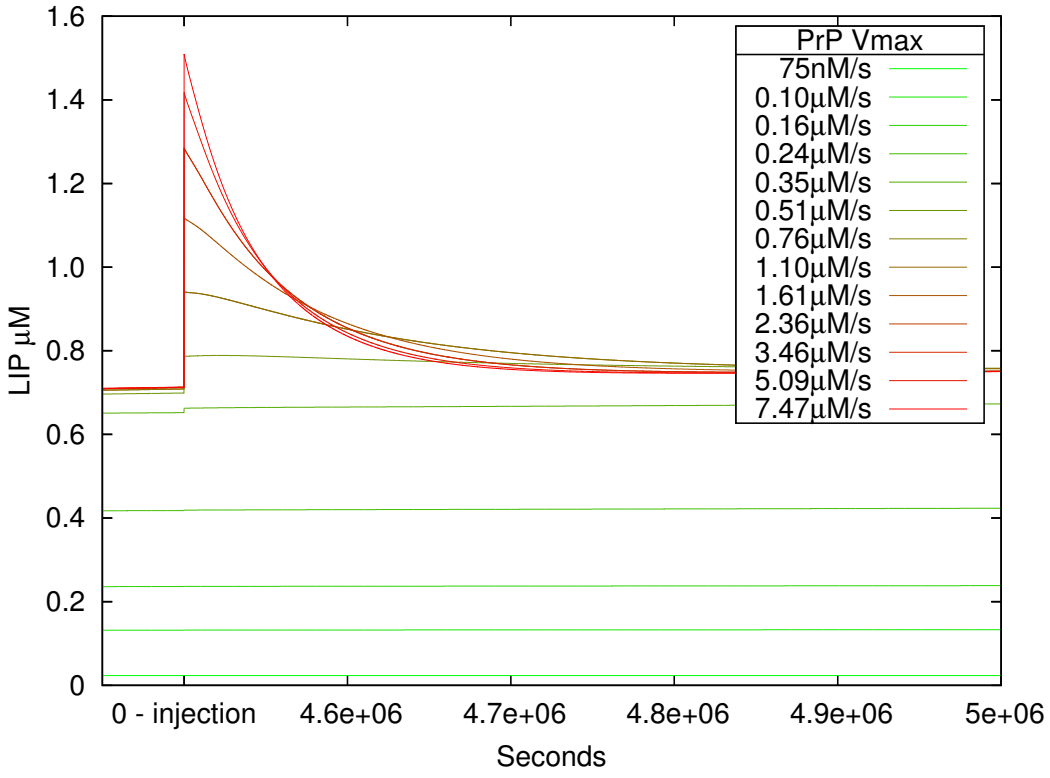

Figure 5.6: **Simulated liver iron pool concentration over time for varying rates of liver iron reduction following injected iron.**

the liver iron pool. The spike in liver iron following an injection event was reduced when liver iron reductase activity was reduced. The simulation recreated both the reduced iron level and the reduced peak following iron injection, which indicated reduced uptake is the underlying cause of the PrP knockout phenotype. This correlates well with the findings of Singh et al. (2013), who found reduced labile iron pool in PrP knockout mice, and less response to injection of iron-dextran. The reduced response to injected iron suggests that the PrP knockout phenotype is a result of reduced iron uptake as opposed to reduced iron availability in the serum. Iron uptake by transferrin receptor-mediated pathways was measured for the post injection-event period to assess whether there was a reduced rate of iron uptake in a simulation with reduced ferric reductase capacity (Figure 5.7). Decreased transferrin receptor-mediated uptake was observed with decreasing ferric reductase activity; this confirmed that the lower LIP levels were due to uptake and not export or storage.

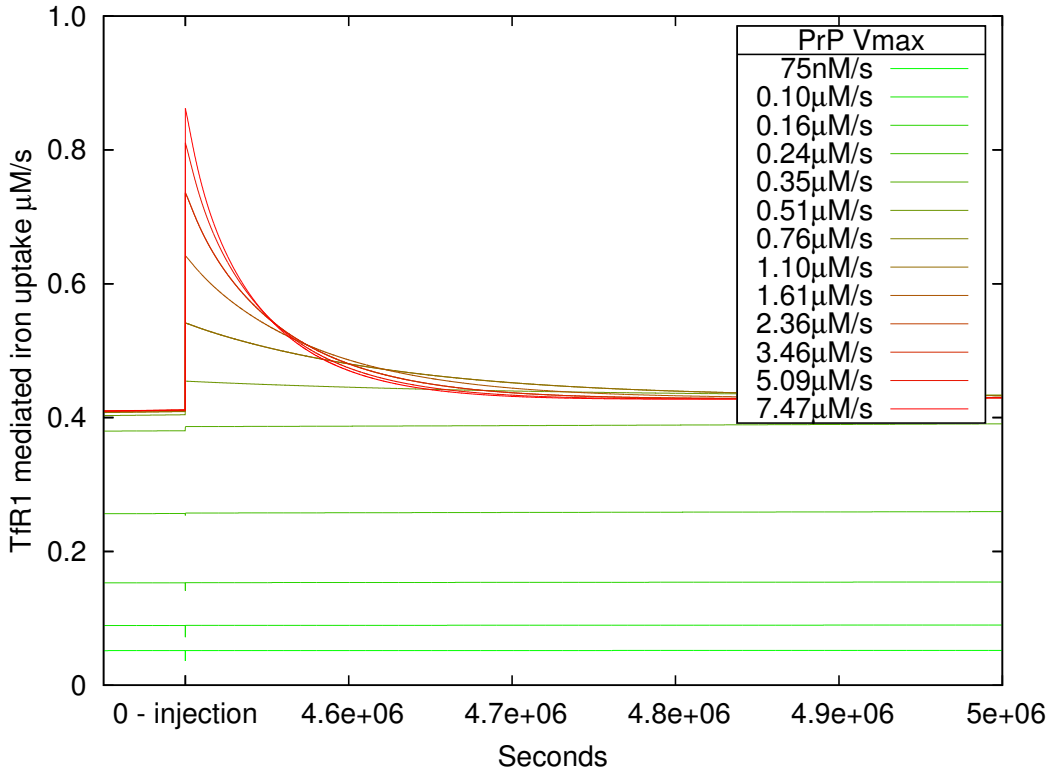

Figure 5.7: **Simulated transferrin receptor-mediated uptake over time for varying hepatocyte iron reduction rates following iron injection.**

The simulation provided the unique opportunity to measure the rate of iron uptake directly, which can be experimentally difficult. While Singh et al. (2013) suggested that the PrP phenotype may be a result of reduced iron uptake, they were unable to untangle possible confounding factors such as improper iron storage or increased iron export from the liver. Overall the phenotype from PrP knockout mice was matched well in the simulation suggesting that the physiological role of cellular prion protein is iron reduction following transferrin receptor mediated uptake.

5.3.3 Ubiquitous PrP Reductase Activity

As PrP is ubiquitously expressed Collinge (2001); Ermonval et al. (2009), it is possible that PrP has an iron-reductive effect at both the brush border of enterocytes and on the plasma membrane of hepatocytes. To establish whether this is likely, a simultaneous parameter scan of reduction rate at both sites was simulated and the results compared to the phenotype observed by Singh et al. (2013).

In the simulation, both decreasing ferrous iron availability and decreasing liver membrane ferric reductase activity lead to decreasing liver LIP size (Figure 5.8). This indicated that the liver phenotype observed in PrP knockout mice could be recreated correctly if PrP's ferric-reductase activity was ubiquitous and active in both cell types.

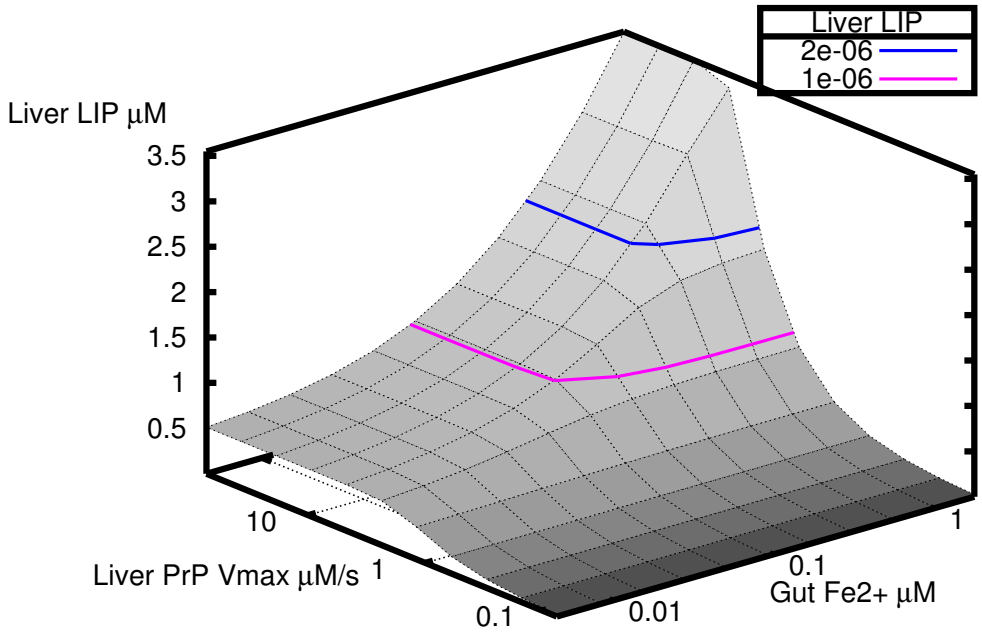

Figure 5.8: **Simulated liver iron pool levels for varying rates of iron reduction in hepatocytes and varying ferrous iron availability to enterocytes**

The $V_{\max}$ of hepatic reduction was found to have little effect until it was reduced below $2\ \mu$M/s. While decreasing the availability of ferrous iron at the brush border was also found to reduce the level of liver iron, this effect was small around the physiological liver iron pool concentration of around 1μM. It was found that if both sites of action (i.e. enterocytes and hepatocytes) were diminished, then the liver iron pool would decrease as seen in PrP knockout mice. A non-negative gradient at all points on the surface of Figure 5.8 indicated that the correct liver iron pool phenotype observed in PrP knockout mice would be recreated by loss of reductase activity in either, or both, cell types.

It was shown that decreasing intestinal reduction in isolation did not recreate the in-

creased iron uptake rate seen in mice (Figure 5.3). However, it was not known whether decreasing reductase rate in both cell types simultaneously could recreate the iron-uptake phenotype, to investigate this the iron uptake rate was assessed in a 2-dimensional parameter scan of iron reduction.

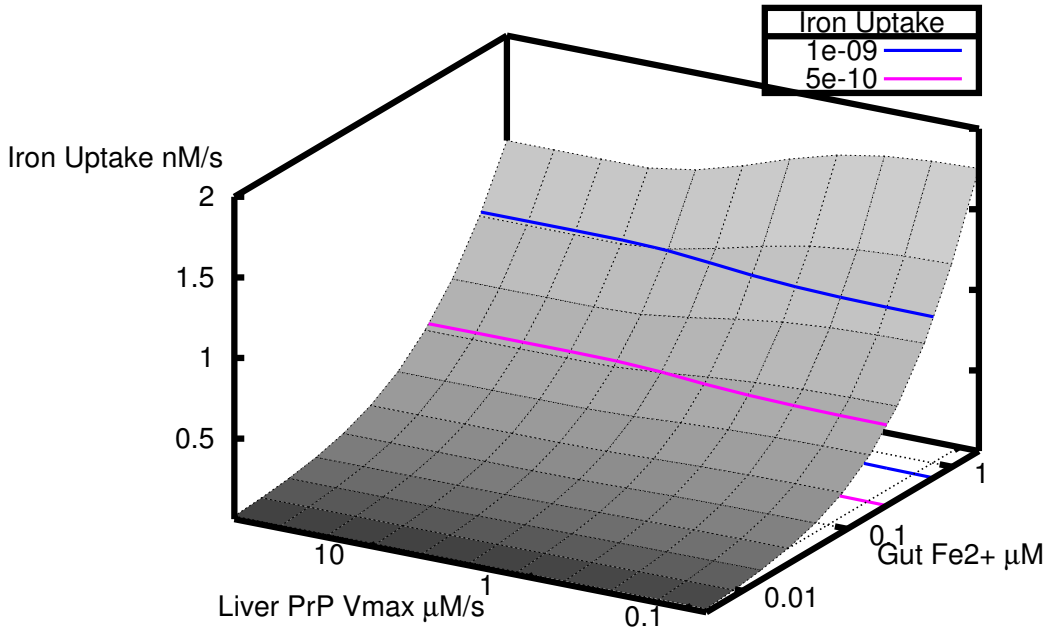

Figure 5.9: **Simulated dietary iron uptake rate for varying rates of iron reduction in hepatocytes and varying ferrous iron availability to enterocytes.**

Lowering liver reduction rates in the simulation was found to increase iron uptake, as seen in PrP knockout mice (Singh et al., 2013) (Figure 5.9). This effect was only seen when the $V_{\max}$ was lowered below around 2 μM/s, as with the liver LIP phenotype seen in Figure 5.8. At no point in the surface of Figure 5.8 does decreasing gut ferrous iron availability in isolation result in increasing iron uptake. Therefore it was found that the only way an increase in iron uptake, through decreased iron reduction, could be achieved in the simulation would be if the decrease in reductive capacity was much smaller in the gut than in the liver. A large decease in the liver's reductive capacity coupled with a small decrease in duodenal reduction created an increase in iron uptake rate as required. Therefore, the simulation predicted that PrP is most likely involved in the transferrin receptor uptake pathway found in the liver, rather than in divalent metal transporter mediated uptake from the diet. The model was able to demonstrate that despite a dietary absorption phenotype, the physiological role of cellular prion protein may not be in intestinal absorptive cells.

The model also made a number of predictions for other metabolites in PrP knockout, which remain to be measured experimentally. The simulation predicted an up-regulation of haem oxygenase 1, which would lead to a consequent reduction in haem in the liver of

PrP knockout organisms. The simulation also predicted a down-regulation of liver ferritin, yet it also unintuitively predicted an up-regulation of hepcidin.

5.4 Discussion

Iron has been implicated in a wide variety of neurological disorders from age-related cognitive decline (Bartzokis et al., 2007b) to Alzheimer's and Parkinson's disease (Gerlach et al., 1994; Pichler et al., 2013). Common to all these neurodegenerative disorders is a lack of understanding of the role of iron. It is not known whether iron plays a causative role in many neurodegenerative disorders or whether perturbations of iron metabolism are a common result of neurodegeneration caused, say, by a pathogenic alteration unrelated to iron. The model presented here provides a tool to assess whether perturbations of iron metabolism can recreate the disease state of conditions that are not traditionally associated with iron.

Cellular prion protein (PrP) came to the fore when it became clear that the key event leading to Creutzfeldt-Jakob disease (sCJD) is a conformational change in cellular prion protein into a β-sheet-rich isoform called PrP scrapie (PrP^{Sc}) (Palmer et al., 1991). The infection then spreads by PrP^{Sc}-templated conversion of cellular prion protein.

Cellular prion protein is ubiquitously expressed. However, it is most abundant on neuronal cells, which can explain why the misfolding of a ubiquitously expressed protein can result in a phenotype seemingly isolated to the brain (Horiuchi et al., 1995). Understanding the physiological role of prion protein will aid understanding of pathological prion disorders, but also has the potential for providing a therapeutic target as active cellular prion protein appears to be required for the pathological effects of PrP^{Sc}. Recent findings showing that PrP is a ferric reductase, and identifying a distinctive iron phenotype in a mouse model of PrP knockout mice (Singh et al., 2013), provides a potential physiological role for PrP.

Here I tested whether PrP's physiological function could be as ferric reductase by simulating whether altering this function could recreate the phenotype observed in mouse models where PrP expression was altered. The model was not fitted to any data relating to prion proteins and furthermore the prion protein was not considered in model construction as the iron reductase metabolite was unknown (with a number of proteins proposed to have this role). In PrP knockout mice, reduced liver iron was observed despite increasing dietary iron uptake (Singh et al., 2013). This phenotype is counter-intuitive as increasing dietary iron uptake in the healthy simulation (or in previously modelled disease states such as haemochromatosis; see Section 4.3.3) leads to tissue iron overload.

If PrP was providing a ferric reductase role *in vivo* then PrP knockout mice would have a reduced ferric reductase capacity. Therefore, to test whether PrPs iron-reducing properties could fully explain the phenotype observed in $PrP^{(-/-)}$ mice, the rate of iron reduction at the cell surface was reduced in the simulation. All other parameters were left

unchanged and a parameter scan was performed on the rate of iron reduction.

It was found that ferric iron reduction at the enterocyte basolateral membrane could not be the sole site of PrPs action, as reducing this activity did not increase iron uptake as seen in PrP knockout mice (Singh et al., 2013). The hepatocyte compartment membrane was then investigated as a potential site of PrPs ferric reductase activity, following TfR-mediated uptake. In the simulation, decreasing the rate of ferric reductase activity in the hepatocyte matched the counter-intuitive phenotype of increased dietary iron uptake but decreased liver iron pool seen in PrP knockout mice.

If, as suggested by the simulation, PrP reduces iron following TfR1/2-mediated uptake then PrP must be present on the cell surface of hepatocytes and presumably endocytosed with the transferrin-TfR complex. Cellular prion protein is ubiquitously expressed and targeted to the cell surface (Ermonval, 2003). While prion protein endocytosis as a result of iron uptake has not been investigated, there is evidence that PrP is involved in an endosomal pathway (Peters et al., 2003) and copper has been shown to stimulate prion protein endocytosis (Pauly and Harris, 1998). It is therefore possible that PrP could be endocytosed along with the transferrin-receptors and reduces iron prior to its export into the cytosol by DMT1. Using the modelling evidence presented here I propose that the physiological role of prion protein is in reducing endocytosed iron following transferrin receptor-mediated uptake.

As cellular prion protein is ubiquitously expressed I cannot simply ignore the simulated brush border reductive effect because the simulation does not match the data (Singh et al., 2013). Importantly, there is evidence for other ferric reductases on the brush border that could compensate for the loss of ferric reductase capacity in PrP knockout. Duodenal cytochrome B (DcytB) is known to reduce iron on the brush border membrane and is located primarily in intestinal cell types (McKie, 2008). Its location explains why it can not also compensate for PrP knockout in hepatic tissue.

Steap3 is usually considered the primary ferric-reductase in hepatic tissue performing the role of post-endocytosis ferric reduction. However Steap3 knockout cells still retain some endosomal iron reduction and iron uptake capacity (Ohgami et al., 2005), suggesting other ferric reductases are present. Our simulated findings suggest that PrP could be one of these, as yet unidentified, compensatory reductases. Singh et al. (2013) were not expecting the iron deficient phenotype found in the red blood cells (RBCs) of PrP knockout mice. However, if PrP does indeed reduce iron following TfR-mediated endocytosis then reduced iron uptake would be expected in RBCs. RBCs uptake iron through the TfR pathway. Therefore, a similar phenotype to that shown for the simulated liver compartment would be expected in RBCs.

Taken as a whole, the simulation results suggest that:

- PrP is either inactive as an iron reductase in intestinal absorptive cells or another reductase (e.g. DcytB) is active and able to compensate for PrP knockout.
- PrP on hepatocytes can not be fully compensated for by Steap3, and therefore PrP

remains important for adequate iron uptake in these cell types, and presumably for other cell types which primarily uptake transferrin-bound iron.

- PrP is endocytosed with transferrin receptors following iron uptake.

In exploring a role for prion protein, this simulation recreated counter-intuitive disease phenotypes for which it had not been fitted. This gives a powerful demonstration of the model's utility and unique value as a hypothesis testing tool, allowing a number of hypotheses, which are challenging to measure experimentally, to be simulated to determine which were most likely.

The approach presented here may be applicable to other enigmatic proteins, such as Huntingtin. Huntingtin, like PrP, is a ubiquitously expressed protein (Brown et al., 2008). The physiological role of the Huntingtin protein remains unclear. A pathogenic alteration, caused by a trinucleotide repeat in the gene encoding the protein, leads to Huntington's disease. Huntington's disease is a neurodegenerative disorder and has been associated with iron misregulation (Bartzokis et al., 2007a; Kell, 2010). I have demonstrated here that the computational model can suggest potential physiological action for poorly understood proteins. Similar modelling efforts to those presented here may improve our understanding of Huntingtin. Furthermore, there is some evidence that Huntingtin may be involved in a similar pathway to PrP as Huntingtin deficient zebra-fish demonstrate blocked receptor-mediated transferrin-bound iron uptake (Lumsden et al., 2007).

CHAPTER

SIX

DISCUSSION

The model created here is the most detailed and comprehensive mechanistic simulation of human iron metabolism to date. The liver simulation is the first quantitative model of liver iron metabolism. The hepatocyte is a cell type with particular importance due to its ability to sense systemic iron levels and control the iron regulatory hormone, hepcidin. Existing models have always considered hepcidin to be a fixed external signal (Mobilia et al., 2012) therefore ignoring its crucial role in system-scale regulation in human iron metabolism.

The model presented here was constructed and validated in stages to ensure accuracy was maintained at each stage as the scope of the model increased. The isolated liver (hepatocyte) model provided insights into how the transferrin receptors work as iron sensors and how hepcidin can become misregulated in haemochromatosis disease.

The need to include the effect of hepcidin on intestinal iron uptake was identified as important to improve the accuracy and utility of the model. The model was therefore expanded to include the intestinal absorptive cells (enterocytes) and the lumen of the gut. The intestinal compartment taken in isolation is, to my knowledge, the most detailed model of enterocyte iron metabolism, to date. However, when the intestinal compartment is coupled with the hepatocyte simulation, the model becomes a powerful *in silico* laboratory for human iron metabolism. The computational model provides a unique tool for investigating the interplay (either cooperation or conflict) between cellular regulation (via IRPs) and system-scale regulation (via hepcidin) in health and disease; this has been achieved by the inclusion of hepcidin's effect on dietery iron uptake in the model.

6.1 Computational Iron Metabolism Modelling in Health

Given expected dietary iron availability, the simulation demonstrates how iron is kept tightly regulated to ensure the labile iron pool remains within safe concentrations. With fixed dietary iron, the system reached a biologically accurate steady state that was validated by a large amount of experimental findings. Validation, reflecting the accuracy of the simulation, was achieved simultaneously at both a small scale, such as the amount of

iron stored in each ferritin cage, and a large scale, such as the overall rates of dietary iron uptake.

Metabolic control analysis of the health simulation indicates that control lies with hepcidin and the proposed role of haemochromatosis protein (HFE) and transferrin receptor 2 (TfR2) as a sensing system for systemic iron, located on the liver compartment (hepatocyte) membrane. This validates the proposed role of hepcidin and identifies promising therapeutic targets. Therapeutic use of hepcidin replacements or agonists are a promising area of ongoing investigation (Ramos et al., 2012). Interestingly, the HFE system has not been targeted as a hepcidin regulator directly and this model suggests this may be a more responsive point of intervention.

6.2 Computational Iron Metabolism Modelling in Disease States

Haemochromatosis disease was modelled mechanistically in a manner analogous to model organisms used to simulate the human disease. HFE knockout mice are used to study haemochromatosis disease as they recreate the phenotype accurately, while model organisms offer greater experimental flexibility. The HFE knockout model presented here provides yet more flexibility to determine any concentration or flux with practically zero time and cost. Potential therapeutic interventions can be tested using the simulation prior to experiments in model organisms to increase the chance of successful experimentation and reduce unneeded suffering of laboratory animals.

The disease model showed how control in haemochromatosis moves away from the iron-sensing components of the liver and hepcidin. Metabolic control analysis in haemochromatosis disease identified ferroportin itself as a good therapeutic target in haemochromatosis disease. Methods of inducing the degradation of ferroportin in the absence of hepcidin remain mainly unexplored experimentally. The simulation also indicates that manipulating the hypoxia-sensing apparatus to treat haemochromatosis disease could be surprisingly effective.

6.3 Iron Metabolism and Hypoxia

The hypoxia and iron metabolism networks are closely linked to the extent that a model of one would not be complete without including relevant components from the other. The model presented here provides the tools to investigate the interaction between the two systems in a comprehensive manner that would be challenging experimentally.

Despite a wide variety of oxygenation conditions, and therefore demands on iron metabolism, the networks were found to regulate iron carefully and always maintain safe iron levels. The increased draw of iron for erythropoiesis was balanced by a combination of up-regulation of iron uptake by hypoxia inducible factors and hepcidin-mediated

regulation of ferroportin. The comprehensive combined simulation of the interaction of hypoxia-sensing and iron metabolism provide novel insight and a level of understanding that would have been difficult to obtain through existing experimental methods.

6.4 Limitations

There was limited availability of quantitative human data for model parameterisation. To overcome this constraint data from multiple sources were used. This enabled data from multiple experimental conditions to improve our understanding of human iron metabolism. However, the quality and applicability of these data can limit the utility of the model. To ensure the limits of the model were well understood global sensitivity analysis was performed at each stage of model construction. These analyses identified reactions for which a wide range of sensitivity was possible if parameters were allowed to change. Care should be taken when drawing conclusions about those reactions with highly variable sensitivity.

The scope of the model, while the most comprehensive to date, limits its utility. Cell types which have not been modelled could impact the results presented here. Additional cell types would be connected to the existing serum compartment and would not directly affect the regulation of hepcidin or iron uptake; therefore, large impact from additional cell types would be unexpected.

The model does not include every potentially important protein or reaction and some modelled reactions are approximations of a more intricate process. The two iron responsive proteins (IRP1 and IRP2) are modelled as a single chemical species, however there is some evidence for distinct regulation by each iron responsive protein (Rouault, 2006). Ferritin is also modelled as a single protein. However, ferritin consists of two distinct subunits, which are the product of different genes (Boyd et al., 1985; Torti and Torti, 2002), and have distinct roles (Lawson et al., 1989). The ratio of the two ferritin subunits varies with cell type and iron status (Arosio et al., 1976). If two distinct ferritin subunits were included, the model could be validated by a wide variety of experimental data available investigating the subunit ratios in different tissues and in response to stimuli. Predictions of ferritin subunit ratios could not be made using the current model.

The model presented here was simulated in isolation, without attempt to model an entire virtual human. This may not reflect the impact that other, non-iron systems can have on human iron metabolism. Importantly the metabolism of other metals, such as copper, was not considered. Copper metabolism interacts with iron metabolism in a number of ways including the ferroxidase caeruloplasmin, which is a copper containing protein (Collins et al., 2010). Care should be taken when interpreting modelling results which may impact systems other than iron-metabolism.

6.5 Future Work

The model presented here has significant scope for further expansion and its potential is compelling. The model can be developed in both breadth and detail. As the mechanism behind the promotion of hepcidin expression becomes better understood this process could be modelled in more detail. Although it is well established that HFE promotes hepcidin expression through the bone morphogenetic protein BMP/SMAD signal transduction pathways, the mechanistic detail of this is only beginning to emerge. It appears that haemojuvelin (HJV) functions as a coreceptor required for the activation of SMAD (Babitt et al., 2006) and that the transmembrane serine protease, TMPRSS6, cleaves HJV reducing this effect (Du et al., 2008). Once this process is better understood and the reactions better characterised, addition of this mechanism into the model would be possible. However care must be taken with the parameterisation as the promoters of hepcidin expression have been found to have high control over the model presented. Increasing mechanistic detail in this way would allow identification of further potential sites for intervention.

The addition of haemosiderin formation, as a result of ferritin degradation, would allow the model to recreate better the phenotype of iron overload disorders. Haemosiderin formation in the model could be validated by a large amount of experimental data such as Perls' Prussian stains which stain for haemosiderin and are regularly used as a measure of iron overload.

The model can also be expanded to include other important cell-types. Priority should be given to include red blood cells, erythropoiesis in bone marrow (a major sink for iron), and recycling of senescent red blood cells by macrophages. Some of these processes should be relatively straightforward to simulate such as haem biosynthesis which consists of 8 well characterised reactions, although care should be taken as this process begins and ends in the macrophage with 4 cytosolic reactions. The modelling of macrophages engulfing erythrocytes and recycling iron requires careful consideration for how a discrete event, where a large amount of iron is released, can be simulated accurately and without numerical discontinuities. Rather than modelling individual engulfing events, an average red blood cell recycling rate proportional to the macrophage activity could be simulated to simplify the process.

Addition of a compartment representing the brain would increase the model's applicability to neurodegenerative disorders. The blood-brain barrier presents a challenge to modelling brain iron metabolism. However it is thought that the transferrin receptor (TfR) on the blood-brain barrier takes up iron into the brain (Jefferies et al., 1984; Fishman et al., 1987). It appears that the central nervous systems iron status controls the expression of blood-brain barrier TfR. If iron is made available through receptor-mediated endocytosis and the subsequent export by ferroportin, then this means the blood brain barrier could be modelled similarly to the existing cell-types (Rouault and Cooperman, 2006). It may be sufficient for initial investigations into neuronal diseases to assess levels of iron that cross the blood-brain barrier, but a model of iron distribution within the central nervous

system, although challenging given the heterogeneity and complex spatial arrangement of neuronal cells, offers even greater potential to help with our understanding of these diseases.

The approach taken here to identify a physiological site of action for cellular prion protein can be applied to other systems. Parkin, Huntingtin and cellular prion protein are all proteins with unclear function that are implicated in neurodegenerative disorders. While knockout of the protein implicated in disease must not be confused with the disease-causing alteration (PrP knockout is not CJD, and Huntingtin knockout is not Hungtinton's disease), knockout of any of these proteins generates a distinctive iron phenotypes in experimental organisms (Lumsden et al., 2007; Roth et al., 2010; Singh et al., 2013). By recreating the iron misregulation of knockout organisms in the model, as done with PrP here, potential sites of action can be identified. Automated parameter estimation techniques, such as those offered by COPASI, can also be used to attempt to fit the model to results from knockout organisms. The parameters that are adjusted to fit the experimental results point towards potential roles for the proteins being investigated. Once the physiological role of these proteins are better understood the model can be utilised to investigate the disease-causing alterations.

The modelling of reactive oxygen species (ROS) could be expanded, by including multiple new chemical species, to improve understanding of the formation of dangerous radicals and identify targets for reducing the damage caused by free iron (Kell, 2009). Modelling of the process by which free radicals lead to apoptotic signalling would help to establish whether excess levels of iron are sufficient to induce apoptosis (Circu and Aw, 2010). As mitochondria are regularly the targets of ROS damage, modelling mitochondrial iron metabolism in detail would improve the applicability of the model. Adding a mitochondrial compartment would enable modelling of the role of mitochondria in iron-sulfur protein biogenesis. This could aid our understanding of disorders such as Friedreich's ataxia, which is caused by a reduction in the levels of mitochondrial protein frataxin (Rötig et al., 1997), an important protein in iron-sulfur cluster biosynthesis (Yoon and Cowan, 2003). The process of iron cluster biogenesis is well characterised (Xu et al., 2013) and would create important feedbacks in the existing simulation as iron response proteins — known to control iron metabolism — are iron-sulfur containing proteins. Phenotypic effects of clinical interest, such as inefficient respiration, could be predicted by inadequate iron incorporation into the mitochondrial complexes.

BIBLIOGRAPHY

S. Abboud and D. J. Haile. A Novel Mammalian Iron-regulated Protein Involved in Intracellular Iron Metabolism. *Journal of Biological Chemistry*, 275(26):19906–19912, June 2000. doi: 10.1074/jbc.M000713200. URL http://dx.doi.org/10.1074/jbc.M000713200.

J. D. Aguirre, H. M. Clark, M. McIlvin, C. Vazquez, S. L. Palmere, D. J. Grab, J. Seshu, P. J. Hart, M. Saito, and V. C. Culotta. A manganese-rich environment supports superoxide dismutase activity in a lyme disease pathogen, borrelia burgdorferi. *Journal of Biological Chemistry*, 288(12):8468–8478, Mar. 2013. ISSN 1083-351X. doi: 10.1074/jbc.m112.433540. URL http://dx.doi.org/10.1074/jbc.m112.433540.

P. Aisen. Transferrin receptor 1. *The International Journal of Biochemistry & Cell Biology*, 36(11):2137–2143, November 2004. ISSN 13572725. doi: 10.1016/j.biocel.2004.02.007. URL http://dx.doi.org/10.1016/j.biocel.2004.02.007.

P. Aisen, A. Leibman, and J. Zweier. Stoichiometric and site characteristics of the binding of iron to human transferrin. *Journal of Biological Chemistry*, 253(6):1930–1937, March 1978. URL http://www.jbc.org/content/253/6/1930.abstract.

P. Aisen, C. Enns, and M. Wessling-Resnick. Chemistry and biology of eukaryotic iron metabolism. *The International Journal of Biochemistry & Cell Biology*, 33(10):940–959, October 2001. ISSN 1357-2725. URL http://view.ncbi.nlm.nih.gov/pubmed/11470229.

R. Albert, H. Jeong, and A.-L. Barabasi. Error and attack tolerance of complex networks. *Nature*, 406(6794):378–382, July 2000. doi: 10.1038/35019019. URL http://dx.doi.org/10.1038/35019019.

B. Alberts, A. Johnson, J. Lewis, M. Raff, K. Roberts, and P. Walter. *Molecular Biology of the Cell*. Garland Science, 5 edition, November 2007. ISBN 0815341059. URL http://www.worldcat.org/isbn/0815341059.

V. Andersen, J. Sonne, S. Sletting, and A. Prip. The volume of the liver in patients correlates to body weight and alcohol consumption. *Alcohol and Alcoholism*, 35(5): 531–532, Sept. 2000. ISSN 1464-3502. doi: 10.1093/alcalc/35.5.531. URL http://dx.doi.org/10.1093/alcalc/35.5.531.

N. C. Andrews. When is a heme transporter not a heme transporter? When it's a folate transporter. *Cell Metabolism*, 5(1):5–6, January 2007. ISSN 1550-4131. doi: 10.1016/j.cmet.2006.12.004. URL http://dx.doi.org/10.1016/j.cmet.2006.12.004.

N. C. Andrews. Forging a field: the golden age of iron biology. *Blood*, 112(2):219–230, July 2008. ISSN 1528-0020. doi: 10.1182/blood-2007-12-077388. URL http://dx.doi.org/10.1182/blood-2007-12-077388.

S. C. Andrews, M. C. Brady, A. Treffry, J. M. Williams, S. Mann, M. I. Cleton, W. de Bruijn, and P. M. Harrison. Studies on haemosiderin and ferritin from iron-loaded rat liver. *Biology of Metals*, 1(1):33–42, 1988. ISSN 0933-5854. URL http://view.ncbi.nlm.nih.gov/pubmed/3152870.

P. Arosio, M. Yokota, and J. W. Drysdale. Structural and immunological relationships of isoferritins in normal and malignant cells. *Cancer Research*, 36(5):1735–1739, May 1976. ISSN 1538-7445. URL http://cancerres.aacrjournals.org/content/36/5/1735.abstract.

A. Asberg. Screening for hemochromatosis: High prevalence and low morbidity in an unselected population of 65,238 persons. *Scandinavian Journal of Gastroenterology*, 36(10):1108–1115, Jan. 2001. doi: 10.1080/003655201750422747. URL http://dx.doi.org/10.1080/003655201750422747.

J. L. Babitt, F. W. Huang, D. M. Wrighting, Y. Xia, Y. Sidis, T. A. Samad, J. A. Campagna, R. T. Chung, A. L. Schneyer, C. J. Woolf, N. C. Andrews, and H. Y. Lin. Bone morphogenetic protein signaling by hemojuvelin regulates hepcidin expression. *Nature Genetics*, 38(5):531–539, May 2006. ISSN 1061-4036. doi: 10.1038/ng1777. URL http://dx.doi.org/10.1038/ng1777.

W. Bao, F. Song, X. Li, S. Rong, W. Yang, M. Zhang, P. Yao, L. Hao, N. Yang, F. B. Hu, and L. Liu. Plasma heme oxygenase-1 concentration is elevated in individuals with type 2 diabetes mellitus. *PLOS ONE*, 5(8):e12371+, Aug. 2010. doi: 10.1371/journal.pone.0012371. URL http://dx.doi.org/10.1371/journal.pone.0012371.

K. J. Barnham and A. I. Bush. Metals in alzheimer's and parkinson's diseases. *Current Opinion in Chemical Biology*, 12(2):222–228, Apr. 2008. ISSN 1367-5931. doi: 10.1016/j.cbpa.2008.02.019. URL http://dx.doi.org/10.1016/j.cbpa.2008.02.019.

G. Bartzokis, J. Mintz, D. Sultzer, P. Marx, J. Herzberg, C. Phelan, and S. Marder. In vivo mr evaluation of age-related increases in brain iron. *American Journal of Neuroradiology*, 15(6):1129–1138, 1994.

G. Bartzokis, P. H. Lu, T. A. Tishler, S. M. Fong, B. Oluwadara, J. P. Finn, D. Huang, Y. Bordelon, J. Mintz, and S. Perlman. Myelin breakdown and iron changes in huntingtonâĂŹs disease: pathogenesis and treatment implications. *Neurochemical Research*, 32(10):1655–1664, 2007a.

G. Bartzokis, T. A. Tishler, P. H. Lu, P. Villablanca, L. L. Altshuler, M. Carter, D. Huang, N. Edwards, and J. Mintz. Brain ferritin iron may influence age- and gender-related risks of neurodegeneration. *Neurobiology of Aging*, 28(3):414–423, Mar. 2007b. ISSN 01974580. doi: 10.1016/j.neurobiolaging.2006.02.005. URL http://dx.doi.org/10.1016/j.neurobiolaging.2006.02.005.

K. Basso, A. A. Margolin, G. Stolovitzky, U. Klein, R. Dalla-Favera, and A. Califano. Reverse engineering of regulatory networks in human B cells. *Nature Genetics*, 37(4): 382–390, April 2005. ISSN 1061-4036. doi: 10.1038/ng1532. URL http://dx.doi.org/10.1038/ng1532.

C. Beaumont, P. Leneuve, I. Devaux, J.-Y. Scoazec, M. Berthier, M.-N. Loiseau, B. Grandchamp, and D. Bonneau. Mutation in the iron responsive element of the l ferritin mRNA in a family with dominant hyperferritinaemia and cataract. *Nature Genetics*, 11(4):444–446, Dec. 1995. doi: 10.1038/ng1295-444. URL http://dx.doi.org/10.1038/ng1295-444.

V. Becker, M. Schilling, J. Bachmann, U. Baumann, A. Raue, T. Maiwald, J. Timmer, and U. Klingmüller. Covering a broad dynamic range: Information processing at the erythropoietin receptor. *Science*, 328(5984):1404–1408, June 2010. ISSN 1095-9203. doi: 10.1126/science.1184913. URL http://dx.doi.org/10.1126/science.1184913.

E. E. Benarroch. Brain iron homeostasis and neurodegenerative disease. *Neurology*, 72 (16):1436–1440, Apr. 2009. ISSN 1526-632X. doi: 10.1212/wnl.0b013e3181a26b30. URL http://dx.doi.org/10.1212/wnl.0b013e3181a26b30.

M. J. Bennett, J. A. Lebrón, and P. J. Bjorkman. Crystal structure of the hereditary haemochromatosis protein HFE complexed with transferrin receptor. *Nature*, 403(6765):46–53, January 2000. ISSN 0028-0836. doi: 10.1038/47417. URL http://dx.doi.org/10.1038/47417.

B. d. Benoist, E. McLean, I. Egll, M. Cogswell, et al. *Worldwide prevalence of anaemia 1993-2005: WHO global database on anaemia.* World Health Organization, 2008.

L. Berglund, E. Bjorling, P. Oksvold, L. Fagerberg, A. Asplund, C. Al-Khalili Szigyarto, A. Persson, J. Ottosson, H. Wernerus, P. Nilsson, E. Lundberg, A. Sivertsson, S. Navani, K. Wester, C. Kampf, S. Hober, F. Ponten, and M. Uhlen. A gene-centric Human Protein Atlas for expression profiles based on antibodies. *Molecular & Cellular Proteomics*, 7(10):2019–2027, October 2008. ISSN 1535-9484. doi: 10.1074/mcp.R800013-MCP200. URL http://dx.doi.org/10.1074/mcp.R800013-MCP200.

D. J. Bertges, S. Berg, M. P. Fink, and R. L. Delude. Regulation of hypoxia-inducible factor 1 in enterocytic cells. *Journal of Surgical Research*, 106(1):157–165, July 2002. ISSN 00224804. doi: 10.1006/jsre.2002.6439. URL http://dx.doi.org/10.1006/jsre.2002.6439.

C. Berzuini, P. Franzone, M. Stefanelli, and C. Viganotti. Iron kinetics: Modelling and parameter estimation in normal and anemic states. *Computers and Biomedical Research*, 11(3):209–227, June 1978. ISSN 00104809. doi: 10.1016/0010-4809(78)90008-3. URL http://dx.doi.org/10.1016/0010-4809(78)90008-3.

C. R. Bhasker, G. Burgiel, B. Neupert, A. Emery-Goodman, L. C. Kühn, and B. K. May. The putative iron-responsive element in the human erythroid 5-aminolevulinate synthase mRNA mediates translational control. *The Journal of Biological Chemistry*, 268 (17):12699–12705, June 1993. ISSN 0021-9258. URL http://view.ncbi.nlm.nih.gov/pubmed/8509404.

D. F. Bishop. Two different genes encode delta-aminolevulinate synthase in humans: nucleotide sequences of cDNAs for the housekeeping and erythroid genes. *Nucleic Acids Research*, 18(23):7187–7188, December 1990. ISSN 0305-1048. URL http://view.ncbi.nlm.nih.gov/pubmed/2263504.

K. Boelmans, B. Holst, M. Hackius, J. Finsterbusch, C. Gerloff, J. Fiehler, and A. Munchau. Brain iron deposition fingerprints in parkinson's disease and progressive supranuclear palsy. *Movement Disorders*, 27(3):421–427, Mar. 2012. ISSN 1531-8257. doi: 10.1002/mds.24926. URL http://dx.doi.org/10.1002/mds.24926.

F. Bou-Abdallah, P. Santambrogio, S. Levi, P. Arosio, and N. D. Chasteen. Unique iron binding and oxidation properties of human mitochondrial ferritin: a comparative analysis with Human H-chain ferritin. *Journal of Molecular Biology*, 347(3): 543–554, April 2005a. ISSN 0022-2836. doi: 10.1016/j.jmb.2005.01.007. URL http://dx.doi.org/10.1016/j.jmb.2005.01.007.

F. Bou-Abdallah, G. Zhao, H. R. Mayne, P. Arosio, and N. D. Chasteen. Origin of the unusual kinetics of iron deposition in human H-chain ferritin. *Journal of the American Chemical Society*, 127(11):3885–3893, March 2005b. ISSN 0002-7863. doi: 10.1021/ja044355k. URL http://dx.doi.org/10.1021/ja044355k.

C. Bouton and J.-C. C. Drapier. Iron regulatory proteins as no signal transducers. *Science Signal Transduction Knowledge Environment*, 2003(182), May 2003. ISSN 1525-8882. doi: 10.1126/stke.2003.182.pe17. URL http://dx.doi.org/10.1126/stke.2003.182.pe17.

D. Boyd, C. Vecoli, D. M. Belcher, S. K. Jain, and J. W. Drysdale. Structural and functional relationships of human ferritin h and l chains deduced from cdna clones. *The Journal of Biological Chemistry*, 260(21):11755–11761, Sept. 1985. ISSN 0021-9258. URL http://view.ncbi.nlm.nih.gov/pubmed/3840162.

V. Braun. Bacterial solutions to the iron-supply problem. *Trends in Biochemical Sciences*, 24(3):104–109, March 1999. ISSN 09680004. doi: 10.1016/S0968-0004(99)01359-6. URL http://dx.doi.org/10.1016/S0968-0004(99)01359-6.

W. Breuer, S. Epsztejn, and I. Z. Cabantchik. Iron Acquired from Transferrin by K562 Cells Is Delivered into a Cytoplasmic Pool of Chelatable Iron(II). *Journal of Biological Chemistry*, 270(41):24209–24215, October 1995a. doi: 10.1074/jbc.270.41.24209. URL http://dx.doi.org/10.1074/jbc.270.41.24209.

W. Breuer, S. Epsztejn, P. Millgram, and I. Z. Cabantchik. Transport of iron and other transition metals into cells as revealed by a fluorescent probe. *The American Journal of Physiology - Cell Physiology*, 268(6):C1354–1361, June 1995b. URL http://ajpcell.physiology.org/cgi/content/abstract/268/6/C1354.

T. B. Brown, A. I. Bogush, and M. E. Ehrlich. Neocortical expression of mutant huntingtin is not required for alterations in striatal gene expression or motor dysfunction in a transgenic mouse. *Human Molecular Genetics*, 17(20):3095–3104, Oct. 2008. ISSN 1460-2083. doi: 10.1093/hmg/ddn206. URL http://dx.doi.org/10.1093/hmg/ddn206.

S. L. Byrne, N. D. Chasteen, A. N. Steere, and A. B. Mason. The unique kinetics of iron release from transferrin: the role of receptor, lobe-lobe interactions, and salt at endosomal ph. *Journal of Molecular Biology*, 396(1):130–140, Feb. 2010. ISSN 1089-8638. doi: 10.1016/j.jmb.2009.11.023. URL http://dx.doi.org/10.1016/j.jmb.2009.11.023.

G. Cairo, L. Tacchini, and A. Pietrangelo. Lack of coordinate control of ferritin and transferrin receptor expression during rat liver regeneration. *Hepatology*, 28(1):173–178, 1998. doi: 10.1002/hep.510280123. URL http://dx.doi.org/10.1002/hep.510280123.

A. Calzolari, C. Raggi, S. Deaglio, N. M. M. Sposi, M. Stafsnes, K. Fecchi, I. Parolini, F. Malavasi, C. Peschle, M. Sargiacomo, and U. Testa. Tfr2 localizes in lipid raft domains and is released in exosomes to activate signal transduction along the mapk

pathway. *Journal of Cell Science*, 119(Pt 21):4486–4498, Nov. 2006. ISSN 0021-9533. doi: 10.1242/jcs.03228. URL http://dx.doi.org/10.1242/jcs.03228.

D. Camacho, P. VERA LICONA, P. Mendes, and R. Laubenbacher. Comparison of reverse-engineering methods using an in silico network. *Annals of the New York Academy of Sciences*, 1115(1):73–89, 2007.

C. Camaschella, A. Roetto, A. Calì, M. De Gobbi, G. Garozzo, M. Carella, N. Majorano, A. Totaro, and P. Gasparini. The gene TFR2 is mutated in a new type of haemochromatosis mapping to 7q22. *Nature Genetics*, 25(1):14–15, May 2000. ISSN 1061-4036. doi: 10.1038/75534. URL http://dx.doi.org/10.1038/75534.

I. Cavill. Erythropoiesis and iron. *Best Practice & Research Clinical Haematology*, 15(2):399–409, June 2002. ISSN 15216926. doi: 10.1053/beha.2002.0004. URL http://dx.doi.org/10.1053/beha.2002.0004.

C. Chaouiya, E. Remy, and D. Thieffry. Petri net modelling of biological regulatory networks. *Journal of Discrete Algorithms*, 6(2):165–177, June 2008. ISSN 15708667. doi: 10.1016/j.jda.2007.06.003. URL http://dx.doi.org/10.1016/j.jda.2007.06.003.

H. Chen, T. Su, Z. K. Attieh, T. C. Fox, A. T. McKie, G. J. Anderson, and C. D. Vulpe. Systemic regulation of Hephaestin and Ireg1 revealed in studies of genetic and nutritional iron deficiency. *Blood*, 102(5):1893–1899, September 2003. ISSN 0006-4971. doi: 10.1182/blood-2003-02-0347. URL http://dx.doi.org/10.1182/blood-2003-02-0347.

H. Chen, Z. K. Attieh, T. Su, B. A. Syed, H. Gao, R. M. Alaeddine, T. C. Fox, J. Usta, C. E. Naylor, R. W. Evans, A. T. McKie, G. J. Anderson, and C. D. Vulpe. Hephaestin is a ferroxidase that maintains partial activity in sex-linked anemia mice. *Blood*, 103(10):3933–3939, May 2004. ISSN 0006-4971. doi: 10.1182/blood-2003-09-3139. URL http://dx.doi.org/10.1182/blood-2003-09-3139.

O. S. Chen, K. P. Blemings, K. L. Schalinske, and R. S. Eisenstein. Dietary iron intake rapidly influences iron regulatory proteins, ferritin subunits and mitochondrial aconitase in rat liver. *The Journal of Nutrition*, 128(3):525–535, Mar. 1998. ISSN 1541-6100. URL http://jn.nutrition.org/content/128/3/525.abstract.

Y. Cheng, O. Zak, P. Aisen, S. C. Harrison, and T. Walz. Structure of the Human Transferrin Receptor-Transferrin Complex. *Cell*, 116(4):565–576, February 2004. ISSN 00928674. doi: 10.1016/S0092-8674(04)00130-8. URL http://dx.doi.org/10.1016/S0092-8674(04)00130-8.

J. Chifman, A. Kniss, P. Neupane, I. Williams, B. Leung, Z. Deng, P. Mendes, V. Hower, F. M. Torti, S. A. Akman, S. V. Torti, and R. Laubenbacher. The core control system of intracellular iron homeostasis: a mathematical model. *Journal of Theoretical Biology*, 300:91–99, May 2012. ISSN 1095-8541. doi: 10.1016/j.jtbi.2012.01.024. URL `http://dx.doi.org/10.1016/j.jtbi.2012.01.024`.

M. Chloupková, A.-S. Zhang, and C. A. Enns. Stoichiometries of transferrin receptors 1 and 2 in human liver. *Blood Cells, Molecules, and Diseases*, 44(1):28–33, Jan. 2010. ISSN 10799796. doi: 10.1016/j.bcmd.2009.09.004. URL `http://dx.doi.org/10.1016/j.bcmd.2009.09.004`.

M. J. Chorney, Y. Yoshida, P. N. Meyer, M. Yoshida, and G. S. Gerhard. The enigmatic role of the hemochromatosis protein (HFE) in iron absorption. *Trends in Molecular Medicine*, 9(3):118–125, March 2003. ISSN 1471-4914. URL `http://view.ncbi.nlm.nih.gov/pubmed/12657433`.

A. C. Chua, R. D. Delima, E. H. Morgan, C. E. Herbison, J. E. Tirnitz-Parker, R. M. Graham, R. E. Fleming, R. S. Britton, B. R. Bacon, J. K. Olynyk, and D. Trinder. Iron uptake from plasma transferrin by a transferrin receptor 2 mutant mouse model of haemochromatosis. *Journal of Hepatology*, 52(3):425–431, Mar. 2010. ISSN 0168-8278. doi: 10.1016/j.jhep.2009.12.010. URL `http://dx.doi.org/10.1016/j.jhep.2009.12.010`.

M. L. Circu and T. Y. Aw. Reactive oxygen species, cellular redox systems, and apoptosis. *Free Radical Biology and Medicine*, 48(6):749–762, Mar. 2010. ISSN 08915849. doi: 10.1016/j.freeradbiomed.2009.12.022. URL `http://dx.doi.org/10.1016/j.freeradbiomed.2009.12.022`.

S. F. Clark. Iron Deficiency Anemia. *Nutrition in Clinical Practice*, 23(2):128–141, April 2008. ISSN 0884-5336. doi: 10.1177/0884533608314536. URL `http://dx.doi.org/10.1177/0884533608314536`.

J. Collinge. Prion diseases of humans and animals: Their causes and molecular basis. *Annual Review of Neuroscience*, 24(1):519–550, 2001. doi: 10.1146/annurev.neuro.24.1.519. URL `http://dx.doi.org/10.1146/annurev.neuro.24.1.519`.

J. Collingwood and J. Dobson. Mapping and characterization of iron compounds in alzheimer's tissue. *Journal of Alzheimer's Disease*, 10(2):215–222, 2006.

J. F. Collins, J. R. Prohaska, and M. D. Knutson. Metabolic crossroads of iron and copper. *Nutrition reviews*, 68(3):133–147, Mar. 2010. ISSN 1753-4887. doi: 10.1111/j.1753-4887.2010.00271.x. URL `http://dx.doi.org/10.1111/j.1753-4887.2010.00271.x`.

M. Constante, W. Jiang, D. Wang, V.-A. Raymond, M. Bilodeau, and M. M. Santos. Distinct requirements for hfe in basal and induced hepcidin levels in iron overload and inflammation. *American Journal of Physiology - Gastrointestinal and Liver Physiology*, 291(2):G229–G237, Aug. 2006. ISSN 1522-1547. doi: 10.1152/ajpgi.00092.2006. URL http://dx.doi.org/10.1152/ajpgi.00092.2006.

B. Corsi, S. Levi, A. Cozzi, A. Corti, D. Altimare, A. Albertini, and P. Arosio. Overexpression of the hereditary hemochromatosis protein, HFE, in HeLa cells induces and iron-deficient phenotype. *FEBS Letters*, 460(1):149–152, October 1999. ISSN 0014-5793. URL http://view.ncbi.nlm.nih.gov/pubmed/10571078.

A. Cozzi. Role of iron and ferritin in tnfa-induced apoptosis in hela cells. *FEBS Letters*, 537(1-3):187–192, Feb. 2003. ISSN 00145793. doi: 10.1016/S0014-5793(03)00114-5. URL http://dx.doi.org/10.1016/S0014-5793(03)00114-5.

J. O. Dada, I. Spasić, N. W. Paton, and P. Mendes. SBRML: a markup language for associating systems biology data with models. *Bioinformatics*, 26(7):932–938, April 2010. ISSN 1367-4811. doi: 10.1093/bioinformatics/btq069. URL http://dx.doi.org/10.1093/bioinformatics/btq069.

T. A. Dailey, J. H. Woodruff, and H. A. Dailey. Examination of mitochondrial protein targeting of haem synthetic enzymes: in vivo identification of three functional haem-responsive motifs in 5-aminolaevulinate synthase. *The Biochemical Journal*, 386(Pt 2):381–386, March 2005. ISSN 1470-8728. doi: 10.1042/BJ20040570. URL http://dx.doi.org/10.1042/BJ20040570.

F. D'Alessio, M. W. Hentze, and M. U. Muckenthaler. The hemochromatosis proteins HFE, TfR2, and HJV form a membrane-associated protein complex for hepcidin regulation. *Journal of Hepatology*, 57(5):1052–1060, Nov. 2012. ISSN 1600-0641. doi: 10.1016/j.jhep.2012.06.015. URL http://dx.doi.org/10.1016/j.jhep.2012.06.015.

A. Dancis, R. D. Klausner, A. G. Hinnebusch, and J. G. Barriocanal. Genetic evidence that ferric reductase is required for iron uptake in Saccharomyces cerevisiae. *Molecular and Cellular Biology*, 10(5):2294–2301, May 1990. ISSN 0270-7306. URL http://view.ncbi.nlm.nih.gov/pubmed/2183029].

A. Dancis, D. G. Roman, G. J. Anderson, A. G. Hinnebusch, and R. D. Klausner. Ferric reductase of Saccharomyces cerevisiae: molecular characterization, role in iron uptake, and transcriptional control by iron. *Proceedings of the National Academy of Sciences of the United States of America*, 89(9):3869–3873, May 1992. ISSN 0027-8424. URL http://view.ncbi.nlm.nih.gov/pubmed/1570306].

G. De Crescenzo, C. Boucher, Y. Durocher, and M. Jolicoeur. Kinetic Characterization by Surface Plasmon Resonance-Based Biosensors: Principle and Emerging Trends.

Cellular and Molecular Bioengineering, 1(4):204–215, December 2008. ISSN 1865-5025. doi: 10.1007/s12195-008-0035-5. URL http://dx.doi.org/10.1007/s12195-008-0035-5.

A. de la Fuente, P. Brazhnik, and P. Mendes. Linking the genes: inferring quantitative gene networks from microarray data. *Trends in Genetics*, 18(8):395–398, 2002.

A. De La Fuente, N. Bing, I. Hoeschele, and P. Mendes. Discovery of meaningful associations in genomic data using partial correlation coefficients. *Bioinformatics*, 20(18): 3565–3574, 2004.

N. Dehne. Cisplatin Ototoxicity: Involvement of Iron and Enhanced Formation of Superoxide Anion Radicals. *Toxicology and Applied Pharmacology*, 174(1):27–34, July 2001. ISSN 0041008X. doi: 10.1006/taap.2001.9171. URL http://dx.doi.org/10.1006/taap.2001.9171.

L. A. Doyle and D. D. Ross. Multidrug resistance mediated by the breast cancer resistance protein BCRP (ABCG2). *Oncogene*, 22(47):7340–7358, October 2003. ISSN 0950-9232. doi: 10.1038/sj.onc.1206938. URL http://dx.doi.org/10.1038/sj.onc.1206938.

A. Droste, C. Sorg, and P. Högger. Shedding of CD163, a novel regulatory mechanism for a member of the scavenger receptor cysteine-rich family. *Biochemical and Biophysical Research Communications*, 256(1):110–113, March 1999. ISSN 0006-291X. doi: 10.1006/bbrc.1999.0294. URL http://dx.doi.org/10.1006/bbrc.1999.0294.

X. Du, E. She, T. Gelbart, J. Truksa, P. Lee, Y. Xia, K. Khovananth, S. Mudd, N. Mann, E. M. M. Moresco, E. Beutler, and B. Beutler. The serine protease TMPRSS6 is required to sense iron deficiency. *Science*, 320(5879):1088–1092, May 2008. ISSN 1095-9203. doi: 10.1126/science.1157121. URL http://dx.doi.org/10.1126/science.1157121.

R. Eberhart and J. Kennedy. A new optimizer using particle swarm theory. In *Micro Machine and Human Science, 1995. MHS '95., Proceedings of the Sixth International Symposium on*, pages 39 –43, oct 1995. doi: 10.1109/MHS.1995.494215.

J. S. Edwards, R. U. Ibarra, and B. O. Palsson. In silico predictions of Escherichia coli metabolic capabilities are consistent with experimental data. *Nature Biotechnology*, 19 (2):125–130, February 2001. ISSN 1087-0156. doi: 10.1038/84379. URL http://dx.doi.org/10.1038/84379.

A. Egyed. Carrier mediated iron transport through erythroid cell membrane. *British Journal of Haematology*, 68(4):483–486, 1988. doi: 10.1111/j.1365-2141.1988.tb04241.x. URL http://dx.doi.org/10.1111/j.1365-2141.1988.tb04241.x.

S. Epsztejn, O. Kakhlon, H. Glickstein, W. Breuer, and Z. I. Cabantchik. Fluorescence Analysis of the Labile Iron Pool of Mammalian Cells. *Analytical Biochemistry*, pages 31–40, May 1997. ISSN 0003-2697. URL http://www.ingentaconnect.com/content/ap/ab/1997/00000248/00000001/art02126.

R. Erlitzki, J. C. Long, and E. C. Theil. Multiple, conserved iron-responsive elements in the 3'-untranslated region of transferrin receptor mrna enhance binding of iron regulatory protein 2. *The Journal of Biological Chemistry*, 277(45):42579–42587, Nov. 2002. ISSN 0021-9258. doi: 10.1074/jbc.m207918200. URL http://dx.doi.org/10.1074/jbc.m207918200.

M. Ermonval. Evolving views in prion glycosylation: functional and pathological implications. *Biochimie*, 85(1-2):33–45, Feb. 2003. ISSN 03009084. doi: 10.1016/s0300-9084(03)00040-3. URL http://dx.doi.org/10.1016/s0300-9084(03)00040-3.

M. Ermonval, A. Baudry, F. Baychelier, E. Pradines, M. Pietri, K. Oda, B. Schneider, S. Mouillet-Richard, J.-M. Launay, and O. Kellermann. The cellular prion protein interacts with the tissue non-specific alkaline phosphatase in membrane microdomains of bioaminergic neuronal cells. *PLOS ONE*, 4(8):e6497+, Aug. 2009. ISSN 1932-6203. doi: 10.1371/journal.pone.0006497. URL http://dx.doi.org/10.1371/journal.pone.0006497.

B. O. Fabriek, C. D. Dijkstra, and T. K. van den Berg. The macrophage scavenger receptor CD163. *Immunobiology*, 210(2-4):153–160, 2005. ISSN 0171-2985. URL http://view.ncbi.nlm.nih.gov/pubmed/16164022.

J. N. Feder, A. Gnirke, W. Thomas, Z. Tsuchihashi, D. A. Ruddy, A. Basava, F. Dormishian, R. Domingo, M. C. Ellis, A. Fullan, L. M. Hinton, N. L. Jones, B. E. Kimmel, G. S. Kronmal, P. Lauer, V. K. Lee, D. B. Loeb, F. A. Mapa, E. McClelland, N. C. Meyer, G. A. Mintier, N. Moeller, T. Moore, E. Morikang, C. E. Prass, L. Quintana, S. M. Starnes, R. C. Schatzman, K. J. Brunke, D. T. Drayna, N. J. Risch, B. R. Bacon, and R. K. Wolff. A novel MHC class I-like gene is mutated in patients with hereditary haemochromatosis. *Nature Genetics*, 13(4):399–408, August 1996. ISSN 1061-4036. doi: 10.1038/ng0896-399. URL http://dx.doi.org/10.1038/ng0896-399.

J. N. Feder, D. M. Penny, A. Irrinki, V. K. Lee, J. A. Lebrón, N. Watson, Z. Tsuchihashi, E. Sigal, P. J. Bjorkman, and R. C. Schatzman. The hemochromatosis gene product complexes with the transferrin receptor and lowers its affinity for ligand binding. *Proceedings of the National Academy of Sciences of the United States of America*, 95(4):1472–1477, February 1998. ISSN 0027-8424. URL http://view.ncbi.nlm.nih.gov/pubmed/9465039.

G. C. Ferreira. Heme biosynthesis: biochemistry, molecular biology, and relationship to disease. *Journal of Bioenergetics and Biomembranes*, 27(2):147–150, April 1995. ISSN 0145-479X. URL http://view.ncbi.nlm.nih.gov/pubmed/7592561.

G. C. Ferreira and J. Gong. 5-Aminolevulinate synthase and the first step of heme biosynthesis. *Journal of Bioenergetics and Biomembranes*, 27(2):151–159, April 1995. ISSN 0145-479X. URL http://view.ncbi.nlm.nih.gov/pubmed/7592562.

J. B. Fishman, J. B. Rubin, J. V. Handrahan, J. R. Connor, and R. E. Fine. Receptor-mediated transcytosis of transferrin across the blood-brain barrier. *Journal of Neuroscience Research*, 18(2):299–304, 1987. ISSN 0360-4012. doi: 10.1002/jnr.490180206. URL http://dx.doi.org/10.1002/jnr.490180206.

R. E. Fleming, C. C. Holden, S. Tomatsu, A. Waheed, E. M. Brunt, R. S. Britton, B. R. Bacon, D. C. Roopenian, and W. S. Sly. Mouse strain differences determine severity of iron accumulation in hfe knockout model of hereditary hemochromatosis. *Proceedings of the National Academy of Sciences*, 98(5):2707–2711, Feb. 2001. ISSN 1091-6490. doi: 10.1073/pnas.051630898. URL http://dx.doi.org/10.1073/pnas.051630898.

P. Flicek, B. L. Aken, K. Beal, B. Ballester, M. Caccamo, Y. Chen, L. Clarke, G. Coates, F. Cunningham, T. Cutts, T. Down, S. C. Dyer, T. Eyre, S. Fitzgerald, J. Fernandez-Banet, S. GrÃÂd'f, S. Haider, M. Hammond, R. Holland, K. L. Howe, K. Howe, N. Johnson, A. Jenkinson, A. KÃÂd'h AÂd'ri, D. Keefe, F. Kokocinski, E. Kulesha, D. Lawson, I. Longden, K. Megy, P. Meidl, B. Overduin, A. Parker, B. Pritchard, A. Prlic, S. Rice, D. Rios, M. Schuster, I. Sealy, G. Slater, D. Smedley, G. Spudich, S. Trevanion, A. J. Vilella, J. Vogel, S. White, M. Wood, E. Birney, T. Cox, V. Curwen, R. Durbin, X. M. Fernandez-Suarez, J. Herrero, T. J. P. Hubbard, A. Kasprzyk, G. Proctor, J. Smith, A. Ureta-Vidal, and S. Searle. Ensembl 2008. *Nucleic Acids Research*, 36(suppl 1):D707–D714, January 2008. ISSN 1362-4962. doi: 10.1093/nar/gkm988. URL http://dx.doi.org/10.1093/nar/gkm988.

P. C. Franzone, A. Paganuzzi, and M. Stefanelli. A mathematical model of iron metabolism. *Journal of Mathematical Biology*, 15(2):173–201, 1982. ISSN 0303-6812. URL http://view.ncbi.nlm.nih.gov/pubmed/7153668.

H. B. Fraser, A. E. Hirsh, L. M. Steinmetz, C. Scharfe, and M. W. Feldman. Evolutionary rate in the protein interaction network. *Science*, 296(5568):750–752, April 2002. ISSN 1095-9203. doi: 10.1126/science.1068696. URL http://dx.doi.org/10.1126/science.1068696.

D. M. Frazer and G. J. Anderson. The orchestration of body iron intake: how and where do enterocytes receive their cues? *Blood Cells, Molecules & Diseases*, 30(3):288–297,

2003. ISSN 1079-9796. URL http://view.ncbi.nlm.nih.gov/pubmed/12737947.

D. M. Frazer, H. R. Inglis, S. J. Wilkins, K. N. Millard, T. M. Steele, G. D. McLaren, A. T. McKie, C. D. Vulpe, and G. J. Anderson. Delayed hepcidin response explains the lag period in iron absorption following a stimulus to increase erythropoiesis. *Gut*, 53(10):1509–1515, October 2004. ISSN 0017-5749. doi: 10.1136/gut.2003.037416. URL http://dx.doi.org/10.1136/gut.2003.037416.

N. Friedman, M. Linial, I. Nachman, and D. Pe'er. Using Bayesian networks to analyze expression data. *Journal of Computational Biology : a Journal of Computational Molecular Cell Biology*, 7(3-4):601–620, August 2000. ISSN 1066-5277. doi: 10.1089/106652700750050961. URL http://dx.doi.org/10.1089/106652700750050961.

A. Funahashi, Y. Matsuoka, A. Jouraku, M. Morohashi, N. Kikuchi, and H. Kitano. CellDesigner 3.5: A Versatile Modeling Tool for Biochemical Networks. *Proceedings of the IEEE*, 96(8):1254–1265, August 2008. ISSN 0018-9219. doi: 10.1109/JPROC.2008.925458. URL http://dx.doi.org/10.1109/JPROC.2008.925458.

J. Gao, J. Chen, M. Kramer, H. Tsukamoto, A.-S. S. Zhang, and C. A. Enns. Interaction of the hereditary hemochromatosis protein hfe with transferrin receptor 2 is required for transferrin-induced hepcidin expression. *Cell Metabolism*, 9(3):217–227, Mar. 2009. ISSN 1932-7420. doi: 10.1016/j.cmet.2009.01.010. URL http://dx.doi.org/10.1016/j.cmet.2009.01.010.

S. G. Gehrke, H. Kulaksiz, T. Herrmann, H.-D. Riedel, K. Bents, C. Veltkamp, and W. Stremmel. Expression of hepcidin in hereditary hemochromatosis: evidence for a regulation in response to the serum transferrin saturation and to non-transferrin-bound iron. *Blood*, 102(1):371–376, July 2003. doi: 10.1182/blood-2002-11-3610. URL http://dx.doi.org/10.1182/blood-2002-11-3610.

M. Gerlach, D. Ben-Shachar, P. Riederer, and M. B. H. Youdim. Altered brain metabolism of iron as a cause of neurodegenerative diseases? *Journal of Neurochemistry*, 63(3):793–807, Sept. 1994. doi: 10.1046/j.1471-4159.1994.63030793.x. URL http://dx.doi.org/10.1046/j.1471-4159.1994.63030793.x.

D. Girelli, P. Trombini, F. Busti, N. Campostrini, M. Sandri, S. Pelucchi, M. Westerman, T. Ganz, E. Nemeth, A. Piperno, and C. Camaschella. A time course of hepcidin response to iron challenge in patients with hfe and tfr2 hemochromatosis. *Haematologica*, 96(4):500–506, Apr. 2011. ISSN 1592-8721. doi: 10.3324/haematol.2010.033449. URL http://dx.doi.org/10.3324/haematol.2010.033449.

N. Gizzatkulov, I. Goryanin, E. Metelkin, E. Mogilevskaya, K. Peskov, and O. Demin. DBSolve Optimum: a software package for kinetic modeling which allows dynamic

visualization of simulation results. *BMC Systems Biology*, 4(1):109+, August 2010. ISSN 1752-0509. doi: 10.1186/1752-0509-4-109. URL http://dx.doi.org/10.1186/1752-0509-4-109.

A. S. Go, J. Yang, L. M. Ackerson, K. Lepper, S. Robbins, B. M. Massie, and M. G. Shlipak. Hemoglobin level, chronic kidney disease, and the risks of death and hospitalization in adults with chronic heart failure. *Circulation*, 113(23):2713–2723, June 2006. ISSN 1524-4539. doi: 10.1161/circulationaha.105.577577. URL http://dx.doi.org/10.1161/circulationaha.105.577577.

D. H. Goetz, M. A. Holmes, N. Borregaard, M. E. Bluhm, K. N. Raymond, and R. K. Strong. The neutrophil lipocalin NGAL is a bacteriostatic agent that interferes with siderophore-mediated iron acquisition. *Molecular cell*, 10(5):1033–1043, November 2002. ISSN 1097-2765. URL http://view.ncbi.nlm.nih.gov/pubmed/12453412.

B. Goldstein, D. Coombs, X. He, A. R. Pineda, and C. Wofsy. The influence of transport on the kinetics of binding to surface receptors: application to cells and BIAcore. *Journal of Molecular Recognition*, 12(5):293–299, 1999. ISSN 0952-3499. URL http://dx.doi.org/10.1002/(SICI)1099-1352(199909/10)12:5%3C293::AID-JMR472%3E3.0.CO;2-M.

P. T. Gomme, K. B. McCann, and J. Bertolini. Transferrin: structure, function and potential therapeutic actions. *Drug Discovery Today*, 10(4):267–273, February 2005. ISSN 1359-6446. doi: 10.1016/S1359-6446(04)03333-1. URL http://dx.doi.org/10.1016/S1359-6446(04)03333-1.

L. Gooman. Alzheimer's disease: a clinico-pathologic analysis of twenty-three cases with a theory on pathogenesis. *The Journal of Nervous and Mental Disease*, 118(2):97–130, 1953.

T. Goswami and N. C. Andrews. Hereditary Hemochromatosis Protein, HFE, Interaction with Transferrin Receptor 2 Suggests a Molecular Mechanism for Mammalian Iron Sensing. *Journal of Biological Chemistry*, 281(39):28494–28498, September 2006. doi: 10.1074/jbc.C600197200. URL http://dx.doi.org/10.1074/jbc.C600197200.

S. Granick. Ferritin: Its properties and significance for iron metabolism. *Chemical Reviews*, 38(3):379–403, June 1946. doi: 10.1021/cr60121a001. URL http://dx.doi.org/10.1021/cr60121a001.

S. Grunwald, A. Speer, J. Ackermann, and I. Koch. Petri net modelling of gene regulation of the Duchenne muscular dystrophy. *Bio Systems*, 92(2):189–205, May 2008. ISSN 0303-2647. doi: 10.1016/j.biosystems.2008.02.005. URL http://dx.doi.org/10.1016/j.biosystems.2008.02.005.

H. Gunshin, B. Mackenzie, U. V. Berger, Y. Gunshin, M. F. Romero, W. F. Boron, S. Nussberger, J. L. Gollan, and M. A. Hediger. Cloning and characterization of a mammalian proton-coupled metal-ion transporter. *Nature*, 388(6641):482–488, July 1997. ISSN 0028-0836. doi: 10.1038/41343. URL http://dx.doi.org/10.1038/41343.

H. Gunshin, C. N. Starr, C. DiRenzo, M. D. Fleming, J. Jin, E. L. Greer, V. M. Sellers, S. M. Galica, and N. C. Andrews. Cybrd1 (duodenal cytochrome b) is not necessary for dietary iron absorption in mice. *Blood*, 106(8):2879–2883, October 2005. doi: 10.1182/blood-2005-02-0716. URL http://dx.doi.org/10.1182/blood-2005-02-0716.

P. Hahn, Y. Qian, T. Dentchev, L. Chen, J. Beard, Z. L. L. Harris, and J. L. Dunaief. Disruption of ceruloplasmin and hephaestin in mice causes retinal iron overload and retinal degeneration with features of age-related macular degeneration. *Proceedings of the National Academy of Sciences of the United States of America*, 101(38):13850–13855, September 2004. ISSN 0027-8424. doi: 10.1073/pnas.0405146101. URL http://dx.doi.org/10.1073/pnas.0405146101.

C. Hahnefeld, S. Drewianka, and F. W. Herberg. Determination of kinetic data using surface plasmon resonance biosensors. *Methods in Molecular Medicine*, 94:299–320, 2004. ISSN 1543-1894. URL http://view.ncbi.nlm.nih.gov/pubmed/14959837.

D. Haile, M. Hentze, T. Rouault, J. Harford, and R. Klausner. Regulation of interaction of the iron-responsive element binding protein with iron-responsive rna elements. *Molecular and Cellular Biology*, 9(11):5055–5061, 1989a.

D. J. Haile, M. W. Hentze, T. A. Rouault, J. B. Harford, and R. D. Klausner. Regulation of interaction of the iron-responsive element binding protein with iron-responsive (rna) elements. *Molecular and Cellular Biology*, 9(11):5055–5061, Nov. 1989b. ISSN 0270-7306. URL http://www.ncbi.nlm.nih.gov/pmc/articles/PMC363657/.

A. P. Han, C. Yu, L. Lu, Y. Fujiwara, C. Browne, G. Chin, M. Fleming, P. Leboulch, S. H. Orkin, and J. J. Chen. Heme-regulated eIF2alpha kinase (HRI) is required for translational regulation and survival of erythroid precursors in iron deficiency. *The EMBO journal*, 20(23):6909–6918, December 2001. ISSN 0261-4189. doi: 10.1093/emboj/20.23.6909. URL http://dx.doi.org/10.1093/emboj/20.23.6909.

J.-D. D. Han, N. Bertin, T. Hao, D. S. Goldberg, G. F. Berriz, L. V. Zhang, D. Dupuy, A. J. Walhout, M. E. Cusick, F. P. Roth, and M. Vidal. Evidence for dynamically organized modularity in the yeast protein-protein interaction network. *Nature*, 430(6995):88–93, July 2004. ISSN 1476-4687. doi: 10.1038/nature02555. URL http://dx.doi.org/10.1038/nature02555.

E. Harju. Clinical pharmacokinetics of iron preparations. *Clinical Pharmacokinetics*, 17 (2):69–89, Aug. 1989. ISSN 0312-5963. URL http://view.ncbi.nlm.nih.gov/pubmed/2673607.

Z. L. Harris, Y. Takahashi, H. Miyajima, M. Serizawa, R. T. MacGillivray, and J. D. Gitlin. Aceruloplasminemia: molecular characterization of this disorder of iron metabolism. *Proceedings of the National Academy of Sciences of the United States of America*, 92 (7):2539–2543, March 1995. ISSN 0027-8424. URL http://view.ncbi.nlm.nih.gov/pubmed/7708681.

Z. L. Harris, A. P. Durley, T. K. Man, and J. D. Gitlin. Targeted gene disruption reveals an essential role for ceruloplasmin in cellular iron efflux. *Proceedings of the National Academy of Sciences of the United States of America*, 96(19):10812–10817, September 1999. ISSN 0027-8424. URL http://view.ncbi.nlm.nih.gov/pubmed/10485908].

Z. L. Harris, S. R. Davis-Kaplan, J. D. Gitlin, and J. Kaplan. A fungal multicopper oxidase restores iron homeostasis in aceruloplasminemia. *Blood*, 103(12):4672–4673, June 2004. doi: 10.1182/blood-2003-11-4060. URL http://dx.doi.org/10.1182/blood-2003-11-4060.

P. M. Harrison. Ferritin: an iron-storage molecule. *Seminars in Hematology*, 14(1):55–70, January 1977. ISSN 0037-1963. URL http://view.ncbi.nlm.nih.gov/pubmed/318769.

S. J. Hayden, T. J. Albert, T. R. Watkins, and E. R. Swenson. Anemia in critical illness: insights into etiology, consequences, and management. *American Journal of Respiratory and Critical Care Medicine*, 185(10):1049–1057, May 2012. ISSN 1535-4970. doi: 10.1164/rccm.201110-1915ci. URL http://dx.doi.org/10.1164/rccm.201110-1915ci.

A. Heinemann, F. Wischhusen, K. Püschel, and X. Rogiers. Standard liver volume in the caucasian population. *Liver Transplantation*, 5(5):366–368, Sept. 1999. doi: 10.1002/lt.500050516. URL http://dx.doi.org/10.1002/lt.500050516.

R. Heinrich and T. A. Rapoport. A linear steady-state treatment of enzymatic chains. *European Journal of Biochemistry*, 42(1):89–95, 1974. doi: 10.1111/j.1432-1033.1974.tb03318.x. URL http://dx.doi.org/10.1111/j.1432-1033.1974.tb03318.x.

M. W. Hentze and L. C. Kühn. Molecular control of vertebrate iron metabolism: mRNA-based regulatory circuits operated by iron, nitric oxide, and oxidative stress. *Proceedings of the National Academy of Sciences of the United States of America*, 93(16): 8175–8182, August 1996. ISSN 0027-8424. URL http://view.ncbi.nlm.nih.gov/pubmed/8710843].

M. W. Hentze, M. U. Muckenthaler, and N. C. Andrews. Balancing acts: molecular control of mammalian iron metabolism. *Cell*, 117(3):285–297, April 2004. ISSN 0092-8674. URL http://view.ncbi.nlm.nih.gov/pubmed/15109490.

S. Hoops, S. Sahle, R. Gauges, C. Lee, J. Pahle, N. Simus, M. Singhal, L. Xu, P. Mendes, and U. Kummer. COPASI - a COmplex PAthway SImulator. *Bioinformatics*, 22(24): 3067–3074, December 2006. ISSN 1367-4811. doi: 10.1093/bioinformatics/btl485. URL http://dx.doi.org/10.1093/bioinformatics/btl485.

M. Horiuchi, N. Yamazaki, T. Ikeda, N. Ishiguro, and M. Shinagawa. A cellular form of prion protein (PrPC) exists in many non-neuronal tissues of sheep. *Journal of General Virology*, 76(10):2583–2587, Oct. 1995. ISSN 1465-2099. doi: 10.1099/0022-1317-76-10-2583. URL http://dx.doi.org/10.1099/0022-1317-76-10-2583.

G. Hounnou, C. Destrieux, J. Desmé, P. Bertrand, and S. Velut. Anatomical study of the length of the human intestine. *Surgical and Radiologic Anatomy*, 24(5):290–294, 2002. doi: 10.1007/s00276-002-0057-y. URL http://dx.doi.org/10.1007/s00276-002-0057-y.

V. Hower, P. Mendes, F. M. Torti, R. Laubenbacher, S. Akman, V. Shulaev, and S. V. Torti. A general map of iron metabolism and tissue-specific subnetworks. *Molecular BioSystems*, 5(5):422–443, May 2009. ISSN 1742-2051. doi: 10.1039/b816714c. URL http://dx.doi.org/10.1039/b816714c.

C. Y. Huang and J. E. Ferrell. Ultrasensitivity in the mitogen-activated protein kinase cascade. *Proceedings of the National Academy of Sciences*, 93(19):10078–10083, Sept. 1996. ISSN 1091-6490. URL http://www.pnas.org/content/93/19/10078.abstract.

L. E. Huang, Z. Arany, D. M. Livingston, and H. F. Bunn. Activation of hypoxia-inducible transcription factor depends primarily upon redox-sensitive stabilization of its Îś subunit. *Journal of Biological Chemistry*, 271(50):32253–32259, Dec. 1996. doi: 10.1074/jbc.271.50.32253. URL http://dx.doi.org/10.1074/jbc.271.50.32253.

N. Hubert and M. W. Hentze. Previously uncharacterized isoforms of divalent metal transporter (DMT)-1: implications for regulation and cellular function. *Proceedings of the National Academy of Sciences of the United States of America*, 99(19):12345–12350, September 2002. ISSN 0027-8424. doi: 10.1073/pnas.192423399. URL http://dx.doi.org/10.1073/pnas.192423399.

M. Hucka, A. Finney, H. M. Sauro, H. Bolouri, J. C. Doyle, H. Kitano, , the rest of the SBML Forum:, A. P. Arkin, B. J. Bornstein, D. Bray, A. Cornish-Bowden, A. A.

Cuellar, S. Dronov, E. D. Gilles, M. Ginkel, V. Gor, I. I. Goryanin, W. J. Hedley, T. C. Hodgman, J. H. Hofmeyr, P. J. Hunter, N. S. Juty, J. L. Kasberger, A. Kremling, U. Kummer, N. Le Novère, L. M. Loew, D. Lucio, P. Mendes, E. Minch, E. D. Mjolsness, Y. Nakayama, M. R. Nelson, P. F. Nielsen, T. Sakurada, J. C. Schaff, B. E. Shapiro, T. S. Shimizu, H. D. Spence, J. Stelling, K. Takahashi, M. Tomita, J. Wagner, and J. Wang. The systems biology markup language (SBML): a medium for representation and exchange of biochemical network models. *Bioinformatics*, 19(4): 524–531, March 2003. ISSN 1367-4803. doi: 10.1093/bioinformatics/btg015. URL http://dx.doi.org/10.1093/bioinformatics/btg015.

M. Hucka, F. T. Bergmann, S. Hoops, S. M. Keating, S. Sahle, J. C. Schaff, L. P. Smith, and D. J. Wilkinson. The systems biology markup language (sbml): Language specification for level 3 version 1 core. *Nature Precedings*, Oct. 2010. ISSN 1756-0357. doi: 10.1038/npre.2010.4959.1. URL http://dx.doi.org/10.1038/npre.2010.4959.1.

H. A. Huebers and C. A. Finch. The physiology of transferrin and transferrin receptors. *Physiological Reviews*, 67(2):520–582, April 1987. ISSN 0031-9333. URL http://view.ncbi.nlm.nih.gov/pubmed/3550839.

D. Hull, K. Wolstencroft, R. Stevens, C. Goble, M. R. Pocock, P. Li, and T. Oinn. Taverna: a tool for building and running workflows of services. *Nucleic Acids Research*, 34(34): W729–732, July 2006. ISSN 1362-4962. doi: 10.1093/nar/gkl320. URL http://dx.doi.org/10.1093/nar/gkl320.

V. Hvidberg, C. Jacobsen, R. K. Strong, J. B. Cowland, S. K. Moestrup, and N. Borregaard. The endocytic receptor megalin binds the iron transporting neutrophil-gelatinase-associated lipocalin with high affinity and mediates its cellular uptake. *FEBS Letters*, 579(3):773–777, January 2005. ISSN 0014-5793. doi: 10.1016/j.febslet.2004.12.031. URL http://dx.doi.org/10.1016/j.febslet.2004.12.031.

B. J. Iacopetta and E. H. Morgan. The kinetics of transferrin endocytosis and iron uptake from transferrin in rabbit reticulocytes. *Journal of Biological Chemistry*, 258 (15):9108–9115, August 1983. URL http://www.jbc.org/content/258/15/9108.abstract.

M. Ivan, K. Kondo, H. Yang, W. Kim, J. Valiando, M. Ohh, A. Salic, J. M. Asara, W. S. Lane, and W. G. Kaelin. Hifalpha targeted for vhl-mediated destruction by proline hydroxylation: implications for o2 sensing. *Science*, 292(5516):464–468, Apr. 2001. ISSN 0036-8075. doi: 10.1126/science.1059817. URL http://dx.doi.org/10.1126/science.1059817.

V. Iyengar, R. Pullakhandam, and K. M. Nair. Iron-zinc interaction during uptake in human intestinal caco-2 cell line: kinetic analyses and possible mechanism. *Indian*

Journal of Biochemistry & Biophysics, 46(4):299–306, Aug. 2009. ISSN 0301-1208. URL http://view.ncbi.nlm.nih.gov/pubmed/19788062.

W. A. Jefferies, M. R. Brandon, S. V. Hunt, A. F. Williams, K. C. Gatter, and D. Y. Mason. Transferrin receptor on endothelium of brain capillaries. *Nature*, 312(5990): 162–163, Nov. 1984. doi: 10.1038/312162a0. URL http://dx.doi.org/10.1038/312162a0.

H. Jeong, B. Tombor, R. Albert, Z. N. Oltvai, and A. L. Barabasi. The large-scale organization of metabolic networks. *Nature*, 407(6804):651–654, October 2000. ISSN 0028-0836. doi: 10.1038/35036627. URL http://dx.doi.org/10.1038/35036627.

H. Jeong, Z. N. Oltvai, and A.-L. Barabási. Prediction of Protein Essentiality Based on Genomic Data. *Complexus*, 1(1):19–28, 2003. ISSN 1424-8506. doi: 10.1159/000067640. URL http://dx.doi.org/10.1159/000067640.

W. Jin, H. Takagi, B. Pancorbo, and E. C. Theil. "Opening" the ferritin pore for iron release by mutation of conserved amino acids at interhelix and loop sites. *Biochemistry*, 40(25):7525–7532, June 2001. ISSN 0006-2960. URL http://view.ncbi.nlm.nih.gov/pubmed/11412106.

J. L. Johnson, D. C. Norcross, P. Arosio, R. B. Frankel, and G. D. Watt. Redox reactivity of animal apoferritins and apoheteropolymers assembled from recombinant heavy and light human chain ferritins†. *Biochemistry*, 38(13):4089–4096, Mar. 1999. doi: 10.1021/bi982690d. URL http://dx.doi.org/10.1021/bi982690d.

M. B. Johnson and C. A. Enns. Diferric transferrin regulates transferrin receptor 2 protein stability. *Blood*, 104(13):4287–4293, Dec. 2004. ISSN 0006-4971. doi: 10.1182/blood-2004-06-2477. URL http://dx.doi.org/10.1182/blood-2004-06-2477.

M. B. Johnson, J. Chen, N. Murchison, F. A. Green, and C. A. Enns. Transferrin receptor 2: evidence for ligand-induced stabilization and redirection to a recycling pathway. *Molecular Biology of the Cell*, 18(3):743–754, March 2007. ISSN 1059-1524. doi: 10.1091/mbc.E06-09-0798. URL http://dx.doi.org/10.1091/mbc.E06-09-0798.

U. Jönsson, L. Fägerstam, B. Ivarsson, B. Johnsson, R. Karlsson, K. Lundh, S. Löfås, B. Persson, H. Roos, and I. Rönnberg. Real-time biospecific interaction analysis using surface plasmon resonance and a sensor chip technology. *BioTechniques*, 11(5):620–627, November 1991. ISSN 0736-6205. URL http://view.ncbi.nlm.nih.gov/pubmed/1804254.

M. P. P. Joy, A. Brock, D. E. Ingber, and S. Huang. High-betweenness proteins in the yeast protein interaction network. *Journal of Biomedicine and Biotechnology*, 2005 (2):96–103, 2005. ISSN 1110-7243. doi: 10.1155/JBB.2005.96. URL http://dx.doi.org/10.1155/JBB.2005.96.

H. Kacser and J. A. Burns. The control of flux. *Symposia of the Society for Experimental Biology*, 27:65–104, 1973. ISSN 0081-1386. URL http://view.ncbi.nlm.nih.gov/pubmed/4148886.

J. Kaplan. Mechanisms of cellular iron acquisition: another iron in the fire. *Cell*, 111 (5):603–606, November 2002. ISSN 0092-8674. URL http://view.ncbi.nlm.nih.gov/pubmed/12464171.

J. Kato, M. Kobune, S. Ohkubo, K. Fujikawa, M. Tanaka, R. Takimoto, K. Takada, D. Takahari, Y. Kawano, Y. Kohgo, and Y. Niitsu. Iron/IRP-1-dependent regulation of mRNA expression for transferrin receptor, DMT1 and ferritin during human erythroid differentiation. *Experimental Hematology*, 35(6):879–887, June 2007. ISSN 0301-472X. doi: 10.1016/j.exphem.2007.03.005. URL http://dx.doi.org/10.1016/j.exphem.2007.03.005.

H. Kawabata, R. Yang, T. Hirama, P. T. Vuong, S. Kawano, A. F. Gombart, and H. P. Koeffler. Molecular Cloning of Transferrin Receptor 2. *Journal of Biological Chemistry*, 274(30):20826–20832, July 1999. doi: 10.1074/jbc.274.30.20826. URL http://dx.doi.org/10.1074/jbc.274.30.20826.

H. Kawabata, R. E. Fleming, D. Gui, S. Y. Moon, T. Saitoh, J. O'Kelly, Y. Umehara, Y. Wano, J. W. Said, and H. P. Koeffler. Expression of hepcidin is down-regulated in tfr2 mutant mice manifesting a phenotype of hereditary hemochromatosis. *Blood*, 105 (1):376–381, Jan. 2005. ISSN 0006-4971. doi: 10.1182/blood-2004-04-1416. URL http://dx.doi.org/10.1182/blood-2004-04-1416.

Y. Ke and Z. Ming Qian. Iron misregulation in the brain: a primary cause of neurodegenerative disorders. *Lancet Neurology*, 2(4):246–253, Apr. 2003. ISSN 1474-4422. URL http://view.ncbi.nlm.nih.gov/pubmed/12849213.

Y. Ke, J. Wu, E. A. Leibold, W. E. Walden, and E. C. Theil. Loops and bulge/loops in iron-responsive element isoforms influence iron regulatory protein binding. fine-tuning of mrna regulation? *The Journal of Biological Chemistry*, 273(37):23637–23640, Sept. 1998. ISSN 0021-9258. URL http://view.ncbi.nlm.nih.gov/pubmed/9726965.

S. B. Keel, R. T. Doty, Z. Yang, J. G. Quigley, J. Chen, S. Knoblaugh, P. D. Kingsley, I. De Domenico, M. B. Vaughn, J. Kaplan, J. Palis, and J. L. Abkowitz. A heme export protein is required for red blood cell differentiation and iron homeostasis. *Science*,

319(5864):825–828, February 2008. ISSN 1095-9203. doi: 10.1126/science.1151133. URL http://dx.doi.org/10.1126/science.1151133.

D. Kell. Iron behaving badly: inappropriate iron chelation as a major contributor to the aetiology of vascular and other progressive inflammatory and degenerative diseases. *BMC Medical Genomics*, 2(1):2+, 2009. ISSN 1755-8794. doi: 10.1186/1755-8794-2-2. URL http://dx.doi.org/10.1186/1755-8794-2-2.

D. B. Kell. Towards a unifying, systems biology understanding of large-scale cellular death and destruction caused by poorly liganded iron: Parkinson's, huntington's, alzheimer's, prions, bactericides, chemical toxicology and others as examples. *Archives of Toxicology*, 84(11):825–889, 2010.

E. Kent, S. Hoops, and P. Mendes. Condor-copasi: high-throughput computing for biochemical networks. *BMC Systems Biology*, 6(1):91, 2012a. ISSN 1752-0509. doi: 10.1186/1752-0509-6-91. URL http://www.biomedcentral.com/1752-0509/6/91.

E. Kent, S. Hoops, and P. Mendes. Condor-copasi: high-throughput computing for biochemical networks. *BMC Systems Biology*, 6(1):91, 2012b.

T. Z. Kidane, E. Sauble, and M. C. Linder. Release of iron from ferritin requires lysosomal activity. *American Journal of Physiology. Cell Physiology*, 291(3), September 2006. ISSN 0363-6143. doi: 10.1152/ajpcell.00505.2005. URL http://dx.doi.org/10.1152/ajpcell.00505.2005.

H. Y. Kim, R. D. Klausner, and T. A. Rouault. Translational repressor activity is equivalent and is quantitatively predicted by in vitro rna binding for two iron-responsive element-binding proteins, irp1 and irp2. *The Journal of Biological Chemistry*, 270(10):4983–4986, Mar. 1995. ISSN 0021-9258. URL http://view.ncbi.nlm.nih.gov/pubmed/7890603.

R. T. Kinobe, R. A. Dercho, J. Z. Vlahakis, J. F. Brien, W. A. Szarek, and K. Nakatsu. Inhibition of the enzymatic activity of heme oxygenases by azole-based antifungal drugs. *Journal of Pharmacology and Experimental Therapeutics*, 319(1):277–284, Oct. 2006. doi: 10.1124/jpet.106.102699. URL http://dx.doi.org/10.1124/jpet.106.102699.

H. Kitano. Computational systems biology. *Nature*, 420(6912):206–210, November 2002. ISSN 0028-0836. doi: 10.1038/nature01254. URL http://dx.doi.org/10.1038/nature01254.

A. M. Konijn, H. Glickstein, B. Vaisman, E. G. Meyron-Holtz, I. N. Slotki, and Z. I. Cabantchik. The Cellular Labile Iron Pool and Intracellular Ferritin in K562 Cells. *Blood*, 94(6):2128–2134, September 1999. ISSN 0006-

4971. URL http://bloodjournal.hematologylibrary.org/cgi/content/abstract/94/6/2128.

A. Krause, S. Neitz, H. J. Mägert, A. Schulz, W. G. Forssmann, P. Schulz-Knappe, and K. Adermann. LEAP-1, a novel highly disulfide-bonded human peptide, exhibits antimicrobial activity. *FEBS Letters*, 480(2-3):147–150, September 2000. ISSN 0014-5793. URL http://view.ncbi.nlm.nih.gov/pubmed/11034317.

P. Krishnamurthy and J. D. Schuetz. Role of ABCG2/BCRP in biology and medicine. *Annual Review of Pharmacology and Toxicology*, 46:381–410, 2006. ISSN 0362-1642. doi: 10.1146/annurev.pharmtox.46.120604.141238. URL http://dx.doi.org/10.1146/annurev.pharmtox.46.120604.141238.

J. J. C. Kroot, H. Tjalsma, R. E. Fleming, and D. W. Swinkels. Hepcidin in human iron disorders: Diagnostic implications. *Clinical Chemistry*, 57(12):1650–1669, Dec. 2011. ISSN 1530-8561. doi: 10.1373/clinchem.2009.140053. URL http://dx.doi.org/10.1373/clinchem.2009.140053.

B. Lang, M. Delmar, and W. Coombs. Surface Plasmon Resonance as a Method to Study the Kinetics and Amplitude of Protein- Protein Binding. In S. Dhein, F. Mohr, and M. Delmar, editors, *Practical Methods in Cardiovascular Research*, chapter 47, pages 936–947. Springer Berlin Heidelberg, Berlin/Heidelberg, 2005. ISBN 3-540-40763-4. doi: 10.1007/3-540-26574-0_47. URL http://dx.doi.org/10.1007/3-540-26574-0_47.

G. O. Latunde-Dada, K. Takeuchi, R. J. Simpson, and A. T. McKie. Haem carrier protein 1 (HCP1): Expression and functional studies in cultured cells. *FEBS Letters*, 580(30):6865–6870, December 2006. ISSN 0014-5793. doi: 10.1016/j.febslet.2006.11.048. URL http://dx.doi.org/10.1016/j.febslet.2006.11.048.

R. Laubenbacher, V. Hower, A. Jarrah, S. V. Torti, V. Shulaev, P. Mendes, F. M. Torti, and S. Akman. A systems biology view of cancer. *Biochimica et Biophysica Acta*, 1796(2):129–139, December 2009. ISSN 0006-3002. doi: 10.1016/j.bbcan.2009.06.001. URL http://dx.doi.org/10.1016/j.bbcan.2009.06.001.

V. Laufberger. Sur la cristallisation de la ferritine. *Bulletin de la Société de chimie biologique*, 19:1575–1582, 1937.

D. M. Lawson, A. Treffry, P. J. Artymiuk, P. M. Harrison, S. J. Yewdall, A. Luzzago, G. Cesareni, S. Levi, and P. Arosio. Identification of the ferroxidase centre in ferritin. *FEBS Letters*, 254(1-2):207–210, Aug. 1989. ISSN 00145793. doi: 10.1016/0014-5793(89)81040-3. URL http://dx.doi.org/10.1016/0014-5793(89)81040-3.

N. Le Novère, B. Bornstein, A. Broicher, M. Courtot, M. Donizelli, H. Dharuri, L. Li, H. Sauro, M. Schilstra, B. Shapiro, J. L. Snoep, and M. Hucka. BioModels database: a free, centralized database of curated, published, quantitative kinetic models of biochemical and cellular systems. *Nucleic Acids Research*, 34(suppl 1):D689–D691, Jan. 2006. ISSN 1362-4962. doi: 10.1093/nar/gkj092. URL http://dx.doi.org/10.1093/nar/gkj092.

N. Le Novère, M. Hucka, S. Hoops, S. Keating, S. Sahle, D. Wilkinson, M. Hucka, S. Hoops, S. M. Keating, N. Le Novère, S. Sahle, and D. Wilkinson. Systems Biology Markup Language (SBML) Level 2: Structures and Facilities for Model Definitions. *Nature Precedings*, December 2008. ISSN 1756-0357. doi: 10.1038/npre.2008.2715.1. URL http://dx.doi.org/10.1038/npre.2008.2715.1.

J. Lebron. Crystal Structure of the Hemochromatosis Protein HFE and Characterization of Its Interaction with Transferrin Receptor. *Cell*, 93(1):111–123, April 1998. ISSN 00928674. doi: 10.1016/S0092-8674(00)81151-4. URL http://dx.doi.org/10.1016/S0092-8674(00)81151-4.

J. A. Lebrón, A. P. West, and P. J. Bjorkman. The hemochromatosis protein HFE competes with transferrin for binding to the transferrin receptor. *Journal of Molecular Biology*, 294(1):239–245, November 1999. ISSN 0022-2836. doi: 10.1006/jmbi.1999.3252. URL http://dx.doi.org/10.1006/jmbi.1999.3252.

P. J. Lee, B. H. Jiang, B. Y. Chin, N. V. Iyer, J. Alam, G. L. Semenza, and A. M. Choi. Hypoxia-inducible factor-1 mediates transcriptional activation of the heme oxygenase-1 gene in response to hypoxia. *The Journal of Biological Chemistry*, 272(9):5375–5381, Feb. 1997. ISSN 0021-9258. URL http://view.ncbi.nlm.nih.gov/pubmed/9038135.

R. J. Lee, S. Wang, and P. S. Low. Measurement of endosome pH following folate receptor-mediated endocytosis. *Biochimica et Biophysica Acta*, 1312(3):237–242, July 1996. ISSN 01674889. doi: 10.1016/0167-4889(96)00041-9. URL http://dx.doi.org/10.1016/0167-4889(96)00041-9.

M. J. Leimberg, E. Prus, A. M. Konijn, and E. Fibach. Macrophages function as a ferritin iron source for cultured human erythroid precursors. *Journal of Cellular Biochemistry*, 103(4):1211–1218, March 2008. ISSN 1097-4644. doi: 10.1002/jcb.21499. URL http://dx.doi.org/10.1002/jcb.21499.

S. Levi, S. J. Yewdall, P. M. Harrison, P. Santambrogio, A. Cozzi, E. Rovida, A. Albertini, and P. Arosio. Evidence of H- and L-chains have co-operative roles in the iron-uptake mechanism of human ferritin. *The Biochemical Journal*, 288 (Pt 2):591–596, December 1992. ISSN 0264-6021. URL http://view.ncbi.nlm.nih.gov/pubmed/1463463.

J. E. Levy, O. Jin, Y. Fujiwara, F. Kuo, and N. C. Andrews. Transferrin receptor is necessary for development of erythrocytes and the nervous system. *Nature Genetics*, 21(4):396–399, April 1999. ISSN 1061-4036. doi: 10.1038/7727. URL http://dx.doi.org/10.1038/7727.

C. Li, M. Donizelli, N. Rodriguez, H. Dharuri, L. Endler, V. Chelliah, L. Li, E. He, A. Henry, M. I. Stefan, J. L. Snoep, M. Hucka, N. Le Novère, and C. Laibe. BioModels Database: An enhanced, curated and annotated resource for published quantitative kinetic models. *BMC Systems Biology*, 4(1):92+, June 2010a. ISSN 1752-0509. doi: 10.1186/1752-0509-4-92. URL http://dx.doi.org/10.1186/1752-0509-4-92.

P. Li, J. Dada, D. Jameson, I. Spasic, N. Swainston, K. Carroll, W. Dunn, F. Khan, N. Malys, H. Messiha, E. Simeonidis, D. Weichart, C. Winder, J. Wishart, D. Broomhead, C. Goble, S. Gaskell, D. Kell, H. Westerhoff, P. Mendes, and N. Paton. Systematic integration of experimental data and models in systems biology. *BMC Bioinformatics*, 11(1):582+, November 2010b. ISSN 1471-2105. doi: 10.1186/1471-2105-11-582. URL http://dx.doi.org/10.1186/1471-2105-11-582.

L. Lin, E. V. Valore, E. Nemeth, J. B. Goodnough, V. Gabayan, and T. Ganz. Iron transferrin regulates hepcidin synthesis in primary hepatocyte culture through hemojuvelin and bmp2/4. *Blood*, 110(6):2182–2189, Sept. 2007. ISSN 1528-0020. doi: 10.1182/blood-2007-04-087593. URL http://dx.doi.org/10.1182/blood-2007-04-087593.

E. Lindholm, J. Nickolls, S. Oberman, and J. Montrym. NVIDIA Tesla: A Unified Graphics and Computing Architecture. *IEEE Micro*, 28(2):39–55, March 2008. ISSN 0272-1732. doi: 10.1109/MM.2008.31. URL http://dx.doi.org/10.1109/MM.2008.31.

M. Litzkow and M. Livny. Experience with the Condor distributed batch system. In *8th International Conference on Distributed Computing Systems*, pages 97–101, 1988. doi: 10.1109/EDS.1990.138057.

M. J. Litzkow, M. Livny, and M. W. Mutka. Condor-a hunter of idle workstations. In *8th International Conference on Distributed Computing Systems*, pages 104–111, 1988.

S. Liu, R. N. Suragani, F. Wang, A. Han, W. Zhao, N. C. Andrews, and J.-J. J. Chen. The function of heme-regulated eIF2alpha kinase in murine iron homeostasis and macrophage maturation. *The Journal of Clinical Investigation*, 117(11):3296–3305, November 2007. ISSN 0021-9738. doi: 10.1172/JCI32084. URL http://dx.doi.org/10.1172/JCI32084.

X. Liu, W. Jin, and E. C. Theil. Opening protein pores with chaotropes enhances Fe reduction and chelation of Fe from the ferritin biomineral. *Proceedings of the National*

Academy of Sciences of the United States of America, 100(7):3653–3658, April 2003. ISSN 0027-8424. doi: 10.1073/pnas.0636928100. URL http://dx.doi.org/10.1073/pnas.0636928100.

C. M. Lloyd, M. D. Halstead, and P. F. Nielsen. CellML: its future, present and past. *Progress in Biophysics and Molecular Biology*, 85(2-3):433–450, July 2004. ISSN 0079-6107. doi: 10.1016/j.pbiomolbio.2004.01.004. URL http://dx.doi.org/10.1016/j.pbiomolbio.2004.01.004.

C. N. Lok and P. Ponka. Identification of a hypoxia response element in the transferrin receptor gene. *The Journal of Biological Chemistry*, 274(34):24147–24152, Aug. 1999. ISSN 0021-9258. URL http://view.ncbi.nlm.nih.gov/pubmed/10446188.

T. Lopes, T. Luganskaja, M. V. Spasic, M. Hentze, M. Muckenthaler, K. Schumann, and J. Reich. Systems analysis of iron metabolism: the network of iron pools and fluxes. *BMC Systems Biology*, 4(1):112+, 2010. ISSN 1752-0509. doi: 10.1186/1752-0509-4-112. URL http://dx.doi.org/10.1186/1752-0509-4-112.

S. Ludwiczek, E. Aigner, I. Theurl, and G. Weiss. Cytokine-mediated regulation of iron transport in human monocytic cells. *Blood*, 101(10):4148–4154, May 2003. doi: 10.1182/blood-2002-08-2459. URL http://dx.doi.org/10.1182/blood-2002-08-2459.

S. Ludwiczek, I. Theurl, S. Bahram, K. Schümann, and G. Weiss. Regulatory networks for the control of body iron homeostasis and their dysregulation in hfe mediated hemochromatosis. *Journal Cellular Physiology*, 204(2):489–499, 2005. doi: 10.1002/jcp.20315. URL http://dx.doi.org/10.1002/jcp.20315.

A. L. Lumsden, T. L. Henshall, S. Dayan, M. T. Lardelli, and R. I. Richards. Huntingtin-deficient zebrafish exhibit defects in iron utilization and development. *Human Molecular Genetics*, 16(16):1905–1920, Aug. 2007. ISSN 0964-6906. doi: 10.1093/hmg/ddm138. URL http://dx.doi.org/10.1093/hmg/ddm138.

Y. Ma, H. de Groot, Z. Liu, R. C. Hider, and F. Petrat. Chelation and determination of labile iron in primary hepatocytes by pyridinone fluorescent probes. *The Biochemical Journal*, 395(1):49–55, April 2006a. ISSN 1470-8728. doi: 10.1042/BJ20051496. URL http://dx.doi.org/10.1042/BJ20051496.

Y. Ma, M. Yeh, K.-Y. Y. Yeh, and J. Glass. Iron Imports. V. Transport of iron through the intestinal epithelium. *American Journal of Physiology. Gastrointestinal and Liver physiology*, 290(3), March 2006b. ISSN 0193-1857. doi: 10.1152/ajpgi.00489.2005. URL http://dx.doi.org/10.1152/ajpgi.00489.2005.

Y. Ma, Z. Liu, R. C. Hider, and F. Petrat. Determination of the labile iron pool of human lymphocytes using the fluorescent probe, CP655. *Analytical Chemistry Insights*, 2:61–67, 2007. ISSN 1177-3901. URL http://view.ncbi.nlm.nih.gov/pubmed/19662178].

I. C. Macdougall, B. Tucker, J. Thompson, C. R. V. Tomson, L. R. I. Baker, and A. E. G. Raine. A randomized controlled study of iron supplementation in patients treated with erythropoietin. *Kidney International*, 50(5):1694–1699, Nov. 1996. doi: 10.1038/ki.1996.487. URL http://dx.doi.org/10.1038/ki.1996.487.

M. Madsen, J. H. Graversen, and S. K. Moestrup. Haptoglobin and CD163: captor and receptor gating hemoglobin to macrophage lysosomes. *Redox Report : Communications in Free Radical Research*, 6(6):386–388, 2001. ISSN 1351-0002. URL http://view.ncbi.nlm.nih.gov/pubmed/11865982.

M. Marignani, S. Angeletti, C. Bordi, F. Malagnino, C. Mancino, G. Delle Fave, and B. Annibale. Reversal of long-standing iron deficiency anaemia after eradication of Helicobacter pylori infection. *Scandinavian Journal of Gastroenterology*, 32(6):617–622, June 1997. ISSN 0036-5521. URL http://view.ncbi.nlm.nih.gov/pubmed/9200297.

A. Martelli, M. Wattenhofer-Donzé, S. Schmucker, S. Bouvet, L. Reutenauer, and H. Puccio. Frataxin is essential for extramitochondrial Fe-S cluster proteins in mammalian tissues. *Human Molecular Genetics*, 16(22):2651–2658, November 2007. ISSN 0964-6906. doi: 10.1093/hmg/ddm163. URL http://dx.doi.org/10.1093/hmg/ddm163.

M. Masoud, G. Sarig, B. Brenner, and G. Jacob. Orthostatic hypercoagulability. *Hypertension*, 51(6):1545–1551, June 2008. ISSN 1524-4563. doi: 10.1161/hypertensionaha.108.112003. URL http://dx.doi.org/10.1161/hypertensionaha.108.112003.

M. Mastrogiannaki, P. Matak, B. Keith, M. C. Simon, S. Vaulont, and C. Peyssonnaux. Hif-2alpha, but not hif-1alpha, promotes iron absorption in mice. *The Journal of Clinical Investigation*, 119(5):1159–1166, May 2009. ISSN 1558-8238. doi: 10.1172/jci38499. URL http://dx.doi.org/10.1172/jci38499.

I. Mateo, J. Infante, P. Sánchez-Juan, I. García-Gorostiaga, E. Rodríguez-Rodríguez, J. L. Vázquez-Higuera, J. Berciano, and O. Combarros. Serum heme oxygenase-1 levels are increased in parkinson's disease but not in alzheimer's disease. *Acta Neurologica Scandinavica*, 121(2):136–138, Feb. 2010. ISSN 1600-0404. doi: 10.1111/j.1600-0404.2009.01261.x. URL http://dx.doi.org/10.1111/j.1600-0404.2009.01261.x.

MATLAB. *version 7.10.0 (R2010a)*. The MathWorks Inc., Natick, Massachusetts, 2010.

A. T. McKie. The role of Dcytb in iron metabolism: an update. *Biochemical Society Transactions*, 36(Pt 6):1239–1241, December 2008. ISSN 1470-8752. doi: 10.1042/BST0361239. URL http://dx.doi.org/10.1042/BST0361239.

A. T. McKie, D. Barrow, G. O. Latunde-Dada, A. Rolfs, G. Sager, E. Mudaly, M. Mudaly, C. Richardson, D. Barlow, A. Bomford, T. J. Peters, K. B. Raja, S. Shirali, M. A. Hediger, F. Farzaneh, and R. J. Simpson. An iron-regulated ferric reductase associated with the absorption of dietary iron. *Science*, 291(5509):1755–1759, March 2001. ISSN 0036-8075. doi: 10.1126/science.1057206. URL http://dx.doi.org/10.1126/science.1057206.

U. Mehdi and R. D. Toto. Anemia, diabetes, and chronic kidney disease. *Diabetes Care*, 32(7):1320–1326, July 2009. ISSN 1935-5548. doi: 10.2337/dc08-0779. URL http://dx.doi.org/10.2337/dc08-0779.

I. Mellman, R. Fuchs, and A. Helenius. Acidification of the endocytic and exocytic pathways. *Annual Review of Biochemistry*, 55:663–700, 1986. ISSN 0066-4154. doi: 10.1146/annurev.bi.55.070186.003311. URL http://dx.doi.org/10.1146/annurev.bi.55.070186.003311.

E. G. Meyron-Holtz, E. Fibach, D. Gelvan, and A. M. Konijn. Binding and uptake of exogenous isoferritins by cultured human erythroid precursor cells. *British Journal of Haematology*, 86(3):635–641, March 1994. ISSN 0007-1048. URL http://view.ncbi.nlm.nih.gov/pubmed/8043447.

M. P. Mims, Y. Guan, D. Pospisilova, M. Priwitzerova, K. Indrak, P. Ponka, V. Divoky, and J. T. Prchal. Identification of a human mutation of DMT1 in a patient with microcytic anemia and iron overload. *Blood*, 105(3):1337–1342, February 2005. ISSN 0006-4971. doi: 10.1182/blood-2004-07-2966. URL http://dx.doi.org/10.1182/blood-2004-07-2966.

S. Mitchell and P. Mendes. A computational model of liver iron metabolism, Aug. 2013a. URL http://arxiv.org/abs/1308.5826.

S. Mitchell and P. Mendes. A computational model of liver iron metabolism. *PLOS Computational Biology*, 9(11), Nov. 2013b. doi: 10.1371/journal.pcbi.1003299. URL http://dx.doi.org/10.1371/journal.pcbi.1003299.

N. Mobilia, A. Donzé, J. M. Moulis, and E. Fanchon. A model of the cellular iron homeostasis network using semi-formal methods for parameter space exploration. *Electronic Proceedings in Theoretical Computer Science*, 92:42–57, Aug. 2012. ISSN 2075-2180. doi: 10.4204/eptcs.92.4. URL http://dx.doi.org/10.4204/eptcs.92.4.

C. G. Moles, P. Mendes, and J. R. Banga. Parameter estimation in biochemical pathways: a comparison of global optimization methods. *Genome Research*, 13(11):2467–2474,

November 2003. ISSN 1088-9051. doi: 10.1101/gr.1262503. URL http://dx.doi.org/10.1101/gr.1262503.

E. R. Monsen, L. Hallberg, M. Layrisse, D. M. Hegsted, J. D. Cook, W. Mertz, and C. A. Finch. Estimation of available dietary iron. *The American Journal of Clinical Nutrition*, 31(1):134–141, Jan. 1978. ISSN 0002-9165. URL http://view.ncbi.nlm.nih.gov/pubmed/619599.

G. Montosi, A. Donovan, A. Totaro, C. Garuti, E. Pignatti, S. Cassanelli, C. C. Trenor, P. Gasparini, N. C. Andrews, and A. Pietrangelo. Autosomal-dominant hemochromatosis is associated with a mutation in the ferroportin (SLC11A3) gene. *The Journal of Clinical Investigation*, 108(4):619–623, August 2001. ISSN 0021-9738. doi: 10.1172/JCI13468. URL http://dx.doi.org/10.1172/JCI13468.

B. Moszkowski. Executing temporal logic programs. In S. Brookes, A. Roscoe, and G. Winskel, editors, *Seminar on Concurrency*, volume 197 of *Lecture Notes in Computer Science*, pages 111–130. Springer Berlin Heidelberg, 1985. doi: 10.1007/3-540-15670-4_6. URL http://dx.doi.org/10.1007/3-540-15670-4_6.

M. Muckenthaler, N. K. Gray, and M. W. Hentze. IRP-1 Binding to Ferritin mRNA Prevents the Recruitment of the Small Ribosomal Subunit by the Cap-Binding Complex eIF4F. *Molecular Cell*, 2(3):383–388, September 1998. URL http://www.cell.com/molecular-cell/abstract/S1097-2765(00)80282-8.

C. K. Mukhopadhyay, B. Mazumder, and P. L. Fox. Role of hypoxia-inducible factor-1 in transcriptional activation of ceruloplasmin by iron deficiency. *The Journal of Biological Chemistry*, 275(28):21048–21054, July 2000. ISSN 0021-9258. doi: 10.1074/jbc.m000636200. URL http://dx.doi.org/10.1074/jbc.m000636200.

E. W. Müllner, B. Neupert, and L. C. Kühn. A specific mrna binding factor regulates the iron-dependent stability of cytoplasmic transferrin receptor mrna. *Cell*, 58(2):373–382, 1989.

D. G. Myszka, X. He, M. Dembo, T. A. Morton, and B. Goldstein. Extending the Range of Rate Constants Available from BIACORE: Interpreting Mass Transport-Influenced Binding Data. *Biophysical Journal*, 75(2):583–594, August 1998. URL http://www.cell.com/biophysj/abstract/S0006-3495(98)77549-6.

E. Nemeth, S. Rivera, V. Gabayan, C. Keller, S. Taudorf, B. K. Pedersen, and T. Ganz. IL-6 mediates hypoferremia of inflammation by inducing the synthesis of the iron regulatory hormone hepcidin. *The Journal of Clinical Investigation*, 113(9):1271–1276, May 2004a. ISSN 0021-9738. doi: 10.1172/JCI20945. URL http://dx.doi.org/10.1172/JCI20945.

E. Nemeth, M. S. Tuttle, J. Powelson, M. B. Vaughn, A. Donovan, D. M. Ward, T. Ganz, and J. Kaplan. Hepcidin Regulates Cellular Iron Efflux by Binding to Ferroportin and Inducing Its Internalization. *Science*, 306(5704):2090–2093, December 2004b. ISSN 0036-8075. doi: 10.1126/science.1104742. URL http://dx.doi.org/10.1126/science.1104742.

G. Nicolas, M. Bennoun, A. Porteu, S. Mativet, C. Beaumont, B. Grandchamp, M. Sirito, M. Sawadogo, A. Kahn, and S. Vaulont. Severe iron deficiency anemia in transgenic mice expressing liver hepcidin. *Proceedings of the National Academy of Sciences of the United States of America*, 99(7):4596–4601, April 2002a. ISSN 0027-8424. doi: 10.1073/pnas.072632499. URL http://dx.doi.org/10.1073/pnas.072632499.

G. Nicolas, C. Chauvet, L. Viatte, J. L. L. Danan, X. Bigard, I. Devaux, C. Beaumont, A. Kahn, and S. Vaulont. The gene encoding the iron regulatory peptide hepcidin is regulated by anemia, hypoxia, and inflammation. *The Journal of Clinical Investigation*, 110(7):1037–1044, October 2002b. ISSN 0021-9738. doi: 10.1172/JCI15686. URL http://dx.doi.org/10.1172/JCI15686.

N. L. Novere, M. Hucka, H. Mi, S. Moodie, F. Schreiber, A. Sorokin, E. Demir, K. Wegner, M. I. Aladjem, S. M. Wimalaratne, F. T. Bergman, R. Gauges, P. Ghazal, H. Kawaji, L. Li, Y. Matsuoka, A. Villeger, S. E. Boyd, L. Calzone, M. Courtot, U. Dogrusoz, T. C. Freeman, A. Funahashi, S. Ghosh, A. Jouraku, S. Kim, F. Kolpakov, A. Luna, S. Sahle, E. Schmidt, S. Watterson, G. Wu, I. Goryanin, D. B. Kell, C. Sander, H. Sauro, J. L. Snoep, K. Kohn, and H. Kitano. The Systems Biology Graphical Notation. *Nature Biotechnology*, 27(8):735–741, August 2009. ISSN 1087-0156. doi: 10.1038/nbt.1558. URL http://dx.doi.org/10.1038/nbt.1558.

M. J. O'Connell, R. J. Ward, H. Baum, and T. J. Peters. Iron release from haemosiderin and ferritin by therapeutic and physiological chelators. *The Biochemical Journal*, 260 (3):903–907, June 1989. ISSN 0264-6021. URL http://www.ncbi.nlm.nih.gov/pmc/articles/PMC1138761/.

R. S. Ohgami, D. R. Campagna, E. L. Greer, B. Antiochos, A. McDonald, J. Chen, J. J. Sharp, Y. Fujiwara, J. E. Barker, and M. D. Fleming. Identification of a ferrireductase required for efficient transferrin-dependent iron uptake in erythroid cells. *Nature Genetics*, 37(11):1264–1269, November 2005. ISSN 1061-4036. doi: 10.1038/ng1658. URL http://dx.doi.org/10.1038/ng1658.

K. S. Olsson, B. Ritter, U. Rosén, P. A. Heedman, and F. Staugård. Prevalence of iron overload in central sweden. *Acta Medica Scandinavica*, 213(2):145–150, 1983. ISSN 0001-6101. URL http://view.ncbi.nlm.nih.gov/pubmed/6837331.

S. Omholt. Description and Analysis of Switchlike Regulatory Networks Exemplified by a Model of Cellular Iron Homeostasis. *Journal of Theoretical Biology*, 195(3):339–350, December 1998. ISSN 00225193. doi: 10.1006/jtbi.1998.0800. URL http://dx.doi.org/10.1006/jtbi.1998.0800.

S. J. Oppenheimer, Gibson, S. B. Macfarlane, J. B. Moody, C. Harrison, A. Spencer, and O. Bunari. Iron supplementation increases prevalence and effects of malaria: report on clinical studies in papua new guinea. *Transactions of the Royal Society of Tropical Medicine and Hygiene*, 80(4):603–612, Jan. 1986. ISSN 00359203. doi: 10.1016/0035-9203(86)90154-9. URL http://dx.doi.org/10.1016/0035-9203(86)90154-9.

F. Ortega, J. L. Garcés, F. Mas, B. N. Kholodenko, and M. Cascante. Bistability from double phosphorylation in signal transduction. *FEBS Journal*, 273(17):3915–3926, Sept. 2006. ISSN 1742-4658. doi: 10.1111/j.1742-4658.2006.05394.x. URL http://dx.doi.org/10.1111/j.1742-4658.2006.05394.x.

S. Osaki, D. A. Johnson, and E. Frieden. The possible significance of the ferrous oxidase activity of ceruloplasmin in normal human serum. *The Journal of Biological Chemistry*, 241(12):2746–2751, June 1966. ISSN 0021-9258. URL http://view.ncbi.nlm.nih.gov/pubmed/5912351.

M. S. Palmer, A. J. Dryden, J. T. Hughes, and J. Collinge. Homozygous prion protein genotype predisposes to sporadic Creutzfeldt-Jakob disease. *Nature*, 352(6333):340–342, July 1991. doi: 10.1038/352340a0. URL http://dx.doi.org/10.1038/352340a0.

K. Pantopoulos, N. K. Gray, and M. W. Hentze. Differential regulation of two related rna-binding proteins, iron regulatory protein (irp) and irpb. *RNA*, 1(2):155–163, Apr. 1995. ISSN 1355-8382. URL http://www.ncbi.nlm.nih.gov/pmc/articles/PMC1369069/.

G. Papanikolaou, M. E. Samuels, E. H. Ludwig, M. L. E. MacDonald, P. L. Franchini, M.-P. Dube, L. Andres, J. MacFarlane, N. Sakellaropoulos, M. Politou, E. Nemeth, J. Thompson, J. K. Risler, C. Zaborowska, R. Babakaiff, C. C. Radomski, T. D. Pape, O. Davidas, J. Christakis, P. Brissot, G. Lockitch, T. Ganz, M. R. Hayden, and Y. P. Goldberg. Mutations in HFE2 cause iron overload in chromosome 1q linked juvenile hemochromatosis. *Nature Genetics*, 36(1):77–82, November 2003. doi: 10.1038/ng1274. URL http://dx.doi.org/10.1038/ng1274.

C. H. Park, E. V. Valore, A. J. Waring, and T. Ganz. Hepcidin, a urinary antimicrobial peptide synthesized in the liver. *The Journal of Biological Chemistry*, 276(11):7806–7810, March 2001. ISSN 0021-9258. doi: 10.1074/jbc.M008922200. URL http://dx.doi.org/10.1074/jbc.M008922200.

P. C. Pauly and D. A. Harris. Copper stimulates endocytosis of the prion protein. *Journal of Biological Chemistry*, 273(50):33107–33110, Dec. 1998. ISSN 1083-351X. doi: 10.1074/jbc.273.50.33107. URL http://dx.doi.org/10.1074/jbc.273.50.33107.

D. Pe'er, A. Regev, G. Elidan, and N. Friedman. Inferring subnetworks from perturbed expression profiles. *Bioinformatics*, 17 Suppl 1(suppl 1):S215–S224, June 2001. ISSN 1367-4803. doi: 10.1093/bioinformatics/17.suppl_1.S215. URL http://dx.doi.org/10.1093/bioinformatics/17.suppl_1.S215.

L. R. Perez and K. J. Franz. Minding metals: tailoring multifunctional chelating agents for neurodegenerative disease. *Dalton Transactions*, 39(9):2177–2187, Mar. 2010. ISSN 1477-9234. doi: 10.1039/b919237a. URL http://dx.doi.org/10.1039/b919237a.

P. J. Peters, A. Mironov, D. Peretz, E. van Donselaar, E. Leclerc, S. Erpel, S. J. DeArmond, D. R. Burton, R. A. Williamson, M. Vey, and S. B. Prusiner. Trafficking of prion proteins through a caveolae-mediated endosomal pathway. *The Journal of Cell Biology*, 162(4):703–717, Aug. 2003. ISSN 0021-9525. doi: 10.1083/jcb.200304140. URL http://dx.doi.org/10.1083/jcb.200304140.

F. Petrat. Determination of the Chelatable Iron Pool of Single Intact Cells by Laser Scanning Microscopy. *Archives of Biochemistry and Biophysics*, 376(1):74–81, April 2000. ISSN 00039861. doi: 10.1006/abbi.2000.1711. URL http://dx.doi.org/10.1006/abbi.2000.1711.

F. Petrat, U. Rauen, and H. de Groot. Determination of the chelatable iron pool of isolated rat hepatocytes by digital fluorescence microscopy using the fluorescent probe, phen green SK. *Hepatology*, 29(4):1171–1179, April 1999. ISSN 0270-9139. doi: 10.1002/hep.510290435. URL http://dx.doi.org/10.1002/hep.510290435.

F. Petrat, H. de Groot, and U. Rauen. Subcellular distribution of chelatable iron: a laser scanning microscopic study in isolated hepatocytes and liver endothelial cells. *The Biochemical Journal*, 356(Pt 1):61–69, May 2001. ISSN 0264-6021. URL http://view.ncbi.nlm.nih.gov/pubmed/11336636].

F. Petrat, D. Weisheit, M. Lensen, H. de Groot, R. Sustmann, and U. Rauen. Selective determination of mitochondrial chelatable iron in viable cells with a new fluorescent sensor. *The Biochemical Journal*, 362(Pt 1):137–147, February 2002. ISSN 0264-6021. URL http://view.ncbi.nlm.nih.gov/pubmed/11829750].

C. Peyssonnaux, V. Nizet, and R. S. Johnson. Role of the hypoxia inducible factors hif in iron metabolism. *Cell Cycle*, 7(1):28–32, 2008.

I. Pichler, D. Greco, M. Gögele, C. M. Lill, L. Bertram, C. B. Do, N. Eriksson, T. Foroud, R. H. Myers, M. Nalls, M. F. Keller, B. Benyamin, J. B. Whitfield, P. P. Pramstaller, A. A. Hicks, J. R. Thompson, and C. Minelli. Serum iron levels and the risk of parkinson disease: A mendelian randomization study. *PLOS Medicine*, 10(6):e1001462+, June 2013. doi: 10.1371/journal.pmed.1001462. URL http://dx.doi.org/10.1371/journal.pmed.1001462.

C. Pigeon, G. Ilyin, B. Courselaud, P. Leroyer, B. Turlin, P. Brissot, and O. Loréal. A new mouse liver-specific gene, encoding a protein homologous to human antimicrobial peptide hepcidin, is overexpressed during iron overload. *The Journal of Biological Chemistry*, 276(11):7811–7819, March 2001. ISSN 0021-9258. doi: 10.1074/jbc.M008923200. URL http://dx.doi.org/10.1074/jbc.M008923200.

N. R. Pimstone, P. Engel, R. Tenhunen, P. T. Seitz, H. S. Marver, and R. Schmid. Inducible heme oxygenase in the kidney: a model for the homeostatic control of hemoglobin catabolism. *The Journal of Clinical Investigation*, 50(10):2042–2050, Oct. 1971. ISSN 0021-9738. doi: 10.1172/JCI106697. URL http://dx.doi.org/10.1172/JCI106697.

A. Piperno, D. Girelli, E. Nemeth, P. Trombini, C. Bozzini, E. Poggiali, Y. Phung, T. Ganz, and C. Camaschella. Blunted hepcidin response to oral iron challenge in hfe-related hemochromatosis. *Blood*, 110(12):4096–4100, Dec. 2007. ISSN 1528-0020. doi: 10.1182/blood-2007-06-096503. URL http://dx.doi.org/10.1182/blood-2007-06-096503.

A. Polonifi, M. Politou, V. Kalotychou, K. Xiromeritis, M. Tsironi, V. Berdoukas, G. Vaiopoulos, and A. Aessopos. Iron metabolism gene expression in human skeletal muscle. *Blood Cells, Molecules, and Diseases*, 45(3):233–237, October 2010. ISSN 10799796. doi: 10.1016/j.bcmd.2010.07.002. URL http://dx.doi.org/10.1016/j.bcmd.2010.07.002.

P. Ponka. Tissue-specific regulation of iron metabolism and heme synthesis: distinct control mechanisms in erythroid cells. *Blood*, 89(1):1–25, January 1997. ISSN 0006-4971. URL http://view.ncbi.nlm.nih.gov/pubmed/8978272.

P. Ponka. Cell biology of heme. *The American Journal of the Medical Sciences*, 318(4):241–256, October 1999. ISSN 0002-9629. URL http://view.ncbi.nlm.nih.gov/pubmed/10522552.

P. Ponka, C. Beaumont, and D. R. Richardson. Function and regulation of transferrin and ferritin. *Seminars in Hematology*, 35(1):35–54, January 1998. ISSN 0037-1963. URL http://view.ncbi.nlm.nih.gov/pubmed/9460808.

F. L. Powell. Functional genomics and the comparative physiology of hypoxia. *Annual Review of Physiology*, 65:203–230, 2003. ISSN 0066-4278. doi: 10.1146/annurev.

physiol.65.092101.142711. URL http://dx.doi.org/10.1146/annurev.physiol.65.092101.142711.

H. Puccio and M. Kœnig. Recent advances in the molecular pathogenesis of friedreich ataxia. *Human Molecular Genetics*, 9(6):887–892, Apr. 2000. ISSN 1460-2083. doi: 10.1093/hmg/9.6.887. URL http://dx.doi.org/10.1093/hmg/9.6.887.

J. G. Quigley, Z. Yang, M. T. Worthington, J. D. Phillips, K. M. Sabo, D. E. Sabath, C. L. Berg, S. Sassa, B. L. Wood, and J. L. Abkowitz. Identification of a human heme exporter that is essential for erythropoiesis. *Cell*, 118(6):757–766, September 2004. ISSN 0092-8674. doi: 10.1016/j.cell.2004.08.014. URL http://dx.doi.org/10.1016/j.cell.2004.08.014.

A. A. Qutub and A. S. Popel. A computational model of intracellular oxygen sensing by hypoxia-inducible factor hif1alpha. *Journal of Cell Science*, 119(16):3467–3480, Aug. 2006. ISSN 1477-9137. doi: 10.1242/jcs.03087. URL http://dx.doi.org/10.1242/jcs.03087.

I. Radovanovic, N. Braun, O. T. Giger, K. Mertz, G. Miele, M. Prinz, B. Navarro, and A. Aguzzi. Truncated prion protein and doppel are myelinotoxic in the absence of oligodendrocytic PrPC. *The Journal of Neuroscience*, 25(19):4879–4888, May 2005. ISSN 1529-2401. doi: 10.1523/jneurosci.0328-05.2005. URL http://dx.doi.org/10.1523/jneurosci.0328-05.2005.

A. Raj and A. van Oudenaarden. Nature, Nurture, or Chance: Stochastic Gene Expression and Its Consequences. *Cell*, 135(2):216–226, October 2008. URL http://www.cell.com//abstract/S0092-8674(08)01243-9.

E. Ramos, P. Ruchala, J. B. Goodnough, L. Kautz, G. C. Preza, E. Nemeth, and T. Ganz. Minihepcidins prevent iron overload in a hepcidin-deficient mouse model of severe hemochromatosis. *Blood*, 120(18):3829–3836, Nov. 2012. ISSN 1528-0020. doi: 10.1182/blood-2012-07-440743. URL http://dx.doi.org/10.1182/blood-2012-07-440743.

E. B. Rankin, M. P. Biju, Q. Liu, T. L. Unger, J. Rha, R. S. Johnson, M. C. Simon, B. Keith, and V. H. Haase. Hypoxia-inducible factor-2 (hif-2) regulates hepatic erythropoietin in vivo. *The Journal of Clinical Investigation*, 117(4):1068–1077, Apr. 2007. ISSN 0021-9738. doi: 10.1172/jci30117. URL http://dx.doi.org/10.1172/jci30117.

P. J. Ratcliffe. Hif-1 and hif-2: working alone or together in hypoxia? *The Journal of Clinical Investigation*, 117(4):862–865, Apr. 2007. ISSN 0021-9738. doi: 10.1172/jci31750. URL http://dx.doi.org/10.1172/jci31750.

U. Rauen, F. Petrat, T. Li, and H. De Groot. Hypothermia injury/cold-induced apoptosis evidence of an increase in chelatable iron causing oxidative injury in spite of low O2-/H2O2 formation. *The FASEB Journal*, 14(13):1953–1964, October 2000. doi: 10.1096/fj.00-0071com. URL http://dx.doi.org/10.1096/fj.00-0071com.

J. L. Reed and B. Ø. Palsson. Thirteen years of building constraint-based in silico models of Escherichia coli. *Journal of Bacteriology*, 185(9):2692–2699, May 2003. ISSN 0021-9193. URL http://view.ncbi.nlm.nih.gov/pubmed/12700248.

A. E. Rice, M. J. Mendez, C. A. Hokanson, D. C. Rees, and P. J. Björkman. Investigation of the biophysical and cell biological properties of ferroportin, a multipass integral membrane protein iron exporter. *Journal of Molecular Biology*, 386(3): 717–732, February 2009. ISSN 1089-8638. doi: 10.1016/j.jmb.2008.12.063. URL http://dx.doi.org/10.1016/j.jmb.2008.12.063.

D. R. Richardson and P. Ponka. The molecular mechanisms of the metabolism and transport of iron in normal and neoplastic cells. *Biochimica et Biophysica Acta*, 1331(1): 1–40, March 1997. ISSN 0006-3002. URL http://view.ncbi.nlm.nih.gov/pubmed/9325434.

H. D. Riedel, M. U. Muckenthaler, S. G. Gehrke, I. Mohr, K. Brennan, T. Herrmann, B. A. Fitscher, M. W. Hentze, and W. Stremmel. Hfe downregulates iron uptake from transferrin and induces iron-regulatory protein activity in stably transfected cells. *Blood*, 94(11):3915–3921, Dec. 1999. ISSN 1528-0020. URL http://bloodjournal.hematologylibrary.org/content/94/11/3915.abstract.

S. Rivera, E. Nemeth, V. Gabayan, M. A. Lopez, D. Farshidi, and T. Ganz. Synthetic hepcidin causes rapid dose-dependent hypoferremia and is concentrated in ferroportin-containing organs. *Blood*, 106(6):2196–2199, Sept. 2005. ISSN 0006-4971. doi: 10.1182/blood-2005-04-1766. URL http://dx.doi.org/10.1182/blood-2005-04-1766.

A. Robb and M. Wessling-Resnick. Regulation of transferrin receptor 2 protein levels by transferrin. *Blood*, 104(13):4294–4299, December 2004. ISSN 0006-4971. doi: 10.1182/blood-2004-06-2481. URL http://dx.doi.org/10.1182/blood-2004-06-2481.

A. Roetto, G. Papanikolaou, M. Politou, F. Alberti, D. Girelli, J. Christakis, D. Loukopoulos, and C. Camaschella. Mutant antimicrobial peptide hepcidin is associated with severe juvenile hemochromatosis. *Nature Genetics*, 33(1):21–22, January 2003. doi: 10.1038/ng1053. URL http://dx.doi.org/10.1038/ng1053.

J. A. Roth, S. Singleton, J. Feng, M. Garrick, and P. N. Paradkar. Parkin regulates metal transport via proteasomal degradation of the 1B isoforms of divalent metal transporter

1. *Journal of Neurochemistry*, 113(2):454–464, Apr. 2010. ISSN 0022-3042. doi: 10.1111/j.1471-4159.2010.06607.x. URL http://dx.doi.org/10.1111/j.1471-4159.2010.06607.x.

A. Rötig, P. de Lonlay, D. Chretien, F. Foury, M. Koenig, D. Sidi, A. Munnich, and P. Rustin. Aconitase and mitochondrial iron-sulphur protein deficiency in Friedreich ataxia. *Nature Genetics*, 17(2):215–217, October 1997. ISSN 1061-4036. doi: 10.1038/ng1097-215. URL http://dx.doi.org/10.1038/ng1097-215.

T. A. Rouault. The role of iron regulatory proteins in mammalian iron homeostasis and disease. *Nature Chemical Biology*, 2(8):406–414, July 2006. ISSN 1552-4450. doi: 10.1038/nchembio807. URL http://dx.doi.org/10.1038/nchembio807.

T. A. Rouault and S. Cooperman. Brain iron metabolism. *Seminars in Pediatric Neurology*, 13(3):142–148, Sept. 2006. ISSN 10719091. doi: 10.1016/j.spen.2006.08.002. URL http://dx.doi.org/10.1016/j.spen.2006.08.002.

S. Sahle, P. Mendes, S. Hoops, and U. Kummer. A new strategy for assessing sensitivities in biochemical models. *Philosophical Transactions of the Royal Society A*, 366(1880):3619–3631, Oct. 2008. ISSN 1364-503X. doi: 10.1098/rsta.2008.0108. URL http://dx.doi.org/10.1098/rsta.2008.0108.

J. C. Salgado, A. O. Nappa, Z. Gerdtzen, V. Tapia, E. Theil, C. Conca, and M. Nunez. Mathematical modeling of the dynamic storage of iron in ferritin. *BMC Systems Biology*, 4(1):147+, 2010. ISSN 1752-0509. doi: 10.1186/1752-0509-4-147. URL http://dx.doi.org/10.1186/1752-0509-4-147.

A. C. Salisbury, K. P. Alexander, K. J. Reid, F. A. Masoudi, S. S. Rathore, T. Y. Wang, R. G. Bach, S. P. Marso, J. A. Spertus, and M. Kosiborod. Incidence, correlates, and outcomes of acute, hospital-acquired anemia in patients with acute myocardial infarction. *Circulation: Cardiovascular Quality and Outcomes*, 3(4):337–346, July 2010. ISSN 1941-7713. doi: 10.1161/circoutcomes.110.957050. URL http://dx.doi.org/10.1161/circoutcomes.110.957050.

A. Saltelli, K. Chan, and Scott. *Sensitivity Analysis*. Wiley Series in Probability and Statistics. Wiley, 1 edition, October 2000. ISBN 0471998923. URL http://www.worldcat.org/isbn/0471998923.

L. Salter-Cid, A. Brunmark, Y. Li, D. Leturcq, P. A. Peterson, M. R. Jackson, and Y. Yang. Transferrin receptor is negatively modulated by the hemochromatosis protein hfe: implications for cellular iron homeostasis. *Proceedings of the National Academy of Sciences of the United States of America*, 96(10):5434–5439, May 1999. ISSN 0027-8424. URL http://www.ncbi.nlm.nih.gov/pmc/articles/PMC21877/.

M. S. Samoilov, G. Price, and A. P. Arkin. From Fluctuations to Phenotypes: The Physiology of Noise. *Science Signaling*, 2006(366):re17+, December 2006. doi: 10.1126/stke.3662006re17. URL http://dx.doi.org/10.1126/stke.3662006re17.

M. Sanchez, B. Galy, M. U. Muckenthaler, and M. W. Hentze. Iron-regulatory proteins limit hypoxia-inducible factor-2[alpha] expression in iron deficiency. *Nature Structural & Molecular Biology*, 14(5):420–426, May 2007. ISSN 1545-9993. doi: 10.1038/nsmb1222. URL http://dx.doi.org/10.1038/nsmb1222.

J. Sarkar, V. Seshadri, N. A. Tripoulas, M. E. Ketterer, and P. L. Fox. Role of ceruloplasmin in macrophage iron efflux during hypoxia. *The Journal of Biological Chemistry*, 278(45):44018–44024, Nov. 2003. ISSN 0021-9258. doi: 10.1074/jbc.m304926200. URL http://dx.doi.org/10.1074/jbc.m304926200.

S. Sassa. Why heme needs to be degraded to iron, biliverdin ixalpha, and carbon monoxide? *Antioxidants & Redox Signaling*, 6(5):819–824, Oct. 2004. ISSN 1523-0864. doi: 10.1089/ars.2004.6.819. URL http://dx.doi.org/10.1089/ars.2004.6.819.

C. Schiller, Fröhlich, T. Giessmann, W. Siegmund, H. Mönnikes, N. Hosten, and W. Weitschies. Intestinal fluid volumes and transit of dosage forms as assessed by magnetic resonance imaging. *Alimentary Pharmacology & Therapeutics*, 22(10):971–979, Nov. 2005. ISSN 0269-2813. doi: 10.1111/j.1365-2036.2005.02683.x. URL http://dx.doi.org/10.1111/j.1365-2036.2005.02683.x.

C. H. Schilling, J. S. Edwards, D. Letscher, and B. Ø. Palsson. Combining pathway analysis with flux balance analysis for the comprehensive study of metabolic systems. *Biotechnology and Bioengineering*, 71(4):286–306, 2000. ISSN 0006-3592. URL http://view.ncbi.nlm.nih.gov/pubmed/11291038.

H. Schmidt and M. Jirstrand. Systems biology toolbox for matlab: a computational platform for research in systems biology. *Bioinformatics*, 22(4):514–515, Feb. 2006. ISSN 1460-2059. doi: 10.1093/bioinformatics/bti799. URL http://dx.doi.org/10.1093/bioinformatics/bti799.

D. Segrè, D. Vitkup, and G. M. Church. Analysis of optimality in natural and perturbed metabolic networks. *Proceedings of the National Academy of Sciences of the United States of America*, 99(23):15112–15117, November 2002. ISSN 0027-8424. doi: 10.1073/pnas.232349399. URL http://dx.doi.org/10.1073/pnas.232349399.

G. L. Semenza. Involvement of oxygen-sensing pathways in physiologic and pathologic erythropoiesis. *Blood*, 114(10):2015–2019, Sept. 2009. ISSN 1528-0020. doi: 10.1182/blood-2009-05-189985. URL http://dx.doi.org/10.1182/blood-2009-05-189985.

M. Shayeghi, G. O. Latunde-Dada, J. S. Oakhill, A. H. Laftah, K. Takeuchi, N. Halliday, Y. Khan, A. Warley, F. E. McCann, R. C. Hider, D. M. Frazer, G. J. Anderson, C. D. Vulpe, R. J. Simpson, and A. T. McKie. Identification of an intestinal heme transporter. *Cell*, 122(5):789–801, September 2005. ISSN 0092-8674. doi: 10.1016/j.cell.2005.06.025. URL http://dx.doi.org/10.1016/j.cell.2005.06.025.

J. C. Sibille, H. Kondo, and P. Aisen. Interactions between isolated hepatocytes and kupffer cells in iron metabolism: a possible role for ferritin as an iron carrier protein. *Hepatology*, 8(2):296–301, 1988. ISSN 0270-9139. URL http://view.ncbi.nlm.nih.gov/pubmed/3356411.

A. Singh, A. O. Isaac, X. Luo, M. L. Mohan, M. L. Cohen, F. Chen, Q. Kong, J. Bartz, and N. Singh. Abnormal brain iron homeostasis in human and animal prion disorders. *PLOS Pathogens*, 5(3):e1000336+, Mar. 2009. ISSN 1553-7374. doi: 10.1371/journal.ppat.1000336. URL http://dx.doi.org/10.1371/journal.ppat.1000336.

A. Singh, S. Haldar, K. Horback, C. Tom, L. Zhou, H. Meyerson, and N. Singh. Prion protein regulates iron transport by functioning as a ferrireductase. *Journal of Alzheimer's Disease*, 35(3):541–552, Jan. 2013. doi: 10.3233/jad-130218. URL http://dx.doi.org/10.3233/jad-130218.

M. E. Smoot, K. Ono, J. Ruscheinski, P.-L. L. Wang, and T. Ideker. Cytoscape 2.8: new features for data integration and network visualization. *Bioinformatics*, 27(3):431–432, Feb. 2011. ISSN 1367-4811. doi: 10.1093/bioinformatics/btq675. URL http://dx.doi.org/10.1093/bioinformatics/btq675.

S. Soe-Lin, A. D. Sheftel, B. Wasyluk, and P. Ponka. Nramp1 equips macrophages for efficient iron recycling. *Experimental Hematology*, 36(8):929–937, August 2008. ISSN 0301-472X. doi: 10.1016/j.exphem.2008.02.013. URL http://dx.doi.org/10.1016/j.exphem.2008.02.013.

R. Srivastava, L. You, J. Summers, and J. Yin. Stochastic vs. deterministic modeling of intracellular viral kinetics. *Journal of Theoretical Biology*, 218(3):309–321, Oct. 2002. ISSN 0022-5193. URL http://view.ncbi.nlm.nih.gov/pubmed/12381432.

T. G. St Pierre, W. Chua-anusorn, J. Webb, D. Macey, and P. Pootrakul. The form of iron oxide deposits in thalassemic tissues varies between different groups of patients: a comparison between thai beta-thalassemia/hemoglobin e patients and australian beta-thalassemia patients. *Biochimica et Biophysica Acta*, 1407(1):51–60, July 1998. ISSN 0006-3002. URL http://view.ncbi.nlm.nih.gov/pubmed/9639673.

G. Stolovitzky, D. Monroe, and A. Califano. Dialogue on Reverse-Engineering Assessment and Methods. *Annals of the New York Academy of Sciences*, 1115(1):

1–22, December 2007. ISSN 1749-6632. doi: 10.1196/annals.1407.021. URL http://dx.doi.org/10.1196/annals.1407.021.

D. M. Stroka, T. Burkhardt, I. Desbaillets, R. H. Wenger, D. A. Neil, C. Bauer, M. Gassmann, and D. Candinas. Hif-1 is expressed in normoxic tissue and displays an organ-specific regulation under systemic hypoxia. *FASEB Journal*, 15(13): 2445–2453, Nov. 2001. ISSN 1530-6860. doi: 10.1096/fj.01-0125com. URL http://dx.doi.org/10.1096/fj.01-0125com.

M. Summers, M. Worwood, and A. Jacobs. Ferritin in normal erythrocytes, lymphocytes, polymorphs, and monocytes. *British Journal of Haematology*, 28(1):19–26, Sept. 1974. doi: 10.1111/j.1365-2141.1974.tb06636.x. URL http://dx.doi.org/10.1111/j.1365-2141.1974.tb06636.x.

D. W. Swinkels, D. Girelli, C. Laarakkers, J. Kroot, N. Campostrini, E. H. Kemna, and H. Tjalsma. Advances in quantitative hepcidin measurements by time-of-flight mass spectrometry. *PlOS ONE*, 3(7), 2008. ISSN 1932-6203. doi: 10.1371/journal.pone.0002706. URL http://dx.doi.org/10.1371/journal.pone.0002706.

A. Tamura, M. Watanabe, H. Saito, H. Nakagawa, T. Kamachi, I. Okura, and T. Ishikawa. Functional validation of the genetic polymorphisms of human atp-binding cassette (abc) transporter abcg2: identification of alleles that are defective in porphyrin transport. *Molecular Pharmacology*, 70(1):287–296, July 2006. ISSN 0026-895X. doi: 10.1124/mol.106.023556. URL http://dx.doi.org/10.1124/mol.106.023556.

C. K. Tang, J. Chin, J. B. Harford, R. D. Klausner, and T. A. Rouault. Iron regulates the activity of the iron-responsive element binding protein without changing its rate of synthesis or degradation. *The Journal of Biological Chemistry*, 267(34):24466–24470, December 1992. ISSN 0021-9258. URL http://view.ncbi.nlm.nih.gov/pubmed/1447194.

G. C. Telling. Prion protein genes and prion diseases: studies in transgenic mice. *Neuropathology and Applied Neurobiology*, 26(3):209–220, June 2000. ISSN 0305-1846. URL http://view.ncbi.nlm.nih.gov/pubmed/10886679.

K. Thorstensen and I. Romslo. The role of transferrin in the mechanism of cellular iron uptake. *The Biochemical Journal*, 271(1):1–9, October 1990. ISSN 0264-6021. URL http://view.ncbi.nlm.nih.gov/pubmed/2222403].

W.-H. H. Tong and T. A. Rouault. Functions of mitochondrial ISCU and cytosolic ISCU in mammalian iron-sulfur cluster biogenesis and iron homeostasis. *Cell Metabolism*, 3 (3):199–210, March 2006. ISSN 1550-4131. doi: 10.1016/j.cmet.2006.02.003. URL http://dx.doi.org/10.1016/j.cmet.2006.02.003.

F. M. Torti and S. V. Torti. Regulation of ferritin genes and protein. *Blood*, 99(10):3505–3516, May 2002. doi: 10.1182/blood.V99.10.3505. URL http://dx.doi.org/10.1182/blood.V99.10.3505.

C. C. Trenor, D. R. Campagna, V. M. Sellers, N. C. Andrews, and M. D. Fleming. The molecular defect in hypotransferrinemic mice. *Blood*, 96(3):1113–1118, August 2000. URL http://bloodjournal.hematologylibrary.org/cgi/content/abstract/96/3/1113.

M. Uhlen, P. Oksvold, L. Fagerberg, E. Lundberg, K. Jonasson, M. Forsberg, M. Zwahlen, C. Kampf, K. Wester, S. Hober, H. Wernerus, L. Bjorling, and F. Ponten. Towards a knowledge-based human protein atlas. *Nature Biotechnology*, 28(12):1248–1250, Dec. 2010. ISSN 1546-1696. doi: 10.1038/nbt1210-1248. URL http://dx.doi.org/10.1038/nbt1210-1248.

C. Uzel and M. E. Conrad. Absorption of heme iron. *Seminars in Hematology*, 35(1):27–34, Jan. 1998. ISSN 0037-1963. URL http://view.ncbi.nlm.nih.gov/pubmed/9460807.

B. Vaisman, E. Fibach, and A. M. Konijn. Utilization of intracellular ferritin iron for hemoglobin synthesis in developing human erythroid precursors. *Blood*, 90(2):831–838, July 1997. ISSN 0006-4971. URL http://view.ncbi.nlm.nih.gov/pubmed/9226184.

B. A. van Dijk, C. M. Laarakkers, S. M. Klaver, E. M. Jacobs, L. J. van Tits, M. C. Janssen, and D. W. Swinkels. Serum hepcidin levels are innately low in hfe-related haemochromatosis but differ between c282y-homozygotes with elevated and normal ferritin levels. *British Journal of Haematology*, 142(6):979–985, Sept. 2008. ISSN 1365-2141. doi: 10.1111/j.1365-2141.2008.07273.x. URL http://dx.doi.org/10.1111/j.1365-2141.2008.07273.x.

K. E. Van Zandt, F. B. Sow, W. C. Florence, B. S. Zwilling, A. R. Satoskar, L. S. Schlesinger, and W. P. Lafuse. The iron export protein ferroportin 1 is differentially expressed in mouse macrophage populations and is present in the mycobacterial-containing phagosome. *Journal of Leukocyte Biology*, 84(3):689–700, Sept. 2008. ISSN 1938-3673. doi: 10.1189/jlb.1107781. URL http://dx.doi.org/10.1189/jlb.1107781.

A. Vander and J. Sherman, editors. *Human physiology: the mechanisms of body function*. McGraw-Hill higher education, Boston, 2001.

A. Veliz-Cuba, A. S. Jarrah, and R. Laubenbacher. Polynomial algebra of discrete models in systems biology. *Bioinformatics*, 26(13):1637–1643, July 2010. ISSN 1367-4811. doi: 10.1093/bioinformatics/btq240. URL http://dx.doi.org/10.1093/bioinformatics/btq240.

C. D. Vulpe, Y.-M. Kuo, T. L. Murphy, L. Cowley, C. Askwith, N. Libina, J. Gitschier, and G. J. Anderson. Hephaestin, a ceruloplasmin homologue implicated in intestinal iron transport, is defective in the sla mouse. *Nature Genetics*, 21(2):195–199, February 1999. doi: 10.1038/5979. URL http://dx.doi.org/10.1038/5979.

A. Wagner and D. A. Fell. The small world inside large metabolic networks. *Proceedings. Biological sciences / The Royal Society*, 268(1478):1803–1810, September 2001. ISSN 0962-8452. doi: 10.1098/rspb.2001.1711. URL http://dx.doi.org/10.1098/rspb.2001.1711.

T. Wajima, G. K. Isbister, and S. B. Duffull. A comprehensive model for the humoral coagulation network in humans. *Clinical Pharmacology & Therapeutics*, 86(3):290–298, June 2009. doi: 10.1038/clpt.2009.87. URL http://dx.doi.org/10.1038/clpt.2009.87.

J. M. Walker, C. Hahnefeld, S. Drewianka, and F. W. Herberg. Determination of Kinetic Data Using Surface Plasmon Resonance Biosensors. In J. Decler and U. Reischl, editors, *Molecular Diagnosis of Infectious Diseases*, volume 94 of *Methods in Molecular Medicine*, pages 299–320. Humana Press, New Jersey, November 2004. ISBN 1-59259-679-7. doi: 10.1385/1-59259-679-7:299. URL http://dx.doi.org/10.1385/1-59259-679-7:299.

D. F. Wallace, L. Summerville, E. M. Crampton, D. M. Frazer, G. J. Anderson, and N. N. Subramaniam. Combined deletion of hfe and transferrin receptor 2 in mice leads to marked dysregulation of hepcidin and iron overload. *Hepatology*, 50(6):1992–2000, Dec. 2009. ISSN 1527-3350. doi: 10.1002/hep.23198. URL http://dx.doi.org/10.1002/hep.23198.

C.-Y. Y. Wang and M. D. Knutson. Hepatocyte divalent metal-ion transporter-1 is dispensable for hepatic iron accumulation and non-transferrin-bound iron uptake in mice. *Hepatology*, page doi:10.1002/hep.26401, Mar. 2013. ISSN 1527-3350. doi: 10.1002/hep.26401. URL http://dx.doi.org/10.1002/hep.26401.

G. L. Wang, B. H. Jiang, E. A. Rue, and G. L. Semenza. Hypoxia-inducible factor 1 is a basic-helix-loop-helix-PAS heterodimer regulated by cellular o2 tension. *Proceedings of the National Academy of Sciences*, 92(12):5510–5514, June 1995. ISSN 1091-6490. URL http://www.pnas.org/content/92/12/5510.abstract.

J. Wang, G. Chen, and K. Pantopoulos. The haemochromatosis protein hfe induces an apparent iron-deficient phenotype in h1299 cells that is not corrected by co-expression of beta 2-microglobulin. *The Biochemical Journal*, 370(Pt 3):891–899, Mar. 2003a. ISSN 0264-6021. doi: 10.1042/BJ20021607. URL http://dx.doi.org/10.1042/BJ20021607.

M. Wang, M. Weiss, M. Simonovic, G. Haertinger, S. P. Schrimpf, M. O. Hengartner, and C. von Mering. Paxdb, a database of protein abundance averages across all three domains of life. *Molecular & Cellular Proteomics*, 11(8):492–500, Aug. 2012. ISSN 1535-9484. doi: 10.1074/mcp.o111.014704. URL http://dx.doi.org/10.1074/mcp.o111.014704.

R.-H. H. Wang, C. Li, X. Xu, Y. Zheng, C. Xiao, P. Zerfas, S. Cooperman, M. Eckhaus, T. Rouault, L. Mishra, and C.-X. X. Deng. A role of SMAD4 in iron metabolism through the positive regulation of hepcidin expression. *Cell Metabolism*, 2(6):399–409, December 2005. ISSN 1550-4131. doi: 10.1016/j.cmet.2005.10.010. URL http://dx.doi.org/10.1016/j.cmet.2005.10.010.

T.-P. P. Wang, L. Quintanar, S. Severance, E. I. Solomon, and D. J. Kosman. Targeted suppression of the ferroxidase and iron trafficking activities of the multicopper oxidase fet3p from saccharomyces cerevisiae. *Journal of Biological Inorganic Chemistry*, 8 (6):611–620, July 2003b. ISSN 0949-8257. doi: 10.1007/s00775-003-0456-5. URL http://dx.doi.org/10.1007/s00775-003-0456-5.

E. D. Weinberg. Iron withholding: a defense against infection and neoplasia. *Physiological Reviews*, 64(1):65–102, January 1984. ISSN 0031-9333. URL http://view.ncbi.nlm.nih.gov/pubmed/6420813.

J. Weise, R. Sandau, S. Schwarting, O. Crome, A. Wrede, W. Schulz-Schaeffer, I. Zerr, and M. Bähr. Deletion of cellular prion protein results in reduced akt activation, enhanced postischemic caspase-3 activation, and exacerbation of ischemic brain injury. *Stroke; a Journal of Cerebral Circulation*, 37(5):1296–1300, May 2006. ISSN 1524-4628. doi: 10.1161/01.str.0000217262.03192.d4. URL http://dx.doi.org/10.1161/01.str.0000217262.03192.d4.

M. Wessling-Resnick. Iron imports. III. Transfer of iron from the mucosa into circulation. *American Journal of Physiology. Gastrointestinal and Liver Physiology*, 290(1), January 2006. ISSN 0193-1857. doi: 10.1152/ajpgi.00415.2005. URL http://dx.doi.org/10.1152/ajpgi.00415.2005.

A. P. West, M. J. Bennett, V. M. Sellers, N. C. Andrews, C. A. Enns, and P. J. Bjorkman. Comparison of the Interactions of Transferrin Receptor and Transferrin Receptor 2 with Transferrin and the Hereditary Hemochromatosis Protein HFE. *Journal of Biological Chemistry*, 275(49):38135–38138, December 2000. doi: 10.1074/jbc.C000664200. URL http://dx.doi.org/10.1074/jbc.C000664200.

A. P. West, A. M. Giannetti, A. B. Herr, M. J. Bennett, J. S. Nangiana, J. R. Pierce, L. P. Weiner, P. M. Snow, and P. J. Bjorkman. Mutational analysis of the transferrin receptor reveals overlapping HFE and transferrin binding sites. *Journal of Molecular Biology*,

313(2):385–397, October 2001. ISSN 0022-2836. doi: 10.1006/jmbi.2001.5048. URL http://dx.doi.org/10.1006/jmbi.2001.5048.

H. V. Westerhoff, C. Winder, H. Messiha, E. Simeonidis, M. Adamczyk, M. Verma, F. J. Bruggeman, and W. Dunn. Systems biology: the elements and principles of life. *FEBS Letters*, 583(24):3882–3890, December 2009. ISSN 1873-3468. doi: 10.1016/j.febslet.2009.11.018. URL http://dx.doi.org/10.1016/j.febslet.2009.11.018.

R. L. Wixom, L. Prutkin, and H. N. Munro. Hemosiderin: nature, formation, and significance. *International Review of Experimental Pathology*, 22:193–225, 1980. ISSN 0074-7718. URL http://view.ncbi.nlm.nih.gov/pubmed/7005144.

J. S. Woods. Regulation of porphyrin and heme metabolism in the kidney. *Seminars in Hematology*, 25(4):336–348, October 1988. ISSN 0037-1963. URL http://view.ncbi.nlm.nih.gov/pubmed/3064315.

D. M. Wrighting and N. C. Andrews. Interleukin-6 induces hepcidin expression through STAT3. *Blood*, 108(9):3204–3209, November 2006. ISSN 0006-4971. doi: 10.1182/blood-2006-06-027631. URL http://dx.doi.org/10.1182/blood-2006-06-027631.

S. Wuchty. Centers of complex networks. *Journal of Theoretical Biology*, 223(1):45–53, July 2003. ISSN 00225193. doi: 10.1016/S0022-5193(03)00071-7. URL http://dx.doi.org/10.1016/S0022-5193(03)00071-7.

S. Wyman, R. Simpson, A. McKie, and P. Sharp. Dcytb (cybrd1) functions as both a ferric and a cupric reductase in vitro. *FEBS Letters*, 582(13):1901–1906, June 2008. ISSN 00145793. doi: 10.1016/j.febslet.2008.05.010. URL http://dx.doi.org/10.1016/j.febslet.2008.05.010.

W. Xu, T. Barrientos, and N. C. Andrews. Iron and copper in mitochondrial diseases. *Cell Metabolism*, 17(3):319–328, Mar. 2013. ISSN 1932-7420. doi: 10.1016/j.cmet.2013.02.004. URL http://dx.doi.org/10.1016/j.cmet.2013.02.004.

M. Yamamoto, N. Hayashi, and G. Kikuchi. Translational inhibition by heme of the synthesis of hepatic delta-aminolevulinate synthase in a cell-free system. *Biochemical and Biophysical Research Communications*, 115(1):225–231, August 1983. ISSN 0006-291X. URL http://view.ncbi.nlm.nih.gov/pubmed/6615529.

J. Yang, D. Goetz, J.-Y. Li, W. Wang, K. Mori, D. Setlik, T. Du, H. Erdjument-Bromage, P. Tempst, and R. Strong. An Iron Delivery Pathway Mediated by a Lipocalin. *Molecular Cell*, 10(5):1045–1056, November 2002. ISSN 10972765. doi: 10.1016/S1097-2765(02)00710-4. URL http://dx.doi.org/10.1016/S1097-2765(02)00710-4.

T. Yoon and J. A. Cowan. Iron-sulfur cluster biosynthesis. Characterization of frataxin as an iron donor for assembly of [2Fe-2S] clusters in ISU-type proteins. *Journal of the American Chemical Society*, 125(20):6078–6084, May 2003. ISSN 0002-7863. doi: 10.1021/ja027967i. URL http://dx.doi.org/10.1021/ja027967i.

T. Yoon and J. A. Cowan. Frataxin-mediated iron delivery to ferrochelatase in the final step of heme biosynthesis. *The Journal of Biological Chemistry*, 279(25):25943–25946, June 2004. ISSN 0021-9258. doi: 10.1074/jbc.C400107200. URL http://dx.doi.org/10.1074/jbc.C400107200.

M. B. Youdim, D. Ben-Shachar, and P. Riederer. The possible role of iron in the etiopathology of parkinson's disease. *Movement Disorders*, 8(1):1–12, 1993. ISSN 0885-3185. doi: 10.1002/mds.870080102. URL http://dx.doi.org/10.1002/mds.870080102.

J. Yu, V. A. Smith, P. P. Wang, A. J. Hartemink, and E. D. Jarvis. Advances to bayesian network inference for generating causal networks from observational biological data. *Bioinformatics*, 20(18):3594–3603, 2004.

X. Yu, Y. Kong, L. C. Dore, O. Abdulmalik, A. M. Katein, S. Zhou, J. K. Choi, D. Gell, J. P. Mackay, A. J. Gow, and M. J. Weiss. An erythroid chaperone that facilitates folding of alpha-globin subunits for hemoglobin synthesis. *The Journal of Clinical Investigation*, 117(7):1856–1865, July 2007. ISSN 0021-9738. doi: 10.1172/JCI31664. URL http://dx.doi.org/10.1172/JCI31664.

G. Zanninelli, O. Loréal, P. Brissot, A. M. Konijn, I. N. Slotki, R. C. Hider, and Z. Ioav Cabantchik. The labile iron pool of hepatocytes in chronic and acute iron overload and chelator-induced iron deprivation. *Journal of Hepatology*, 36(1):39–46, January 2002. ISSN 0168-8278. URL http://view.ncbi.nlm.nih.gov/pubmed/11804662.

J. Zaritsky, B. Young, B. Gales, H.-J. Wang, A. Rastogi, M. Westerman, E. Nemeth, T. Ganz, and I. B. Salusky. Reduction of serum hepcidin by hemodialysis in pediatric and adult patients. *Clinical Journal of the American Society of Nephrology*, 5(6):1010–1014, June 2010. doi: 10.2215/CJN.08161109. URL http://dx.doi.org/10.2215/CJN.08161109.

L. Zecca, M. B. H. Youdim, P. Riederer, J. R. Connor, and R. R. Crichton. Iron, brain ageing and neurodegenerative disorders. *Nature Reviews Neuroscience*, 5(11):863–873, Nov. 2004. ISSN 1471-003X. doi: 10.1038/nrn1537. URL http://dx.doi.org/10.1038/nrn1537.

J. H. Zivny, M. P. Gelderman, F. Xu, J. Piper, K. Holada, J. Simak, and J. G. Vostal. Reduced erythroid cell and erythropoietin production in response to acute anemia in

prion protein-deficient (prnp-/-) mice. *Blood Cells, Molecules & Diseases*, 40(3):302–307, 2008. ISSN 1096-0961. doi: 10.1016/j.bcmd.2007.09.009. URL `http://dx.doi.org/10.1016/j.bcmd.2007.09.009`.

APPENDIX

A

LIST OF EQUATIONS

These equations make up the model described initially in Chapter 4. They are also used for Chapter 5. A subset of these equations (those which appear in Figure 3.5) comprise the liver model described in Chapter 3.

$$\begin{aligned}\frac{\mathrm{d}\left([\mathrm{Hamp}]\right)}{\mathrm{d}t} = &+\frac{a_{(\text{"Hepcidin expression"})}\cdot[\text{"2HFE}-\text{TfR2"}]^{n_{(\text{"Hepcidin expression"})}}}{K^{n_{(\text{"Hepcidin expression"})}}_{(\text{"Hepcidin expression"})}+[\text{"2HFE}-\text{TfR2"}]^{n_{(\text{"Hepcidin expression"})}}}\\ &+\frac{\mathrm{a1}_{(\text{"Hepcidin expression"})}\cdot[\text{"2(Tf}-\text{Fe)}-\text{TfR2"}]}{\mathrm{K1}_{(\text{"Hepcidin expression"})}+[\text{"2(Tf}-\text{Fe)}-\text{TfR2"}]}\\ &-\mathrm{k1}_{(\text{"Hepcidin degradation"})}\cdot[\mathrm{Hamp}]\end{aligned} \tag{A.0.1}$$

$$\begin{aligned}\frac{\mathrm{d}\left([\text{"Fe}-\text{FT"}]\right)}{\mathrm{d}t} = &\ \mathrm{k1}_{(\text{"Ferritin Iron binding"})}\cdot[\mathrm{LIP}]\cdot[\mathrm{FT}]\\ &-\mathrm{k1}_{(\text{"Ferritin Iron release"})}\cdot[\text{"Fe}-\text{FT"}]\\ &-\mathrm{k1}_{(\text{"Ferritin Iron internalisation"})}\cdot[\text{"Fe}-\text{FT"}]\end{aligned} \tag{A.0.2}$$

$$\begin{aligned}\frac{\mathrm{d}\left([\mathrm{FT}]\right)}{\mathrm{d}t} = &-\mathrm{k1}_{(\text{"Ferritin Iron binding"})} \cdot [\mathrm{LIP}] \cdot [\mathrm{FT}] \\ &+ \mathrm{k1}_{(\text{"Ferritin Iron release"})} \cdot [\text{"Fe} - \mathrm{FT}\text{"}] \\ &+ \mathrm{k1}_{(\text{"Ferritin Iron internalisation"})} \cdot [\text{"Fe} - \mathrm{FT}\text{"}] \\ &+ a_{(\text{"ferritin expression"})} \cdot \left(1 - \frac{[\mathrm{IRP}]^{n_{(\text{"ferritin expression"})}}}{K^{n_{(\text{"ferritin expression"})}}_{(\text{"ferritin expression"})} + [\mathrm{IRP}]^{n_{(\text{"ferritin expression"})}}}\right) \\ &- \mathrm{k1}_{(\text{"Ferritin Degredation Full"})} \cdot [\mathrm{FT}]\end{aligned} \tag{A.0.3}$$

$$\begin{aligned}\frac{\mathrm{d}\left([\mathrm{FT1}]\right)}{\mathrm{d}t} = &+\mathrm{k1}_{(\text{"Ferritin Iron internalisation"})} \cdot [\text{"Fe} - \mathrm{FT}\text{"}] \\ &- [\mathrm{FT1}] \cdot \mathrm{kloss}_{(\text{"Ferritin internalised iron release"})} \cdot \left(1 + \frac{0.048 \cdot \frac{[\mathrm{FT1}]}{[\mathrm{FT}]}}{1 + \frac{[\mathrm{FT1}]}{[\mathrm{FT}]}}\right) \\ &- K_{(\text{"Ferritin Degredation Full Iron Release"})} \cdot \frac{[\mathrm{FT1}]}{[\mathrm{FT}]} \cdot [\mathrm{FT}]\end{aligned} \tag{A.0.4}$$

$$\begin{aligned}\frac{\mathrm{d}\left([\text{"HO} - 1\text{"}]\right)}{\mathrm{d}t} = &+\frac{\mathrm{a2}_{(\text{"HO1 exp"})} \cdot [\mathrm{Halpha}]^{n_{(\text{"HO1 exp"})}}}{\mathrm{K2}^{n_{(\text{"HO1 exp"})}}_{(\text{"HO1 exp"})} + [\mathrm{Halpha}]^{n_{(\text{"HO1 exp"})}}} \\ &+ \frac{a_{(\text{"HO1 exp"})} \cdot [\mathrm{Heme}]^{n_{(\text{"HO1 exp"})}}}{K^{n_{(\text{"HO1 exp"})}}_{(\text{"HO1 exp"})} + [\mathrm{Heme}]^{n_{(\text{"HO1 exp"})}}} \\ &- \mathrm{k1}_{(\text{"HO1 Deg"})} \cdot [\text{"HO} - 1\text{"}]\end{aligned} \tag{A.0.5}$$

$$\begin{aligned}\frac{\mathrm{d}\left([\mathrm{Heme}]\right)}{\mathrm{d}t} = &+\frac{V_{(\text{"Heme uptake"})} \cdot [\mathrm{Heme\_intercell}]}{\mathrm{Km}_{(\text{"Heme uptake"})} + [\mathrm{Heme\_intercell}]} \\ &- \frac{V_{(\text{"Heme export"})} \cdot [\mathrm{Heme}]}{\mathrm{Km}_{(\text{"Heme export"})} + [\mathrm{Heme}]} \\ &- \frac{[\text{"HO} - 1\text{"}] \cdot C_{(\text{"Heme oxygenation"})} \cdot [\mathrm{Heme}]}{K_{(\text{"Heme oxygenation"})} + [\mathrm{Heme}]}\end{aligned} \tag{A.0.6}$$

$$
\begin{aligned}
\frac{\mathrm{d}\left([\mathrm{LIP}]\right)}{\mathrm{d}t} &= -2 \cdot a_{(\text{"Fpn Export"})} \cdot \frac{[\mathrm{Fpn}]^{n_{(\text{"Fpn Export"})}}}{K^{n_{(\text{"Fpn Export"})}}_{(\text{"Fpn Export"})} + [\mathrm{Fpn}]^{n_{(\text{"Fpn Export"})}}} \cdot [\mathrm{LIP}] \\
&\quad - \mathrm{k1}_{(\mathrm{outFlow})} \cdot [\mathrm{LIP}] \\
&\quad - \mathrm{k1}_{(\text{"Ferritin Iron binding"})} \cdot [\mathrm{LIP}] \cdot [\mathrm{FT}] \\
&\quad + \mathrm{k1}_{(\text{"Ferritin Iron release"})} \cdot [\text{"Fe} - \text{FT"}] \\
&\quad + [\mathrm{FT1}] \cdot \mathrm{kloss}_{(\text{"Ferritin internalised iron release"})} \cdot \left(1 + \frac{0.048 \cdot \frac{[\mathrm{FT1}]}{[\mathrm{FT}]}}{1 + \frac{[\mathrm{FT1}]}{[\mathrm{FT}]}}\right) \\
&\quad + K_{(\text{"Ferritin Degredation Full Iron Release"})} \cdot \frac{[\mathrm{FT1}]}{[\mathrm{FT}]} \cdot [\mathrm{FT}] \\
&\quad + \frac{[\text{"HO} - 1\text{"}] \cdot C_{(\text{"Heme oxygenation"})} \cdot [\mathrm{Heme}]}{K_{(\text{"Heme oxygenation"})} + [\mathrm{Heme}]} \\
&\quad + \frac{V_{(\text{"DMT1 endosomal export"})} \cdot [\mathrm{endoFe2}]}{\mathrm{Km}_{(\text{"DMT1 endosomal export"})} + [\mathrm{endoFe2}]} \\
&\quad - \mathrm{k1}_{(\text{"Fe2 oxidation by H202"})} \cdot [\mathrm{LIP}] \cdot [\mathrm{H202}] \\
&\quad - \mathrm{k1}_{(\text{"Fe2 PD2 binding"})} \cdot [\mathrm{LIP}] \cdot [\mathrm{PD2}] - \mathrm{k2}_{(\text{"Fe2 PD2 binding"})} \cdot [\text{"PD2} - \text{Fe2"}] \\
&\quad + \mathrm{k1}_{(\text{"Fe3 reduction by AS and O2"})} \cdot [\mathrm{Fe3}] \cdot [\mathrm{O2}] \cdot [\mathrm{AS}] \\
&\quad - a_{(\text{"outFlow erythropoiesis"})} \\
&\quad \cdot \frac{[\mathrm{H2alpha}]^{n_{(\text{"outFlow erythropoiesis"})}}}{K^{n_{(\text{"outFlow erythropoiesis"})}}_{(\text{"outFlow erythropoiesis"})} + [\mathrm{H2alpha}]^{n_{(\text{"outFlow erythropoiesis"})}}} \cdot [\mathrm{LIP}]
\end{aligned}
\tag{A.0.7}
$$

$$
\begin{aligned}
\frac{\mathrm{d}\left([\mathrm{Fpn}]\right)}{\mathrm{d}t} &= +a_{(\text{"Ferroportin Expression"})} \\
&\quad \cdot \left(1 - \frac{[\mathrm{IRP}]^{n_{(\text{"Ferroportin Expression"})}}}{K^{n_{(\text{"Ferroportin Expression"})}}_{(\text{"Ferroportin Expression"})} + [\mathrm{IRP}]^{n_{(\text{"Ferroportin Expression"})}}}\right) \\
&\quad - a_{(\text{"Fpn degradation"})} \cdot \frac{[\mathrm{Hamp}]^{n_{(\text{"Fpn degradation"})}}}{K^{n_{(\text{"Fpn degradation"})}}_{(\text{"Fpn degradation"})} + [\mathrm{Hamp}]^{n_{(\text{"Fpn degradation"})}}} \cdot [\mathrm{Fpn}]
\end{aligned}
\tag{A.0.8}
$$

$$
\begin{aligned}
\frac{\mathrm{d}\left([\mathrm{IRP}]\right)}{\mathrm{d}t} &= +a_{(\text{"IRP expresion"})} \cdot \left(1 - \frac{[\mathrm{LIP}]^{n_{(\text{"IRP expresion"})}}}{K^{n_{(\text{"IRP expresion"})}}_{(\text{"IRP expresion"})} + [\mathrm{LIP}]^{n_{(\text{"IRP expresion"})}}}\right) \\
&\quad - \mathrm{k1}_{(\text{"IRP degradation"})} \cdot [\mathrm{IRP}]
\end{aligned}
\tag{A.0.9}
$$

$$\frac{\mathrm{d}\left([\mathrm{Fe3}]\right)}{\mathrm{d}t} = +\mathrm{k1}_{(\text{"Fe2 oxidation by H202"})} \cdot [\mathrm{LIP}] \cdot [\mathrm{H202}] - \mathrm{k1}_{(\text{"Fe3reductionbyASandO2"})} \cdot [\mathrm{Fe3}] \cdot [\mathrm{O2}] \cdot [\mathrm{AS}] \tag{A.0.10}$$

$$\frac{\mathrm{d}\left([\mathrm{endoFe3}]\right)}{\mathrm{d}t} = +4 \cdot \left(\mathrm{k1}_{(\text{"TfR1 iron internalisation"})} \cdot [\text{"2(Tf} - \mathrm{Fe}) - \mathrm{TfR1"}]\right) + 4 \cdot \left(\mathrm{k1}_{(\text{"TfR2 iron internalisation"})} \cdot [\text{"2(Tf} - \mathrm{Fe}) - \mathrm{TfR2"}]\right) - \frac{V_{(\text{"Steap3 iron reduction"})} \cdot [\mathrm{endoFe3}]}{\mathrm{Km}_{(\text{"Steap3 iron reduction"})} + [\mathrm{endoFe3}]} \tag{A.0.11}$$

$$\frac{\mathrm{d}\left([\mathrm{endoFe2}]\right)}{\mathrm{d}t} = +\frac{V_{(\text{"Steap3 iron reduction"})} \cdot [\mathrm{endoFe3}]}{\mathrm{Km}_{(\text{"Steap3 iron reduction"})} + [\mathrm{endoFe3}]} - \frac{V_{(\text{"DMT1 endosomal export"})} \cdot [\mathrm{endoFe2}]}{\mathrm{Km}_{(\text{"DMT1 endosomal export"})} + [\mathrm{endoFe2}]} \tag{A.0.12}$$

$$\frac{\mathrm{d}\left([\mathrm{Halpha}]\right)}{\mathrm{d}t} = -\left(\mathrm{k1}_{(\text{"Halpha binding"})} \cdot [\mathrm{Halpha}] \cdot [\text{"PD2} - \mathrm{Fe2} - \mathrm{DG} - \mathrm{O2} - \mathrm{AS"}] - \mathrm{k2}_{(\text{"Halpha binding"})} \cdot [\text{"Halpha} - \mathrm{PHD2} - \mathrm{Fe2} - \mathrm{AS} - \mathrm{DG} - \mathrm{O2"}]\right) - \left(\mathrm{k1}_{(\text{"Halpha binding without AS"})} \cdot [\text{"PD2} - \mathrm{Fe2} - \mathrm{DG} - \mathrm{O2"}] \cdot [\mathrm{Halpha}] - \mathrm{k2}_{(\text{"Halpha binding without AS"})} \cdot [\text{"Halpha} - \mathrm{PHD2} - \mathrm{Fe2} - \mathrm{AS} - \mathrm{DG} - \mathrm{O2"}]\right) + v_{(\text{"Halpha expression"})} \tag{A.0.13}$$

$$\frac{\mathrm{d}\left(["\mathrm{Halpha-PHD2-Fe2-AS-DG-O2"}]\right)}{\mathrm{d}t} =$$
$$+ \left(\mathrm{k1}_{("\text{Halpha binding}")} \cdot [\mathrm{Halpha}] \cdot ["\mathrm{PD2-Fe2-DG-O2-AS"}]\right.$$
$$\left. - \ \mathrm{k2}_{("\text{Halpha binding}")} \cdot ["\mathrm{Halpha-PHD2-Fe2-AS-DG-O2"}]\right)$$
$$+ \left(\mathrm{k1}_{("\text{Halpha binding without AS}")} \cdot ["\mathrm{PD2-Fe2-DG-O2"}] \cdot [\mathrm{Halpha}]\right.$$
$$\left. - \ \mathrm{k2}_{("\text{Halpha binding without AS}")} \cdot ["\mathrm{Halpha-PHD2-Fe2-AS-DG-O2"}]\right)$$
$$- \mathrm{k1}_{("\text{Halpha hydroxylation}")} \cdot ["\mathrm{Halpha-PHD2-Fe2-AS-DG-O2"}]$$

(A.0.14)

$$\frac{\mathrm{d}\left([\mathrm{hydroxylRadical}]\right)}{\mathrm{d}t} = +\mathrm{k1}_{("\text{Fe2 oxidation by H202}")} \cdot [\mathrm{LIP}] \cdot [\mathrm{H202}]$$
$$- \mathrm{k1}_{("\text{hydroxylRadical to water}")} \cdot [\mathrm{hydroxylRadical}]$$

(A.0.15)

$$\frac{\mathrm{d}\left([\mathrm{PD2}]\right)}{\mathrm{d}t} = -\left(\mathrm{k1}_{("\text{Fe2 PD2 binding}")} \cdot [\mathrm{LIP}] \cdot [\mathrm{PD2}] \ - \ \mathrm{k2}_{("\text{Fe2 PD2 binding}")} \cdot ["\mathrm{PD2-Fe2"}]\right)$$
$$+ [\mathrm{Halpha}] \cdot K_{("\text{PD2 expression}")}$$

(A.0.16)

$$\frac{\mathrm{d}\left(["\mathrm{PD2-Fe2"}]\right)}{\mathrm{d}t} = -\left(\mathrm{k1}_{("\text{DG binding}")} \cdot [\mathrm{DG}] \cdot ["\mathrm{PD2-Fe2"}]\right.$$
$$\left. - \mathrm{k2}_{("\text{DG binding}")} \cdot ["\mathrm{PD2-Fe2-DG"}]\right)$$
$$+ \left(\mathrm{k1}_{("\text{Fe2 PD2 binding}")} \cdot [\mathrm{LIP}] \cdot [\mathrm{PD2}]\right.$$
$$\left. - \mathrm{k2}_{("\text{Fe2 PD2 binding}")} \cdot ["\mathrm{PD2-Fe2"}]\right)$$

(A.0.17)

$$\frac{\mathrm{d}\left([\text{"PD2}-\text{Fe2}-\text{DG"}]\right)}{\mathrm{d}t} =$$
$$+\left(\mathrm{k1}_{(\text{"DG binding"})} \cdot [\mathrm{DG}] \cdot [\text{"PD2}-\text{Fe2"}] - \mathrm{k2}_{(\text{"DG binding"})} \cdot [\text{"PD2}-\text{Fe2}-\text{DG"}]\right)$$
$$-\left(\mathrm{k1}_{(\text{"O2 Binding"})} \cdot [\mathrm{O2}] \cdot [\text{"PD2}-\text{Fe2}-\text{DG"}]\right.$$
$$\left.-\mathrm{k2}_{(\text{"O2 Binding"})} \cdot [\text{"PD2}-\text{Fe2}-\text{DG}-\text{O2"}]\right)$$

(A.0.18)

$$\frac{\mathrm{d}\left([\text{"PD2}-\text{Fe2}-\text{DG}-\text{O2"}]\right)}{\mathrm{d}t} =$$
$$-\left(\mathrm{k1}_{(\text{"As binding"})} \cdot [\text{"PD2}-\text{Fe2}-\text{DG}-\text{O2"}] \cdot [\mathrm{AS}]\right.$$
$$\left.-\mathrm{k2}_{(\text{"As binding"})} \cdot [\text{"PD2}-\text{Fe2}-\text{DG}-\text{O2}-\text{AS"}]\right)$$
$$-\left(\mathrm{k1}_{(\text{"Halpha binding without AS"})} \cdot [\text{"PD2}-\text{Fe2}-\text{DG}-\text{O2"}] \cdot [\mathrm{Halpha}]\right.$$
$$\left.-\mathrm{k2}_{(\text{"Halpha binding without AS"})} \cdot [\text{"Halpha}-\text{PHD2}-\text{Fe2}-\text{AS}-\text{DG}-\text{O2"}]\right)$$
$$+\left(\mathrm{k1}_{(\text{"O2 Binding"})} \cdot [\mathrm{O2}] \cdot [\text{"PD2}-\text{Fe2}-\text{DG"}]\right.$$
$$\left.-\mathrm{k2}_{(\text{"O2 Binding"})} \cdot [\text{"PD2}-\text{Fe2}-\text{DG}-\text{O2"}]\right)$$
$$-\left(\mathrm{k1}_{(\text{"H2alpha binding without AS"})} \cdot [\text{"PD2}-\text{Fe2}-\text{DG}-\text{O2"}] \cdot [\mathrm{H2alpha}]\right.$$
$$\left.-\mathrm{k2}_{(\text{"H2alpha binding without AS"})} \cdot [\text{"H2alpha}-\text{PHD2}-\text{Fe2}-\text{AS}-\text{DG}-\text{O2"}]\right)$$

(A.0.19)

$$\frac{\mathrm{d}\left([\text{"PD2}-\text{Fe2}-\text{DG}-\text{O2}-\text{AS"}]\right)}{\mathrm{d}t} =$$
$$+\left(\mathrm{k1}_{(\text{"As binding"})} \cdot [\text{"PD2}-\text{Fe2}-\text{DG}-\text{O2"}] \cdot [\mathrm{AS}]\right.$$
$$\left.-\mathrm{k2}_{(\text{"As binding"})} \cdot [\text{"PD2}-\text{Fe2}-\text{DG}-\text{O2}-\text{AS"}]\right)$$
$$-\left(\mathrm{k1}_{(\text{"Halpha binding"})} \cdot [\mathrm{Halpha}] \cdot [\text{"PD2}-\text{Fe2}-\text{DG}-\text{O2}-\text{AS"}]\right.$$
$$\left.-\mathrm{k2}_{(\text{"Halpha binding"})} \cdot [\text{"Halpha}-\text{PHD2}-\text{Fe2}-\text{AS}-\text{DG}-\text{O2"}]\right)$$
$$-\left(\mathrm{k1}_{(\text{"H2alpha binding"})} \cdot [\mathrm{H2alpha}] \cdot [\text{"PD2}-\text{Fe2}-\text{DG}-\text{O2}-\text{AS"}]\right.$$
$$\left.-\mathrm{k2}_{(\text{"H2alpha binding"})} \cdot [\text{"H2alpha}-\text{PHD2}-\text{Fe2}-\text{AS}-\text{DG}-\text{O2"}]\right)$$

(A.0.20)

$$\frac{\mathrm{d}\left([\mathrm{HalphaH}]\right)}{\mathrm{d}t} = +\,\mathrm{k1}_{(\text{"Halpha hydroxylation"})} \cdot [\text{"Halpha} - \mathrm{PHD2} - \mathrm{Fe2} - \mathrm{AS} - \mathrm{DG} - \mathrm{O2"}] - \mathrm{k1}_{(\text{"HalphaH degradation"})} \cdot [\mathrm{HalphaH}]$$

(A.0.21)

$$\begin{aligned}\frac{\mathrm{d}\left([\mathrm{H2alpha}]\right)}{\mathrm{d}t} = \\ &+ a_{(\text{"H2alpha expression"})} \cdot \left(1 - \frac{[\mathrm{IRP}]}{K_{(\text{"H2alpha expression"})} + [\mathrm{IRP}]}\right) \\ &- \Big(\mathrm{k1}_{(\text{"H2alpha binding"})} \cdot [\mathrm{H2alpha}] \cdot [\text{"PD2} - \mathrm{Fe2} - \mathrm{DG} - \mathrm{O2} - \mathrm{AS"}] \\ &\quad - \mathrm{k2}_{(\text{"H2alpha binding"})} \cdot [\text{"H2alpha} - \mathrm{PHD2} - \mathrm{Fe2} - \mathrm{AS} - \mathrm{DG} - \mathrm{O2"}]\Big) \\ &- \Big(\mathrm{k1}_{(\text{"H2alpha binding without AS"})} \cdot [\text{"PD2} - \mathrm{Fe2} - \mathrm{DG} - \mathrm{O2"}] \cdot [\mathrm{H2alpha}] \\ &\quad - \mathrm{k2}_{(\text{"H2alpha binding without AS"})} \cdot [\text{"H2alpha} - \mathrm{PHD2} - \mathrm{Fe2} - \mathrm{AS} - \mathrm{DG} - \mathrm{O2"}]\Big)\end{aligned}$$

(A.0.22)

$$\begin{aligned}\frac{\mathrm{d}\left([\text{"H2alpha} - \mathrm{PHD2} - \mathrm{Fe2} - \mathrm{AS} - \mathrm{DG} - \mathrm{O2"}]\right)}{\mathrm{d}t} = \\ &+ \Big(\mathrm{k1}_{(\text{"H2alpha binding"})} \cdot [\mathrm{H2alpha}] \cdot [\text{"PD2} - \mathrm{Fe2} - \mathrm{DG} - \mathrm{O2} - \mathrm{AS"}] \\ &\quad - \mathrm{k2}_{(\text{"H2alpha binding"})} \cdot [\text{"H2alpha} - \mathrm{PHD2} - \mathrm{Fe2} - \mathrm{AS} - \mathrm{DG} - \mathrm{O2"}]\Big) \\ &+ \Big(\mathrm{k1}_{(\text{"H2alpha binding without AS"})} \cdot [\text{"PD2} - \mathrm{Fe2} - \mathrm{DG} - \mathrm{O2"}] \cdot [\mathrm{H2alpha}] \\ &\quad - \mathrm{k2}_{(\text{"H2alpha binding without AS"})} \cdot [\text{"H2alpha} - \mathrm{PHD2} - \mathrm{Fe2} - \mathrm{AS} - \mathrm{DG} - \mathrm{O2"}]\Big) \\ &- \mathrm{k1}_{(\text{"H2alpha hydroxylation"})} \cdot [\text{"H2alpha} - \mathrm{PHD2} - \mathrm{Fe2} - \mathrm{AS} - \mathrm{DG} - \mathrm{O2"}]\end{aligned}$$

(A.0.23)

$$\frac{\mathrm{d}\left([\mathrm{H2alphaH}]\right)}{\mathrm{d}t} = +\,\mathrm{k1}_{(\text{"H2alpha hydroxylation"})} \cdot [\text{"H2alpha} - \mathrm{PHD2} - \mathrm{Fe2} - \mathrm{AS} - \mathrm{DG} - \mathrm{O2"}] - \mathrm{k1}_{(\text{"H2alphaH degradation"})} \cdot [\mathrm{H2alphaH}]$$

(A.0.24)

$$
\begin{aligned}
&\frac{\mathrm{d}\left([\text{"Tf}-\text{Fe\_intercell"}]\right)}{\mathrm{d}t} = \\
&+\left(a_{(\text{"Fpn Export"})} \cdot \frac{[\mathrm{Fpn}]^{n_{(\text{"Fpn Export"})}}}{K^{n_{(\text{"Fpn Export"})}}_{(\text{"Fpn Export"})} + [\mathrm{Fpn}]^{n_{(\text{"Fpn Export"})}}} \cdot [\mathrm{LIP}]\right) \\
&-\mathrm{k1}_{(\text{"TfR1 binding"})} \cdot [\text{"Tf}-\text{Fe\_intercell"}] \cdot [\mathrm{TfR}] \\
&+\mathrm{k1}_{(\text{"TfR1 release"})} \cdot [\text{"Tf}-\text{Fe}-\text{TfR1"}] \\
&-\mathrm{k1}_{(\text{"TfR2 binding"})} \cdot [\text{"Tf}-\text{Fe\_intercell"}] \cdot [\mathrm{TfR2}] \\
&+\mathrm{k1}_{(\text{"TfR2 release"})} \cdot [\text{"Tf}-\text{Fe}-\text{TfR2"}] \\
&-\mathrm{k1}_{(\text{"TfR1 binding 2"})} \cdot [\text{"Tf}-\text{Fe}-\text{TfR1"}] \cdot [\text{"Tf}-\text{Fe\_intercell"}] \\
&+\mathrm{k1}_{(\text{"TfR1 release 2"})} \cdot [\text{"2(Tf}-\text{Fe)}-\text{TfR1"}] \\
&-\mathrm{k1}_{(\text{"TfR2 binding 2"})} \cdot [\text{"Tf}-\text{Fe}-\text{TfR2"}] \cdot [\text{"Tf}-\text{Fe\_intercell"}] \\
&+\mathrm{k1}_{(\text{"TfR2 release 2"})} \cdot [\text{"2(Tf}-\text{Fe)}-\text{TfR2"}] \\
&+\left(a_{(\text{"int Fpn Export"})} \cdot \frac{[\mathrm{intFpn}]^{n_{(\text{"int Fpn Export"})}}}{K^{n_{(\text{"int Fpn Export"})}}_{(\text{"int Fpn Export"})} + [\mathrm{intFpn}]^{n_{(\text{"int Fpn Export"})}}} \cdot [\mathrm{intLIP}]\right)
\end{aligned}
\tag{A.0.25}
$$

$$
\begin{aligned}
&\frac{\mathrm{d}\left([\mathrm{TfR}]\right)}{\mathrm{d}t} = \\
&+\frac{\mathrm{a2}_{(\text{"TfR1 expression"})} \cdot [\mathrm{Halpha}]^{n_{(\text{"TfR1 expression"})}}}{\mathrm{K2}^{n_{(\text{"TfR1 expression"})}}_{(\text{"TfR1 expression"})} + [\mathrm{Halpha}]^{n_{(\text{"TfR1 expression"})}}} \\
&+\frac{a_{(\text{"TfR1 expression"})} \cdot [\mathrm{IRP}]^{n_{(\text{"TfR1 expression"})}}}{K^{n_{(\text{"TfR1 expression"})}}_{(\text{"TfR1 expression"})} + [\mathrm{IRP}]^{n_{(\text{"TfR1 expression"})}}} \\
&-\mathrm{k1}_{(\text{"HFE TfR1 binding"})} \cdot [\mathrm{HFE}] \cdot [\mathrm{TfR}] \\
&+\mathrm{k1}_{(\text{"HFE TfR1 release"})} \cdot [\text{"HFE}-\text{TfR"}] \\
&-\mathrm{k1}_{(\text{"TfR1 binding"})} \cdot [\text{"Tf}-\text{Fe\_intercell"}] \cdot [\mathrm{TfR}] \\
&+\mathrm{k1}_{(\text{"TfR1 release"})} \cdot [\text{"Tf}-\text{Fe}-\text{TfR1"}] \\
&-\mathrm{k1}_{(\text{"TfR1 degradation"})} \cdot [\mathrm{TfR}] \\
&+\left(\mathrm{k1}_{(\text{"TfR1 iron internalisation"})} \cdot [\text{"2(Tf}-\text{Fe)}-\text{TfR1"}]\right)
\end{aligned}
\tag{A.0.26}
$$

$$\begin{aligned}\frac{\mathrm{d}\left([\text{"Tf}-\text{Fe}-\text{TfR1"}]\right)}{\mathrm{d}t} = &+V_{\text{intercell}} \cdot \left(\mathrm{k1}_{(\text{"TfR1 binding"})} \cdot [\text{"Tf}-\text{Fe\_intercell"}] \cdot [\text{TfR}]\right)\\ &-\mathrm{k1}_{(\text{"TfR1 release"})} \cdot [\text{"Tf}-\text{Fe}-\text{TfR1"}]\\ &-\mathrm{k1}_{(\text{"TfR1 binding 2"})} \cdot [\text{"Tf}-\text{Fe}-\text{TfR1"}] \cdot [\text{"Tf}-\text{Fe\_intercell"}]\\ &+\mathrm{k1}_{(\text{"TfR1 release 2"})} \cdot [\text{"2(Tf}-\text{Fe)}-\text{TfR1"}]\end{aligned}$$

(A.0.27)

$$\begin{aligned}\frac{\mathrm{d}\left([\text{HFE}]\right)}{\mathrm{d}t} = &-\mathrm{k1}_{(\text{"HFE TfR1 binding"})} \cdot [\text{HFE}] \cdot [\text{TfR}]\\ &+\mathrm{k1}_{(\text{"HFE TfR1 release"})} \cdot [\text{"HFE}-\text{TfR"}]\\ &-2 \cdot \mathrm{k1}_{(\text{"HFE TfR2 binding"})} \cdot [\text{HFE}] \cdot [\text{HFE}] \cdot [\text{TfR2}]\\ &+2 \cdot \mathrm{k1}_{(\text{"HFE TfR2 release"})} \cdot [\text{"2HFE}-\text{TfR2"}]\\ &-\mathrm{k1}_{(\text{"HFE TfR1 binding 2"})} \cdot [\text{"HFE}-\text{TfR"}] \cdot [\text{HFE}]\\ &+\mathrm{k1}_{(\text{"HFE TfR1 release 2"})} \cdot [\text{"2HFE}-\text{TfR"}]\\ &-\mathrm{k1}_{(\text{"HFE degradation"})} \cdot [\text{HFE}]\\ &+v_{(\text{"HFE expression"})}\end{aligned}$$

(A.0.28)

$$\begin{aligned}\frac{\mathrm{d}\left([\text{"HFE}-\text{TfR"}]\right)}{\mathrm{d}t} = &+\mathrm{k1}_{(\text{"HFE TfR1 binding"})} \cdot [\text{HFE}] \cdot [\text{TfR}]\\ &-\mathrm{k1}_{(\text{"HFE TfR1 release"})} \cdot [\text{"HFE}-\text{TfR"}]\\ &-\mathrm{k1}_{(\text{"HFE TfR1 binding 2"})} \cdot [\text{"HFE}-\text{TfR"}] \cdot [\text{HFE}]\\ &+\mathrm{k1}_{(\text{"HFE TfR1 release 2"})} \cdot [\text{"2HFE}-\text{TfR"}]\end{aligned}$$

(A.0.29)

$$\begin{aligned}\frac{\mathrm{d}\left([\text{"Tf}-\text{Fe}-\text{TfR2"}]\right)}{\mathrm{d}t} = &+\mathrm{k1}_{(\text{"TfR2 binding"})} \cdot [\text{"Tf}-\text{Fe\_intercell"}] \cdot [\text{TfR2}]\\ &-\mathrm{k1}_{(\text{"TfR2 release"})} \cdot [\text{"Tf}-\text{Fe}-\text{TfR2"}]\\ &-\mathrm{k1}_{(\text{"TfR2 binding 2"})} \cdot [\text{"Tf}-\text{Fe}-\text{TfR2"}] \cdot [\text{"Tf}-\text{Fe\_intercell"}]\\ &+\mathrm{k1}_{(\text{"TfR2 release 2"})} \cdot [\text{"2(Tf}-\text{Fe)}-\text{TfR2"}]\end{aligned}$$

(A.0.30)

$$\frac{\mathrm{d}\left(["2(\mathrm{Tf}-\mathrm{Fe})-\mathrm{TfR1"}]\right)}{\mathrm{d}t} = +\ \mathrm{k1}_{("\mathrm{TfR1\ binding\ 2"})} \cdot ["\mathrm{Tf}-\mathrm{Fe}-\mathrm{TfR1"}] \cdot ["\mathrm{Tf}-\mathrm{Fe\_intercell"}] - \mathrm{k1}_{("\mathrm{TfR1\ release\ 2"})} \cdot ["2(\mathrm{Tf}-\mathrm{Fe})-\mathrm{TfR1"}] - \mathrm{k1}_{("\mathrm{TfR1\ iron\ internalisation"})} \cdot ["2(\mathrm{Tf}-\mathrm{Fe})-\mathrm{TfR1"}] \tag{A.0.31}$$

$$\frac{\mathrm{d}\left(["2\mathrm{HFE}-\mathrm{TfR"}]\right)}{\mathrm{d}t} = +\mathrm{k1}_{("\mathrm{HFE\ TfR1\ binding\ 2"})} \cdot ["\mathrm{HFE}-\mathrm{TfR"}] \cdot [\mathrm{HFE}] - \mathrm{k1}_{("\mathrm{HFE\ TfR1\ release\ 2"})} \cdot ["2\mathrm{HFE}-\mathrm{TfR"}] - \mathrm{k1}_{("\mathrm{HFETfR\ degradation"})} \cdot ["2\mathrm{HFE}-\mathrm{TfR"}] \tag{A.0.32}$$

$$\frac{\mathrm{d}\left(["2\mathrm{HFE}-\mathrm{TfR2"}]\right)}{\mathrm{d}t} = +\mathrm{k1}_{("\mathrm{HFE\ TfR2\ binding"})} \cdot [\mathrm{HFE}] \cdot [\mathrm{HFE}] \cdot [\mathrm{TfR2}] - \mathrm{k1}_{("\mathrm{HFE\ TfR2\ release"})} \cdot ["2\mathrm{HFE}-\mathrm{TfR2"}] \; xs \; - \mathrm{k1}_{("\mathrm{HFETfR2\ degradation"})} \cdot ["2\mathrm{HFE}-\mathrm{TfR2"}] \tag{A.0.33}$$

$$\frac{\mathrm{d}\left(["2\mathrm{HFE}-\mathrm{TfR2"}]\right)}{\mathrm{d}t} = +\mathrm{k1}_{("\mathrm{HFE\ TfR2\ binding"})} \cdot [\mathrm{HFE}] \cdot [\mathrm{HFE}] \cdot [\mathrm{TfR2}] - \mathrm{k1}_{("\mathrm{HFE\ TfR2\ release"})} \cdot ["2\mathrm{HFE}-\mathrm{TfR2"}] - \mathrm{k1}_{("\mathrm{HFETfR2\ degradation"})} \cdot ["2\mathrm{HFE}-\mathrm{TfR2"}] \tag{A.0.34}$$

$$\frac{\mathrm{d}\left(["2\mathrm{HFE}-\mathrm{TfR2"}]\right)}{\mathrm{d}t} = +\mathrm{k1}_{("\mathrm{HFE\ TfR2\ binding"})} \cdot [\mathrm{HFE}] \cdot [\mathrm{HFE}] \cdot [\mathrm{TfR2}] - \mathrm{k1}_{("\mathrm{HFE\ TfR2\ release"})} \cdot ["2\mathrm{HFE}-\mathrm{TfR2"}] - \mathrm{k1}_{("\mathrm{HFETfR2\ degradation"})} \cdot ["2\mathrm{HFE}-\mathrm{TfR2"}] \tag{A.0.35}$$

$$\frac{\mathrm{d}\left([\text{"2(Tf}-\text{Fe)}-\text{TfR2"}]\right)}{\mathrm{d}t} =$$
$$+ \mathrm{k1}_{(\text{"TfR2 binding 2"})} \cdot [\text{"Tf}-\text{Fe}-\text{TfR2"}] \cdot [\text{"Tf}-\text{Fe\_intercell"}]$$
$$- \mathrm{k1}_{(\text{"TfR2 release 2"})} \cdot [\text{"2(Tf}-\text{Fe)}-\text{TfR2"}]$$
$$- \mathrm{k1}_{(\text{"TfR2 iron internalisation"})} \cdot [\text{"2(Tf}-\text{Fe)}-\text{TfR2"}] \tag{A.0.36}$$

$$\begin{aligned}\frac{\mathrm{d}\left([\mathrm{TfR2}]\right)}{\mathrm{d}t} =& - a_{(\text{"TfR2 degradation"})} \cdot [\mathrm{TfR2}] \\ & \cdot \left(1 - \frac{[\text{"Tf}-\text{Fe\_intercell"}]^{n_{(\text{"TfR2 degradation"})}}}{K^{n_{(\text{"TfR2 degradation"})}}_{(\text{"TfR2 degradation"})} + [\text{"Tf}-\text{Fe\_intercell"}]^{n_{(\text{"TfR2 degradation"})}}}\right) \\ & - \mathrm{k1}_{(\text{"HFE TfR2 binding"})} \cdot [\mathrm{HFE}] \cdot [\mathrm{HFE}] \cdot [\mathrm{TfR2}] \\ & + \mathrm{k1}_{(\text{"HFE TfR2 release"})} \cdot [\text{"2HFE}-\text{TfR2"}] \\ & - \mathrm{k1}_{(\text{"TfR2 binding"})} \cdot [\text{"Tf}-\text{Fe\_intercell"}] \cdot [\mathrm{TfR2}] \\ & + \mathrm{k1}_{(\text{"TfR2 release"})} \cdot [\text{"Tf}-\text{Fe}-\text{TfR2"}] \\ & + \left(\mathrm{k1}_{(\text{"TfR2 iron internalisation"})} \cdot [\text{"2(Tf}-\text{Fe)}-\text{TfR2"}]\right) \\ & + v_{(\text{"TfR2 expression"})}\end{aligned} \tag{A.0.37}$$

$$\begin{aligned}\frac{\mathrm{d}\left([\text{Heme\_intercell}]\right)}{\mathrm{d}t} =& - \frac{V_{(\text{"Heme uptake"})} \cdot [\text{Heme\_intercell}]}{\mathrm{Km}_{(\text{"Heme uptake"})} + [\text{Heme\_intercell}]} \\ & +, \left(\frac{V_{(\text{"Heme export"})} \cdot [\mathrm{Heme}]}{\mathrm{Km}_{(\text{"Heme export"})} + [\mathrm{Heme}]}\right) \\ & + \left(\frac{V_{(\text{"int Heme Export"})} \cdot [\mathrm{intHeme}]}{\mathrm{Km}_{(\text{"int Heme Export"})} + [\mathrm{intHeme}]}\right)\end{aligned} \tag{A.0.38}$$

$$
\begin{aligned}
\frac{\mathrm{d}\left([\mathrm{intLIP}]\right)}{\mathrm{d}t} = &+ K_{(\text{"int Ferritin Degredation Full Iron Release"})} \cdot \frac{[\mathrm{intFT1}]}{[\mathrm{intFT}]} \cdot [\mathrm{intFT}] \\
&+ [\mathrm{intFT1}] \cdot \mathrm{kloss}_{(\text{"int Ferritin internalised iron release"})} \\
&\cdot \left(1 + \frac{0.048 \cdot \frac{[\mathrm{intFT1}]}{[\mathrm{intFT}]}}{1 + \frac{[\mathrm{intFT1}]}{[\mathrm{intFT}]}}\right) \\
&- \mathrm{k1}_{(\text{"int Ferritin Iron binding"})} \cdot [\mathrm{intLIP}] \cdot [\mathrm{intFT}] \\
&+ \mathrm{k1}_{(\text{"int Ferritin Iron release"})} \cdot [\text{"intFe} - \text{FT"}] \\
&- 2 \cdot \left(a_{(\text{"int Fpn Export"})} \cdot \frac{[\mathrm{intFpn}]^{n_{(\text{"int Fpn Export"})}}}{K^{n_{(\text{"int Fpn Export"})}}_{(\text{"int Fpn Export"})} + [\mathrm{intFpn}]^{n_{(\text{"int Fpn Export"})}}}\right. \\
&\left. \cdot [\mathrm{intLIP}]\right) \\
&+ \frac{[\mathrm{intDMT1}] \cdot C_{(\text{"int Iron Import DMT1"})} \cdot [\mathrm{gutFe2}]}{K_{(\text{"int Iron Import DMT1"})} + [\mathrm{gutFe2}]} \\
&+ \frac{[\text{"intHO} - 1\text{"}] \cdot C_{(\text{"int Heme Oxygenation"})} \cdot [\mathrm{intHeme}]}{K_{(\text{"int Heme Oxygenation"})} + [\mathrm{intHeme}]} \\
&- \mathrm{k1}_{(\text{"int outflow"})} \cdot [\mathrm{intLIP}] \\
&- \mathrm{k1}_{(\text{"int Fe2 oxidation by H202"})} \cdot [\mathrm{intLIP}] \cdot [\mathrm{intH202}] \\
&- \left(\mathrm{k1}_{(\text{"int Fe2 PD2 binding"})} \cdot [\mathrm{intLIP}] \cdot [\mathrm{intPD2}] - \right. \\
&\left. \mathrm{k2}_{(\text{"int Fe2 PD2 binding"})} \cdot [\text{"intPD2} - \text{Fe2"}]\right) \\
&+ \left(\mathrm{k1}_{(\text{"}int\ Fe3\ reduction\ by\ AS\ and\ O2\text{"})} \cdot [\mathrm{intFe3}] \cdot [\mathrm{intO2}] \cdot [\mathrm{intAS}]\right)
\end{aligned}
\tag{A.0.39}
$$

$$
\begin{aligned}
\frac{\mathrm{d}\left([\mathrm{intDMT1}]\right)}{\mathrm{d}t} = &- \mathrm{k1}_{(\text{"int Dmt1 Degradation"})} \cdot [\mathrm{intDMT1}] \\
&+ \frac{\mathrm{a2}_{(\text{"int DMT1 Expression"})} \cdot [\mathrm{intH2alpha}]^{n_{(\text{"int DMT1 Expression"})}}}{\mathrm{K2}_{(\text{"int DMT1 Expression"})} n_{(\text{"int DMT1 Expression"})} + [\mathrm{intH2alpha}]^{n_{(\text{"int DMT1 Expression"})}}} \\
&+ \frac{a_{(\text{"int DMT1 Expression"})} \cdot [\mathrm{intIRP}]^{n_{(\text{"int DMT1 Expression"})}}}{K_{(\text{"int DMT1 Expression"})} n_{(\text{"int DMT1 Expression"})} + [\mathrm{intIRP}]^{n_{(\text{"int DMT1 Expression"})}}}
\end{aligned}
\tag{A.0.40}
$$

$$\frac{\mathrm{d}\left([\mathrm{intIRP}]\right)}{\mathrm{d}t} =$$
$$+ a_{(\text{"int IRP Expression"})} \cdot \left(1 - \frac{[\mathrm{intLIP}]^{n_{(\text{"int IRP Expression"})}}}{K^{n_{(\text{"int IRP Expression"})}}_{(\text{"int IRP Expression"})} + [\mathrm{intLIP}]^{n_{(\text{"int IRP Expression"})}}}\right)$$
$$- \mathrm{k1}_{(\text{"int IRP degradation"})} \cdot [\mathrm{intIRP}]$$

(A.0.41)

$$\frac{\mathrm{d}\left([\mathrm{intFpn}]\right)}{\mathrm{d}t} =$$
$$+ a_{(\text{"int Ferroportin Expression"})} \cdot \left(1 - \frac{[\mathrm{intIRP}]^{n_{(\text{"int Ferroportin Expression"})}}}{K^{n_{(\text{"int Ferroportin Expression"})}}_{(\text{"int Ferroportin Expression"})} + [\mathrm{intIRP}]^{n_{(\text{"int Ferroportin Expression"})}}}\right)$$
$$- a_{(\text{"int Fpn degradation"})} \cdot \frac{[\mathrm{intHamp}]^{n_{(\text{"int Fpn degradation"})}}}{K^{n_{(\text{"int Fpn degradation"})}}_{(\text{"int Fpn degradation"})} + [\mathrm{intHamp}]^{n_{(\text{"int Fpn degradation"})}}} \cdot [\mathrm{intFpn}]$$

(A.0.42)

$$[\mathrm{intHamp}] = [\mathrm{Hamp}]$$

(A.0.43)

$$\frac{\mathrm{d}\left([\mathrm{intHeme}]\right)}{\mathrm{d}t} = + \left(\frac{V_{(\text{"gutHeme uptake"})} \cdot [\mathrm{gutHeme}]}{\mathrm{Km}_{(\text{"gutHeme uptake"})} + [\mathrm{gutHeme}]}\right)$$
$$- \left(\frac{V_{(\text{"int Heme Export"})} \cdot [\mathrm{intHeme}]}{\mathrm{Km}_{(\text{"int Heme Export"})} + [\mathrm{intHeme}]}\right)$$
$$- \left(\frac{[\text{"intHO} - 1\text{"}] \cdot C_{(\text{"int Heme Oxygenation"})} \cdot [\mathrm{intHeme}]}{K_{(\text{"int Heme Oxygenation"})} + [\mathrm{intHeme}]}\right)$$

(A.0.44)

$$\frac{\mathrm{d}\left([\text{"intFe} - \mathrm{FT}\text{"}]\right)}{\mathrm{d}t} = + \mathrm{k1}_{(\text{"int Ferritin Iron binding"})} \cdot [\mathrm{intLIP}] \cdot [\mathrm{intFT}]$$
$$- \mathrm{k1}_{(\text{"int Ferritin Iron internalisation"})} \cdot [\text{"intFe} - \mathrm{FT}\text{"}]$$
$$- \mathrm{k1}_{(\text{"int Ferritin Iron release"})} \cdot [\text{"intFe} - \mathrm{FT}\text{"}]$$

(A.0.45)

$$\begin{aligned}\frac{\mathrm{d}\left([\mathrm{intFT}]\right)}{\mathrm{d}t} =& -\mathrm{k1}_{(\text{"int Ferritin Degradation Full"})} \cdot [\mathrm{intFT}] \\ &+ a_{(\text{"int ferritin expression"})} \\ &\cdot \left(1 - \frac{[\mathrm{intIRP}]^{n_{(\text{"int ferritin expression"})}}}{K^{n_{(\text{"int ferritin expression"})}}_{(\text{"int ferritin expression"})} + [\mathrm{intIRP}]^{n_{(\text{"int ferritin expression"})}}}\right) \\ &- \mathrm{k1}_{(\text{"int Ferritin Iron binding"})} \cdot [\mathrm{intLIP}] \cdot [\mathrm{intFT}] \\ &+ \mathrm{k1}_{(\text{"int Ferritin Iron internalisation"})} \cdot [\text{"intFe} - \mathrm{FT"}] \\ &+ \mathrm{k1}_{(\text{"int Ferritin Iron release"})} \cdot [\text{"intFe} - \mathrm{FT"}]\end{aligned} \tag{A.0.46}$$

$$\begin{aligned}\frac{\mathrm{d}\left([\mathrm{intFT1}]\right)}{\mathrm{d}t} =& , -K_{(\text{"int Ferritin Degredation Full Iron Release"})} \cdot \frac{[\mathrm{intFT1}]}{[\mathrm{intFT}]} \cdot [\mathrm{intFT}] \\ &- [\mathrm{intFT1}] \cdot \mathrm{kloss}_{(\text{"int Ferritin internalised iron release"})} \cdot \left(1 + \frac{0.048 \cdot \frac{[\mathrm{intFT1}]}{[\mathrm{intFT}]}}{1 + \frac{[\mathrm{intFT1}]}{[\mathrm{intFT}]}}\right) \\ &+ \mathrm{k1}_{(\text{"int Ferritin Iron internalisation"})} \cdot [\text{"intFe} - \mathrm{FT"}]\end{aligned} \tag{A.0.47}$$

$$\begin{aligned}\frac{\mathrm{d}\left([\text{"intHO} - 1\text{"}]\right)}{\mathrm{d}t} =& + \frac{\mathrm{a2}_{(\text{"int HO1 exp"})} \cdot [\mathrm{intHalpha}]^{n_{(\text{"int HO1 exp"})}}}{\mathrm{K2}^{n_{(\text{"int HO1 exp"})}}_{(\text{"int HO1 exp"})} + [\mathrm{intHalpha}]^{n_{(\text{"int HO1 exp"})}}} \\ &+ \frac{a_{(\text{"int HO1 exp"})} \cdot [\mathrm{intHeme}]^{n_{(\text{"int HO1 exp"})}}}{K^{n_{(\text{"int HO1 exp"})}}_{(\text{"int HO1 exp"})} + [\mathrm{intHeme}]^{n_{(\text{"int HO1 exp"})}}} \\ &- \mathrm{k1}_{(\text{"int HO1 deg"})} \cdot [\text{"intHO} - 1\text{"}]\end{aligned} \tag{A.0.48}$$

$$\begin{aligned}\frac{\mathrm{d}\left([\mathrm{intFe3}]\right)}{\mathrm{d}t} =& + \mathrm{k1}_{(\text{"int Fe2 oxidation by H202"})} \cdot [\mathrm{intLIP}] \cdot [\mathrm{intH202}] \\ &- \left(\mathrm{k1}_{(\text{"int Fe3 reduction by AS and O2"})} \cdot [\mathrm{intFe3}] \cdot [\mathrm{intO2}] \cdot [\mathrm{intAS}]\right)\end{aligned} \tag{A.0.49}$$

$$[\text{intH202}] = [\text{H202}]$$

(A.0.50)

$$\frac{\mathrm{d}\left([\text{intHalpha}]\right)}{\mathrm{d}t} =$$
$$-\left(\text{k1}_{(\text{"int Halpha binding"})} \cdot [\text{intHalpha}] \cdot [\text{"intPD2} - \text{Fe2} - \text{DG} - \text{O2} - \text{AS"}]\right.$$
$$\left. - \text{k2}_{(\text{"int Halpha binding"})} \cdot [\text{"intHalpha} - \text{PHD2} - \text{Fe2} - \text{AS} - \text{DG} - \text{O2"}]\right)$$
$$-\left(\text{k1}_{(\text{"int Halpha binding without AS"})} \cdot [\text{"intPD2} - \text{Fe2} - \text{DG} - \text{O2"}] \cdot [\text{intHalpha}]\right.$$
$$\left. - \text{k2}_{(\text{"int Halpha binding without AS"})} \cdot [\text{"intHalpha} - \text{PHD2} - \text{Fe2} - \text{AS} - \text{DG} - \text{O2"}]\right)$$
$$+ v_{(\text{"int Halpha expression"})}$$

(A.0.51)

$$\frac{\mathrm{d}\left([\text{"intHalpha} - \text{PHD2} - \text{Fe2} - \text{AS} - \text{DG} - \text{O2"}]\right)}{\mathrm{d}t} =$$
$$+\left(\text{k1}_{(\text{"int Halpha binding"})} \cdot [\text{intHalpha}] \cdot [\text{"intPD2} - \text{Fe2} - \text{DG} - \text{O2} - \text{AS"}]\right.$$
$$\left. - \text{k2}_{(\text{"int Halpha binding"})} \cdot [\text{"intHalpha} - \text{PHD2} - \text{Fe2} - \text{AS} - \text{DG} - \text{O2"}]\right)$$
$$+\left(\text{k1}_{(\text{"int Halpha binding without AS"})} \cdot [\text{"intPD2} - \text{Fe2} - \text{DG} - \text{O2"}] \cdot [\text{intHalpha}]\right.$$
$$\left. - \text{k2}_{(\text{"int Halpha binding without AS"})} \cdot [\text{"intHalpha} - \text{PHD2} - \text{Fe2} - \text{AS} - \text{DG} - \text{O2"}]\right)$$
$$- \text{k1}_{(\text{"int Halpha hydroxylation"})} \cdot [\text{"intHalpha} - \text{PHD2} - \text{Fe2} - \text{AS} - \text{DG} - \text{O2"}]$$

(A.0.52)

$$\frac{\mathrm{d}\left([\text{intHalphaH}]\right)}{\mathrm{d}t} =$$
$$+ \text{k1}_{(\text{"int Halpha hydroxylation"})} \cdot [\text{"intHalpha} - \text{PHD2} - \text{Fe2} - \text{AS} - \text{DG} - \text{O2"}]$$
$$- \text{k1}_{(\text{"int HalphaH degradation"})} \cdot [\text{intHalphaH}]$$

(A.0.53)

$$\frac{\mathrm{d}\left([\mathrm{inthydroxylRadical}]\right)}{\mathrm{d}t} = +\,\mathrm{k1}_{(\text{"int Fe2 oxidation by H202"})} \cdot [\mathrm{intLIP}] \cdot [\mathrm{intH202}] - \mathrm{k1}_{(\text{"int hydroxylRadical to water"})} \cdot [\mathrm{inthydroxylRadical}]$$

(A.0.54)

$$[\mathrm{intO2}] = [\mathrm{O2}]$$

(A.0.55)

$$\frac{\mathrm{d}\left([\mathrm{intPD2}]\right)}{\mathrm{d}t} = -\left(\mathrm{k1}_{(\text{"int Fe2 PD2 binding"})} \cdot [\mathrm{intLIP}] \cdot [\mathrm{intPD2}] - \mathrm{k2}_{(\text{"int Fe2 PD2 binding"})} \cdot [\text{"intPD2} - \mathrm{Fe2"}]\right) + [\mathrm{intHalpha}] \cdot K_{(\text{"int PD2 expression"})}$$

(A.0.56)

$$\frac{\mathrm{d}\left([\text{"intPD2} - \mathrm{Fe2"}]\right)}{\mathrm{d}t} = -\left(\mathrm{k1}_{(\text{"int DG binding"})} \cdot [\mathrm{intDG}] \cdot [\text{"intPD2} - \mathrm{Fe2"}] - \mathrm{k2}_{(\text{"int DG binding"})} \cdot [\text{"intPD2} - \mathrm{Fe2} - \mathrm{DG"}]\right) + \left(\mathrm{k1}_{(\text{"int Fe2 PD2 binding"})} \cdot [\mathrm{intLIP}] \cdot [\mathrm{intPD2}] - \mathrm{k2}_{(\text{"int Fe2 PD2 binding"})} \cdot [\text{"intPD2} - \mathrm{Fe2"}]\right)$$

(A.0.57)

$$\frac{\mathrm{d}\left([\text{"intPD2} - \mathrm{Fe2} - \mathrm{DG"}]\right)}{\mathrm{d}t} = +\left(\mathrm{k1}_{(\text{"int DG binding"})} \cdot [\mathrm{intDG}] \cdot [\text{"intPD2} - \mathrm{Fe2"}] - \mathrm{k2}_{(\text{"int DG binding"})} \cdot [\text{"intPD2} - \mathrm{Fe2} - \mathrm{DG"}]\right) - \left(\mathrm{k1}_{(\text{"int O2 Binding"})} \cdot [\mathrm{intO2}] \cdot [\text{"intPD2} - \mathrm{Fe2} - \mathrm{DG"}] - \mathrm{k2}_{(\text{"int O2 Binding"})} \cdot [\text{"intPD2} - \mathrm{Fe2} - \mathrm{DG} - \mathrm{O2"}]\right)$$

(A.0.58)

$$\frac{\mathrm{d}\left([\text{"intPD2} - \text{Fe2} - \text{DG} - \text{O2"}]\right)}{\mathrm{d}t} =$$
$$- \left(\mathrm{k1}_{(\text{"int H2alpha binding without AS"})} \cdot [\text{"intPD2} - \text{Fe2} - \text{DG} - \text{O2"}] \cdot [\text{intH2alpha}]\right.$$
$$\left. - \mathrm{k2}_{(\text{"int H2alpha binding without AS"})} \cdot [\text{"intH2alpha} - \text{PHD2} - \text{Fe2} - \text{AS} - \text{DG} - \text{O2"}]\right)$$
$$- \left(\left(\mathrm{k1}_{(\text{"int As binding"})} \cdot [\text{"intPD2} - \text{Fe2} - \text{DG} - \text{O2"}] \cdot [\text{intAS}]\right.\right.$$
$$\left.\left. - \mathrm{k2}_{(\text{"int As binding"})} \cdot [\text{"intPD2} - \text{Fe2} - \text{DG} - \text{O2} - \text{AS"}]\right)\right)$$
$$- \left(\mathrm{k1}_{(\text{"int Halpha binding without AS"})} \cdot [\text{"intPD2} - \text{Fe2} - \text{DG} - \text{O2"}] \cdot [\text{intHalpha}]\right.$$
$$\left. - \mathrm{k2}_{(\text{"int Halpha binding without AS"})} \cdot [\text{"intHalpha} - \text{PHD2} - \text{Fe2} - \text{AS} - \text{DG} - \text{O2"}]\right)$$
$$+ \left(\mathrm{k1}_{(\text{"int O2 Binding"})} \cdot [\text{intO2}] \cdot [\text{"intPD2} - \text{Fe2} - \text{DG"}]\right.$$
$$\left. - \mathrm{k2}_{(\text{"int O2 Binding"})} \cdot [\text{"intPD2} - \text{Fe2} - \text{DG} - \text{O2"}]\right)$$

(A.0.59)

$$\frac{\mathrm{d}\left([\text{"intPD2} - \text{Fe2} - \text{DG} - \text{O2} - \text{AS"}]\right)}{\mathrm{d}t} =$$
$$- \left(\mathrm{k1}_{(\text{"int H2alpha binding"})} \cdot [\text{intH2alpha}] \cdot [\text{"intPD2} - \text{Fe2} - \text{DG} - \text{O2} - \text{AS"}]\right.$$
$$\left. \mathrm{k2}_{(\text{"int H2alpha binding"})} \cdot [\text{"intH2alpha} - \text{PHD2} - \text{Fe2} - \text{AS} - \text{DG} - \text{O2"}]\right)$$
$$+ \left(\left(\mathrm{k1}_{(\text{"int As binding"})} \cdot [\text{"intPD2} - \text{Fe2} - \text{DG} - \text{O2"}] \cdot [\text{intAS}]\right.\right.$$
$$\left.\left. - \mathrm{k2}_{(\text{"int As binding"})} \cdot [\text{"intPD2} - \text{Fe2} - \text{DG} - \text{O2} - \text{AS"}]\right)\right)$$
$$- \left(\mathrm{k1}_{(\text{"int Halpha binding"})} \cdot [\text{intHalpha}] \cdot [\text{"intPD2} - \text{Fe2} - \text{DG} - \text{O2} - \text{AS"}]\right.$$
$$\left. - \mathrm{k2}_{(\text{"int Halpha binding"})} \cdot [\text{"intHalpha} - \text{PHD2} - \text{Fe2} - \text{AS} - \text{DG} - \text{O2"}]\right)$$

(A.0.60)

$$\frac{\mathrm{d}\left([\text{intH2alpha}]\right)}{\mathrm{d}t} =$$
$$- \left(\mathrm{k1}_{(\text{"int H2alpha binding"})} \cdot [\text{intH2alpha}] \cdot [\text{"intPD2} - \text{Fe2} - \text{DG} - \text{O2} - \text{AS"}]\right.$$
$$\left. - \mathrm{k2}_{(\text{"int H2alpha binding"})} \cdot [\text{"intH2alpha} - \text{PHD2} - \text{Fe2} - \text{AS} - \text{DG} - \text{O2"}]\right)$$
$$- \left(\mathrm{k1}_{(\text{"int H2alpha binding without AS"})} \cdot [\text{"intPD2} - \text{Fe2} - \text{DG} - \text{O2"}] \cdot [\text{intH2alpha}]\right.$$
$$\left. - \mathrm{k2}_{(\text{"int H2alpha binding without AS"})} \cdot [\text{"intH2alpha} - \text{PHD2} - \text{Fe2} - \text{AS} - \text{DG} - \text{O2"}]\right)$$
$$+ a_{(\text{"int H2alpha expression"})} \cdot \left(1 - \frac{[\text{intIRP}]}{K_{(\text{"int H2alpha expression"})} + [\text{intIRP}]}\right)$$

(A.0.61)

$$\frac{\mathrm{d}\left([\text{"intH2alpha} - \text{PHD2} - \text{Fe2} - \text{AS} - \text{DG} - \text{O2"}]\right)}{\mathrm{d}t} =$$
$$+ \left(\mathrm{k1}_{(\text{"int H2alpha binding"})} \cdot [\text{intH2alpha}] \cdot [\text{"intPD2} - \text{Fe2} - \text{DG} - \text{O2} - \text{AS"}]\right.$$
$$\left. - \mathrm{k2}_{(\text{"int H2alpha binding"})} \cdot [\text{"intH2alpha} - \text{PHD2} - \text{Fe2} - \text{AS} - \text{DG} - \text{O2"}]\right)$$
$$- \mathrm{k1}_{(\text{"int H2alpha hydroxylation"})} \cdot [\text{"intH2alpha} - \text{PHD2} - \text{Fe2} - \text{AS} - \text{DG} - \text{O2"}]$$
$$+ \left(\mathrm{k1}_{(\text{"int H2alpha binding without AS"})} \cdot [\text{"intPD2} - \text{Fe2} - \text{DG} - \text{O2"}] \cdot [\text{intH2alpha}]\right.$$
$$\left. - \mathrm{k2}_{(\text{"int H2alpha binding without AS"})} \cdot [\text{"intH2alpha} - \text{PHD2} - \text{Fe2} - \text{AS} - \text{DG} - \text{O2"}]\right)$$

(A.0.62)

$$\frac{\mathrm{d}\left([\text{intH2alphaH}]\right)}{\mathrm{d}t} =$$
$$+ \mathrm{k1}_{(\text{"int H2alpha hydroxylation"})} \cdot [\text{"intH2alpha} - \text{PHD2} - \text{Fe2} - \text{AS} - \text{DG} - \text{O2"}]$$
$$- \mathrm{k1}_{(\text{"int H2alphaH degradation"})} \cdot [\text{intH2alphaH}]$$

(A.0.63)